NNT/NL : 0000AIXM0000/000ED000

THÈSE DE DOCTORAT

Soutenue à Aix-Marseille Université
le 23 février 2024 par

Kilian Zuchan

Caractérisation phylogénétique et thermodynamique de l'électron confurcante hydrogénase à [Fe-Fe] HydABC de *Thermotoga maritima*

Discipline
Biologie-Santé

Spécialité
Biochimie structurale

École doctorale
62 – Sciences de la vie et de la santé

Laboratoire/Partenaires de recherche
Bioénergétique et Ingénierie des Protéines
UMR7281, CNRS-AMU

Composition du jury

Anne-Frances MILLER PR, University of Kentucky, USA	Rapporteuse
Matthias BOLL PR, University of Freiburg, Germany	Rapporteur
Winfried LEIBL DR, CEA, I2BC, UMR-8221	Examinateur
James STURGIS PR, LISM, CNRS-AMU	Président du jury
Wolfgang NITSCHKE DR, BIP, CNRS-AMU	Directeur de thèse
Frauke BAYMANN CR, BIP, CNRS-AMU	Co-directrice de thèse

Affidavit

I, undersigned, Kilian Zuchan, hereby declare that the work presented in this manuscript is my own work, carried out under the scientific supervision of Frauke Baymann and Wolfgang Nitschke, in accordance with the principles of honesty, integrity and responsibility inherent to the research mission. The research work and the writing of this manuscript have been carried out in compliance with both the french national charter for Research Integrity and the Aix-Marseille University charter on the fight against plagiarism.

This work has not been submitted previously either in this country or in another country in the same or in a similar version to any other examination body.

Marseille 14/12/2023



Liste de publications et/ou brevets et participation aux conférences

1.) Liste des publications et/ou brevet 1 réalisées dans le cadre du projet de thèse:

1. **Chapter 4** Zuchan, K., Nina, B. , Christoph, L. *et al.* **(2023)** Thermodynamic landscape of the redox-centres in the electron-confurcating [FeFe]-Hydrogenase (HydABC) of *Thermotoga maritima*, *in preparation*

2. Nitschke W., Schoepp-Cothenet B., Zuchan, K., *et al.* **(2022)** Aqueous electrochemistry: The toolbox for life's emergence from redox disequilibria, *Electrochemical Science Advances* doi: 10.1002/elsa.202100192

3. **Chapter 3** Zuchan, K., Baymann, F. , Baffert, C. *et al.* **(2021)** The dyad of the Y-junction-and a flavin module unites diverse redox enzymes, *BBA-Bioenergetics* doi: 10.1016/j.bbabio.2021.148401

4. Duval S. Zuchan, K., Baymann, F. *et al.* **(2021)** MILS, Metals, Microbes, and Minerals – The Biogeochemical Side of Life *Book Chapter*. doi: 10.1515/9783110589771-011

2.) Participation aux conférences et écoles d'été au cours de la période de thèse:

1. November 2023 (oral communication) Thermodynamic landscape of the redox-centres in the electron-confurcating [FeFe]-Hydrogenase (HydABC) of *Thermotoga maritima*. *3rd Integrative Structural Biology meeting*, Marseille, France.

2. June 2023 (oral communication) Thermodynamic landscape of the redox-centres in the electron-confurcating [FeFe]-Hydrogenase (HydABC) of *Thermotoga maritima*. - A study on the flavin-binding HydB subunit - *Gordon Bioenergetics - Research Seminar*, New Hampshire, USA.

3. June/July 2023 (poster presentation) Thermodynamic landscape of the redox-centres in the electron-confurcating [FeFe]-Hydrogenase (HydABC) of *Thermotoga maritima*. - A study on the flavin-binding HydB subunit - *Gordon Bioenergetics - Research Conference*, New Hampshire, USA.

4. June 2023 (invited speaker oral presentation) Characterization of the redox-centres in the electron-confurcating [FeFe]-Hydrogenase (HydABC) of *Thermotoga maritima*. *Molecular-scale biophysics Research Infrastructure (MOSBRI) Conference*, Zaragoza, Spain.

5. June 2023 (oral presentation) Characterization of the redox-centres in the electron-confurcating [FeFe]-Hydrogenase (HydABC) of *Thermotoga maritima*. *Junior Scientist Microbiology Meeting of Marseille 2023*, Marseille, France.

6. Februrary 2023 (poster presentation) Conformational & redox flexibility - a case study in the electron confurcating [FeFe]-Hydrogenase (HydABC) from *Thermotoga maritima*. *Internal Symposium Max Planck Institute for Chemical Energy Conversion, Department of Inorganic Spectroscopy & Max-Planck-Institut für Kohlenforschung, Department of Molecular Theory and Spectroscopy*, Mülheim, Germany.

7. August 2022 (oral presentation) Characterization of the redox-centres in the electron-confurcating [FeFe]-Hydrogenase (HydABC) of *Thermotoga maritima*. *Colloque -ED 62- Sciences de la vie et de la santé, AMU*, Marseille, France.

8. August 2022 (2 poster presentation) Characterization of the redox-centres in the electron-confurcating [FeFe]-Hydrogenase (HydABC) of *Thermotoga maritima*. & NAD(H)-induced flavosemiquinone stabilization in the electron-confurcating [FeFe]-Hydrogenase (HydABC) of *Thermotoga maritima*. *European Bioenergetics Conference*, Aix-en-Provence, France.

Résumé

L' hydrogénase à [FeFe], HydABC(D), représente un groupe de flavoenzymes catalysant la réaction de la bifurcation/confurcation des électrons qui a été découverte récemment. Le mécanisme de cette réaction, catalysé par la flavine, n'est pas encore compris.

HydABC(D) partage son architecture modulaire avec d'autres déshydrogénases à NAD(P)H telles que le complexe I de la chaîne respiratoire, les hydrogénases à [NiFe] et la formiate déshydrogénase. Toutes comportent deux modules protéiques distincts, ici appelés modules "jonction Y" et module à "flavine", qui assurent le transfert d'électrons entre le $NAD(P)^+$/NAD(P)H et divers substrats bioénergétiques. Le module jonction Y héberge trois centres [4Fe-4S] et un centre [2Fe-2S] disposés en forme de Y. Le module à flavine comporte un seul FMN, avec deux clusters FeS voisins, un cluster [2Fe-2S] de type thiorédoxine et un cluster [4Fe-4S], disposés en triangle. Notre analyse phylogénétique de ce module à flavine a conduit à un regroupement de ces enzymes en deux groupes distincts qui sont caractérisés par des signatures de séquences spécifiques qui corrèlent avec leur capacité à coupler la réduction/oxydation de la ferrédoxine à celle du $NAD(P)^+$/NAD(P)H. La présence requise des deux substrats, démontrée expérimentalement pour HydABC ainsi que pour les autres membres de la famille de ces déhydrogénases à NADPH dépendant de la présence la ferrédoxine, définit le mécanisme de la bifurcation ou de la confurcation des électrons au niveau de la flavine (FBEB/FBEC). Elle va de pair avec la présence de certains domaines mobiles à centres FeS du sous-complexe HydBC. Les paramètres physico-chimiques de l'ensemble des cofacteurs de ce groupe d'enzymes n'ont pas encore été caractérisés.

Dans ce travail, les caractéristiques spectrales et les potentiels rédox de 10 des 11 cofacteurs de l'apo-HydABC de *Thermotoga maritima*, produite de façon hétérologue chez *Escherichia coli*, ainsi que de ses sous-unités isolées, ont été déterminés. La flavine de HydB montre, à des valeurs de pH inférieures à 7, un potentiel rédox de -160 mV pour la première transition électronique ($E_{OX/SR}$). Un $pK_{a,OX}$ de 7 peut être attribué à la protonation de l'azote N(5) des cycles isoalloxazine de la FMN. La deuxième transition électronique ($E_{SR/RED}$) ayant lieu en dessous de -500 mV, indiquant un état semi-réduit neutre de la flavine est fortement stabilisé avec un $\log(K_s)$ d'environ 6.8. Ces propriétés rédox du FMN dans la sous-unité isolée HydB pourraient correspondre à l'état de ce cofacteur dans le complex entier, dans lequel le domaine adjacent à HydB, c'est-à-dire la partie de HydC mobile portant

le cluster [2Fe-2S] de type thiorédoxine est dans une position loin de HydB. Dans l'apo-HydABC, des propriétés rédox différentes ont été déterminées pour la flavine avec les deux transitions rédox individuelles beaucoup plus rapprochées l'une de l'autre et autour de -120 mV (pH 7), ce qui est bien plus élevé que celles des centres FeS voisins autour -400 mV.

Dans aucun des échantillons étudiés, HydB ou apo-HydABC, les propriétés rédox de la flavine et des clusters FeS environnants ne satisfont aux exigences d'une réaction de confurcation des électrons comme celle décrite pour le site Qtextsubscripto des complexes Rieske/cyt*b*, avec les potentiels rédox de la flavine présentant une forte coopérativité positive et le potentiel rédox global à deux électrons ($E_{OX/RED}$) de la flavine situé entre les potentiels rédox des deux donneurs d'électrons.

Cependant, les caractéristiques spectrales des cofacteurs rédox dans HydABC reflètent celles d'autres membres de la famille des NAD(P)H-déshydrogénases, en particulier en ce qui concerne les clusters FeS proches de la flavine. Ceci fournit la base pour les investigations expérimentales d'autres membres de la famille, en mettant l'accent sur les propriétés thermodynamiques de la flavine et des cofacteurs adjacents, pour élucider les capacités catalytiques du FMN et ses implications dans la FBEB/FBEC.

Abstract

The [FeFe]-hydrogenase, HydABC(D), represents a group of flavoenzymes that catalyze the recently discovered reaction of flavin-based electron bifurcation/confurcation (FBEB/FBEC), in a mechanistically not yet understood manner.

This complex shares its modular architecture with other bioenergetic NAD(P)H dehydrogenases such as respiratory complex I, [NiFe]-hydrogenases and formate dehydrogenase. They exhibit two distinctive protein modules, here termed "Y-junction"- and "flavin"-modules, that assure electron transfer between $NAD(P)^+$/NAD(P)H and various bioenergetic substrates. The Y-junction module harbors three [4Fe-4S]- and one [2Fe-2S]-cluster in a Y-shaped arrangement. The flavin module has a single FMN, with two neighboring FeS-clusters, a [2Fe-2S]-cluster of the thioredoxin-type and a [4Fe4S]-cluster, in a branching architecture. Our phylogenetic analysis of this flavin-module led to a clustering of these enzymes into two groups that are distinguished by specific sequence signatures that were congruent with their proposed capacity to use ferredoxin as a second, thermodynamically-coupled substrate besides $NAD(P)^+$/NAD(P)H. The experimentally demonstrated requirement for both substrates, as one defining attribute of FBEB/FBEC, in HydABC alongside other ferredoxin-dependent members of this family was shown to correlate with the expression of additional FeS-cluster-containing domains in the HydBC-subcomplex, which exhibit different degrees of conformational rearrangements and have never been thermodynamically characterized.

Here, for the first time the complete set of equilibrium redox midpoint potentials and spectral signatures of all but one FeS cluster was determined for the heterologously expressed, electron-confurcating apo-HydABC and its constitutive subunits from *Thermotoga maritima*. The redox properties of the single flavin in the isolated HydB subunit feature a redox midpoint potential for the first electron reduction ($E_{OX/SR}$) of -160 mV at pH below 7 with a $pK_{a,OX}$-value of 7 that was attributed to the protonation of the isoalloxazine's nitrogen, N(5), of the FMN. Another redox midpoint potential below -500 mV for the second electron transition ($E_{SR/RED}$) is indicative for a strongly stabilized neutral semi-reduced flavin-state characterized by a $\log(K_s)$ around 6.8. These redox properties of the FMN in the isolated HydB subunit may reflect an observed conformational state of the HydABC complex in which the mobile thioredoxin-like C1 [2Fe-2S]-cluster domain of the HydC subunit is far from the adjacent flavin-binding site in HydB. In the apo-HydABC, the redox properties of the flavin

are different with the two individual redox transitions much closer together, occurring at overall higher potentials (E° ∼ -120 mV) as compared to the neighboring FeS-clusters (E∼ -400 mV).

In none of the investigated samples, HydB or apo-HydABC, the redox properties of the flavin and the surrounding FeS-clusters fulfill the requirements for a flavin-based electron confurcating reaction, in analogy to the redox scheme determined for the Q_o-site in Rieske/cyt*b*-complexes, with the flavin redox potentials exhibiting strong positive cooperativity and the overall two-electron midpoint potential ($E_{OX/RED}$) of the flavin located in between the redox potentials of two adjacent one-electron donors.

The spectral characteristics of redox cofactors in HydABC mirror those in other NAD(P)H dehydrogenase family members, specifically the clusters proximal to the flavin. This provides the basis for the experimental investigations of additional family members with a focus on thermodynamic properties of the flavin and its adjacent cofactors, to elucidate the catalytic abilities of FMN and its implication in FBEB/FBEC.

Acknowledgements

First, I want to thank the members of the jury for the time spent in examining and evaluating my work.

I would like to express my sincere gratitude to the individuals who have played pivotal roles in the completion of this thesis work. I am immensely grateful to my thesis advisors, or as they are affectionately referred to in German as my "Doktormutter" Frauke and my "Doktorvater" Wolfgang. It is a privilege beyond measure to have had both of them on my side through this now more than 4-year long journey. I still remember the morning of first contact that we had spent nearly 5 years ago in Marseille. The serendipity of having two Germans as thesis advisors in the picturesque South of France is a delightful coincidence. Thanks for teaching me how to be resourceful in the lab and all the fun EPR redox titration pizza nights! Even in the face of my perplexing Nernstian $n = 2$ signal interpretations for FeS-clusters, their patient guidance remained unwavering. I owe a considerable debt of gratitude to the members of BIP9, particularly Barbara, the guiding and nurturing head of the group and now the entire laboratory. Simon, a part of my daily coffee routine and my garant has been a source of inspiration and camaraderie. Maybe I really should have done the two PhD-approach, "bifurcation" during the day and "green rust" during the night, as planned in the beginning, so we would have been able to spend more fun time at the CINAM, with Olivier and Daniel. The entire BIP has been an essential part of my academic journey, and I feel deeply obliged to acknowledge some people as they have shaped my PhD experience in different time points along the way. Thanks to Arlette for teaching me the intricate art of cultivating the stinky Desulfovibrio and purifying the Hnd from it, Carole for her assistance in activity tests of the Hnd, Myriam for her unwavering calm and ever-present smile. Mathieu Luglia for his inspiring microbiological expertise in Desulfovibrio cultivation strategies. I'm indebted to the BIP7 for exploiting their EPR redox titration setups, therefore thanks to Eric for his ever-smiling assistance with glove box booking, Emilien for planning our EPR experiments, and Bruno for giving me some leads in interpretion of the iron-sulfur EPR signals. Valerie for introducing me to the great MOSBRI-consortium which funded nearly all my EPR experiments. Finally, the dedicated team at the BIP's laverie, as well as Aurelia, and Isabelle, deserve recognition for their tireless efforts in maintaining the laboratory equipment and handling the administrative complexities.

I extend my deepest appreciation to Studienstiftung des deutschen Volkes for their ideal and financial support over the last 3.5 years. Without their scholarship, I would not have enjoyed the scientific freedom that allowed me to work on this subject to the extent that I did. Additionally, it provided me with access to a wealth of information and invaluable connections to other like-minded people in Germany. I am also thankful to Ecole Doctoral 62 for accepting my candidature under these unusual financial circumstances. The “Committee Suivi de thèse”, including Christophe Léger, Goetz Parsiegla, Maryam Seif-Eddine, and Batoul Srour, have been instrumental in reviewing my progress at the 2 and 3-year marks and providing valuable insights into the direction of this project. My sincere appreciation goes out to Nicolas Vita, who served as "mon parrain de la thèse" and consistently expressed interest in the state of affairs.

James Birrell, without whom this thesis would certainly also not have been possible, deserves special recognition for the collaboration that emerged from an initial request for his PhD-thesis document. Nina Breuer, the technical expert of the biotechnological unit at the MPI, played a crucial role in the success of my research. Christoph Laurich, the creator of the electro-chemical setup I used for HydB and HydABC characterization, was unwavering in his support, especially after the initial system crash. I am also grateful to Kushal Sengupta, the new group leader at the MPI, for his kind support over the last year. My heartfelt thanks go to my friends and family in Germany, who provided not only warm hugs and well-wishes but also provided me with by beloved “Mate” and German bread spreads. Your support meant the world to me.

Acting as the president of the JSM3, “Junior Scientist Microbiology Meeting of Marseille”, was without doubt one of the most enriching experiences during my PhD. I feel immensely honored of having headed our journey for the organization of such a big event after the pandemic. Promoting the scientific exchange with such a large, interdisciplinary and multicultural team of PhD students has filled me with so much joy, besides the struggles of juggling everything at once. I am immensely grateful to my friends in Marseille, including Giulia, who began this journey at the BIP9 with me and shared the everyday struggles with me. Momo, a friend from day one. I want to acknowledge the entire big, chaotic family that I’ve found in Marseille, including Natalie, Anna-Lisa, Mel, Christina, Vincent, Giulia Fish, Julian, Ketty, Brice, Andrea, Nil, Aurore, Dan, Cassy, Anna and Orion. Thanks for all the laughs, the hikes, the apero’s, the evenings, the dinners, the activities and enriching my PhD experience.

Last but certainly not least, to Léa, one of my most significant discoveries in Marseille. Your presence has filled my life with countless emotions, and I am deeply thankful for your love and support.

"Le véritable voyage de découverte ne consiste pas à chercher de nouveaux paysages, mais d'avoir d'autres yeux, de voir l'univers avec les yeux d'un autre, de cent autres, de voir les cent univers que chacun d'eux voit, que chacun d'eux est."

Marcel Proust,
À LA RECHERCHE DU TEMPS PERDU
- LA PRISONNIÈRE (1923) P.69

Contents

1 Introduction **16**

1.1 Energy Acquisition and Transformation in Living Organisms:
The Fundamental Role of Redox Disequilibrium 17

1.1.1 Bioenergetic proteins as coupling devices 18

1.1.2 Electron-confurcating [FeFe]-hydrogenase HydABC from *T. maritima* 19

1.2 Quinone-based Electron bifurcation 22

1.2.1 Quinones 22

1.2.2 Rieske/cyt*b*-family 23

1.2.3 A short excursion into redox cooperativity 26

1.2.4 Electron Bifurcation at the Q_o-site 29

1.3 Electron Bifurcation in flavoenzymes 36

1.3.1 Etf - Electron transferring flavoprotein 38

1.3.2 Nfn - NADH-dependent ferredoxin:NADP oxidoreductase 40

1.3.3 Hdr - Heterodisulfide reductase 41

1.4 Structure - Function Relationship in HydABC 43

1.4.1 Conformational arrangements of three domains in the HydBC subcomplex . . 46

1.4.2 Ferredoxin-like C-terminal domain in HydB with B3 and B4 46

1.4.3 Thioredoxin-like N-terminal domain in HydB with B1 47

1.4.4 Thioredoxin-like C-terminal domain in HydC with C1 48

1.4.5 A single flavin in HydABC catalyzes FBEB and NADH oxidation 49

1.4.6 Conformational changes in HydABC driven by redox transitions? 50

1.5 Thermodynamic and spectral properties of the FeS-Flavoenzyme HydABC 51

1.5.1 Thioredoxin-type [2Fe-2S]-clusters 51

1.5.2 Spectral characteristics of Trx-like [2Fe-2S] 55

1.5.3 Ferredoxin-like [4Fe-4S]-clusters 56

1.6 The Flavoenzyme-environment tunes the electrochemical properties of its flavin . . . 58

1.6.1 pK_a-values of the isoalloxazine's N(1) , N(3) and N(5) 59

1.6.2 Proton-coupled redox transitions induce pH-dependent redox potentials . . . 60
1.6.3 pH-dependent redox potentials of flavins and flavoenzymes 63
1.6.4 Interaction of FMN with NADH involves a hydride transfer to N(5) 64
1.6.5 Spectroscopic means of studying flavins and flavoenzymes 66
1.7 Aim of the thesis 69

2 Methods **71**
2.1 UV/Vis absorbance spectroscopy 71
2.2 Electron paramagnetic resonance (EPR) spectroscopy 71
2.2.1 The influence of Temperature, Spin Relaxation and Power-Saturation 73
2.2.2 g-value anisotropy 75
2.2.3 X-band EPR-signals and characteristics of FeS-clusters 76
2.3 Equilibrium Redox titrations 76
2.3.1 Chemical redox titrations monitored by EPR-spectroscopy 77
2.3.2 Electrochemical redox titrations followed by UV/Vis-Spectroscopy 78

3 The dyad of the Y-junction- and a flavin module unites diverse redox enzymes **80**

4 Thermodynamic landscape of the redox-centres in the electron-confurcating [FeFe]-Hydrogenase (HydABC) of *Thermotoga maritima* **114**

5 Discussion and Perspectives **152**
5.1 The thermodynamic architecture of the HydABC 155
5.1.1 FeS-cofactor geometries across the NAD(P)H dehydrogenase family 155
5.1.2 Comparable geometry doesn't dictate thermodynamics 155
5.1.3 Ambiguities in the redox potential assignment for the Trx-like [2Fe-2S]-cluster B1 in HydB between EPR and UV/Vis 158
5.2 Thermodynamic properties of the FMN in HydB and HydABC 161
5.2.1 A neutral semi-reduced redox state of the FMN in HydB 161
5.2.2 The fully-reduced redox state of FMN in HydB 163
5.2.3 Assignments of pK_a-values to N(1), N(3) and N(5) to the FMN in HydB 166
5.2.4 The FMN environment in structure models of HydABC 167
5.2.5 Summary of the assigned pK_a-values for the FMN in HydB 169
5.2.6 Characterization of the FMN in HydABC 171
5.2.7 Interactions of HydABC and HydB with NAD^+/NADH 171
5.3 An electron-transferring redox landscape in HydB and HydABC 172

6 Conclusions **175**

6.1 Conclusions 175

A Appendix **176**

Bibliography **182**

List of Abbreviations

8Fe Fd	8 iron = 2 [4Fe-4S] **F**erre**d**oxin
ASR	**A**nionic **S**emi-**R**educed species
Complex I	**N**ADH:**(ubi)quinone** oxidoreductase
Complex III	bc_1-complex or **ubiquinol**:**cytochrome** c oxidoreductase
Cryo-EM	Single-particle **C**ryo-**E**lectron **M**icroscopy
Cw-EPR	**C**ontinuous **w**ave-**E**lectron **P**aramagnetic **R**esonance
CTD	**C**-**T**erminal **D**omain
EPR	**E**lectron **P**aramagnetic **R**esonance (spectroscopy)
Cw-EPR	**C**ontinuous **w**ave **EPR**
Etf	**E**lectron **t**ransferring **f**lavoprotein
EB	**E**lectron **B**ifurcation
EC	**E**lectron **C**onfurcation
FMN	**F**lavin **M**ono**N**ucleotide
FAD	**F**lavin **A**denine **D**inucleotide
FBEB	**F**lavin-**B**ased **E**lectron **B**ifurcation
FBEC	**F**lavin-**B**ased **E**lectron **C**onfurcation
Fd	**F**erre**d**oxin
FeS	**I**ron-**S**ulfur (cluster)
[2Fe-2S]-cluster	**T**wo **I**ron-**T**wo **S**ulfur-cluster
[4Fe-4S]-cluster	**F**our **I**ron-**F**our **S**ulfur-cluster
Fld	**Fl**avo**d**oxin
H-bond	**H**ydrogen **B**onds
Hdr	**H**eterodisulfide **r**eductase
LUCA	**L**ast **U**niversal **C**ommon **A**ncestor
MV	**M**ethyl **V**iologen
NSR	**N**eutral **S**emi-**R**educed species
NAD(P)$^+$	**N**icotinamide **A**denine **D**inucleotide (**P**hosphate)
NAD(P)H	Reduced **N**icotinamide **A**denine **D**inucleotide (**P**hosphate)
NTD	**N**-**T**erminal **D**omain
PDB	**P**rotein **D**ata**B**ank
Nfn	**N**ADH-dependent reduced **f**erredoxin: **N**ADP$^+$ **o**xidoreductase
PMF	**P**roton **M**otive **F**orce
PCET	**P**roton-**C**oupled **E**lectron **T**ransfers
OX	**Ox**idized (species)
QBEB	**Q**uinone-**B**ased **E**lectron **B**ifurcation
SHE	**S**tandard **H**ydrogen **E**lectrode
SR	**S**emi-**R**educed (species)
RED	Fully-**Red**uced (species)
Trx-like [2Fe-2S]	**T**hioredoxin-like [2Fe-2S]-cluster
UV/Vis	**UV/V**isible (spectroscopy)
WT	**W**ild-**T**ype

Chapter 1
Introduction

1.1 Energy Acquisition and Transformation in Living Organisms: The Fundamental Role of Redox Disequilibrium

Irrespective of form, degree of complexity, time or place, all known living organisms are united in their necessity to capture, convert, store and use energy to maintain all metabolic processes to stay alive, reproduce and thrive.

Cells, as the smallest unit of life, are in a constant state of disequilibrium and require a steady supply of energy to uphold their well-structured form. Energy is essential for the production of intricate molecules from basic building blocks (such as crafting proteins from amino acids), maintaining differences in concentrations of different chemical substances inside and outside the cell, and powering mechanical activities like internal cell transport or muscle contractions.

Redox disequilibrium is the source of energy utilized by life[166;190]. It involves the exploitation of the natural tendency of electrons to flow from redox transitions at low to high redox potential. Oxidation-reduction (hereafter redox) reactions that occur as electron transfer reactions from low redox potential electron donors (D_{red}) to high redox potential electron acceptors (A_{ox}) are thermodynamically favored and proceed spontaneously, under the release of free energy ($\Delta G_{ET} < 0$) which sustains life [a] This forms the basis of bioenergetics (figure 1.1).

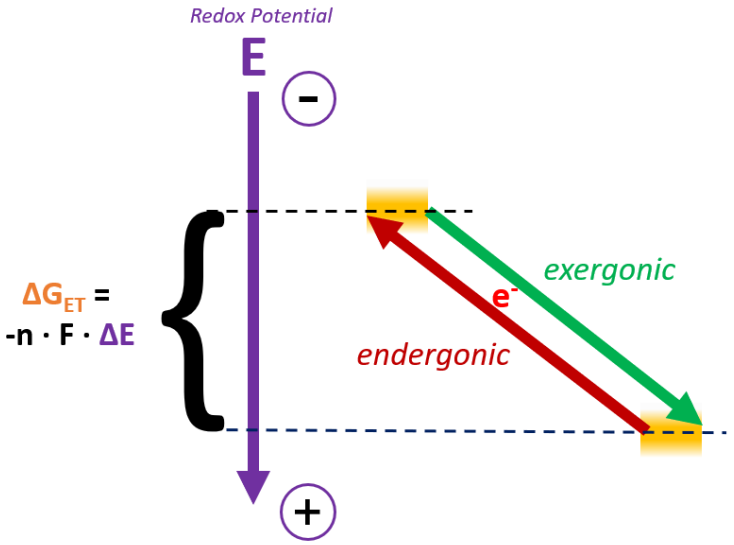

Figure 1.1: General energetic relationship of exergonic and endergonic redox reactions. Exergonic redox reactions occur thermodynamically "downhill" ($\Delta G^{\circ}_{ET} < 0$) in a spontaneous process from a low potential donor to a high potential acceptor (as yellow bars), whereas endergonic redox reactions require energy to "push" the electron "uphill" ($\Delta G^{\circ}_{ET} > 0$).

Under standard conditions[b], the thermodynamic driving force or standard free energy change

[a] For completion: In photosynthetic organisms these low potential donors and high potential acceptors are internally generated from photon energy.

[b] i.e., 25°C or 298.15 K, 10^{-7} M of proton concentration (= pH 7), aqueous substrate and product concentrations of 1 M at 1 unit atmospheric (1 bar, 10^5 Pa) gas pressure. Standard conditions are denoted throughout this thesis by the addition of a degree sign (°). All potentials are given in milliVolt (mV) in reference to the standard hydrogen electrode (SHE).

of the electron transfer ($\Delta G^{\circ}_{\mathrm{ET}}$) is directly proportional to the difference in standard redox potential (ΔE°) of the electron acceptor (E°_{A}) and donor (E°_{D}) via:

$$\Delta E^{\circ} = E^{\circ}_{\mathrm{D}} - E^{\circ}_{\mathrm{A}} \tag{1.1}$$

$$\Delta G^{\circ}_{\mathrm{ET}} = -n \cdot F \cdot \Delta E^{\circ} \tag{1.2}$$

where n is the number of transferred electrons and F is the Faraday constant ($F = 96.485\,\mathrm{kJ\,V^{-1}}$).

$\Delta G^{\circ}_{\mathrm{ET}} < 0$ or $\Delta G^{\circ}_{\mathrm{ET}} > 0$ describes an energetically "downhill" (exergonic) process or energetically "uphill" (endergonic) process, respectively. Exergonic processes release energy along the way, which is either consequently dissipated to the surroundings as heat or can be coupled to an "uphill" process, i.e., an endergonic process. In the case of an energetic coupling of an exergonic with an endergonic process, the net energy released by the exergonic reaction must exceed the energy required for the endergonic reaction for a net forward reaction to occur.

1.1.1 Bioenergetic proteins as coupling devices

Inside the cell, life employs specific protein machines as "coupling devices" that harness the redox disequilibrium by coupling energy-releasing (exergonic) reactions to energy-demanding (endergonic) processes in overall exergonic reactions, i.e., the energy-releasing event liberates overall more energy than the endergonic process requires[28].

Prokaryotes employ a diverse ensemble of electron-transferring redox enzymes[12;190] that enable them to thrive in a variety of ecological niches. These electron transfer chains empower them to exploit diverse environmental redox sources while maximizing the energy output from each substrate. The utilization of these redox sources sustains their internal redox disequilibrium.

Upon closer inspection, it becomes evident that numerous individual coupling devices within different electron transfer chains exhibit similar traits. This stems from the fact that a limited set of building blocks are assembled to build up different bioenergetic proteins. These building blocks, refer to distinct protein subunits or domains, which frequently make use of specific cofactors, such as quinones, flavins, hemes, iron-sulfur (FeS) clusters, or other metal centers, to catalyze a variety of electron transfer reactions[12;35;63;87;203].

The modular make-up of these bioenergetic "building blocks" allows organisms to repurpose existing protein subunits or complexes in adaptation to changing environmental conditions or even entirely new redox sources, ensuring a supply of both electron donors and electron acceptors. Exploring the phylogenetic relationship of homologous building blocks reveal unique metabolic pathways of ancient life forms, possibly dating back to the last universal common ancestor (LUCA)[12;88;181;190].

In recent years, a new type of bioenergetic coupling mechanism in various classes of flavin-containing complexes was discovered[7;13;32;95]. These enzymes have been hypothesized to employ the two-electron carrier, Flavin, together with other redox cofactors to realize a direct thermodynamic coupling of an electron pair. An endergonic electron transfer is thereby coupled to an exergonic electron transfer in an overall exergonic process.

Organisms use these coupling devices to exploit the energy release of the exergonic reduction of a high redox potential electron acceptor from the intermediate redox potential two-electron donating flavin, under the apparently simultaneous production of more reducing electron donors, such as reduced low-potential ferredoxins (Fd). This minimizes energy dissipation by capitalizing on the free energy released during exergonic electron transfers for the thermodynamically coupled, unfavorable electron transfers in a process termed **E**lectron **B**ifurcation (EB).

Oppositely, some protein complexes physiologically catalyze "**E**lectron **C**onfurcation" (EC), enabling the oxidation of a high redox potential 1-electron redox carrier by coupling it to the exergonic oxidation of a partnering lower redox potential single-electron substrate for the reduction of an intermediate potential two-electron acceptor. Both coupling mechanisms, EB and EC, allow living entities to enlarge their vital redox disequilibrium beyond the redox span that is imposed by the available electron-donating and electron-accepting environmental substrates. The two-electron coupling mechanism of this group of flavoenzymes is known as **F**lavin-**b**ased **E**lectron **B**ifurcation (FBEB) or **F**lavin-**b**ased **E**lectron **C**onfurcation (FBEC).

The heterotrimeric [FeFe]-hydrogenase, HydABC, from the anaerobic, hyperthermophilic *Thermotoga maritima* represents one example of this newly discovered group of flavoenzymes. This complex catalyzes FBEC to simultaneously oxidize two thermodynamically different electron acceptors, NAD^+ and ferredoxin in an hydrogen (H_2)-evolving reaction during glucose fermentation.

1.1.2 Electron-confurcating [FeFe]-hydrogenase HydABC from *T. maritima*

The marine bacteria *Thermotoga maritima* was first isolated in 1990 in ocean floor sediments at hydrothermal vents near Volcano Island, Italy. This microorganism grows optimally at 80°C in the strict absence of oxygen[97]. It powers its internal redox disequilibrium from fermentation of organic carbohydrates, the simplest being glucose, producing acetate, carbon dioxide (CO_2), and hydrogen (H_2).

Initial characterizations of the only H_2-producing enzyme in *T. maritima*, the trimeric [FeFe]-hydrogenase HydABC, noticed a substantially lower catalytic H_2 evolution activity in this complex with reduced Methyl-Viologen (MV) as an electron donor compared to the better-characterized, clostridial monomeric [FeFe]-hydrogenases[c]. Meanwhile, the H_2 affinity (K_m) in the H_2 oxidation as-

[c] V_{max} = 164 U mg^{-1} at 80°C in HydABC as compared to 5500 U mg^{-1} in *C. pasterianum* [FeFe]-hydrogenase I (CpI),

says was comparable[d]. Furthermore, it was established that ferredoxin (Fd), which typically serves as the primary electron donor under native conditions for the majority of known [FeFe]-hydrogenases, does not function as an electron substrate for the HydABC complex[107]. Subsequent experiments on cell-free extracts showed, however, considerable H_2-dependent reduction of the internal reducing equivalent NAD^+ ($\sim 0.3\,\mu$mol NADH min^{-1} mg^{-1}), an activity that was lost upon purification of the protein[215].

Schut *et al.* (2009)[194] first demonstrated that HydABC uses neither the low-potential reduced ferredoxin nor the high-potential NADH as the sole electron donors, but both of these substrates in a synergistic way for the two-electron reduction of protons (H^+) to H_2 ($E°_{H^+/H_2}$ = -414 mV[210]).

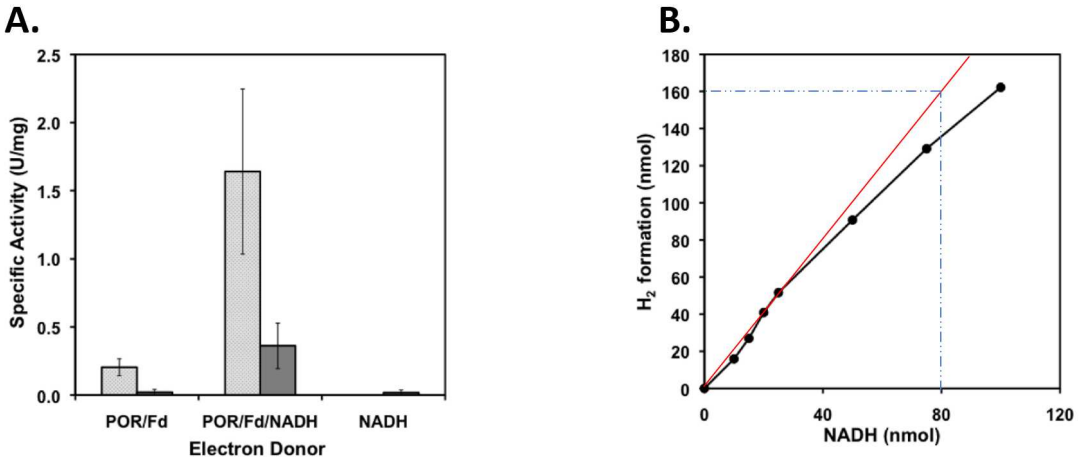

Figure 1.2: **A.** Substrate dependence of the electron-confurcating [FeFe]-hydrogenase of *T. maritima*. The specific activity at 80°C in the standard H_2-production assay containing a ferredoxin-regenerating system with the pyruvate oxidoreductase (Fd/POR), NADH, or Fd/POR and NADH was determined for the cytoplasmic extract (dark bars) and the purified hydrogenase at pH 7.5 (light bars). **B.** H_2-production using limiting amounts of NADH as the electron donor in the presence of the non-limiting ferredoxin (with the Fd/POR system). The amounts of NADH added to the standard H_2-production assay and the amounts of H_2 produced are indicated. The stoichiometry slightly deviates from the 1 to 2 ratio (red line) of NADH to H_2, leading to published ratio of 1 to 1.8 ± 0.2. Graphs and Data adapted with permission from Schut *et al.* (2009)[194]. Copyright 2009 American Society for Microbiology.

Activity assays on cell extracts and the purified enzyme (represented as light and dark gray bars of figure 1.2A, respectively) from *T. maritima* using the reduced form of the native ferredoxin *Tm*Fd1 (TM0927, $E_{m,pH8}$ = -415 mV[41;131]) with a regenerating pyruvate oxidoreductase (POR) system, showed an order of magnitude increased H_2-evolution upon the presence of both electron donors, the higher redox potential NADH ($E°$ = -320 mV[210]) alongside the reduced Fd. Once purified, the synergistic production of H_2 from these two-electron donors by HydABC was further enhanced by the supply of flavin mononucleotide (FMN). This underscored the critical role of this prosthetic group in the coupling mechanism, despite its loose binding and susceptibility to loss during the purification procedure. This led to the proposal of flavin-based electron confurcation (FBEC) by HydABC, which

with 1 U defined as 1 μmol of H_2 produced per minute and per mg of protein[2].

[d] $K_{m,\mathrm{HydABC}} = 100\,\mu$ M vs $K_{\mathrm{m,\ CpI}} = 32$ to $310\,\mu$ M

entails the coupled reduction of the confurcating FMN from the thermodynamically and spatially different electron donors, Fd_{RED} and NADH in an apparently strictly stoichiometric fashion. Since NAD^+/NADH is an obligatory two-electron donor (as will be outlined below) and the ferredoxin TmFd1 harbors a single [4Fe-4S]-cluster, this stoichiometric ratio approaches 1:2 (as shown in figure 1.2B). The electrons from both donors are then transferred to the reduction of protons (H^+) to H_2:

$$2\ Fd_{RED} + NADH + 4\ H^+ \rightleftharpoons 2\ Fd_{OX} + NAD^+ + H^+ + 2\ H_2 \tag{1.3}$$

After the initial description of the electron-confurcating HydABC in *T. maritima*, the same enzyme complex has been found and described in other bacteria, notably in the acetogens *Acetobacterium woodii* (HydABCD[192]), *Moorella thermoacetica* (HydABC[226]), and *Ruminococcus albus* (HydABC[252]), but also in the sulfate-reducing *Desulfovibrio fructosovorans* (HndABCD[115]).

The heterologously produced *T. maritima* HydABC enzyme in *E. coli* was demonstrate to catalyze the FBEB as well with a stoichiometry of NADH to $TmFd1_{RED}$ of 1 to 2.01 (± 0.1)[41]. However, the same heterologously expressed enzyme was also shown to reduce NAD^+ in the absence of oxidized ferredoxin, however, with an approximately 35-fold lower rate[e]. A similar observation was documented for the homologous, electron-bifurcating enzyme complex HndABCD from the sulfate-reducing *D. fructosovorans* with a roughly 10 to 20-fold decrease in the NAD^+ reduction as compared to the coupled electron-bifurcating reduction of NAD^+ and Fd_{OX}[115]. Finally, in HydABC of the acetogen *M. thermoacetica* a strongly decreased but still detectable rate of 0.2 U mg^{-1} of H_2-production was recorded with reduced Fd (with 2 [4Fe-4S] clusters from *Clostridium pasteurianum*, $E°_{Fd}$ = -400 mV[199]) in a re-reducing POR system as a sole electron donor as compared to 7.8 U mg^{-1} during the electron-confurcating assay with both Fd_{RED} and NADH. Meanwhile, in *M. thermoacetica* no oxidoreduction activity was documented for the NAD^+/NADH- and H^+/H_2- redox couples in any direction in the absence of ferredoxins[226].

In the electron-bifurcating enzyme assays of these homologs of HydABC, a near stoichiometric coupling of the two-electron acceptors has been demonstrated, leading to a near 1:1 partition of the supposedly low- and high-potential branch. The NAD^+ to Fd_{OX} reduction ratios observed were 1:0.92 in *R. albus*[252], 1:0.84 in *M. thermoacetica*[226], and 1:1 in *A. woodii*[192] in the electron-bifurcating direction, all of them using *C. pasteurianum* Fd as noted above, which accepts two electrons, as does NAD^+. The stoichiometric ratio is maintained even if both of the respective substrate/product couples during the confurcating or bifurcating reaction are globally exergonic under the conditions applied as it is the case for the study of the tetrameric HydABCD in *A. woodii*[192].

[e] 0.5 ± 0.1 µmol NADH min^{-1} mg^{-1} without Fd_{OX} as compared to 16.6 ± 0.2 µmol NADH min^{-1} mg^{-1} with Fd_{OX}[41]

HydABC represents a flavoenzyme family that catalyzes EB/EC reactions with initially described representatives across diverse phylogenetic and bioenergetic backgrounds, spanning Firmicutes, Thermotogae, and Proteobacteria, each involved in distinct metabolic processes like acetogenesis, fermentation, and sulfate-reduction, respectively. These studies point toward a generally consistent reaction scheme across these variants, which emphasize the central role of the flavin in the coupling reaction. However, the underlying molecular processes leading to the EB/EC reaction, along with varying degrees of stoichiometric coupling that has been observed between redox substrates, remain to be determined.

For the mechanistic understanding of the EB/EC catalytic process in HydABC and other flavoenzymes, the vast experimental evidence from the Q-cycle in the bc_1-complex and the entire related Rieske/cyt*b*-family, which are catalyzing quinone-based electron bifurcation has been fundamental in guiding the experimental design and interpretation of the results. For this electron-bifurcating protein complex, the physicochemical basis of the mechanism has been dissected for more than 50 years[48].

In the following chapter, I will explain the main experimental insights that motivated the development of a molecular model for the mechanisms of the electron-bifurcating reaction in the Rieske/cyt*b*-family as it will facilitate the understanding of the challenges related to the molecular details of this coupling process in the flavin-containing counterpart.

1.2 Quinone-based Electron bifurcation

1.2.1 Quinones

Within biological processes, quinones, a class of lipophilic cyclic organic molecules, serve as essential membrane-integral shuttles of electrons (e^-) and protons (H^+), enabling efficient electron transfer between proteins that reside in the membrane environment, while also contributing to proton transfer across the membrane and the build-up of the proton motive force. In nature, three types of quinones are most commonly found, ubiquinone, plastoquinone and menaquinone, which differ in their respective redox potential (figure 1.3).

The ability of quinones to act as transporters of e^- and H^+ is enabled by the redox chemistry of quinones. Quinones are capable of occupying three redox states: an oxidized quinone state, the one-electron "semi-reduced" (semiquinone) state and the two-electron, "fully-reduced" (hydroquinone) state. With two protonatable sites, for each of these redox states the quinone can be found deprotonated, "semi-protonated" with one of the two sites protonated or "fully-protonated" with both sites protonated, resulting in a thermodynamic 3-by-3 scheme as shown in figure 1.4.

Redox and protonation characteristics influence each other. Simply due to coulombic effects,

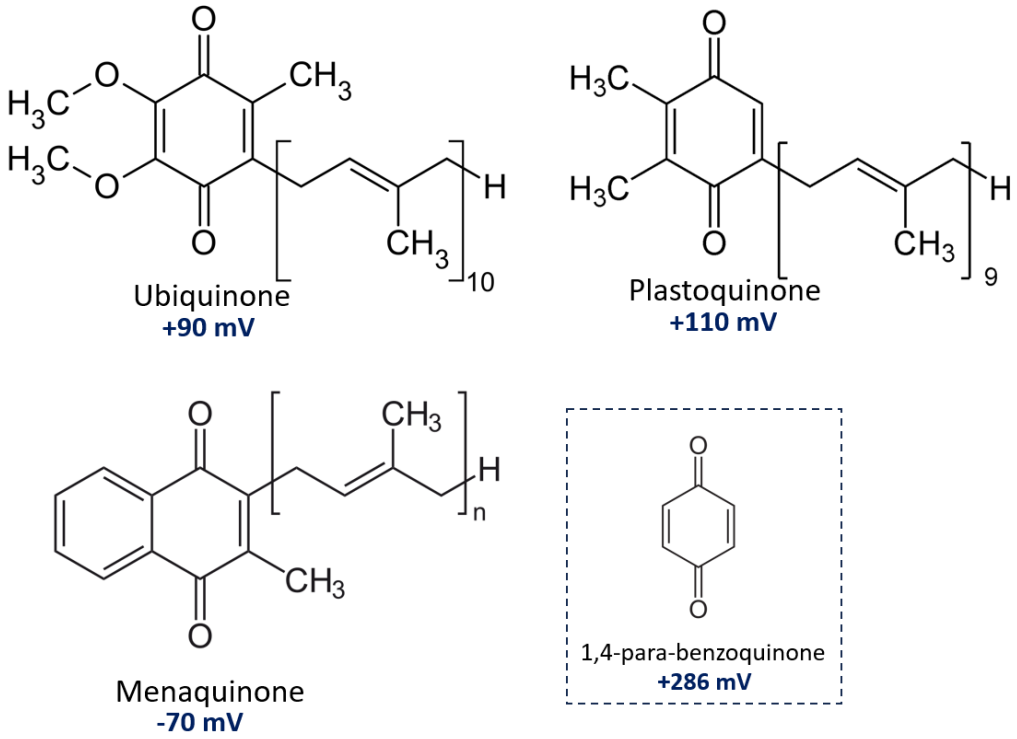

Figure 1.3: The biologically most commonly employed quinone molecules. Ubiquinone is universally used in the bc_1-complex in mitochondria as well as in proteobacteria, plastoquinone is used in the b_6f-complex of chloroplasts and menaquinone is found primarily in anaerobic organisms. 1,4-para-benzoquinone without any substituents and will be used as a "model quinone" for figures 1.4 and 1.5.

a reduction causes an increase in proton-affinity, i.e., an upshift of the corresponding pK_a-value, whereas a protonation of the quinone increases the electron-affinity, i.e., increases the redox potential. Therefore, the general tendency is observed: $pK_{a,OX} < pK_{a,SR} < pK_{a,RED}$.

Quinones are influenced by the physicochemical composition of the surroundings[180]. In aqueous solutions, quinones exhibit a strict two-electron transfer (n = 2) behavior, transitioning directly between the oxidized quinone and the hydroquinone state, while acquiring protons along the reduction[183]. However, when placed in aprotic solvents or within binding pockets of specific proteins that limit their hydrogen-bonding capabilities, the redox behavior of quinones changes, ultimately leading to a one-by-one electron transfer (n = 1)[91]. Such a phenomenon is observed in various respiratory and photosynthetic chains, resulting in the formation of detectable levels of the one-electron semiquinone (as further outlined below), among others in Complex I [242], Complex II[188;237] as well as the Q_B-site in Photosystem II[54].

1.2.2 Rieske/cyt*b*-family

The Rieske/cyt*b* complexes are highly prevalent transmembrane enzymes comprising of the mitochondrial bc_1-complex (also referred to as complex III in the respiratory chain), the photosynthetic cytochrome b_6f-complex, and other bacterial variants[195]. The most studied example of this enzyme

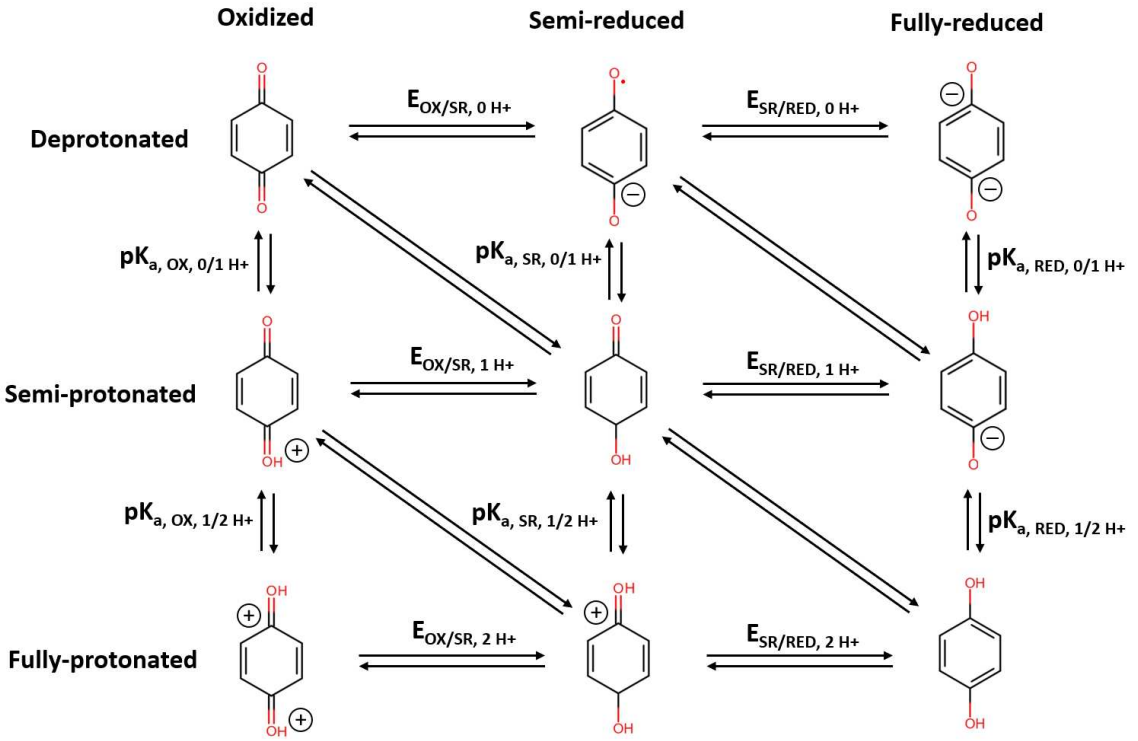

Figure 1.4: Thermodynamic 3-by-3 square scheme for the redox transitions and protonation events of quinones. Each redox transition is associated with a redox potential $E_{OX/SR}$ or $E_{SR/RED}$ along the horizontal axis, each protonation event is characterized by a pK_a-value for the first (1 H^+) or second (2 H^+) proton along the vertical axis. Proton-coupled electron transfer (PCET) occurs along the diagonal lines.

family, the bc_1-complex from the phototrophic proteobacterium *Rhodobacter sphaeroides*, contains 4 one-electron redox cofactors and 2 quinone binding sites (shown in figure 1.5). The complex in this organism exclusively relies on ubiquinone ($E°_{m,OX/RED}$ +90 mV)[207]. Two central *b*-type hemes, named b_L and b_H according to their respective redox potential (b_L: $E°_{Low}$ = -120 mV, b_H: $E°_{High}$ = +80 mV), are arranged in a linear fashion, perpendicular to the membrane plane. This *b*-heme chain electronically connects the two different binding sites for quinones near opposite sides of the membrane: the Q_i-site located closer to the cytoplasmic and the Q_o-site near the periplasmic space. The latter site is also found proximal to a Rieske-type [2Fe-2S]-cluster ($E°_{[2Fe-2S]}$ = +320 mV) that connects the complex to the c_1-type heme ($E°_{c_1}$ = +320 mV), which then transfers the electrons to the soluble cytochrome *c* ($E°_{cyt\ c}$ = +360 mV)[37;177].

The protein environments of the two quinone binding sites, Q_i- and Q_o-site, cause radically different thermodynamic properties of the quinone, which were initially conceptualized by Peter Mitchell as an essential part of the Q(quinone)-cycle in the mitochondrial bc_1-complex[154;155]. In the Q-cycle model (figure 1.5), the fully-reduced hydroquinone donates an electron pair ($n = 2$) onto two thermodynamically and spatially different one-electron acceptors at the Q_o-site:

$$QH_2 + \text{heme } b_{L,OX} + \text{Rieske-[2Fe-2S]}_{OX} \rightleftharpoons Q + 2\ H^+ + \text{heme } b_{L,RED} + \text{Rieske-[2Fe-2S]}_{RED}$$

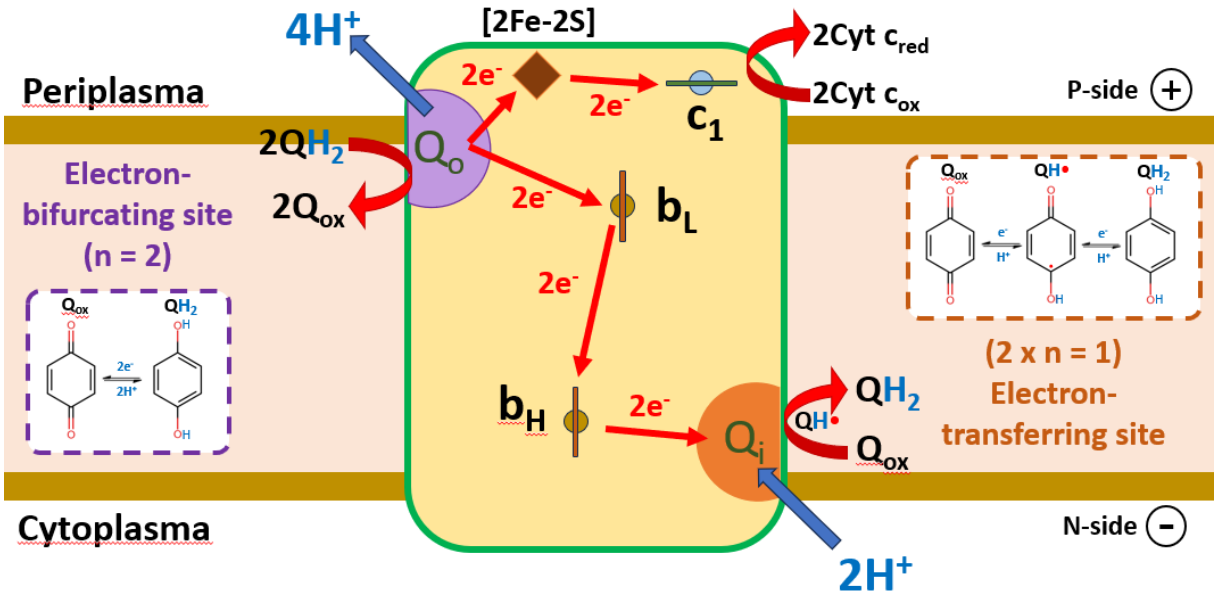

Figure 1.5: Schematic model of the bc_1-complex from *Rhodobacter sphaeroides* including the Q-cycle, with two functionally different quinone-binding sites, Q_o (in magenta) and Q_i (in orange). Electrons from the hydroquinone-oxidizing Q_o-site are bifurcated (n = 2) to the high-potential Rieske-[2Fe-2S]-cluster (brown diamond) and the low-potential b_L-heme. The bifurcated electron pair is consecutively transferred along the high-potential chain via the Rieske-[2Fe-2S]-cluster to heme c_1 (green/blue) and cytochrome *c* and the low-potential *b*-heme chain along b_L and b_H, (both orange/brown). The low-potential chain sequentially transfers the electrons onto the oxidized quinone in the electron-transferring Q_i-site. For stoichiometric reasons, two hydroquinone molecules need to be oxidized at the Q_o site for every oxidized quinone to become fully reduced at the Q_i site. Protons (in blue) are translocated from the negative (N)-side (matrix) to the positive (P)-side (intermembrane space) against the electrochemical gradient as a consequence of the membrane-soluble reduced hydroquinones diffusing from the Q_i site to the Q_o site, as proposed by Mitchell's Q-cycle [154;155]. Chemical representation of the simplest (non-biologically active) quinone, 1,4-(para)-benzoquinone, in all three states. The bc_1-complex from *R sphaeroides* utilizes ubiquinone (see figure 1.3). Figure inspired by Cape, Bowman, Kramer (2005) [37]

The hydroquinone (QH_2) thereby reduces the high-potential Rieske [2Fe-2S]-cluster and the heme b_L, which exhibits a low redox potential relative to the intermediate-potential two-electron donor[50]. The low-potential electrons are passed via the *b*-heme chain against the membrane potential to the other quinone binding site, the Q_i-site, where oxidized quinones are sequentially reduced by two one-electron transfers ($n = 1$):

$$\text{heme } b_{H,\text{RED}} + \text{Q} + \text{H}^+ \rightleftharpoons \text{heme } b_{H,\text{OX}} + \text{QH}$$

$$\text{heme } b_{H,\text{RED}} + \text{QH} + \text{H}^+ \rightleftharpoons \text{heme } b_{H,\text{OX}} + \text{QH}_2$$

The observation of a two-electron transfer ($n = 2$) by the quinone at the Q_o-site and two single-electron transfers ($n = 1$) by the quinone in the Q_i-site is a consequence of different degrees of redox cooperativity between the individual electrons of the quinone in these two binding sites. The concept of redox cooperativity is central to the understanding of electron bifurcation in Rieske/cyt*b*-complexes.

1.2.3 A short excursion into redox cooperativity

At the Q_o-site the surrounding amino acids and the electron acceptors, heme b_L and Rieske-[2Fe-2S]-cluster, cause the quinone to follow an "inverted" (or "crossed-over") redox potential scheme for the individual electron transfers[13;68;69;169] (figure 1.6). The individual redox potentials of the first and second oxidation are conceptually arranged in a way that features the first oxidation ($E_{SR/RED}$), i.e., from fully-reduced to semi-reduced state to be characterized by a higher redox potential as compared to the second oxidation ($E_{OX/SR}$), from the semi-reduced semiquinone to the oxidized quinone state:

$$E_{OX/SR} < E_{SR/RED}$$

This redox behavior in which it is energetically easier to fully oxidize the semi-reduced state as compared to the formation of this semi-reduced state is the defining attribute of redox potential inversion. It characterizes what has been termed in the literature as "cooperative two-electron transfers", more accurately, positively cooperative two-electron transfer, in which the first electron's release, facilitates the discharge of the second. The thermodynamic stabilization of the electronic configuration of the fully-reduced hydroquinone and oxidized quinone state, thus effectively destabilizes the semiquinone state and leads to the observation of a two-electron transfer ($n = 2$). The redox midpoint potential (E_m) of the resulting two-electron transition characterizes the direct transition of the oxidized to the fully-reduced species ($E_m = E_{OX/RED}$) and is located conceptually in the middle of the individual crossed-over one-electron transitions (figure 1.6, lower row), both of which are in this case not easily observable by conventional techniques. Redox potential inversion has been observed in various two-electron compounds, including quinones and flavins[68;69].

In the more straight-forward "non-inverted" or "uncrossed" redox behavior, due to electrostatic interactions, the liberation of the more reducing electron in the initial oxidation of the fully-reduced state ($E_{SR/RED}$) occurs at lower redox potentials than the second oxidation ($E_{OX/SR}$).

The resulting "normal ordering of redox potentials"[69] follows:

$$E_{OX/SR} > E_{SR/RED}$$

As a consequence, two separate, apparently independent one-electron processes from the two-electron compound are observed. These are characterized by, in the oxidizing direction, the first electron presenting more reducing characteristics compared to the second one, leading to a semi-reduced species that therefore is stabilized across a specific redox range. This redox behavior has been termed "negative cooperativity" between the individual electron transfers[13;68;169].

The degree of redox cooperativity between individual electron transfers of the two-electron component forms a continuous spectrum, leading to the apparent disappearance (for positive redox co-

operativity) or the observation of semi-reduced species across a wide redox potential range indicative for negative redox cooperativity.

Since the amount of the observable semi-reduced species is an important indicator for the assessment of the degree of redox cooperativity, its stability constant, K_s, is a useful metric. The K_s value related the population of oxidized (OX), semi-reduced (SR), and fully-reduced (RED) species to one to one another[44;147]:

$$K_s = \frac{[\mathrm{SR}]^2}{[\mathrm{OX}] \cdot [\mathrm{RED}]} \tag{1.4}$$

It is most commonly derived from the splitting (ΔE) of the individual one-electron redox potentials $E_{OX/SR}$ and $E_{SR/RED}$ in a way:

$$\Delta E = E_{\mathrm{OX/SR}} - E_{\mathrm{SR/RED}} = \frac{F}{R \cdot T} \cdot \ln(K_s) \tag{1.5}$$

where T is the temperature, F is the Faraday constant ($F = 96485\,\mathrm{J\,V^{-1}}$) and the gas constant ($R = 8.314\,\mathrm{J\,mol^{-1}\,K^{-1}}$). At 30°C, the K_s value boils down to[44]:

$$\log(K_s) = \frac{\Delta E}{60\mathrm{mV}} \tag{1.6}$$

I will use the $\log(K_s)$-nomenclature in order to compare different semiquinone stability constants more easily throughout this thesis:

- For $\log(K_s) > 0$, it is that $E_{OX/SR} > E_{SR/RED}$, the individual single-electron transitions tend to exhibit more negative cooperativity, leading to an observation of a one-by-one redox behavior ($n = 1$, Upper Row in figure 1.6).
- At $\log(K_s) = 0$ (thus, $K_s = 1$), both redox transitions occur at the same redox potential, and 33% of the semi-reduced species is observed at E_m (Central Row in figure 1.6).
- If $\log(K_s) < 0$, it is that $E_{OX/SR} < E_{SR/RED}$, and the individual single-electron transitions show more positively cooperated redox behavior, leading to the observation of a coupled two-electron transition from the oxidized to the fully-reduced species ($n = 2$) and thus a thermodynamically suppressed semi-reduced state (Bottom Row in figure 1.6).

The maximal fraction of the semi-reduced species (%SR) is calculated from[44;149]:

$$\%SR = \frac{\sqrt{K_s}}{2 + \sqrt{K_s}} \tag{1.7}$$

Figure 1.6 summarizes the redox behavior of a two-electron compound under the three different situations for the relationship between $E_{OX/SR}$ and $E_{SR/RED}$ with a positive 120 mV split (upper

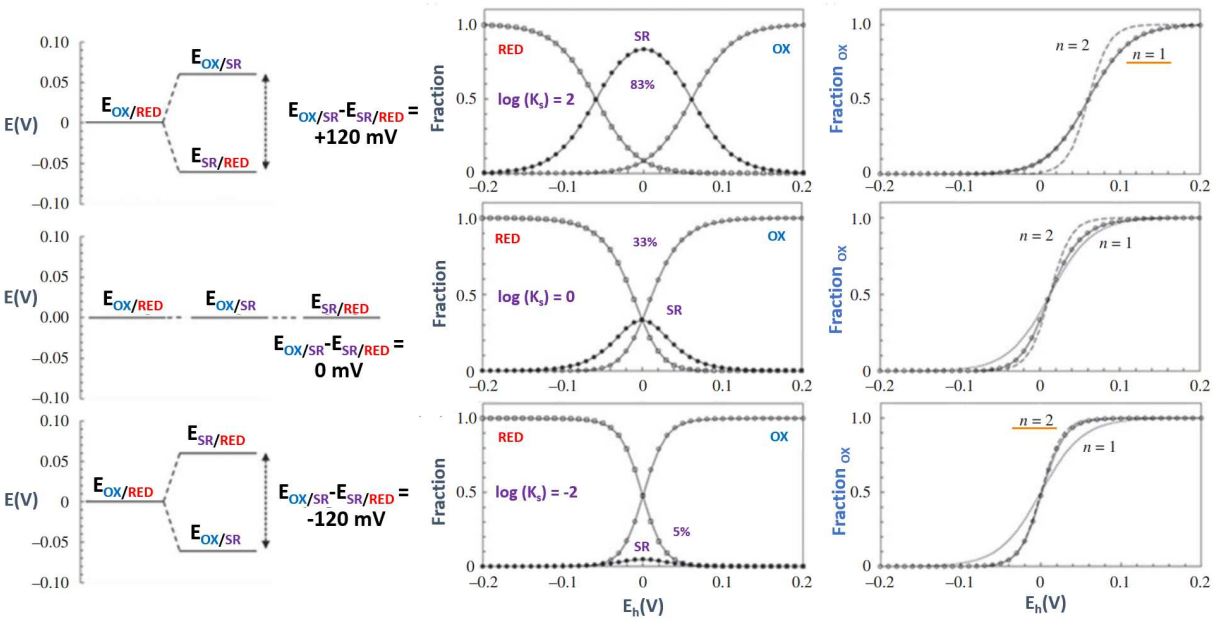

Figure 1.6: Titration behavior simulation for a two-electron compound under three different redox configurations regarding $E_{OX/SR}$ and $E_{SR/RED}$ (depicted in the left column). The fractional concentrations of the oxidized (OX), one-electron semi-reduced (SR) and two-electron fully-reduced (RED) species as a function of the electrode potential (E_h) is shown in the central column. The Nernst-fit (n = 1, solid line; n = 2 dashed line) of the titration behavior of the oxidized species on the right column. The difference (ΔE) between the redox potential values of $E_{OX/SR}$ and $E_{SR/RED}$ is set to +120 mV (top row), 0 mV (middle row) and -120 mV (bottom row). The midpoint potential of the $E_{m,\,OX/RED}$ couple is set to 0 mV. Figure adapted from Vanoni *et al.* (2021)[214] under a Creative Commons Attribution License.

row), equivalent redox potentials (middle row), and negative 120 mV split (bottom row) over redox potentials.

An inverted redox regime as presented in the bottom row of figure 1.6 is indicative of positive redox cooperativity between two one-electron transfers and forms the electrochemical basis for EB/EC, i.e., the simultaneous oxidation of a two-electron compound by two different electron acceptors[13;32;169].

Light-flash experiments in mutated photosynthetic bacteria at alkaline pH have allowed the split between the crossed-over redox couples (ΔE) for the quinone in the Q_o site to be estimated[249]. The individual redox transitions were approximated to be -880 mV apart, with the crossed-over high-potential electron $E_{OX/SR}$ being at about +410 mV at this pH. Thus an effective semiquinone stability constant, $\log(K_s)$ of about -14 was determined[248;249], exceeding the destabilization of semiquinones in aqueous solutions by four orders of magnitude and by ten orders of magnitude in apolar environments such as the membrane. [f]

The explanation of the molecular origin leading to inverted redox potentials are manifold but all invoke an influence of the surrounding medium, i.e., the solvent and direct environment around the two-electron compounds. The direct coupling of two individual electron transfers in some two-

[f]For biologically relevant quinones (see figure 1.3) with $\log(K_s)_{,HOH}$ around -10 in aqueous solutions and $\log(K_s)_{,\,membrane}$ around -4 in the membrane depending on the substituent according to Song and Buettner (2010)[202].

electron compounds (such as flavins[114;165;253] or 3,6-dinitrodurene[116]) has been rationalized by a change in the geometric structure of the compound in the fully-reduced state[68]. Redox potential inversion in biological systems such as quinones and flavins is thought to be primarily affected by hydrogen-bonding additives and thus the proticity of the solvent. The individual electron transfers are thereby assisted by thermodynamically coupled proton transfers that effectively lead to proton-coupled electron transfers (PCET).

The experimentally best supported model for the EB reaction from the hydroquinone in the Q_o-site involves such a PCET, with a consecutive two-electron and two-proton transfer, which will be presented next.

1.2.4 Electron Bifurcation at the Q_o-site

Following Wikström and Berden's 1972 study[230] on the "oxidant-induced reduction" of low-potential cytochrome b_L upon the introduction of a high-potential acceptor shortly before the conceptualization in Mitchell's Q-cycle[154;155], three different lines of empirical support have underpinned a mechanistic proposition that entails a stepwise reduction of both the high-potential and low-potential chains enabled by thermodynamically coupled deprotonation events of the quinone during the electron bifurcation process at the Q_o site:

1. Structural data on enzyme complexes of various members of the Rieske/cyt*b* family allowed for the approximation of distances between each of the cofactors and thus the predictions of theoretical electron transfer rates according to Marcus theory. In addition, mechanistically important residues at the Q_o-sites were shown to be hydrogen-bonded to an inhibitor in place of the substrate hydroquinone.

2. Redox titrations of the different Rieske/cyt*b*-complexes monitored by EPR and UV/Vis spectroscopy allowed for the assignment of redox potentials of all the cofactors and the identification of the high- and low-potential chain as well as the redox potential of the quinone. pH-dependent redox titrations led to the identification of pH-dependent redox compounds and the determination of pK_a-values of protonatable residues.

3. Kinetic studies observed an apparently simultaneous reduction of both high- and low-potential acceptors in a kinetically rate-limiting step and the successive reduction of the high- and low-potential chain.

In the following pages, I will briefly summarize the main findings from these three approaches and follow up on how this led to the proposal of a sequential bifurcating electron transfer scheme.

1.) Structural data on the Rieske/cyt*b*-complex allowed distance assignments between redox cofactors and the observation of H-bonding

Structural models derived from X-ray crystallography [99;104;235] and more recently Cryo-Electron Microscopy[254] of various Rieske/cyt*b*-complexes from different organism showed the Rieske-[2Fe-2S]-cluster containing domain unresolved or in different positions. This has been interpreted for the Rieske-[2Fe-2S]-cluster domain to be structurally mobile. The observation of multiple conformational states has initially led to the proposal of a conformationally gated mechanism[46;234;251]. However, whenever quinone-like inhibitors, such as the Q_o-specific-inhibitor stigmatellin [g], are supplemented and observed in the Q_o-site, the Rieske is located closer to the Q_o-site as the static low-potential acceptor, the heme b_L, therefore suggesting a theoretically faster electron transfer to the Rieske-[2Fe-2S]-cluster according to Marcus theory.

The Rieske-[2Fe-2S]-cluster itself is coordinated by 2 cysteine and 2 histidine residues[92]. When the Rieske-[2Fe-2S]-cluster domain is in the position next to the Q_o-site the quinone-like inhibitor is observed to form a hydrogen-bond (H-bond) to the imidazolate of one of the Rieske-coordinating histidine residues (His-152, *R.sphaeroides* bc_1 nomenclature[251]). In a recently published Cryo-EM structure model of the Q_o-ubiquinone-bound bc_1-complex the quinone in the Q_o is has been observed in H-bond distance to His-152[23]. This strong H-bond from the hydroquinone to the histidine's imidazolate in the Q_o-site has been proposed to be important for the a proton-coupled electron transfer mechanism[47].

2.) The assignment of redox potentials to all the individual redox compounds

As outlined above, the membrane-bound Rieske/cyt*b*-complexes are one of the most ubiquitous enzyme complexes employed by life. Whereas ubiquinone is universally used in mitochondrial bc_1-complex as well as in proteobacteria, related protein complexes from other organisms use chemically different quinones, such as plastoquinones in the b_6f-complex of chloroplasts and cyanobacteria or menaquinone primarily in anaerobic organisms. These quinones differ in their substituents and thus exhibit varying redox potentials, ranging from -70 mV to +100 mV (figure 1.3).

Equilibrium redox titrations of these complexes from different organisms, each employing different quinones, have drawn a surprisingly conserved picture in the redox potential landscape of all major redox compounds (see figure 1.8)[16]. In adaptation to the redox potential of their respective quinones, each of these complexes maintained a constant redox potential difference between the two electron acceptors (high-potential Rieske [2Fe-2S]-cluster and low-potential heme b_L) of the bifurcating electron transfer at the Q_o of roughly -450 mV centered around the midpoint potential of the quinone, while conserving a 130 mV redox potential difference between the two *b*-hemes, allowing

[g] which is proposed to bind in the same position as the bifurcating quinone molecule

for the energy-conserving electron transfer against the membrane potential.

The difference in redox potential between the Rieske [2Fe-2S]-cluster and the heme b_L predicts the required individual, crossed-over redox potentials of the quinone in the Q_o to realize the thermodynamically coupled bifurcating reaction of the electron pair.

Theoretical calculations using Marcus theory for electron transfer kinetics[133] of the bifurcating electron transfer at the Q_o-site necessitated the determination of the redox potential for the Rieske [2Fe-2S]-cluster and heme b_L as electron acceptors for quantifying the theoretical ΔG_{ET} of the electron transfer reaction. Additionally, the reorganization energy (λ) of the medium, along with the distances between the cofactors mentioned earlier, were essential parameters for the assessment of the global reaction kinetics[48].

Meanwhile, redox titrations at different pH values identified pH-dependent redox compounds in the bc_1-complex. The redox potential of the Rieske [2Fe-2S]-cluster was shown to exhibit a pH-dependence induced by the protonation of the coordinating histidine (His-152, *R.sphaeroides* nomenclature) causing a -60 mV/pH dependence of the $E_{[2Fe\text{-}2S]}$ above pH 8[168]. This has been confirmed by ATR-FTIR where this coordinating His-152 of the Rieske [2Fe-2S]-cluster has been shown to undergo redox-linked protonation associated with the electron transfer of the [2Fe-2S]-cluster[103].

3.) Kinetic studies highlight an apparently simultaneous reduction of heme b_L and Rieske [2Fe-2S]-cluster

Kinetic investigations[50;255] were conducted using a rapid mixing/freeze-quench apparatus coupled to EPR spectroscopy to examine the bifurcating oxidation of the fully-reduced hydroquinone in the Q_o-site. They observed the two-electron oxidation of the hydroquinone leading to the apparently simultaneous reduction of the high-potential Rieske-[2Fe-2S]-cluster and the low-potential heme b_L. In the employed setup with a time-resolution in the sub-millisecond region, no indication of detectable semiquinone concentrations were observed, whereas both acceptors were found to be reduced in a relatively slow time frame ($t_{1/2} \sim 250\ \mu$sec).[50;255]

Mechanistic model of EB at the Q_o-site

The observations of the apparently simultaneous and unexpectedly slow reduction kinetics of high- and low-potential acceptor initially seemed to contradict the predicted much faster electron transfer kinetics especially to the high-potential Rieske-[2Fe-2S]-cluster, which were derived from the structural models in conjunction with the thermodynamic data of the high and low redox potential components, according to Marcus theory.

This has given rise to the proposal of an initial rate-limiting, endergonic reduction, acting as an activation barrier for the entire coupled two-electron reaction. This process entails a sequen-

tially tightly-coupled (thus, apparently simultaneous) reduction of both the high- and low-potential chains, proposed to be regulated by the concomitant deprotonation events of the hydroquinone (see figure 1.7 and 1.8)[47]:

The binding of the fully-reduced hydroquinone in the Q_o-site is accompanied by the Rieske-[2Fe-2S]-cluster domain taking up a position proximal to the Q_o-site. A critical H-bond is established between the hydroquinone and the Rieske-coordinating His-152 which protrudes into the active site. For a successful binding process, the His-152 therefore needs to be deprotonated and thus able to act as an H-bond acceptor from the fully-reduced and protonated quinone. It has been proposed that an initial rate-limiting proton-transfer along this H-bond from the hydroquinone in the Q_o-site to the His-152 initiates the endergonic electron transfer via a stepwise PCET reaction following a "proton-first then electron sequence"[48]. It follows, for purely electrostatic reasons, that the release of the proton affects the redox potential of the quinone in a way to promote the release of the first electron. The rate-limiting initial oxidation of the hydroquinone is thermodynamically endergonic, since the inverted redox potential scheme renders the redox transition of the fully-reduced hydroquinone to the semi-reduced semiquinone ($E_{SR/RED} \sim +410$ mV, see section 1.2.3) at overall higher redox potentials as compared to the electron accepting, high-potential Rieske-[2Fe-2S]-cluster ($E^{\circ}_{[2Fe-2S]} = +320$ mV[49]). As a consequence, the electron remains on the fully-reduced hydroquinone until it eventually overcomes the endergonic barrier, assisted by the proton transfer (and aided by thermal activation, see[175]). This results in the formation of the short-lived, strongly reducing semiquinone state.

This semi-reduced state ($E_{OX/SR} \sim$ -470 mV see section 1.2.3) is immediately further oxidized by the next-by electron acceptor, in this case the low-potential b_L-heme ($E^{\circ}_{Low} =$ -120 mV). Due to the steep redox potential gradient and thus the strongly exergonic nature of this reaction, this second oxidation thermodynamically drives the entire reaction. Similar to His-152 for the first electron transfer to the Rieske-[2Fe-2S]-cluster, shall a conserved glutamic acid (Glu-295, *R.sphaeroides* nomenclature[218]) located in the highly conserved PEWY motif then enable the deprotonation of the semiquinone during the exergonic electron transfer to the heme b_L[48]. The involvement and essential nature of Glu-295 however is experimentally less well-supported and strongly debated (see below).

The molecular configuration as presented here, leading to an initial endergonic electron transfer which is kinetically rate-limiting, followed by the immediate (i.e., kinetically rapid) exergonic electron transfer, leading to a molecular escapement mechanism[13;27;48], ensures a tight coupling of the individual electron transfers and directionality of the entire process. The initial endergonic part of the reaction thermodynamically favors the educt state, i.e., for the electron to remain on the fully-reduced hydroquinone. The departure of the high-potential electron to the Rieske-[2Fe-2S]-cluster

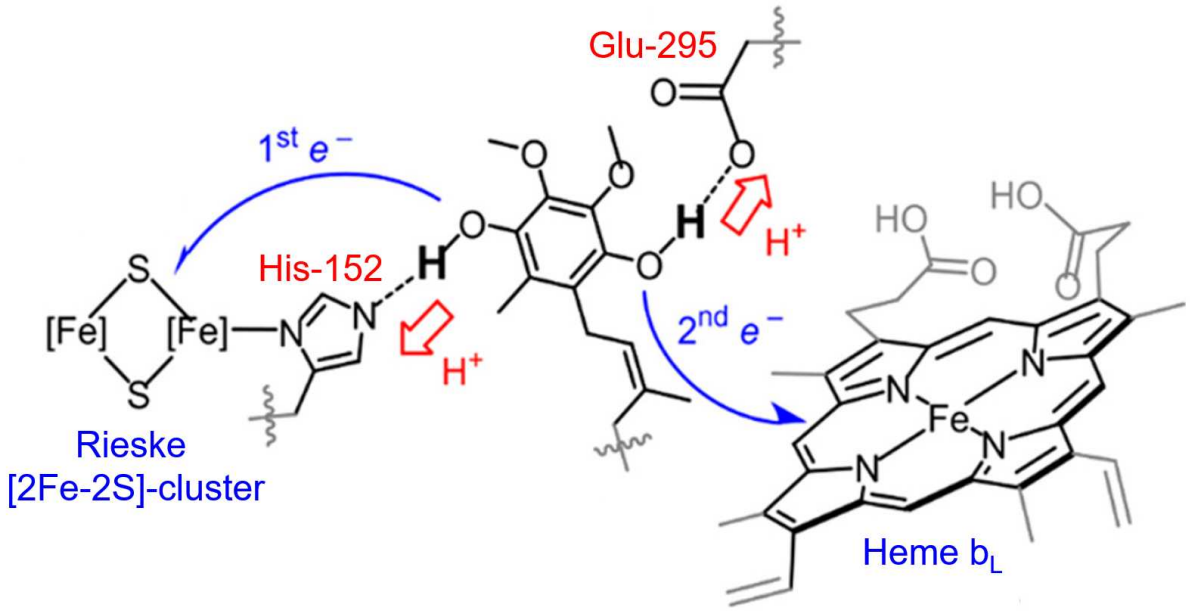

Figure 1.7: Schematic representation of the stepwise PCET of the reduced ubiquinone in the Q_o-site. The hydroquinone (in a position modeled as the structurally similar inhibitor stigmatellin) at the electron-bifurcating Q_o-site is shown in hydrogen bonding with the His-152 and Glu-295. The first (high-potential) electron is proposed to reduce the high-potential Rieske-[2Fe-2S]-cluster after the His-152 becomes protonated. In a similar way, the second (low-potential) electron is proposed to reduce the heme b_L after Glu-295 has abstracted the proton from the semiquinone. Proton transfer and proton acceptors in red, electron transfers and electron acceptors in blue. Figure adapted with permission from Agarwal *et al.* (2022)[4]. Copyright 2022 American Chemical Society.

is immediately followed by the escape of the low-potential electron to the b_L. The high-potential electron thus finds itself "trapped" on the high-potential Rieske-[2Fe-2S]-cluster with the reverse reaction back to the quinone being thermodynamically not feasible, as the quinone is already in the fully oxidized quinone state with crossed-over redox potentials and thus requiring a lower redox potential donor to initiate the back reaction (as will be discussed below for electron confurcation).

To summarize, the thermodynamic coupling of these two redox reactions during electron bifurcation is rationalized on the basis of redox potential inversion of the quinone in Q_o-site. It yields one electron of a high redox potential and one electron of a low redox potential. The high-potential electron reduces the high-potential Rieske-[2Fe-2S]-cluster endergonically which effectively forms an activation barrier for the entire process. Once the barrier is overcome and the high-potential electron is transferred to the Rieske-[2Fe-2S]-cluster, a highly reactive semiquinone state immediately reduces the low-potential heme b_L, latter of which thermodynamically drives the entire reaction.

The importance of proton transfer for the regulation of the redox-properties of the quinone

The escapement-type mechanism[13;27;48] described above is proposed to be dependent on the involvement of protons that orchestrate the entire electron-bifurcating reaction. Each oxidation is proposed to occur alongside a protonation event (see figure 1.7), facilitated by conserved amino acids that

form transient hydrogen bonds with the quinone[45;48]. The involvement of His-152 from the Rieske-[2Fe-2S]-cluster is strongly supported by experiments as part of the described "thermodynamically gated" mechanism, which encompasses both electron and proton transfers, as demonstrated by the aforementioned ATR-FTIR and Cryo-EM studies[17;23;103].

However apart from the observation of this histidine, there is no direct evidence for any of the proton transfers at the Q_o-site. The construction of deletion mutant strains has so far been inconclusive in that regard. Deletion of His-152 results in a disrupted Rieske domain, due to its [2Fe-2S]-cluster coordinating functionality[53]. Mutant strains in which Glu-295, the amino acid that is proposed to be involved in the second deprotonation of the quinone, is replaced by non-protonatable amino acids remain active *in vivo* with partially impaired electron transfer kinetics[174]. From the suggested non-essential nature of Glu-295, several other protonatable residues (such as Tyr-147, *R.sphaeroides* nomenclature) in the Q_o-site residues have been proposed to form an extended hydrogen bond network, which could potentially illustrate a considerable resilience of Q_o-site activity to mutational change in Q_o-site environments[23]. Amino acid residues and water molecules thereby appear to cooperate in providing a physical and chemical environment for supporting efficient hydroquinone oxidation rates. However, understanding the implications of these protonation events and their potential impact on the control of the kinetics of the bifurcating electron transfers remains uncertain. Acquiring pertinent information about these proton transfer faces strong challenges arising from the limited availability of suitable experimental techniques to unambiguously capture such intermediates alongside the rapid nature of the electron-bifurcating reaction. The transient binding state of the quinone at the Q_o-site further complicates in-depth investigations.

The discovery of flavin-based electron bifurcation (FBEB), which is proposed to function by the same molecular principle[13;31–33;169], has induced high hopes to resolve the role of proton transfers for the mechanism. As it will be further elaborated below, some protonation states alongside the redox states of the flavin are easily detectable by UV/Vis and EPR-spectroscopy (section 1.6.5). Furthermore, the electron-bifurcating flavins were identified to be non-covalently bound inside flavoenzymes as prosthetic groups[58;80;129;222] and do not act as diffusible substrates. Hence, flavins are readily observed in protein structure models, even in different redox states such as in the case for flavodoxin[34;200;229], which facilitates the identification of functionally important physicochemical influences by the protein pocket.

Summary: Electron Bifurcation (EB) and Electron Confurcation (EC)

Electron bifurcation (EB) necessarily requires 3 functional redox components: a two-electron bifurcating center of intermediate redox potential featuring inverted redox potentials as well as a high-potential and low-potential electron acceptor in a one-electron accepting state. As depicted in

figure 1.8, the reaction proceeds via an "escapement mechanism"[13;27;46] that involves an initial slow, endergonic electron transfer to the high-potential acceptor, which represents an activation barrier and is kinetically restricting the entire coupled reaction. Once the high-potential electron reduces the high-potential acceptor in the kinetically rate-limiting step, the more rapid, low-potential electron follows immediately and exergonically reduces the low-potential acceptor.

EB thus involves the coupling of two individual electron transfers from an intermediate-potential two-electron donor towards two energetically and spatially different pathways inside one enzyme. This pivotal process thereby couples a strongly favorable electron transfer to an unfavored one allowing for the generation of low-potential electrons.

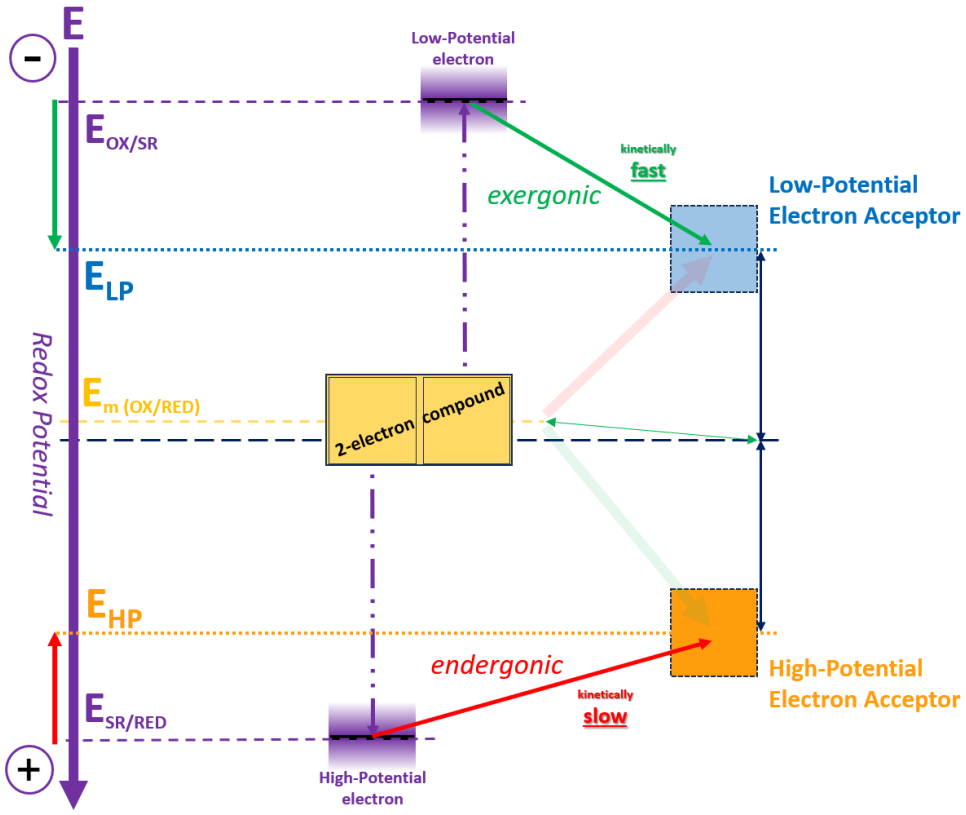

Figure 1.8: Thermodynamic redox-scheme of a coupled electron bifurcating two-electron transfer. The two-electron compound (in yellow) at an intermediate redox potential $E_{m,\,OX/RED}$ exhibiting crossed redox potentials of the individual one-electron transitions ($E_{OX/SR}$ and $E_{SR/RED}$, in magenta). The reduction of the high-potential electron acceptor (orange) is thermodynamically "uphill" due to the overall higher redox potential of the high-potential electron ($E_{SR/RED}$) as compared to the high-potential acceptor (E_{HP}). This endergonic reaction thus proceeds slowly and is the rate-limiting step. The entire bifurcating reaction is energetically driven by the kinetically fast, exergonic reduction of the low-potential electron acceptor (blue) with an overall higher redox potential (E_{LP}) as compared to the low-potential electron ($E_{OX/SR}$). The entire coupled two-electron transfer (n = 2) is thermodynamically favored as the overall two-electron transition ($E_{m,\,OX/RED}$) occurs at a lower redox potential as compared to the average of the redox midpoint potentials of the two one-electron acceptors.

Reversibility is a recurring theme in bioenergetic systems which leads to a change of the overall directionality of the reaction in response to changing environmental conditions. Whereas the here presented "forward" electron transfer of the bc_1-complex involving the bifurcated electron transfer at the Q_o-site contributes to the generation of a proton-motive force, the proton backflow from the

proton gradient can be coupled to the reversed electron transfer[150].

The reversed reaction of Electron Bifurcation (EB) has been termed "Electron Confurcation" (EC), since the electrons are sourced from two thermodynamically and spatially different one-electron donors, a high potential donor and a low potential donor are "confurcated" onto a single intermediate potential two-electron acceptor. The above presented thermodynamic scheme (as shown in figure 1.8) of the energetics for the two individual one-electron transitions in EB involving redox potential inversion applies in the same way for EC.

The confurcating cofactor due to the crossed potential exhibits a low-potential $E_{OX/SR}$ transition and a high-potential $E_{SR/RED}$ transition. The low-potential donor reduces the confurcating cofactor in an endergonic and rate-limiting step. The entire reaction is driven by the apparently simultaneous, more exergonic oxidation of the high-potential donor to the same confurcating cofactor.

Whereas EB allows the organism to generate a more potent, low-potential electron donor, provided that an acceptor for a high-potential electron is available, EC allows the generation of high-potential electron acceptor under the condition that a lower redox potential electron can be delivered to the same acceptor. The bioenergetic utility of this coupling mechanism minimizes energy dissipation by exploiting the free energy release of exergonic electron transfers for the simultaneous thermodynamically unfavorable electron transfers. Through the use of the inherent redox chemistry of two-electron compounds life is able to increase the exploitable redox gradient beyond the redox span given by the available electron donor/acceptor pairs, through the generation of high- and low-potential redox species.

The thermodynamic coupling of two electron transfers by protein complexes belonging to the Rieske/cyt*b*-family during Quinone-based electron bifurcation (QBEB) enables the proton-motive force production during electron transfer from hydroquinone to cytochrome *c*. The generation of a low-potential electron at the Q_o-site that is transferred against the membrane potential from an intermediate potential donor allows the re-generation of a reduced quinone at the Q_i-site and is coupled to the translocation of protons.

1.3 Electron Bifurcation in flavoenzymes

Flavin (lat. meaning "yellow") is a term reserved for a group of compounds that contain an isoalloxazine moiety, i.e., a tricyclic pteridine-derivative with a delocalized π-electron system that is responsible for the yellow color and forms the molecular basis for the chemical function of flavins in living systems. In nature, mainly three types of flavins of increasing chemical complexity are employed (figure 1.9): riboflavin (also known as Vitamin B2), flavin mononucleotide (FMN) and flavin adenosine dinucleotide (FAD).

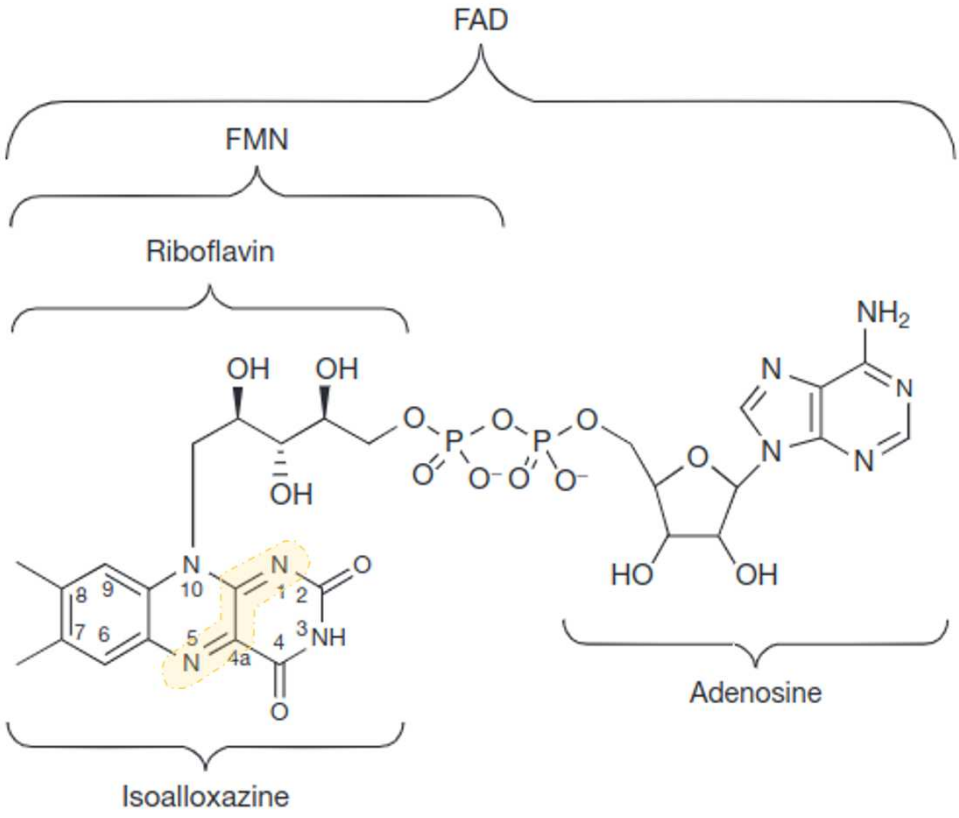

Figure 1.9: The three main types of biologically relevant flavins (shown from the *si*-face) in the oxidized, N(5)-protonated form. The redox reactivity of the isoalloxazine ring has been attributed to the N(5)-N(1) axis (yellow highlighted), featuring a α-diimine bond N(5) = C(4a) - C(10a) = N(1) of the oxidized state as shown here and ethene-1,2-diamine N(5) - C(4a) = C(10a) - N(1) in the fully reduced state with the nitrogens in the protonated form (see below)[159]. Figure adapted with permission from Entsch and Ballou (2013)[67]. Copyright 2013 Elsevier Inc. All rights reserved.

Similar to the quinones, the functional basis for flavins to realize electron transfer (ET) reactions in nature is their ability to occupy three redox states[82]: oxidized, semi-reduced, and fully-reduced[h].

Flavins are involved in a wide variety of enzymatic redox reactions involving either one-electron or two-electron transfers, with both functions often catalyzed by the same enzyme[132]. In many cases, flavoenzymes interact both with obligatory one-electron compounds such as ferredoxin (Fd) or cytochromes as well as obligatory two-electron couples such as lactate / pyruvate[112;119], fumarate / succinate[38;121], and most commonly the two-electron couple $NADP^+$/NAD(P)H during their catalytic cycle[136;223].

The recognition of the similarity in redox behavior between flavins and quinones coincided with Mitchell's proposal of the electron-bifurcating Q-cycle in the 1970's[62]. However, it took over 30 years from this realization for electron bifurcation (EB) to be experimentally observed in flavoenzymes.

A key distinction between flavins and quinones concerning EB/EC lies in their binding sites within flavoenzymes or quinone-binding enzymes. In the latter case, the membrane-soluble quinone pre-

[h]In analogy to quinones discussed in Section 1.2.1, the semi-reduced and fully-reduced states are often referred in literature as semiquinone (or "flavo-semiquinone") and hydroquinone (or "flavo-hydroquinone") species, respectively. I will abstain from this terminology for the sake of clearly distinguishing flavins from quinones.

viously reduced by other enzymes attaches to specific binding sites that tunes its chemical redox characteristics, i.e., the degree of redox cooperativity (Section 1.2.3), allowing it either to bifurcate (as in the Q_o-site of the bc_1-complex) or to undergo a one-by-one redox reaction (as in the Q_i-site, Section 1.2.2). In contrast, flavins typically reside inside flavoenzymes and are non-covalently linked to the protein's binding site. In the context of EB, the flavoenzyme must orchestrate the electron arrival at the flavin, achieved either (as will be shown below) through the two-electron donor NAD(P)H or in a one-by-one manner, followed by the consecutive electron bifurcation onto two distinct one-electron acceptors. To date, in addition to the electron-bifurcating [FeFe]-hydrogenase HydABC, 3 other flavoenzyme families, namely Etf, Nfn, and Hdr, catalyzing FBEB/FBEC have been discovered[31–33]. These will now be further discussed in detail with regard to the EB/EC mechanistic models and flavin's function.

For the electron-transferring flavoprotein (Etf) family and the NADH-dependent ferredoxin:NADP oxidoreductase (Nfn) family, the mechanistic proposal of the FBEB reaction at the bifurcating flavin strongly resembles that of the Q_o-site in the Rieske/cyt*b* family shown above (Section 1.2). In the EB reaction, for both of these enzymes, the flavin receives an electron pair from the intermediate redox potential NADH via a hydride transfer, which is consecutively bifurcated to the two thermodynamically and spatially different, high- and low-potential acceptors (more in detail below).

Contrarily, for the two other flavoenzyme families that were shown to catalyze EB/EC, namely the heterodisulfide reductases (Hdr) and the [FeFe]-hydrogenase, HydABC, a straightforward adaptation of the bifurcating mechanism in analogy to the QBEB does not seem to be possible.

1.3.1 Etf - Electron transferring flavoprotein

In 2008, the groups around Wolfgang Buckel and Rudolf Thauer showed the coupled and stoichiometric reduction of the high-potential crotonyl-CoA and the low-potential ferredoxin (Fd) by the intermediate potential two-electron donor NADH catalyzed by the electron-transferring flavoprotein/ butyryl-CoA dehydrogenase (EtfAB-Bcd) complex[95]. The discovery solved the thermodynamic enigma of how cell-free extracts of the strictly anaerobic, butyrate-producing *Clostridium kluyveri* could catalyze the endergonic formation of hydrogen ($E^\circ_{H^+/H_2}$ = -414 mV) from NADH (E° = -320 mV) in the presence of crotonyl-CoA (E° = -10 mV)[126;210].

Characterized by a remarkable exergonicity ($\Delta G^\circ = -60\,\mathrm{kJ\ mol^{-1}}$), the conversion of crotonyl-CoA to butyryl-CoA via NADH by the EtfAB-Bcd complex remains notably diminished unless supplied by oxidized ferredoxin (E°_{Fd} = -440 mV). This highlights the need for a low redox potential electron acceptor, i.e., oxidized Fd, for the bifurcating flavin to release both electrons[126]. It allows for the thermodynamically coupled generation of reduced Fd and butyryl-CoA, despite the endergonic Fd reduction by NADH.

The protein's exclusive prosthetic group being FAD, and the bifurcating reaction's reliance on this compound[126], led to the proposal of flavins as the only plausible catalysts for flavin-based electron bifurcation (FBEB). The exclusive reliance on flavins invited the design of spectroscopic studies on the EtfAB complex[189] and its respective subunits[206] mainly by UV/Vis and EPR (for reasons outlined in Section 1.6.5). Together with structural studies, these spectroscopic investigations make the EtfAB-Bcd complex today the best understood FBEB-system[30;58;113;151;153;157;158;206;220].

EtfAB features two functionally different flavins

The quaternary structures of this electron-bifurcating protein complex showed a tetramer constructed of two subunits of the electron-transferring flavoprotein (EtfAB) and a homodimer of two butyryl-CoA dehydrogenase (Bcd) subunits[58]. Electron-Bifurcating EtfAB features two FAD prosthetic groups, one in each subunit. The observation of inverted redox potentials for the FAD in EtfA identified the electron- bifurcating flavin (^{Bf}FAD)[189], whereas the second FAD in EtfB is an electron-transferring flavin (^{ET}FAD) which catalyzes exclusively a single-electron transfer while cycling between an anionic semi-reduced state and the anionic fully-reduced state[58;206]. The catalytic mechanism of EtfAB involves an initial two-electron oxidation of NADH by ^{Bf}FAD. In the electron-bifurcating reaction, the reduced ^{Bf}FAD reduces both the soluble low-potential ferredoxin (which binds in 6 Å distance to ^{Bf}FAD) and the high-potential ^{ET}FAD, which is proposed to reside in the one-electron accepting anionic semi-reduced state. The release of the reduced ferredoxin is accompanied by a significant conformational change of the fully-reduced anionic ^{ET}FAD undergoing a movement from the bifurcating site (separated by 14 Å from the ^{Bf}FAD) to the single-electron accepting subunits of Bcd [i] (then 18 Å from the ^{Bf}FAD, in *Acidaminococcus fermentans* Etf-Bcd)[42]. The extensive movement of the ^{ET}FAD domain in EtfB due to a conserved loop region has been observed in other bifurcating and even non-bifurcating Etf's[212]. Over the course of the last 15 years our understanding of the physiological role of the electron-bifurcating EtfAB functional unit has been enlarged by discovering it coupled to various other bioenergetic protein complexes that are in different compartments (soluble and membrane-associated), interacting with different substrates and thus enabling energy conservation in different metabolic pathways (see figure 1.10, Table 1.1). The structural conservation of the main EtfAB module highlights the evolutionary "LEGO-building block"[77] principle of proteins in bioenergetic chains, a general concept that has been identified for all currently discovered FBEB enzymes[7;13;258].

[i] For focus, the redox properties of the Bcd complex are no further discussed here.

Table 1.1: Comparison of the biophysical properties of the characterized EtfAB-module containing EB/EC flavoenzymes. All these complexes couple the EB/EC of low-potential ferredoxin ($E^\circ = \sim$ -500 mV) and the intermediate potential two-electron compound NAD^+/NADH (E° = - 320 mV) to the one-electron oxidation/reduction of a second flavin. In order to fully reduce/oxidize the high potential(HP) electron component two cycles of the entire reaction to or form NAD^+/NADH occur.

Enzyme	Compartment	Direction	HP electron component	E° (mV)	Ref.
EtfAB-Bcd	Cytoplasm	EB	crotonyl-CoA/butyryl-CoA	-10	95;126
CarCDE	Cytoplasm	EB	caffeyl-CoA/dihydro-caffeyl-CoA	+33 to -10	56
Ldh-EtfAB	Cytoplasm	EC	lactate/pyruvate	-190	112;119
EtfABCX	Membrane	EB	$menaquinone_{OX/RED}$	-80	73

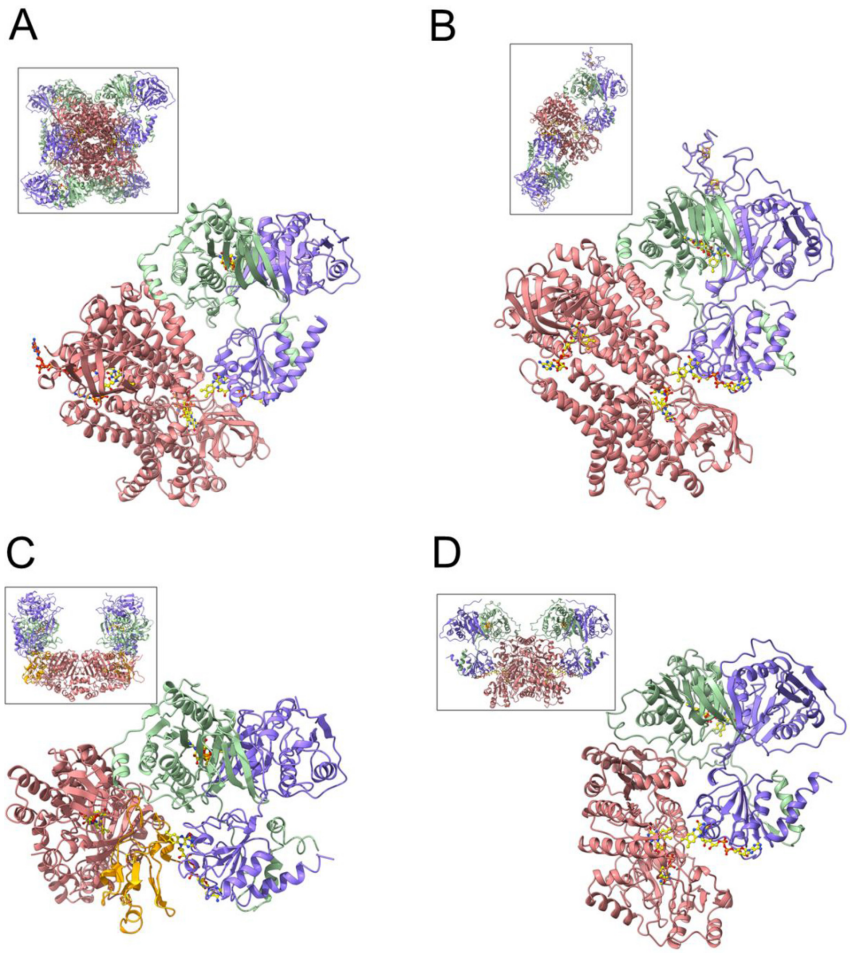

Figure 1.10: Structurally characterized electron-bifurcating EtfAB protein modules associated with different dehydrogenase/oxidoreductase high-potential effector subunits. The four characterized EtfAB complexes are **(A)** $(Bcd\text{-}EtfAB)_4$, **(B)** $(CarCDE)_4$, **(C)** $(FixABCX)_2$ and **(D)** $(Ldh\text{-}EtfAB)_2$. The electron-bifurcating conserved core of EtfA and EtfB (in blue and green, respectively) are shown together with the dehydrogenase/oxidoreductase subunits drawn in salmon (and orange). The EtfAB module for all complexes is presented in the same orientation. Insets show the entire complex. Figure taken from Kayastha *et al.* (2022) [112] under a Creative Commons Attribution License.

1.3.2 Nfn - NADH-dependent ferredoxin:NADP oxidoreductase

Nfn is the most widespread flavoenzyme yet described to catalyze EB/EC [127]. It is composed of two subunits (NfnL and NfnS) that contain a total of five functional cofactors (2 FAD, 1 [2Fe-2S]- and

2 [4Fe-4S]-cluster, figure 1.11)[57] to shuttle electrons between the three universal electron carriers NAD^+/NADH, $NADP^+$/NADPH and Fd. Initial crystallographic and electrochemical studies have resulted in a first model of the bifurcating mechanism in this protein[57;59;129], which, similar to EtfAB, revolves around two functionally different flavins, one in each subunit. The bifurcating ^{Bf}FAD inside the NfnL subunit, catalyzes NADPH oxidation and the subsequent electron bifurcation, whereas the other, an electron-transferring ^{ET}FAD accepts two electrons one-by-one during two consecutive cycles and then reduces NAD^+ to NADH. Positive redox cooperativity of the two electron transfers at the ^{Bf}FAD produces a high-potential electron that allows the reduction of the high-potential [2Fe-2S]-cluster. The second electron then exhibits a more reducing property (as outlined in Section 1.2.3) that permits the reduction of the low-potential [4Fe-4S]-cluster chain, leading ultimately to the reduction of ferredoxin (figure 1.11)[96;246;250].

Nfn represents the only flavoenzymes for which a widely cited stability constant of the semi-reduced species for the ^{Bf}FAD of $\log(K_s) = -21$ has been approximated via transient absorption spectroscopy experiments[129], suggesting a 1.2 V split (ΔE) between the redox potentials of the individual redox-inverted high-potential and low-potential electron transfers. However, this estimation has been controversial and was recently questioned by the same research group[231].

1.3.3 Hdr - Heterodisulfide reductase

Heterodisulfide reductases (Hdr) are found in different microbial metabolism, most notably sulfate reduction, acetogenesis and methanogenesis[7]. Only in the latter, in methanogenic archaea, Hdr was shown to catalyze EB/EC[222;228]. In this flavoenzyme family, a single bifurcating ^{Bf}FAD molecule is found in the HdrA subunit of the HdrABC-subcomplex together with multiple FeS-clusters. The latter were proposed to electronically connect the high-potential electrons from the bifurcating reaction to the high-potential acceptor, heterodisulfide (CoM-S-S-CoB, E°=-140 mV[211]), which after two turnovers of the ^{Bf}FAD in an exergonic reduction results in the liberation of coenzyme M (CoM-SH) and coenzyme B (CoB-SH). The HdrABC core is completed by the recruitment of additional subcomplexes[7] which are proposed to supply the intermediate-potential electrons to the flavin and/or guide the low-potential electrons after the bifurcating reaction to the terminal acceptors. Initial crystallographic structure models from *Methanothermobacter marburgensis* (shown in figure 1.12) have indicated the cytoplasmic HdrABC core module of the H_2-oxidizing CO_2-reducing species to be complexed with the MvhAGD hydrogenase. It was proposed that electrons liberated from the oxidation of hydrogen ($E^\circ_{H^+/H_2}$ = -414 mV[210]) are transferred via a single chain of FeS-clusters to the bifurcating FAD and further to the low-potential Fd and high-potential heterodisulfide in a bifurcating manner via two different FeS-cluster pathways[222]. Later, in Cryo-EM structures of a large (3 MDa) flavoenzyme-complex from *Methanospirillum hungatei*, the HdrABC core was shown to recruit other subunits that

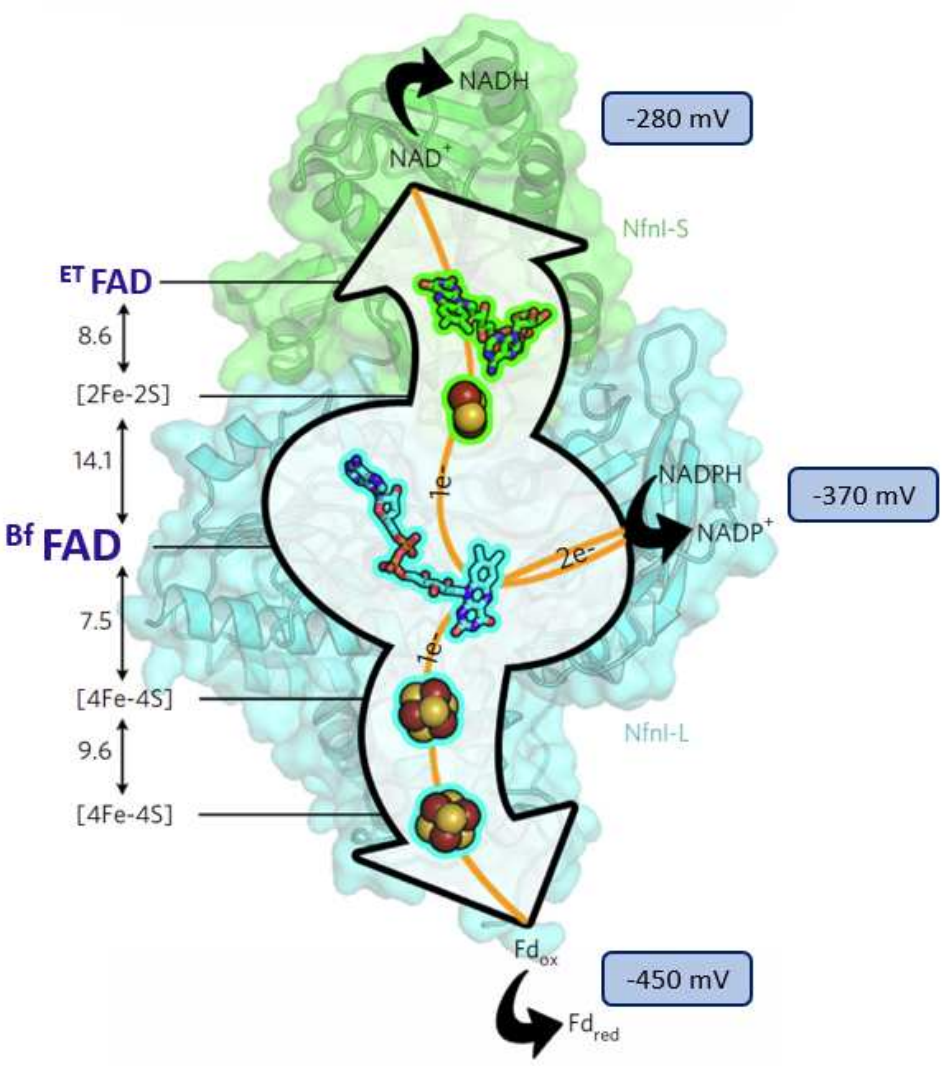

Figure 1.11: Structure model and schematic electron-transfer pathways in the electron-bifurcating Nfn from *Pyrococcus furiosus*. Nfn is a heterodimer of NfnS (31 kDa) and NfnL (53 kDa). NfnS contains the electron-transferring ^{ET}FAD and a 1 Asp/3 Cys-ligated [2Fe-2S]-cluster. NfnL contains the electron bifurcating ^{Bf}FAD and two [4Fe-4S]-clusters. The ferredoxin (Fd) binding site has been proposed near the distal [4Fe-4S]-cluster of NfnL. Edge-to-edge distances between cofactors are given in Ångström (Å), redox potentials of substrate couples (in blue boxes) as assumed under physiological conditions. Data and figure with permission from Lubner *et al.* (2016) [129]. Copyright 2017, Springer Nature America, Inc.

act as electron input modules from the redox substrates $F_{420}H_2$ [240] or formate [228]. Whereas this protein also transfers the low-potential electrons from the FBEB reaction to the reduction of Fd as the HdrABC-MvhAGD complex from *M. marburgensis*, an additional branching architecture made up of iron-sulfur cluster domains also transfer these strongly reducing electrons for the immediate utilization at a molybdenum-formyl-methanofuran containing CO_2-fixation site ($E^{\circ}_{CO_2/HCO_2^-} = -420$ mV [210]) [228]. Whereas the paths of the electrons inside the Hdr flavoenzyme complexes are traced out by chains of FeS-clusters to and from the FAD, the immediately neighboring FeS-clusters that act as direct electron-partners with the bifurcating flavin appear too far in distance for physiologically relevant electron transfer. The ^{Bf}FAD was hypothesized to receive the intermediate redox potential electrons in a consecutive manner from a neighboring iron-sulfur cluster potentially aided by a pair

of cysteines and not through a coupled two-electron transfer from the single two-electron donor, such as NAD(P)H as is the case for Nfn or Etf[228].

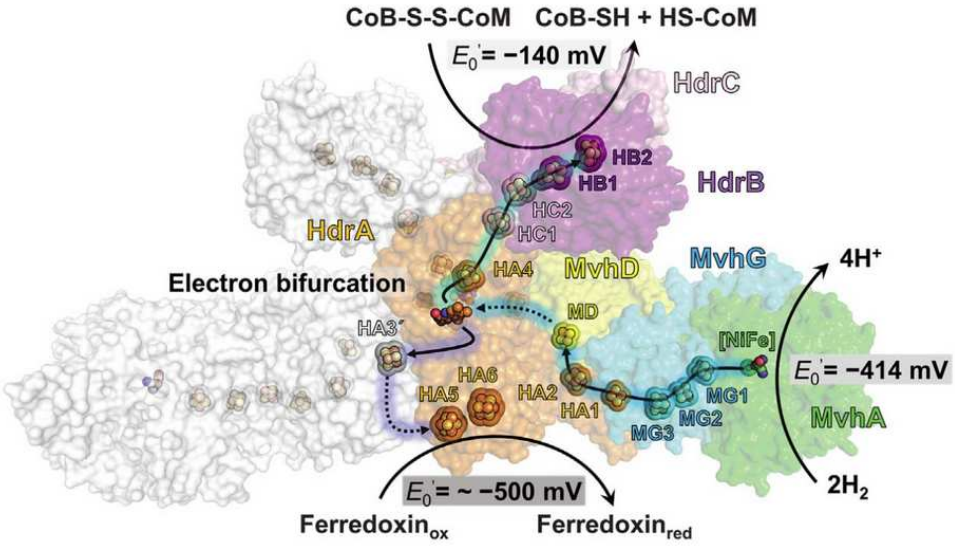

Figure 1.12: Structure model and proposed electron-transfer pathways in the electron-bifurcating HdrABC-MvhAGD from *M. marburgensis*. The solid arrows indicate the electron-transfer pathway composed of iron-sulfur clusters at distances less than 13.5 Å. The dashed arrows correspond to a hypothetical electron-transfer pathway with distances longer than 15 Å between the redox centers. For the full reduction of heterodisulfide (CoM-S-S-CoB), the 2 molecules of H_2 are oxidized and alongside an ferredoxin (with 2 [4Fe-4S]-clusters) is reduced. Figure taken from Wagner *et al.*(2017)[222]. Reprinted with permission from AAAS.

How the single FAD molecule in HdrA is able to switch between different functional modes, an electron-accepting mode and a bifurcating-mode, is not clear. Conformational rearrangements in HdrA were experimentally observed and are hypothesized to mediate electron bifurcation by fine-tuning the accessibility of the low-potential acceptor chain and the electron-supplying chain, but experimental evidence on the molecular details are missing for the moment[228]. Given the presence of numerous FeS-clusters within this enzyme complex, conducting spectroscopic studies around the bifurcating FAD appear rather daunting. This is mainly because the signals arising from the FeS-clusters overlap with the flavin, thereby obscuring the spectral features of the FAD. The adaptation of the single flavin to occupy different functional modes, electron-bifurcating or not, has also been proposed in a structurally simpler flavoenzyme, the [FeFe]-hydrogenase HydABC.

1.4 Structure - Function Relationship in HydABC

In the [FeFe]-hydrogenase (HydABC) from *T. maritima*, NADH (E°=-320 mV[210]) acts as a high-potential donor and has been shown to be stoichiometrically oxidized alongside the low-potential electron donor ferredoxin (Fd, $E_{m,pH8}$=-415 mV[41;131]), in the overall exergonic, electron-confurcating reaction, leading to the two-electron reduction of protons to hydrogen ($E^\circ_{H^+/H_2}$ = -414 mV[210])[194].

As outlined in the chapters above, the minimal requirement for a coupled two-electron transfer

via electron confurcation (EC) is the existence of a two-electron confurcating center, the FMN in this case, and two spatially and thermodynamically different one-electron donors. The native ferredoxin *Tm*Fd1 (TM0927) fulfills the requirement of a one-electron donor. NADH, contrarily, is an obligatory two-electron donor, which transfers a hydride (H^-), i.e., a coupled $2e^-$ and $1H^+$, directly to the flavin. It's not understood how these three electrons from these two respective electron donors are processed by the enzyme.

In the absence of a structural model and due to difficulties in quantifying the FMN as a consequence of its inherently loosely bound nature, initial mechanistic proposals for HydABC in analogy to the electron-bifurcating EtfAB and NfnAB complexes involved a 2-FMN model, "one being required for NADH dehydrogenation and second for flavin-based electron-bifurcation"[31]. This proposal entailed one FMN would interact with the obligatory two-electron donor NADH, and then consecutively transfer a high-potential electron to a second FMN, which also accepts a low-potential electron from ferredoxin, in a confurcating manner. This hypothesis dominated the scientific discourse for multiple years until the beginning of this thesis[32].

Due to the "building block"-architecture of bioenergetic electron transport chains and the homology of HydABC to other structurally and functionally better studied protein complexes, a phylogenetic approach based on structure-guided protein sequence alignments which were interpreted in the light of the biophysical properties of the enzymes and their reactions, was well-suited to explore the properties of HydABC. Many of these homologous proteins belonging to a common NAD(P)H dehydrogenase family such as respiratory complex I, formate dehydrogenase, or [NiFe]-hydrogenases are NAD(P)H-dependent and feature a similar domain architecture, however, were not described to catalyze the energetically coupled reduction or oxidation of two thermodynamically different electron acceptors/donors onto/from an intermediate potential 2-electron donor/acceptor according to the here presented EB/EC scheme.

The analysis of the modular composition of HydABC and its structurally characterized homologs from these different bioenergetic backgrounds rendered the hypothesis on the presence of multiple functionally important flavins in this protein family as invalid[258] (see Chapter 3).

Cryo-EM structure models of the heterotrimeric HydABC enzyme complex of *T. maritima*[80] have shown a single FMN alongside 10 FeS-centers that connect the H_2-converting H-cluster in the HydA-subunit to the flavin in the HydB-subunit and to the two electron donors, reduced ferredoxin (Fd_{RED}) and NADH (figure 1.13).

Interestingly, only half of these FeS-clusters directly form a chain from the FMN to the H-cluster with less than 14 Å between each of the neighboring centers, compatible with fast electron transfer[160;175]. The electron-transferring capabilities of this FeS-cluster wire has been noticed already

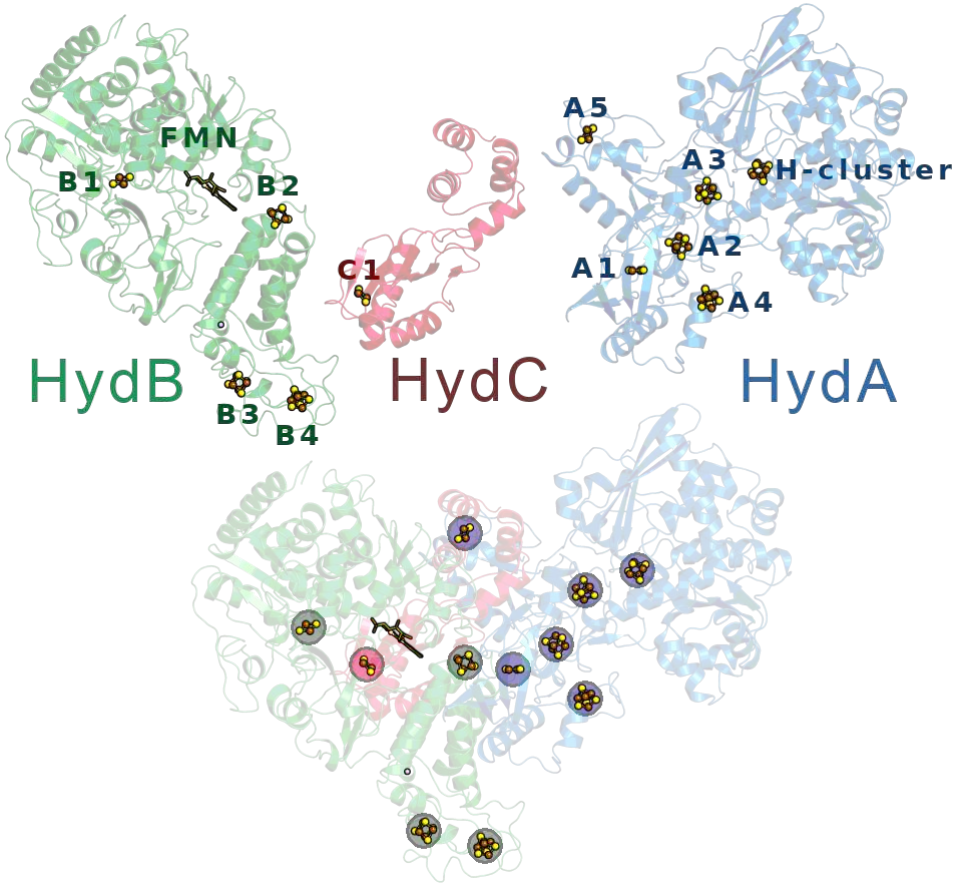

Figure 1.13: Cryo-EM structure model of the heterotrimeric HydABC flavoenzyme complex of *T.maritima*. The minimal functional unit of the flavoenzyme complex is composed of HydA (73 kDa, marine blue), HydB (69 kDa, green), HydC (19 kDa, red) in a 1:1:1 stoichiometry. Beside the prosthetic group FMN in the HydB-subunit (planar top view, shown in green), HydABC utilizes a total of six [4Fe-4S]-clusters and four [2Fe-2S]-clusters (irons : brown, sulfurs : yellow) (PDB-codes: 7P8N, 7P5H, 7P91, 7P92). Cluster nomenclature as originally published in Furlan *et al.* (2022).[80]

during the initial description of the enzyme complex of an H_2-dependent reduction activity of the NAD^+, via the FMN as the only NAD^+/NADH interaction site[215]. The remaining FeS-clusters are found in partially flexible protein domains, which seem to orchestrate the electron transfer to and from the FMN with ferredoxin. No experimental evidence for the binding site of the ferredoxin was obtained so far. However, based on different structural and bioinformatical/computational observations two proposals of the ferredoxin docking site were put forward.

Furlan *et al.* (2022)[80] proposed an N-terminal "fishing-rod"-like α-helix on the flavin-containing HydB subunit, which, by means of electrostatic interactions through highly conserved positive residues (arginines and lysines), attracts the negatively charged ferredoxin. This proposal would favor a Trx-like B1 [2Fe-2S]-cluster as the primary low-potential electron interchanging site.

In a more recent Cryo-EM study from two different homologous electron-bifurcating hydrogenases in the acetogenic bacteria *Acetobacterium woodii* and *Thermoanaerobacter kivui*[111], a different ferredoxin docking site has been proposed. Molecular dynamics (MD) protein docking simulations showed the anionic ferredoxin non-covalently attached to a conserved Lys-rich loop on the direct sur-

face of the C-terminal ferredoxin-like domain of HydB (involving K570 and K572 in *A. woodii*[111]). Consequently, the two [4Fe-4S]-clusters in the C-terminal domain, B3 and B4, would then directly exchange electrons with the soluble ferredoxin.

1.4.1 Conformational arrangements of three domains in the HydBC subcomplex

The FeS-clusters directly or indirectly implicated to exchange electrons with the low-potential ferredoxin are located in three peripheral protein domains of the electron-bifurcating HydBC subcomplex and have been proposed to exhibit various degrees of conformational heterogeneity.[j] These domains include:

1. A ferredoxin-like domain at the C-terminus of the HydB subunit, featuring two [4Fe-4S]-clusters, termed B3 and B4[80] (Section 1.4.2, orange in figure 1.14)
2. Two thioredoxin-like [2Fe-2S]-cluster domains:
    - one in the N-terminus of HydB, containing B1[72;111] (Section 1.4.3, green in figure 1.14)
    - another in the C-terminus of HydC, containing C1[72;111] (Section 1.4.4, red in figure 1.14)

In the above-mentioned Cryo-EM studies of the electron-bifurcating [FeFe]-hydrogenase[80;111] as well as homologous bifurcating proteins, containing HydBC-like subunits, a [NiFe]-hydrogenase from *Acetomicrobium mobile*[72] and a Sporomusa-type Nfn transhydrogenase (Stn) from *Sporomusa ovata*[118], these conformational changes have been assessed either by the observation of discrete conformational states[111] or by having encountered difficulties in fitting a precise model to the Cryo-EM maps[72;111].

1.4.2 Ferredoxin-like C-terminal domain in HydB with B3 and B4

A ferredoxin-like domain (from now 8Fe Fd-like domain) in the C-terminus of HydB (orange in figure 1.14) featuring two [4Fe-4S]-clusters, termed B3 and B4, and was shown in all structural studies to exhibit the highest degree of flexibility in HydABC. This 8Fe Fd-like domain is C-terminally connected to the rest of HydB by an extensive linker. This stretch of amino acids is restricted by a "hinge-like" conserved Zn^{2+} coordination site (grey sphere in figure 1.14) [k], built from 3 Cys and 1 His residue at the direct HydB interface region[80], which conformationally restrains the degree of

[j] Note that the FeS-cluster nomenclature of each HydABC-homologous enzymes[72;111;118] differ slightly from the one first proposed by Furlan *et al.*[80] (2022) for HydABC from *T.maritima*. For consistency, homologous and structurally equivalent FeS-clusters from these other enzymes were renamed to the nomenclature of the here characterized HydABC-complex from *T.maritima*.

[k] In the homologous, pentameric [NiFe]-hydrogenase from *A. mobile* an additional pentacoordinate [2Fe-2S]-cluster in a position coinciding with this Zn^{2+}-binding site in HydABC was documented[72]. The proposed center seems to be restricted to this [NiFe]-hydrogenase while all the other flavoenyzmes with the HydBC-like architecture feature the aforementioned Zn^{2+}-binding site[80;110;118] It is therefore not further considered here.

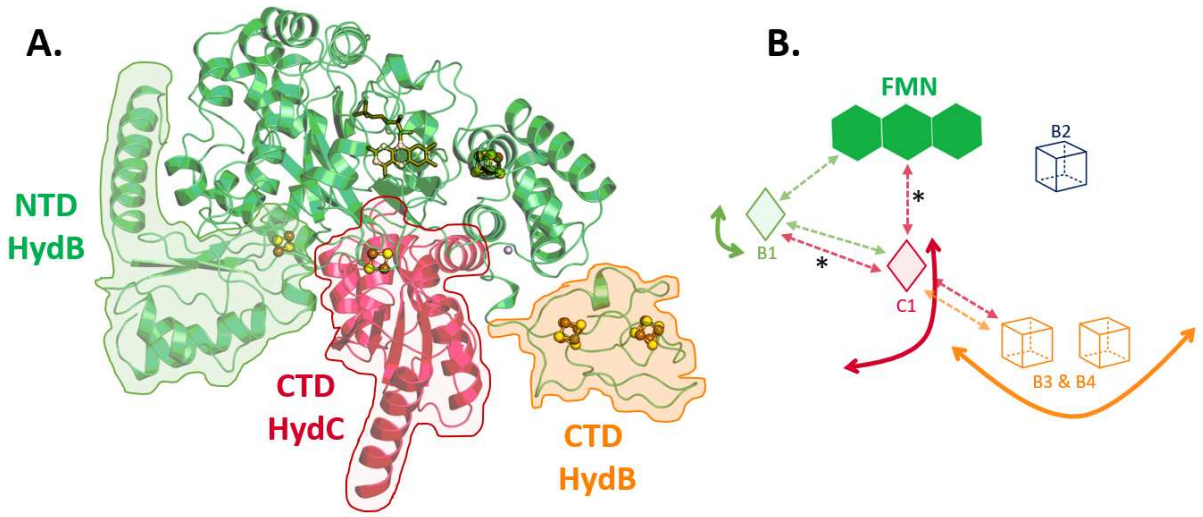

Figure 1.14: Schematic of the observed conformational dynamics of the HydBC-subcomplex. **A.** Structural model of the HydBC from *T.maritima* showing the flavin-containing HydB subunit (in green cartoon representation) and the thioredoxin-like [2Fe-2S]-cluster containing HydC subunit (in red cartoon). Conformational domain rearrangement was proposed for the N-terminal domain (NTD) of HydB (green) due to difficulties in fitting a precise model and the C-terminal domain (CTD) of both HydB (orange) and HydC (red) which were resolve in different conformations. **B.** The degree of domain movement (as solid arrows, colored in respect to the concerned domain as in figure A. with lengths of the arrow indicating the magnitude of conformational change) were proposed to affect electron-transferring distance (as dotted lines, color regarding to the concerned domain) of the respective [2Fe-2S]-clusters (as diamonds) and [4Fe-4S]-clusters (as cubes) inside these domains. Asterisk denotes distances between cofactors that would allow for efficient electron transfer in at least one observed configuration, with distances below 14 Å according to Moser and Dutton[160;175].

freedom. In the structure models of *T.maritima*, this 8Fe Fd-like domain has been resolved in two different states, termed “open” (PDB:7P92) and “closed”(PDB:7P91). In the latter conformation, this domain has been interpreted to be closing a “bridge” to another flexible thioredoxin-like [2Fe-2S]-cluster domain at the C-terminal of the neighboring HydA subunit, which is only resolved in this conformation. The thioredoxin-like domain in HydA including the [2Fe-2S]-cluster A5 is found beyond electron transfering distance to any FeS-cluster (> 30 Å) and absent in all other hydrogenases that have been shown to catalyze EB/EC and but only in a small subset of hydrogenases[258] (Chapter 3) and thus not conserved, questioning its importance in the bifurcating/confurcating mechanism. The 8Fe Fd-like domain however is found highly conserved among bifurcating flavoenzymes using the HydBC-like architecture. Moreover, mutant strains with the deleted 8Fe Fd-like domain in the acetogen *T. kivui* caused the EB activity to cease (right orange bar in figure 1.15), highlighting the essential nature of this domain with its electron-transferring 2 [4Fe-4S]-clusters, B3 and B4[111].

1.4.3 Thioredoxin-like N-terminal domain in HydB with B1

On the opposite side, in the N-terminus of HydB a thioredoxin-like [2Fe-2S]-cluster domain (from now on Trx-like [2Fe-2S], green in figure 1.14) was also suspected to exhibit conformational flexibil-

ity, as it could not be adequately resolved in Cryo-EM maps of the HydABCD[1] structures of *A.woodii*[111] and the homologous [NiFe]-hydrogenase of *A. mobile*[72]. This domain coordinates a Trx-like [2Fe-2S]-cluster, referred as "B1" in the *T. maritima* HydABC structure, and is situated approximately 19 Å away from the bifurcating FMN, when resolved[80].

Similar to the C-terminal 8Fe Fd-like domain, this N-terminal domain with the B1 Trx-like [2Fe-2S]-cluster is highly conserved among all HydBC-like subunits that have been documented catalyzing electron bifurcation. The importance of the [2Fe-2S]-center was also demonstrated in deletion mutants (depicted by the green center bar in figure 1.15), where two of the four coordinating cysteines were mutated to glycine. In such cases, the catalytic activity of electron bifurcation decreased by an order of magnitude as compared to the wildtype (WT) HydABC from *T. kivui*[111].

1.4.4 Thioredoxin-like C-terminal domain in HydC with C1

Finally, a third conformationally dynamic domain is found at the C-terminus of the small HydC subunit (red in figure 1.14). It strongly resembles the N-terminal domain of HydB, as it is also in a Trx-like [2Fe-2S]-cluster coordinating architecture. This domain contains the C1 [2Fe-2S]-cluster which was resolved in two conformations in the oxidized, NAD^+-bound structure models of *A.woodii*[111] (PDB: 7Q4V).

In the "HydC-in" (or "closed") -conformation, the C-terminal domain is found tightly bound to the core domain of the HydB subunit. In this configuration, C1 is in electron transfer distance to both, B1 and the bifurcating FMN ($\sim$ 14 Å to both sites). NAD^+ was not resolved in this site.

Contrarily, in the "HydC-out" (or "open")-conformation, C1 moves away from these two cofactors ($>$ 15 Å to B1 and $>$ 20 Å to the FMN) and instead is observed closer to the 8Fe Fd-like-domain clusters B3 and B4 (observed in $\sim$ 15 to 18 Å distance, as compared to >25 Å in "HydC-in"), which however still doesn't allow for efficient electron transfer especially considering the high dielectric of the aqueous media. In this site, NAD^+ was resolved with the nicotinamide group in 3.8 Å distance from the flavins isoalloxazine. Variance analysis of the homologous electron-bifurcating [NiFe]-hydrogenase from *A. mobile* observed a similar conformational change in HydC[72], although no structural model of the "HydC-out" is available.

Deletion mutants which target the coordinating cysteines of the C1-cluster brought the bifurcating activity to a halt in the recent study of the Stn-transhydrogenase from *S. ovata*, highlighting its essential nature[118].

[1] The absence of a properly resolved model in the case of the hydrogenase of *A.woodii* might have been due to the use of a trimeric HydABC model, whereas the bifurcating [FeFe]-hydrogenase was shown to be tetrameric (HydABCD)[111;192].

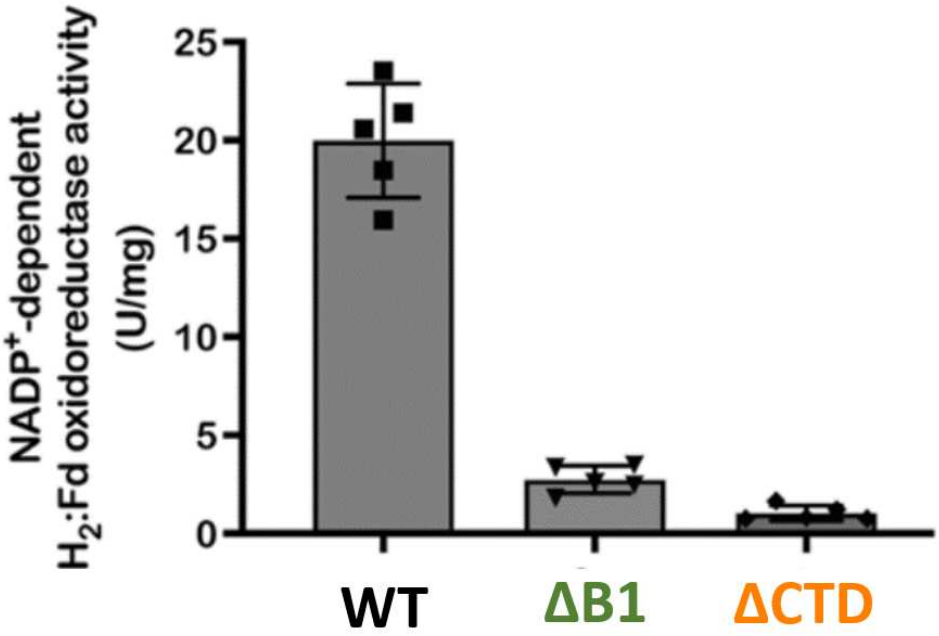

Figure 1.15: Electron bifurcation activity assay of different HydABC variants of *T. kivui* with mutated FeS-cluster (domains) in HydB. $NADP^+$-dependent reduction of ferredoxin by H_2 in a coupled electron-bifurcating reaction is compared for the wild-type (WT) protein, the ΔB1 mutant with the N-terminal thioredoxin-like [2Fe-2S]-cluster in HydB mutated (double mutant on coordinating cysteines: G82G, C86G) and the ΔCTD mutant (entire C-terminus deleted: P565-G630) with the C-terminal ferredoxin-like 2 [4Fe-4S]-cluster domain in HydB deleted. All enzymes were His-tagged. For all data, the error bars show the standard deviation. Figure and Data taken with permission from Katsyv *et al.* (2023)[111] under a Creative Commons Attribution License.

1.4.5 A single flavin in HydABC catalyzes FBEB and NADH oxidation

The phylogenetic analysis in Chapter 3 and the subsequently published structures of HydABC[73;80;111;118] clear demonstrated the presence of a single FMN per HydABC protomer. In addition, these analysis showed the formation a dimer of trimers, where the interaction surface between the protomers is realized by a Y-shaped arrangement of 4 FeS-clusters (termed Y-junction module in the Chapter 3, N-terminal of the catalytic HydA subunit. Interestingly, one of the [4Fe-4S]-cluster, A4, which features a characteristic histidyl-ligand alongside three cysteines is observed at the direct interface of the dimer formation in electron-transferring distance (8.8 Å in HydABC of *T.maritima*) to the A4 cluster of the neighboring protomer[80], which sparked the hypothesis for a cooperative mechanism of the individual flavins during EB/EC. ΔA4-Deletion mutants (by substituting all coordinating cysteines to glycines) of HydABC from *T.kivui*, however, were shown to feature comparable rates of the coupled electron bifurcating reduction of $NADP^{+m}$ and ferredoxin from H_2 as the WT[111]. Analytic Size-Exclusion chromatography of this mutant thereby indicated that the otherwise dimerized enzyme complex (dimer of trimers), breaks apart into the protomers. This supports the functional role of A4 in forming the dimer while not influencing EB/EC.

[m]HydABC from *T.kivui* is currently the only known [FeFe]-hydrogenase that uses $NADP^+$ instead of NAD^+ as high-potential acceptor in the EB reaction.[110]

This finding clearly showed that a single FMN cofactor in HydB is catalyzing the reduction or oxidation of the two-electron compound $NAD(P)^+/NAD(P)H$ and the thermodynamic coupling reaction of $Fd_{OX/RED}$, $NAD(P)^+/NAD(P)H$ and H^+/H_2 during EB/EC[111]. The conformational dynamics of the flavin-surrounding domains in HydBC are thereby proposed to enable for such a coupling mechanism.

1.4.6 Conformational changes in HydABC driven by redox transitions?

The conformational heterogeneity of these three domains in the HydBC subcomplex (figure 1.14), namely the two Trx-like [2Fe-2S] domains, containing C1 in HydC and B1 in HydB as well as the 8Fe Fd-like domain with B3 and B4 in the C-terminus of HydB, have been speculated to correlate with the redox state of the protein. Specifically, the conformational transition from "HydC-in" to "HydC-out" of the C-terminal domain in HydC (section 1.4.4) has been hypothesized to be induced by the reduction of the Trx-like [2Fe-2S]-cluster C1, which has been the result of MD simulations[111]. In the same study, Microscale thermophoresis has been employed to assess the binding affinity of the high-potential acceptor $NADP^+$ in HydABC of *T.kivui*. Here, the reduction of the protein, primarily attributed to Trx-like [2Fe-2S]-cluster B1 in HydB, was proposed to convey a 15-fold higher affinity for $NADP^+$, potentially due to conformational changes. It was speculated that via this binding-affinity modulating mechanism, the single FMN performs to switch between the one-by-one redox behavior allowing the reduction of C1 and B1, and a hydride-transfering mode leading to $NADP^+$ reduction[111].

These Cryo-EM and MD studies[72;111] have put forward a model for the electron-bifurcating mechanism in the HydBC-subcomplex based on the conformational dynamics of these three FeS-containing domains. They favor a kinetic gating model in which the rate of the electron transfer between the different domains is gated primarily by the distance between the respective FeS-clusters and the presence or absence of electron-accepting $NADP^+$. However, these models entail numerous assertions that have been made without reference to data. Whereas most of these statements will be assessed in detail in the final discussion section, the absence of any experimentally determined thermodynamic data, foremost redox potentials of the aforementioned cofactors as well as any spectroscopic data, have motivated the study shown in Chapter 4 on the redox properties of HydABC in *T.maritima*. The observation of considerable dynamic nature of these FeS-cofactors, containing the [2Fe-2S]-clusters B1 and C1 as well as the [4Fe-4S]-clusters B3 and B4, near the central FMN, alongside their strictly conserved nature across all described HydABC homologs indicates their essential importance for the EB/EC mechanism[128;258]. Interestingly, prior studies have already examined some thermodynamic parameters of these cofactors, particularly the Trx-like [2Fe-2S]-cluster domain in isolated subunit of HydC[18] and the homologous protein NuoE[19] from complex I. This thesis will expand upon these insights using spectroscopic techniques coupled to equilibrium redox titrations.

The following section outlines the previously determined thermodynamic and spectral properties of these FeS centers in general, primarily Trx-like [2Fe-2S]-clusters and 8Fe Fd-like domain. Subsequently, we delve into an in-depth examination of the central flavin prosthetic group.

1.5 Thermodynamic and spectral properties of the FeS-Flavoenzyme HydABC

1.5.1 Thioredoxin-type [2Fe-2S]-clusters

Thioredoxin-like [2Fe-2S]-clusters (Trx-like [2Fe-2S] hereafter) were first observed and studied as a rather rare family of soluble ferredoxins (Fd) from different bacteria[40;146]. The name was derived from the structurally similar α/β architecture between this FeS-protein with thioredoxins, a class of small disulfide-containing proteins commonly acting as redox regulators[187]. The structure is characterized by 5 β-sheets, 2 long α-helices, and variable shorter $\alpha/3_{10}$-helices (see figure 1.16). In the first crystallographically observed Trx-like ferredoxins, the formation of dimers along the β-sheets was proposed to stabilize the [2Fe-2S]-clusters near the dimer surface[146]. An interesting peculiarity of the Trx-like [2Fe-2S] is the location of the [2Fe-2S]-cluster at the base of an extended flexible loop between one β-sheet and an α-helix (see figure 1.16A[244]).

The protruding surface loop in these ferredoxins dictates the [2Fe-2S]-cluster's redox properties[146], yet does not shield it from the aqueous environment. The surface-exposed nature of the [2Fe-2S]-cluster is hypothesized to cause variable redox properties depending on the surrounding medium. Monomeric Trx-like [2Fe-2S]-domains are fused as C- and N-terminal extensions to redox enzymes across diverse bioenergetic chains. Their incorporation is also observed in formate dehydrogenase[171], [NiFe]- and [FeFe]-hydrogenases[213], and the respiratory complex I[76]. The fusion of the Trx-like domain is accompanied by a loss of the above-mentioned extended flexible loop between one of the β-sheets and α-helices, which allows the surface-exposed [2Fe-2S]-cluster to be buried inside protein pockets[146]. In all the mentioned cases, including HydABC, the loss of this loop consequently minimizes the distance of the [2Fe-2S]-cluster to the FMN prosthetic group in the neighboring subunit.

HydABC from *T.maritima* is an extreme example of this evolutionary duplicative process, where this Trx-like [2Fe-2S]-domain was fused once to each of the three subunits. It is observed in the C-terminus of HydA, the N-terminus of HydB and the C-terminus of HydC. As elaborated in detail above, the HydA Trx-like [2Fe-2S]-domain was found to be restricted to a small subset of electron-bifurcating [FeFe]-hydrogenases, and therefore not proposed to be fundamentally important for the catalytic properties of the enzyme[258] (Chapter 3). Contrarily, the Trx-like [2Fe-2S]-domain in HydB and HydC are highly conserved and essential for a proper electron-bifurcating activity (section 1.4.1).

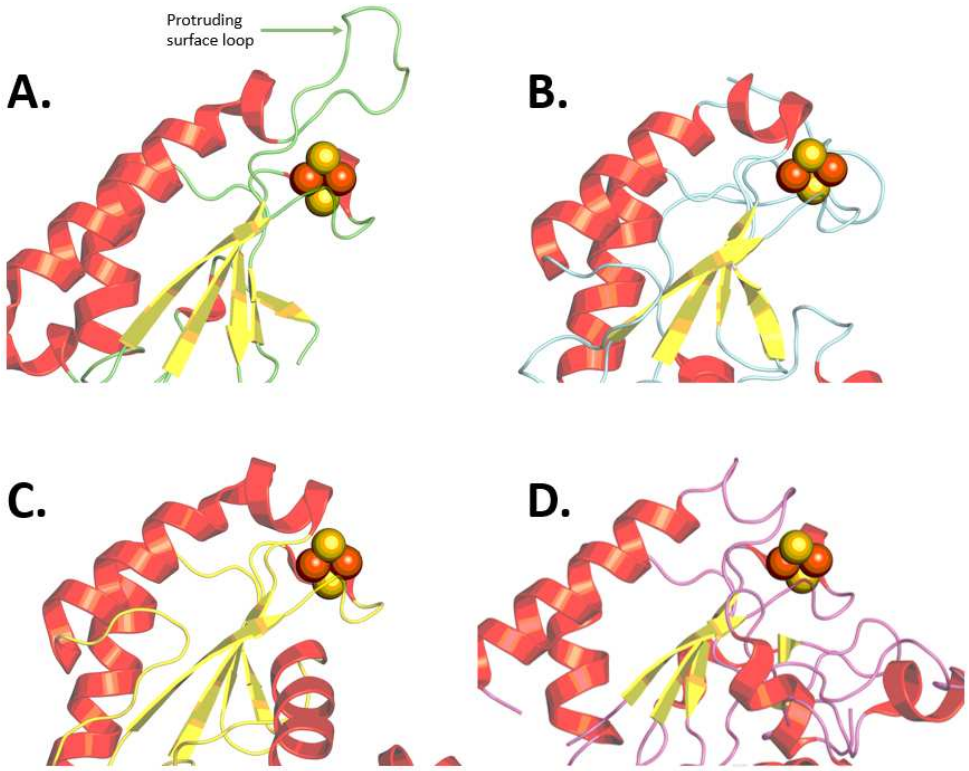

Figure 1.16: Structural comparison of the thioredoxin-like [2Fe-2S] cluster domain in 4 different proteins: **A.** wild-type Trx-like [2Fe-2S] ferredoxin from *Aquifex aeolicus* (PDB-code: 1M2A), **B.** "N1a"-cluster of NuoE in respiratory complex I from *Thermus thermophilus* (PDB-code: 4HEA), **C.** "B1"-cluster of the N-terminus of HydB and **D.** "C1"-cluster of C-terminus of HydC in *Thermotoga maritima*(PDB-code: 7P92). Color code chosen as followed, α-helices in red, β-sheets in yellow, loops in different colors, FeS-clusters as brown-gold spheres. The surface-exposed position of the [2Fe-2S]-cluster in this domain family is thought to be at the origin of the redox-variability of the cluster.

Hydrogen bonding as primary determining factor of redox potentials

The redox properties of Trx-like [2Fe-2S]-cluster were initially studied in WT proteins of the Trx-like [2Fe-2S] Fd from different bacteria, where redox midpoint potentials in the range of -300 mV were determined (such as in *A.aeolicus*[146]). An understanding of the modulation of the redox potential by the Trx-like [2Fe-2S]-domain was gained through site-directed mutagenesis studies on these Fd's. Three factors are proposed to play important roles in influencing the redox potential of the [2Fe-2S]-center:

- hydrogen bonding (H-bond) to the cluster and the H-bond network surrounding the cluster,
- solvation effects, i.e., the degree of solvent exposure leading to the presence or absence of nearby waters,
- the presence or absence of nearby charged residues.

H-bonds with the Fe-coordinating sulfido- and thiolato-sulfur atoms (which act as H-bond acceptors) are thought to stabilize the reduced form of the cluster by dissipating charge density from

the metal-bound sulfur atom. Therefore, more and stronger H-bonds are expected to increase the reduction potential of the clusters.

The degree of solvent exposure of an FeS cluster influences the redox potential of the center in two opposing terms of entropic and enthalpic nature, respectively[61]. Aqueous, polar solvents are prone to form extensive hydrogen bonds to FeS-cluster, thereby increasing the redox potential of the cluster by reducing FeS-covalency, as just mentioned above. A second term comes into play in combination with the ionic strength of the solvent caused by high salt concentration, which is explained by a charge screening effect. Cations and water dipoles orient themselves via Coulomb forces with the positive charge towards the reduced (i.e., negatively charged) FeS-center. The rearrangement of the solvent molecules in response to the reduction of the iron-sulfur cluster entropically disfavors the negatively charged state, effectively decreasing the redox potential of the cluster. Similar trends were proposed for [4Fe-4S]-clusters[60;227;247]. The protein toolset for the modulation of the redox potential is additive and extends further, including coulombic effects through nearby charged residues or co-factors[205].

In the Trx-like [2Fe-2S] ferredoxins, a charge inversion mutant of a nearby H-bonded arginine (the R13E mutant in *A.aeolicus*) caused a drop in redox potential by 90 mV, highlighting the importance of charges around the [2Fe-2S]-center and the effect of H-bonds[146]. In Trx-like [2Fe-2S] cluster domains inserted into bioenergetic proteins, similar mutagenesis experiments supported the redox potential determining factors elaborated from Trx-like [2Fe-2S] Fd, especially highlighting the effects of H-bonding and solvation. The "N1a" [2Fe-2S]-cluster in the small (24 kDa) NuoE subunit of the well-studied complex I (*E.coli* nomenclature) is found in the C-terminal Trx-like [2Fe-2S] domain fused to an N-terminal 4-helix bundle. The experiments on this domain were motivated by the curious observation of widely variable redox potentials of the same [2Fe-2S]-cluster in the same protein complex from different organisms, ranging from -150 mV in *P. denitrificans*[142] to -420 mV in *T. thermophilus*[143]. Furthermore, in some of the characterized complex I, a pH-dependent redox behavior has been observed, which is rather uncommon for an all-cysteine-coordinated FeS cluster[198].

Two studies by Zu *et al.*(2002)[256] and Birrell *et al.*(2013)[19] of the isolated, overexpressed NuoE subunit from different organisms have dissected the effect of pH and ionic strength[256] from the influence of specific charged amino acids by site-directed mutagenesis[19]. Birrell's mutation study highlighted the importance of the H-bonding network around the cluster and the overall protein charge as the main determining factors for the observed redox properties of the cluster. Specific mutations of charged residues near the iron-sulfur center that would influence the electrostatic environment around the cluster surprisingly seemed to exhibit only a marginal effect. Instead, the presence or

absence of a sulfido-hydrogen-bonded Asn142 (*E.coli* Nomenclature) has been attributed to an increase or decrease of the redox potential of 50 to 80 mV, respectively. The largest decrease in redox potential was observed for the *E.coli* NuoE double mutant V96P/N142M with a potential drop of 100 mV (E°_{WT} = -295 mV, $E^{\circ}_{V96P/N142M}$ = -395 mV). The effect of this mutation was mainly attributed to the absence of a hydrogen bond (by N142M) in conjunction with increased water accessibility (by V96P), which lowers the redox potential due to higher solvation[19].

Zu et al.(2002)[256] confirmed a pH-dependence of the redox potential in isolated NuoE subunits from different organisms (bovine, *E. coli*, *P. denitrificans*, and *T. thermophilus*) which is masked by increasing salt concentrations and completely abolished under 2 M NaCl. At low ionic strength (10 mM), a 60 mV/pH dependence is observed, leading to the identification of pK_a-values in the oxidized and reduced redox state around pH 6. Due to the inability to have identified the responsible protonatable amino acids by site-directed mutagenesis, such as nearby histidines (H79A, H129A), aspartates (D114N), and glutamates (E123Q), in which all mutants showed the same pH/ionic strength behavior, the observed pH-dependence of the redox potential is hypothesized to be a result of non-specific protonation events, which alter the overall protein charge[256]. A similar tendency of redox potential modulation favoring the importance of the protein's overall charge instead of specific residues was predicted for the *C. pasteurianum* Trx-like [2Fe-2S]-Fd[146]. The molecular details of this dependence are not understood.

For the isolated HydC subunit in the [FeFe]-hydrogenase HydABC of *T. maritima*, a NuoE-homolog, similar studies confirmed the importance of hydrogen bonds as determining factors of the redox potential[18;216]. The WT Trx-like [2Fe-2S]-cluster, termed C1 in HydC, features a redox potential (E°) of -368 mV. The introduction of large non-polar amino acids (such as Ile, Leu, Met) decreased this redox potential, while smaller and more polar amino acids which could form hydrogen bonds to the cluster increased the redox potential[18]. For all the tested mutants and the WT, only a marginal pH-dependence [n] was observed.

The here presented studies highlight the redox properties of the isolated Trx-like subunits. However, the effects from the neighboring subunits on these properties have not yet been assessed in detail. Due to the observation of two different conformational states of the Trx-like [2Fe-2S] domain in HydC, termed "HydC-in" and "HydC-out" (see Section 1.4.1,[111]), the redox properties of the surface-exposed C1 in the "HydC-out" state are expected to change in accordance with a difference in solvation as compared to the "HydC-in" state when the cluster is buried inside the HydB subunit. From the above conducted studies, the more solvent exposed "HydC-out" state is expected to feature different redox properties than the "HydC-in" state.

[n] $\sim$ -8 pH/mV in absence of NaCl, $\sim$ -2 pH/mV with 0.5 M NaCl; redox range: -360 to -420 mV[18]

1.5.2 Spectral characteristics of Trx-like [2Fe-2S]

UV/Vis-Spectroscopy: Trx-like [2Fe-2S]

Trx-like-[2Fe-2S] feature unique optical absorbance characteristics which distinguishes them from the generally rather feature-less UV/Vis spectra of other FeS-clusters. These characteristics have been exploited during this thesis. In the oxidized $[2Fe\text{-}2S]^{2+}$ state, Trx-like-[2Fe-2S] display broad absorption bands around 333, 420, 460, and 550 nm[146]. Upon reduction, most of the absorbances in the visible range of the resulting $[2Fe\text{–}2S]^{+}$ state disappear to the exception of a single peak observable at ca. 560 nm, which is red-shifted by ∼10 nm and with approximately half of the extinction properties as compared to its oxidized counterpart (figure 1.17).

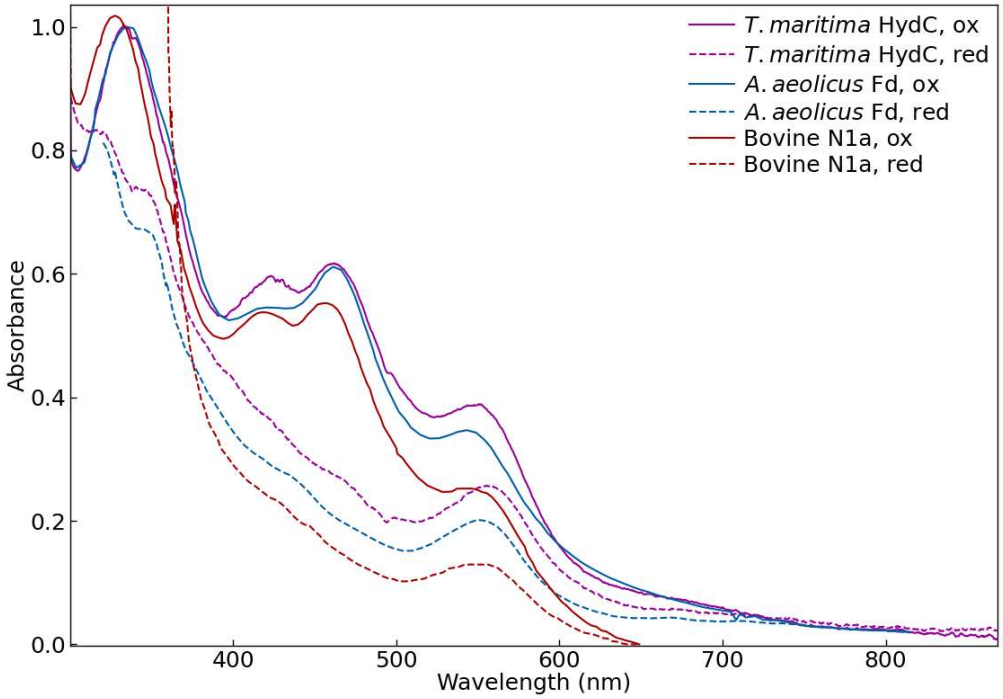

Figure 1.17: UV/Vis-Spectra of the Thioredoxin-like [2Fe-2S]-cluster from three different proteins in the oxidized (solid line) and reduced (dashed line) states. The literature spectra were extracted for the C1-cluster in *T.maritima* HydC[19], Trx-like-[2Fe-2S] ferredoxin of *A.aeolicus*[40] and the N1a-cluster in NuoE from bovine complex I[256]

EPR-Spectroscopy: Trx-like [2Fe-2S]

In the oxidized diferric $[2Fe\text{-}2S]^{2+}$-cluster, both Fe atoms are in the 3+ state, antiferromagnetically coupled, resulting in an overall diamagnetic $S = 0$. Upon reduction, one of the Fe atoms undergoes a transition to the 2+ state, while the other remains in the 3+ state, resulting in the EPR-detectable paramagnetic S = ½ species. Due to their slower relaxation rates, [2Fe-2S]-clusters are observed by EPR in a wider temperature range generally below 100 K. Trx-like [2Fe-2S] features a rhombic spectrum with a characteristic g_z at an unusually high field, around the radical $g = 2.000$

signal (figure 1.18), whereas the g_z of most other [2Fe-2S]-clusters is found at lower fields (i.e. higher g-values).

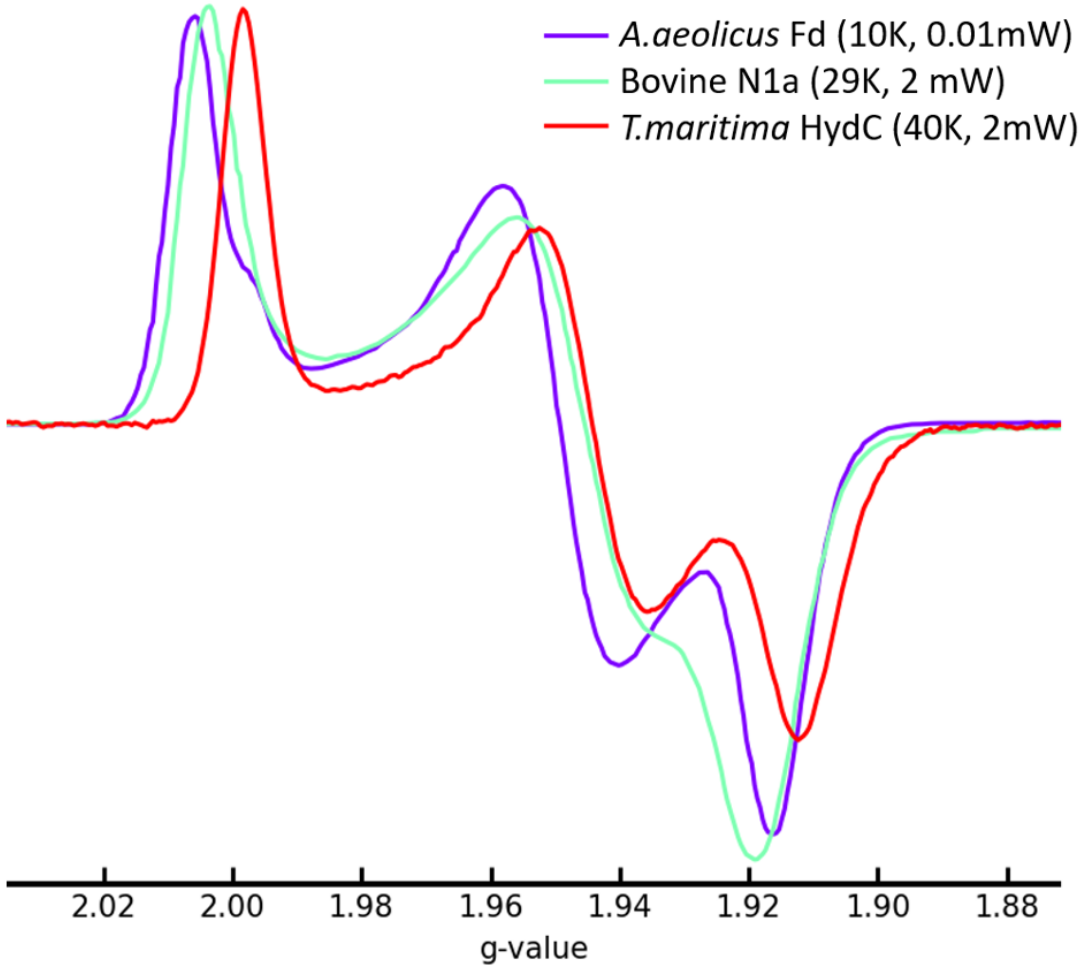

Figure 1.18: EPR-Spectra of Thioredoxin-like [2Fe-2S]-cluster from three different proteins. The literature spectra were extracted for the *T.maritima* HydC C1 spectra in red with g_z=1.998, g_y=1.948 and g_x=1.913, Trx-like-[2Fe-2S]-containing ferredoxin of *A.aeolicus*[40] in violet with g_z=2.006, g_y=1.950 and g_x=1.918 and the N1a-cluster in NuoE from bovine complex I[256] in light green with g_z=2.003, g_y=1.944 and g_x=1.917.

1.5.3 Ferredoxin-like [4Fe-4S]-clusters

While various types of ferredoxins (Fd) that harbor [2Fe-2S]-clusters exist, such as the Trx-like Fd mentioned above, [4Fe-4S]-cluster containing Fd, potentially due to the increased redox-stability of the cubic [4Fe-4S] assembly, outnumber their 2Fe counterparts[145]. Organisms employ these redox-proteins as soluble electron shuttles, which realize electron flux between electron donors to appropriate electron acceptors inside the cell. The “clostridial-type” Fd contains an evolutionarily ancient motif[64] and characteristically harbors a pair of [4Fe-4S]-clusters (hereafter 8Fe-Fd), that are coordinated in a $\beta\alpha\beta\beta\alpha\beta$-architecture, with the individual [4Fe-4S]-centers in electron-transfer distance (ranging around 10 to 13 Å^3). Thus, 8Fe-Fd are typically able to shuttle 2 electrons, in a redox

potential range around -400 mV[199].Some 8Fe-Fd, however, have lost one of the [4Fe-4S]-clusters, while retaining the entire fold and others have lost one coordinating cysteine and have become [7Fe-8S]-ferredoxins.

Besides being expressed as separate redox-proteins, 8Fe-Fd are also found as N- and C-terminal extensions in various proteins such as pyruvate ferredoxin oxidoreductase (PFOR[144]), photosystem I[70], respiratory complex II[173] or the above-mentioned electron-bifurcating Etf-homolog CarCDE[56] as well as in the Ldh-EtfAB, the latter of which represents an example where one [4Fe-4S]-cluster was lost[112]. In addition, in the electron-bifurcating HdrABC-MvhAGD-complex (see figure 1.12) an 8Fe Fd-like domain is evident, inserted between two domains in the HdrA subunit[7;222].

In HydABC, such an 8Fe Fd-like domain containing 2 [4Fe-4S]-clusters B3 and B4 is found in the C-terminal domain (short CTD) of the FMN-containing HydB subunit (figure 1.13). In addition, between the FMN and the H-cluster, inside the N-terminus of HydA an inserted 8Fe Fd-like domain with the [4Fe-4S]-clusters A2 and A3 is found inside a Y-shaped arrangement of 4 FeS clusters (also called the Y-junction module[258], see Chapter 3).

Spectral characteristics of Ferredoxin-like [4Fe-4S]-clusters: EPR-Spectroscopy and Spin-Spin coupling

Whereas [4Fe-4S]-clusters in UV/Vis-spectroscopy feature rather broad absorbance bands centered around 410 nm, the EPR characteristics are more refined. In oxidized [4Fe-4S]-clusters, two of the four iron atoms exist formally as ferric (Fe^{3+}), the other two as ferrous (Fe^{2+}). The delocalization of the electrons over the entire cluster causes all four iron atoms to effectively exhibit an $Fe^{2.5+}$. Anti-ferromagnetic coupling between these single irons yields an overall EPR-invisible $S = 0$ state, as for [2Fe-2S]-clusters. The reduction of a [4Fe-4S]-cluster causes one of the two ferric irons to take up an electron and become 2+ from 3+, which results in an overall S = ½. Due to their faster relaxation properties [4Fe-4S]-clusters are studied by EPR at lower temperatures, usually below 40K.

EPR-spectra on many 8Fe-Fd upon strong reduction, show considerably more structure than could be accounted for from two individual S = ½paramagnets. This is due to spin-spin coupling interactions between the individual reduced centers, that can differently affect the observed spectral properties. Primarily, two types of interactions can be distinguished: dipole-dipole interactions and electrostatic exchange interactions[138].

The dipole-dipole interaction (also known as dipolar coupling) arises from the magnetic dipole moments of the individual paramagnetic centers. When these two paramagnets are in close proximity, their magnetic dipoles interact. The strength of the dipolar coupling primarily depends on the distance between the paramagnetic centers, with closer proximity leading to stronger coupling. This interaction can be observed by broadening of the EPR signals and/or a splitting of the reso-

nance lines, apparent as additional signals (so-called "wings") flanking the central resonance, as demonstrated for various soluble 8Fe ferredoxins and 8Fe ferredoxin-like domains[9;138;185].

Electrostatic exchange interaction (or simply exchange coupling) arises from the overlap of electron wave functions between neighboring paramagnetic centers. It depends on the relative orientation and spatial overlap of the magnetic orbitals of the centers. Exchange coupling can lead to a shift in the one or multiple g-values of the EPR signals, as for the 8Fe Fd FeS-clusters in photosystem I[1;74].

1.6 The Flavoenzyme-environment tunes the electrochemical properties of its flavin

The establishment of redox potential inversion for the individual redox transitions of the flavin within flavoenzymes required for electron bifurcation (EB) is presumed to be achieved through analogous mechanisms as those demonstrated for the QBEB process occurring at the Q_o-site of Rieske/cyt*b*-complexes (section 1.2.4). The flavin's isoalloxazine is a highly polarizable chemical group, i.e., the electron distribution on the heterocyclic π-electron system and therefore the individual electron transitions $E_{OX/SR}$ and $E_{SR/RED}$ are greatly influenced by its direct microenvironment. In aqueous solution, flavins feature a low populated single-electron semi-reduced state accounting for less than 5% in equimolar mixtures of fully oxidized and fully-reduced flavins[84;163]. This phenomenon points to inverted redox potentials for the individual one-electron transitions (as outlined in section 1.2.3). Thus, an apparent two-electron transition from the oxidized to the fully-reduced species at a standard midpoint potential (E_m°) for free FMN of -207 mV is observed[140]. The underlying single-electron potentials were determined by EPR spectroscopy of this low-concentrated, semi-reduced population as well as by pulse radiolysis[6;62]. The redox potentials for the reduction of the oxidized flavin to the semi-reduced species $E_{OX/SR}$ and the reduction of this semi-reduced species to the fully-reduced species $E_{SR/RED}$ were determined at -313 mV and -101 mV respectively (reviewed in Mayhew (1999)[140]). Thus, with a $\Delta E = -212$ mV, the inverted redox potentials of $E_{OX/SR}$ and $E_{SR/RED}$ are characterized by a stability constant of the semi-reduced flavin of $\log(K_s) = -3.5$.

The flavin's redox properties significantly change with the proticity of the medium, due to effects on the hydrogen-bonding (H-bonding) abilities of the isoalloxazine with the nearby bonding partners[208;209]. This leads to the observation of redox midpoint potentials $E_{m,OX/RED}$ for flavins in flavoenzymes ranging from -400 mV to +70 mV[81]. Inside the protein microenvironment, a multitude of parameters, such as electrostatic-, π-stacking- or van der Waals- interactions are proposed to electronically fine-tune the isoalloxazine's redox properties[75;156;176;179]. This leads to the observation of a continuum of different redox transitions between the three redox states with crossed or

uncrossed redox potentials in various flavoenzymes[13;81].

1.6.1 pK_a-values of the isoalloxazine's N(1) , N(3) and N(5)

The flavin's isoalloxazine forms H-bonds with its immediate environment. The presence or absence of these H-bonds in the different redox states are one of the main determinants of the thermodynamic redox-properties of the flavin[102;191]. The isoalloxazine features primarily three protonation sites namely the nitrogens N(1), N(3) and N(5) (figure 1.20). The propensity of these nitrogen's to get protonated is foremost determined by the redox state of the flavin and tuned by the H-bond network surrounding the isoalloxazine together with other factors such as electrostatic interactions. In the deprotonated state these nitrogens act as a H-bond-acceptor, whereas when protonated they become H-bond-donors. Also the neighboring oxygens O(2) and O(4)[o] in the isoalloxazine act as H-bond-acceptors, which are thought to enhance the electron-accepting capacity of the N(5) and could also theoretically be protonated[94;167;257].

In the biological context, the most common H-bond partner for the flavin are amino acid residues in the binding pocket of the flavoenzyme. H-bonding of the flavin with these amino acids either occurs via their functional side chain residues such as for example, the hydroxyl (-OH) of Serin254 to the N(5) of the isoalloxazine as in the non-electron-bifurcating wEtf from the methylotopic bacteria W3A1[241], but also from the peptide backbone. In the well-studied flavodoxin from *Clostridium beijerinckii*[26;100;130], the backbone carbonyl (C=O) in between the Gly57 and Asp58 acts as a H-bond-acceptor, thereby stabilizing the neutral semi-reduced redox state of the N(5) protonated FMN[25;39;75]. In flavodoxin and many other proteins, the main-chain amide-groups (NH2) function as H-bond donors to the isoalloxazine O(2) and O(4).

In many flavoenzymes, specific protein folds such as the commonly observed flavin-binding Rossmann fold[196], are characterized by a solvent accessible flavin-binding cavity[221]. Structurally conserved water molecules inside such Rossmann Fold-like binding pockets[24], attach the flavin to the enzyme and stabilize the surrounding protein domains. These waters make up one of the most frequent H-bond partners to the isoalloxazine, with an average interaction distance of 3 to 5 Å[221]. In various flavoenzymes, such as glucose oxidase, oxynitrilase[221] and Etf[86], waters are proposed to act as H-bond donors or H-bond acceptors to the N(5) for the anionic or neutral semi-reduced redox state, respectively. Their role in tuning the redox properties of the isoalloxazine is rather unclear. A modified Rossmann Fold-like protein architecture is observed in the NuoEF from Complex I where an extensive H-bond network around the flavin was demonstrated in multiple redox states [193]. In the homologous HydBC-subcomplex the presence of some water molecules are only evident in the

[o]Since the protonation of the isoalloxazine oxygens has to my knowledge never been experimentally observed, they will not be further considered.

Cryo-EM structure models of *T.maritima*[80].

1.6.2 Proton-coupled redox transitions induce pH-dependent redox potentials

There exists an intricate relationship between the redox potentials of the individual electron transfer reactions of the isoalloxazine (n = 1 : $E_{OX/SR}$, $E_{SR/RED}$; n = 2: $E_{OX/RED}$) and the proton stabilization constant, the pK_a-value, for each of these sites. In the microscopic framework, the pK_a-value of N(1), N(3), and N(5) change with the redox state of the flavin. In a mutual fashion, changes in the protonation behavior for one or more of these sites induce shifts in the respective redox potentials and the degree of redox cooperativity between the individual electron transfers. This relationship leads to pH-dependent redox-potentials of the flavin, where the protonation of a certain site is directly thermodynamically coupled to a redox transition, short proton-coupled electron transfer (PCET).

This relationship is dissected in the following on a simple thermodynamically coupled one-electron/one-proton transfer.

The Nernst equation 1.8 relates the redox potential of the entire system ($E_{h,pH}$) at a specific pH to the relative populations of oxidized (OX) and reduced species (RED) [p] of the redox compound with a redox midpoint potential ($E_{m,pH}$) at this pH-value:

$$E_{h,\mathrm{pH}} = E_{m,\mathrm{pH}} + \frac{RT}{nF} \ln\left(\frac{[\mathrm{OX}]}{[\mathrm{RED}]}\right) \tag{1.8}$$

where n is the number of transferred electrons, F is the Faraday constant ($F = 96485\,\mathrm{J\,V^{-1}}$) and R the gas constant ($R = 8.314\ \mathrm{J\ mol^{-1}\ K^{-1}}$). The conversion from natural to decadic $\log_{10}$ ($\ln = 2.303 \cdot \log_{10}$) and at ambient temperature ($T = 30°C = 303$ K) gives a rounded prefactor of 60 mV/n (or 59 mV/n at 21°C):

$$E_{h,\mathrm{pH}} = E_{m,\mathrm{pH}} + \frac{0.06}{n} \cdot \log_{10}\left(\frac{[\mathrm{OX}]}{[\mathrm{RED}]}\right) \tag{1.9}$$

Similarly, the Henderson-Hasselbalch expression, the proton-analog to the Nernst Equation, describes the dependence of the proton-affinity (correctly the change in free energy associated with the (de)-protonation) expressed as the pK_a-value to the pH of the solution and the relative populations[q] of the protonated acid (HA) and its corresponding deprotonated base species (A^-):

$$\mathrm{pH} = pK_a + \log_{10}\left(\frac{[\mathrm{A^-}]}{[\mathrm{HA}]}\right) \tag{1.10}$$
$$\text{with } \mathrm{pH} = -\log_{10}([H^+])$$

[p]The Nernst equation actually relates the activity coefficients (γ) of the oxidized and reduced species to each other and the redox potential. Under the assumption that the activity coefficient of both redox species is the same, the relative concentrations are used to simplify the equation.

[q]Again the activity coefficients (γ) of the protonated and deprotonated species, which will be set to one thus the relative concentrations can be taken to simplify the equation.

Due to purely electrostatic reasons, the oxidized and reduced forms of the redox species are expected to feature different proton affinities. The reduced form with n additional negative charges attracts the positively charged protons (H^+) to a larger degree[125]. The difference in proton affinity of the oxidized and reduced species leads to the observation of a $pK_{a,\,OX}$ and $pK_{a,\,RED}$ for a single protonatable site, respectively, with $pK_{a,\,OX} < pK_{a,\,RED}$.

Experimentally, the two pK_as of a redox component that undergoes a thermodynamically coupled proton-transfer with a single electron transfer, are determined by performing redox titration experiments in different pH-buffered solutions to determine the $E_{m,\mathrm{pH}}$ over a range of pH values. In this case, three pH-regions are distinguished (figure 1.19):

1. At pH-values below the $pK_{a,\,OX}$ (below pH 4 in figure 1.19), both redox species are predominantly protonated, and thus no proton is transferred alongside the electron transfer:

$$[\mathrm{RED}]H \rightleftharpoons [\mathrm{OX}]^+H + e^-$$

2. At low proton concentration, thus pH-values above the $pK_{a,\,RED}$ (above pH 10 in figure 1.19), both redox species are primarily found in the deprotonated state, and protons don't participate in the redox reaction:

$$[\mathrm{RED}]^- + H^+ \rightleftharpoons [\mathrm{OX}] + e^- + H^+$$

3. For redox reactions in which the ambient pH is in between $pK_{a,\,OX}$ and $pK_{a,\,RED}$, a direct relationship between the protonation and redox events is observed, resulting from a tightly coupled net release or binding of a proton during the redox reaction:

$$[\mathrm{RED}]H \rightleftharpoons [\mathrm{OX}] + H^+ + e^-$$

From this behavior, the Nernst expression of a single electron transfer, which is thermodynamically coupled to a protonation event, can be shown to follow[152]:

$$E_h = E_{m,\mathrm{pH0}} - 0.06\,\mathrm{V} \cdot \log_{10}\left(\frac{1+\frac{K_{a,\mathrm{OX}}}{[H^+]}}{1+\frac{K_{a,\mathrm{RED}}}{[H^+]}}\right) \tag{1.11}$$

with $pK_{a,\mathrm{OX}}$ and $pK_{a,\mathrm{RED}}$ defined as proton association constants K_a with $pK_a = -\log_{10}(K_a)$:

$$K_{a,\mathrm{OX}} = \frac{[OX] + [H^+]}{[[OX]^+H]}$$
$$K_{a,\mathrm{RED}} = \frac{[RED^-] + [H^+]}{[REDH]}$$

$E_{m,\ \mathrm{pH0}}$ represents the redox potential at 1 molar proton concentration (pH 0), where (presumably) both species, as shown in case 1, are in their protonated form, and thus, no proton is exchanged alongside the electron transfer. Experimentally, $E_{m,\mathrm{pH0}}$ can only be extrapolated due to the instability of the protein system at such high proton concentrations.

Similarly, the behavior of a coupled one proton release/binding during the redox reaction can be described, initially from case 2, i.e., at high pH-value, with the proton concentration approaching zero, such as if the redox reaction would be measured in aprotic solvents, with $\mathrm{E}_{m,\mathrm{pH}\to\infty}$ describing the redox potential at high pH ($\mathrm{pH}\to\infty$) [125]:

$$E_h = E_{m,\mathrm{pH}\to\infty} - 0.06\cdot\log_{10}\left(\frac{1+\frac{[H^+]}{K_{a,\mathrm{OX}}}}{1+\frac{[H^+]}{K_{a,\mathrm{RED}}}}\right) \tag{1.12}$$

As shown in figure 1.19, when $pK_{a,\mathrm{OX}}$ and $pK_{a,\mathrm{RED}}$ are widely separated, this manifests itself as a 60 mV-shift of the E_m per pH-unit for a one-electron ($n=1$)/one-proton transfer and a 30 mV/pH dependence for a two-electron ($n=2$)/one-proton transfer. The latter of which is characteristic for the hydride-transferring cofactor $\mathrm{NADP^+/NAD(P)H}$.

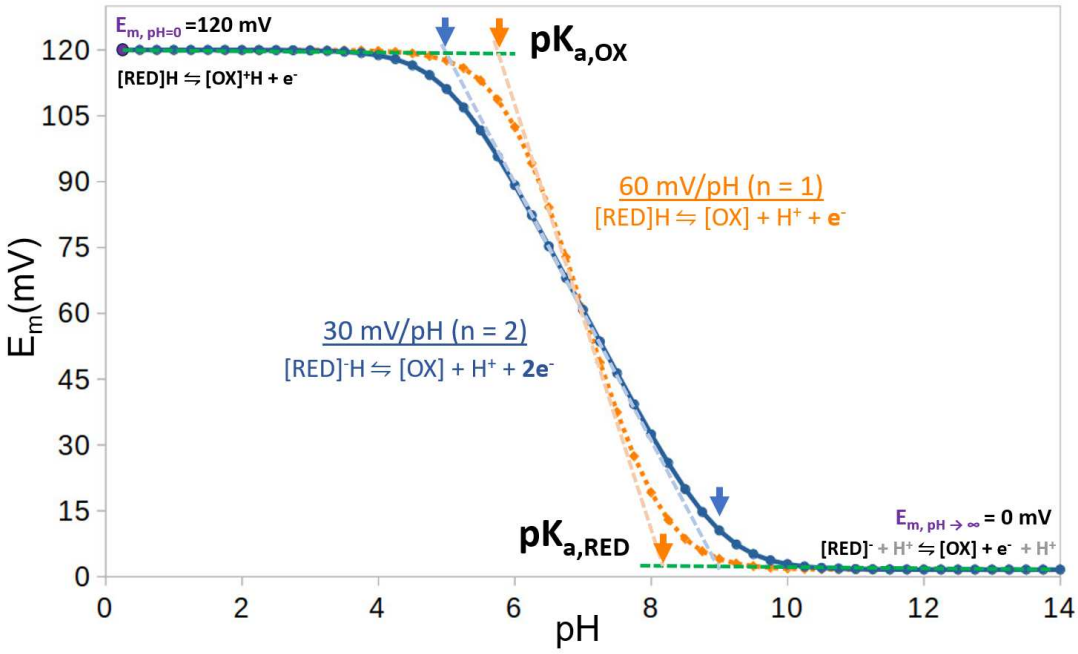

Figure 1.19: E-vs-pH diagram of a simulated $n=1$ and $n=2$ electron transfer coupled to a single proton transfer. The simulated curves permit an identification of a $\mathrm{pK_{a,OX}}$ and $\mathrm{pK_{a,RED}}$ for a two-electron transfer (blue, $\mathrm{pK_{a,OX}}=5$; $\mathrm{pK_{a,RED}}=9$) and one-electron transfer (orange, $\mathrm{pK_{a,OX}}=6$; $\mathrm{pK_{a,RED}}=8$). The curves were simulated to feature the same $E_{m,\mathrm{pH0}}=+120$ mV and $E_{m,\mathrm{pH}\to\infty}=0$ mV and follow the mentioned pH-dependence slope of 30 mV/pH and 60 mV/pH for $n=2$ and $n=1$, respectively.

1.6.3 pH-dependent redox potentials of flavins and flavoenzymes

This E_m-pK_a-formalism described above was initially summarized in Clark's "Oxidation-reduction potentials of organic systems"(1960)[44] and can be extended to any number of thermodynamically coupled protonation and redox events performed by a single chemical compound.

The equation 1.12 can be easily adapted to *n* numbers of transferred electrons per proton via the 0.06 V/n prefactor. Under the assumption of mainly three protonatable sites for flavins (section 1.6.1), the resulting equation must include the $pK_{a,\,OX}$, $pK_{a,\,SR}$ and $pK_{a,\,RED}$ of all three isoalloxazine nitrogens N(1), N(3), N(5).

An ensemble of different experimental techniques on free flavins in aqueous solutions in conjunction with the fitting of the above described equations to the pH-dependent redox potentials of the individual waves allowed for the attribution of $pK_{a,\,OX}$, $pK_{a,\,SR}$ and $pK_{a,\,RED}$ of all three isoalloxazine nitrogens N(1), N(3), N(5) (see figure 1.20, Table 1.2) as reviewed in Mayhew (1999)[140].

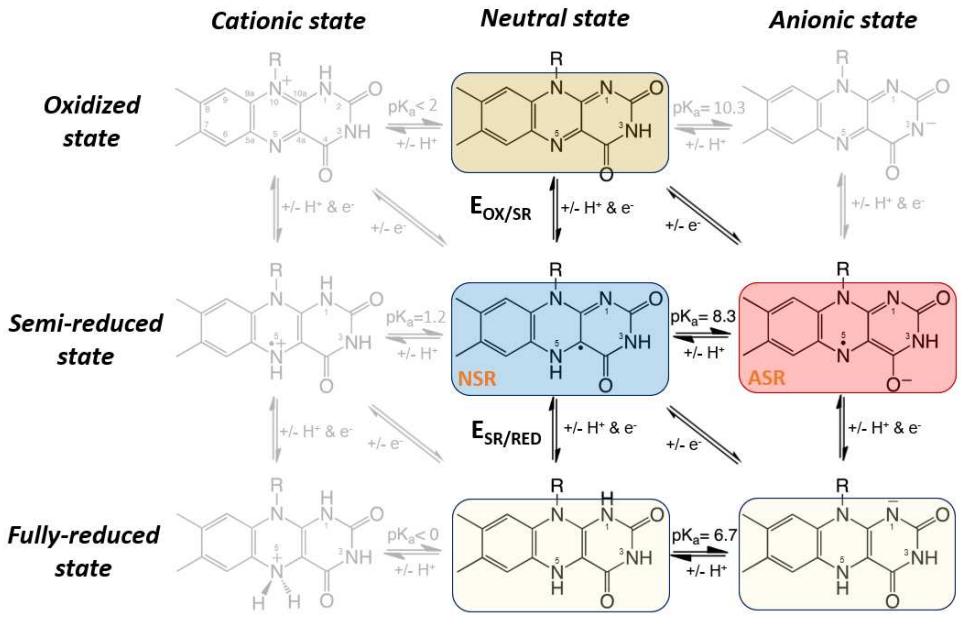

Figure 1.20: Thermodynamic transition scheme for flavin. Scheme highlights the thermodynamically most populated microstates of the flavin (shown in the *si*-face orientation) under physiological conditions. Horizontal transitions denote protonation events, diagonal transitions involve electron transfers, while vertical transitions involve proton-coupled electron transfers (PCET) between two microstates. The strongly yellow colored oxidized state (yellow box) is the name-giving feature of this compound class. The neutral "blue" (NSR) and the anionic "red" semi-reduced state (ASR) are well-distinguished spectroscopically (see below) and are highlighted in blue and red boxes, respectively. The reduced states are pale yellow colored (pale yellow colored box). Note that due to the π-bond character of the isoalloxazine-moiety many of these states exist in multiple resonance structures, but only one of these structures is shown here. pK_a values are taken from FMN in aqueous solution[140] as shown in Table 1.2. Figure adapted with permission from Sobrado (2012)[201] under a Creative Commons Attribution License.

As shown in figure 1.20 and Table 1.2 for each oxidation state of free FMN, there are protonation events that affect the redox potentials observed at physiological pH in aqueous solution: the pK_a of 10.3 for the oxidized on N(3) ($pK_{a,\,OX,\,N(3)}$), the pK_a of 8.3 for the semi-reduced on N(5) ($pK_{a,\,SR,\,N(5)}$) and the pK_a of 6.7 at the fully-reduced FMN on N(1) ($pK_{a,\,RED,\,N(1)}$).

Table 1.2: pK_a values from the three nitrogens N(1), N(3) and N(5) of the isoalloxazine in FMN in aqueous solution in the different redox states. Values obtained from [6;62;148;149] and reviewed in Mayhew (1999) [140].

	$\mathbf{pK}_{a,OX}$	$\mathbf{pK}_{a,SR}$	$\mathbf{pK}_{a,RED}$
N(1)	< 2	1.2	6.7
N(3)	10.3	> 12	$>> 12$
N(5)	-0.5	8.3	> 12

The protein environment has the capacity to significantly influence the individual redox transitions of the flavin by means of H-bonding with the isoalloxazine's N(1) , N(3) and N(5) (section 1.6.1) and therefore shifting the respective pK_a values of the three nitrogens. To illustrate this, the FMN in flavodoxin (Fldx) from *Clostridium beijerincki* is one of the best-studied flavoenzymes (Table 1.3). In Fldx, a stabilizing H-bond interaction of the nearby glutamate (Glu59) to the N(3)H (affecting the $pK_{a,\,OX}$) has been postulated to anchor the isoalloxazine inside the protein [25;26]. The N(5) $pK_{a,\,SR}$ of the semi-reduced FMN redox state is upshifted by more than 5 pH-units to $pK_{a,\,SR,\,N(5)} = 13.9$ (as compared to 8.3 in free FMN), leading to a strongly stabilized NSR species protonated at the N(5). Therefore, the above-mentioned crossed-over redox potentials in free FMN become uncrossed in flavodoxin leading to $E°_{OX/SR}$ = -92 mV and $E°_{SR/RED}$ = -399 mV (Table 1.3) [100;102;130].

The N(5)H proton on the semi-reduced FMN is thereby stabilized by the H-bond accepting protein backbone carbonyl (C=O) group from a glycine (Gly57) which is found inside a flexible loop and approximately 3 Å away from the N(5)H [229]. Mutation of this residue to a threonine (G57T) causes a more rigid loop and a less favorable N(5) H-bond, effectively lowering the proton affinity of the N(5) to $pK_{a,\,SR,\,N(5)} = 11.3$. Indeed, the NSR state in this G57T-mutant strain is more destabilized compared to the WT Fldx which is reflected by the redox potentials $E_{OX/SR}$ = -270 mV and $E_{SR/RED}$ = -320 mV [130]. This illustrates how a single H-bond on the isoalloxazine N(5) affects the redox properties of the flavin.

Table 1.3: Comparison of $pK_{a,SR,N(5)}$ and $E_{OX/SR}/E_{SR/RED}$ in free FMN as compared to wildtype (WT) and Glycine-57-Threonine (G57T) mutant of *C. beijerincki* flavodoxin (Fldx). [130]

	$\mathbf{pK}_{a,SR,N(5)}$	$\mathbf{E}_{OX/SR}$ **(mV)**	$\mathbf{E}_{OX/SR}$ **(mV)**	$E_{m,OX/RED}$ **(mV)**	ΔE **(mV)**	$\mathbf{log(K_s)}$
Free FMN	8.3	-313	-101	-207	-212	-3.5
Fldx WT	13.9	-92	-399	-245	307	5.2
Fldx G57T	11.3	-270	-320	-295	50	0.9

1.6.4 Interaction of FMN with NADH involves a hydride transfer to N(5)

One of the main functions of flavin-containing enzymes in the bioenergetic context is as NAD(P)H-dehydrogenase. Here, the ability of flavins to occupy and change in between three redox states and

thus being able to interact with both one- and two-electron partners is fully exploited[82].

The NAD(P)$^+$/NAD(P)H couple features strongly crossed-over redox potentials, necessitating a coupled, two-electron transfer process. The kinetics of this two-electron transfer (with an accompanying proton) greatly outcompetes the kinetics of the individual one-electron oxidation or reduction reaction and thus renders the role of the one-electron intermediate (NAD•) in biochemical contexts negligible[89]. Pulse-radiolysis experiments[5] determined the redox potentials of the individual redox-transitions. The determined one-electron oxidation of the fully reduced NADH, $E_{NAD\bullet/NADH} = +290$ mV together with the redox midpoint potential of $E_{m\ NAD^+/NADH}$ = -320 mV[210] allowed the first reduction (NAD$^+$/NAD•) to be determined around -930 mV[5;71;210]. The large redox potential difference ($\Delta E = -1.2$ V) between the different waves results in a thermodynamically strongly destabilized semi-reduced species with $\log(K_s) = -20$.

During the NAD(P)H-dehydrogenation by flavins, electrons are transferred as proton-coupled electron transfer (PCET) involving a hydride anion (H^-) composed of two electrons together with one proton[120;184]. During NAD(P)H oxidation the aromatic rings of NADH and FMN therefore accommodate a π-stacked reactant geometry with ca. 3.5 Å distance from each other (figure 1.21). The reaction proceeds via hydride abstraction, involving the proton transfer from C(3) of the dehydridonicotinamide to the N(5) of the isoalloxazine[20;21;233].

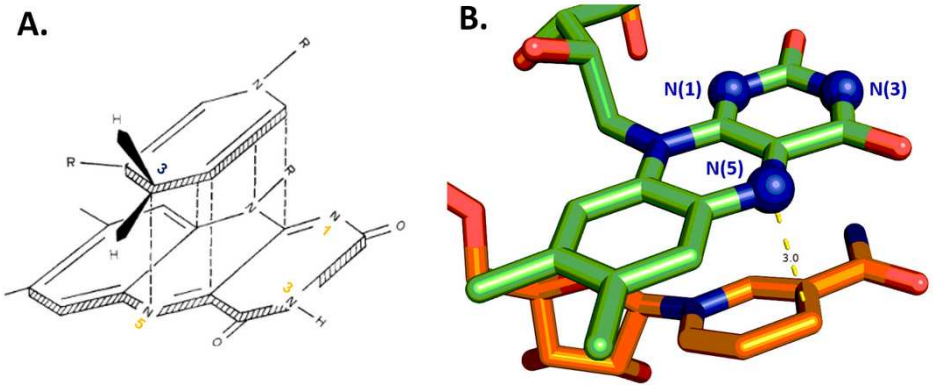

Figure 1.21: Charge-transfer complex of NAD$^+$/NADH and flavin. **A.** Schematic of the pyridine of the nicotinamide (without amide carbonyl (-(C=O)NH2) residue) of NADH (on top) with the isoalloxazine ring of the flavin (*si*-face orientation, on the bottom). **B.** π-stacked configuration of the NADH (carbons in orange) with the FMN (carbons in green) as shown in various crystal structures such as here, in complex I from *A.aeolicus* (PDB-code: 6Q9C) allows for the activation-less hydride transfer involving a proton transfer from C(3) of the nicotinamide to N(5) of the isoalloxazine, over a distance of 3 Ångström (yellow dashed line). Figure adapted with permission from Blankenhorn (1974)[20] under a Creative Commons Attribution License.

The NAD(P)$^+$/NAD(P)H binding can dramatically alter the redox properties of the flavin. This has been proposed for the mammalian xanthine dehydrogenase (XDH)[101]. In this enzyme, the FAD features a one-by-one redox transitions with $E_{OX/SR}$ = -270 mV and $E_{SR/RED}$ = -410 mV (at pH 7.5), thus with a stabilized NSR state of maximal population at $E_{m,OX/RED}$ = -340 mV[98].

The binding of the two-electron acceptor, NAD$^+$ was calculated to destabilize the NSR state by

upshifting the semi-reduced to fully-reduced transition by more than +175 mV, to $E_{SR/RED}$ = -226 mV. Only in this π-stacked NAD^+-FAD configuration the second electron reduction from the high-potential [2Fe-2S]-cluster (Fe/S-II) to the FAD was proposed to occur, which is consequently followed by the two-electron reduction of the NAD^+ in a hydride transfer by the flavin[101].

1.6.5 Spectroscopic means of studying flavins and flavoenzymes

For the assessment of the protonation and redox states of the isoalloxazine, UV/Vis spectroscopy has proven highly effective in diverse flavoenzymes (see figure 1.22)[83;109;137;152]. The addition or abstraction of electrons to or from the isoalloxazine induces an alteration in the delocalized π-electron system of the isoalloxazine, resulting in distinct UV/Vis absorbance spectra for each redox state[83;109;137].

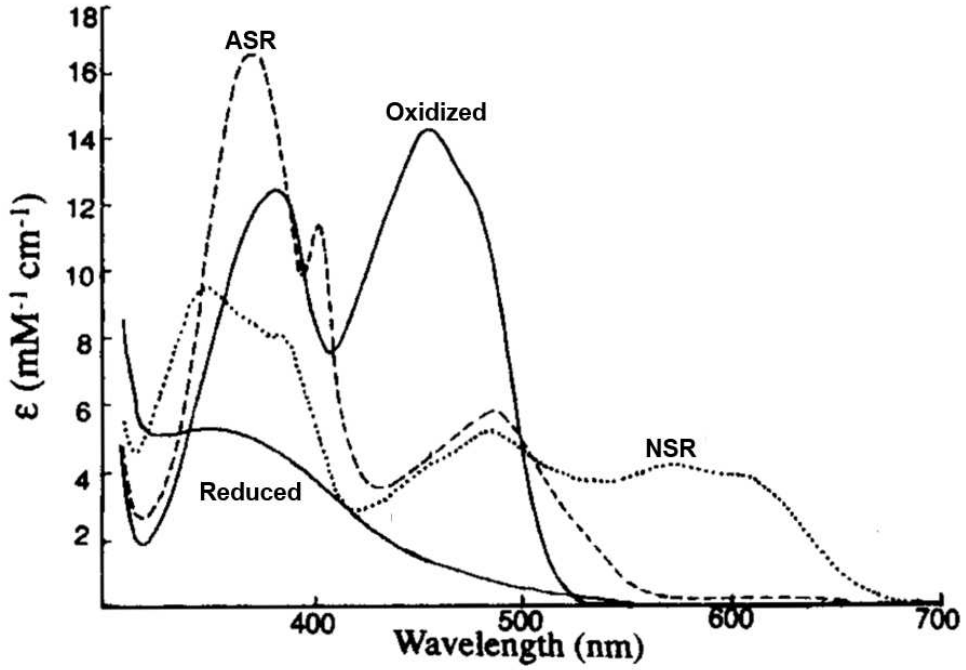

Figure 1.22: UV/Visible absorbance spectra of the oxidized (solid line), neutral semi-reduced (NSR, dotted line) and anionic semi-reduced (ASR, dashed line) and fully-reduced (full line on the bottom) redox state of the FAD in the flavoenzyme glucose oxidase. Figure taken with permission from Massey (1999)[134] under a Creative Commons Attribution License.

The oxidized flavin species, typically in the N(3)-protonated form as indicated by the yellow box in figure 1.20, consistently exhibits three primary bands. These $\pi \rightarrow \pi^*$ transition bands include one in the near-UV region at approximately 260 nm and two in the far-UV-visible region, notably at around 375 nm and 450 nm (figure 1.22). Although the precise position of each band is distinctive for a particular environment and thus protein-specific (see section 1.6.5), it is observed that spectral contributions beyond 500 nm for the oxidized redox state of the flavin are either absent or minimal.

For the fully-reduced flavin species (both anionic and neutral form), the experimental spectra are typically strongly decreased in the 400-450 and 290-300 nm absorbances. Instead, they fea-

ture primarily one ill-defined peak in the 320-355 nm region with large broadened shoulders that protrude further into the visible region[83]. This has been attributed to the bent geometry of the otherwise planar isoalloxazine moiety in the reduced state collapsing the delocalized electron cloud as a means of energy minimization[114]. The isoalloxazine reduced planarity ultimately forms a so-called "butterfly" structure with a folding crest along the N(5)-N(1) axis[165;253]. The phenomenon of a geometrically distorted fully-reduced state has been observed for the flavin in some flavoenzymes such as thioredoxin reductase[123] and in several two-electron compounds exhibiting redox potential inversion[68]. It is suggested to serve as an additional mechanism for fine-tuning the redox potentials of flavins[68;69;224]. Subtle differences in the absorbance spectra between the neutral and anionic reduced species are observed due to their slightly different propensities to occupy these folded states[83].

UV/Vis absorbance spectroscopy has been instrumental in characterizing two physiologically relevant semi-reduced species that are easily distinguishable by their distinct colors. These species include the "blue" neutral and the "red" anionic semi-reduced states, each displaying distinct absorbance properties related to N(5) protonation[137]. The neutral semi-reduced (NSR) state features characteristic low-energy transition bands primarily between 500 nm and 650 nm with a maximum at 580-600 nm, giving it a blue coloration (see figure 1.22). It is thus easily distinguishable from the oxidized species[162]. The N(5)-deprotonated anionic semi-reduced (ASR) species in concentrated solution appears in a red color, due to an overall much stronger absorbance band around 370 nm and a comparably low absorbance band at around 500 nm[66]. For various model flavoenzymes, such as glucose oxidase or xanthine oxidase, all three redox states and both above-mentioned semi-reduced states are well distinguishable if the protein is reduced at different pH-values (figure 1.22)[178;204].

The variability of the UV/Vis-absorbance properties in different flavoenzymes

As outlined above the ability of flavoenzymes to fine-tune the redox properties of their flavins resides mainly in their ability to form H-bonds with the flavin and thus affecting the pK_a values of the protonatable groups. As the electronic transitions of the isoalloxazine and thus the observable absorbance bands of the flavins, are strongly influenced by these protonation events and the presence or absence of the surrounding H-bonding partners, noticeable differences in the spectral features in different flavoenzymes in all redox states are observed[135;141;167;238].

Figure 1.23 highlights the differences in the optical absorbance spectra of the NSR flavin species from 4 different flavoenzymes. Since the stabilization of such a semi-reduced species as outlined above can be realized through different means (H-bonding partners, π-π-interaction, solvent accessibility etc.), the spectral properties belonging to the same microscopic state, here the NSR differ among flavoenzymes. Since these spectral differences offer a rather broad measure of these underlying molecular causes, they have been correlated to techniqes such as NMR spectroscopy[52;161;186;221].

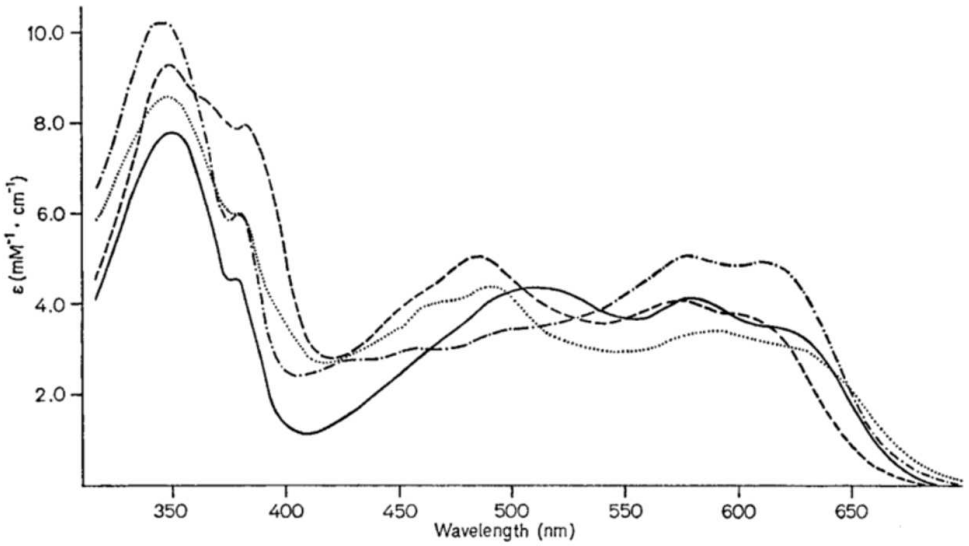

Figure 1.23: Variation in the optical spectra of the neutral semi-reduced (NSR) form of the flavin in various flavoenzymes. The selected spectra are taken from *A. vinelandii* flavodoxin (· - ·), glucose oxidase (- - -), D-amino acid oxidase in the presence of 3-fluorobenzoate (· · ·) and *P. elsdenii* flavodoxin (-). The spectra show the semi-reduced species of the flavin at his highest amplitude which corresponds to a state at the midpoint potential $E_{m,\,OX/RED}$. Figure taken with permission from Müller *et al.* (1972)[162] under a Creative Commons Attribution License.

The same tendencies have been observed for other flavin microstates, i.e. the anionic semi-reduced, oxidized and reduced species[219;239].

X-band EPR-signatures of the flavin's NSR and ASR

Contrarily to UV/Vis-spectroscopy, electron paramagnetic resonance (EPR) spectroscopy require the presence of an unparied, paramagnetic electron on the flavin to allow its detection. This condition is only fulfilled for the semi-reduced radical states of the flavin. As elaborated above, flavins mainly exhibit two different semi-reduced forms, the NSR and ASR state. The X-band EPR signal of these two redox states are easily distinguished by their respective peak-to-trough linewidth (figure 1.24). Due to the presence of a strongly coupled proton at the N(5) position, the EPR spectra of the NSR species exhibit a peak-to-trough linewidth of 19-20 Gauss[163]. Upon incubation of the flavoenzyme in deuterated water (D_2O) this coupling of the N(5) proton decreases, reducing the linewidth to 15 Gauss[65]. The same linewidth (14-15 Gauss) is measured for the ASR radical where no strongly coupled exchangeable proton is present[164].

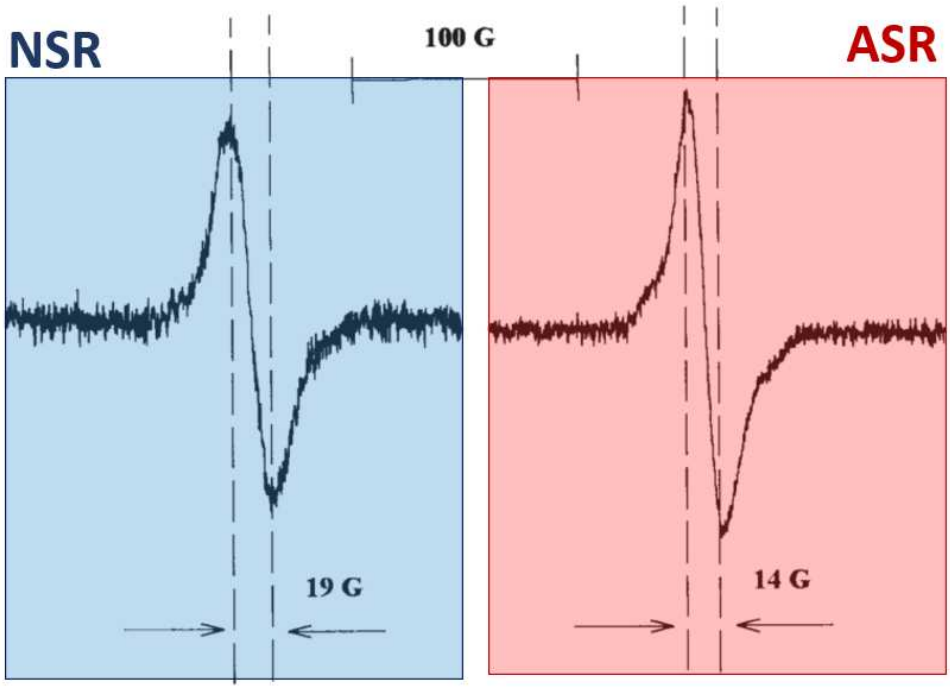

Figure 1.24: X-band EPR spectra of the neutral (NSR) and anionic (ASR) semi-reduced forms of the FAD in the flavoenzyme glucose oxidase. Spectra from 50 μM enzyme-bound photoreduced FAD illuminated for 150 min in buffered solutions at pH 6.0 for the generation of the neutral (blue, NSR), which is identified by a peak-to-trough linewidth of 19 Gauss (G). Same procedure at pH 9.2 for the generation of the anionic semi-reduced (red, ASR) species shows a 14 Gauss separation. Figure adapted with permission from Murataliev (1999) [164]. Copyright 1999, Humana Press Inc., Totowa, NJ

1.7 Aim of the thesis

Flavin-based electron bifurcation/confurcation (FBEB/FBEC) was discovered 15 years ago and recognized as one of the fundamental mechanisms of bioenergetics. The molecular basis of this reaction is well studied for quinone-based electron bifurcation (QBEB) as catalyzed by Rieske/cyt_b complexes [48] and resides in the proton-coupled electron transfers leading to inverted redox potentials (Section 1.2.3) of the hydroquinone in the Q_o-site. The reaction scheme employed by Rieske/cyt_b complexes could be analogously applied to elucidate FBEB in the electron-bifurcating flavoenzymes Etf (Section 1.3.1) and Nfn (Section 1.3.2). However, extending such a projection to the single flavin and its neighboring FeS-cluster in Hyd, the electron-bifurcating/confurcating [FeFe]-hydrogenase, doesn't appear straightforward.

In this thesis, I therefore set out to explore the phylogenetic history and to determine the thermodynamic properties of Hyd in order to lay the basis for a molecular understanding of the reactions catalyzed by the enzyme and more specifically the flavin and its adjacent cofactors.

A phylogenetic approach (chapter 3) has been proven fruitful for bioenergetic enzymes [12;35;63;87;203], including enzymes catalyzing FBEB/FBEC [7;127], due to the evolutionary conservation of structural building blocks in bioenergetic chains. Placing HydABC, as a member of a NAD(P)H dehydrogenase family, in a phylogenetic context of its homologous sister enzymes should allow to detect functionally

important sequence stretches or amino acid residues and to transpose results obtained on homologous enzymes for the formulation of predictions and hypotheses for the enzyme under study.

A thermodynamic characterization (chapter 4), as a complementary approach, will permit the attribution of physicochemical parameters, such as redox potentials and pK_a-values to the flavin and the FeS-cofactors in a particular Hyd complex. The electron-confurcating HydABC enzyme from *Thermotoga maritima* was chosen since it is particularly suitable for this analysis due to its enhanced protein stability arising from its hyperthermophilic origin. The availability of a Cryo-EM structure model[80] of HydABC from this organism, along with the ability to heterologously express the entire complex and its constitutive subunits in *E.coli*[41], should facilitate the attribution of these thermodynamic parameters to specific redox cofactors.

Chapter 2 Methods

In the following chapter, UV/Vis spectroscopy and electron paramagnetic resonance (EPR) spectroscopy for the characterization of flavins and iron-sulfur clusters will be presented. These two spectroscopic techniques have been coupled to redox titrations for the study of the thermodynamic properties of HydABC in *T.maritima* as part of this thesis.

2.1 UV/Vis absorbance spectroscopy

The conjugated π-electron system within the isoalloxazine not only enables flavins to catalyze redox reactions but also imparts them with distinctive spectral properties. The isoalloxazine moiety forms a chromophore, which permits delocalized electrons to transition from lower-energy electronic ground states to higher-energy excited states by absorbing energy from photons at specific wavelengths in the UV/Vis spectrum, as illustrated in figure 2.1. Photon absorption induces the elevation of electrons from the highest occupied molecular orbital (HOMO) in the ground state to the lowest unoccupied molecular orbital (LUMO) in an excited state. Given that each electronic energy state feature multiple vibronic states, transitions from each vibronic state in the electronic ground state to each of the vibronic states in the electronic excited state, result in the observation of specific absorbance lines at mutliple wavelengths which form the characteristic spectra[108].

2.2 Electron paramagnetic resonance (EPR) spectroscopy

Electron Paramagnetic Resonance (EPR) spectroscopy, also known as Electron Spin Resonance (ESR) spectroscopy, allows the study of paramagnetic species, such as molecules or ions with unpaired electrons. It exploits the magnetic properties of unpaired electrons, which have inherent magnetic moments (μ) due to their intrinsic spin, making them paramagnetic and thus responsive to the presence of an external magnetic field. Inside a magnetic field, the unpaired electrons align their spins with the external magnetic field, resulting in the occupation of two distinct energy states for the electron's magnetic moment. In the energetically lower state the electron's spin aligns parallel (S_p, m_s = -½) with the magnetic field, while the other state possesses higher energy as the electron spins

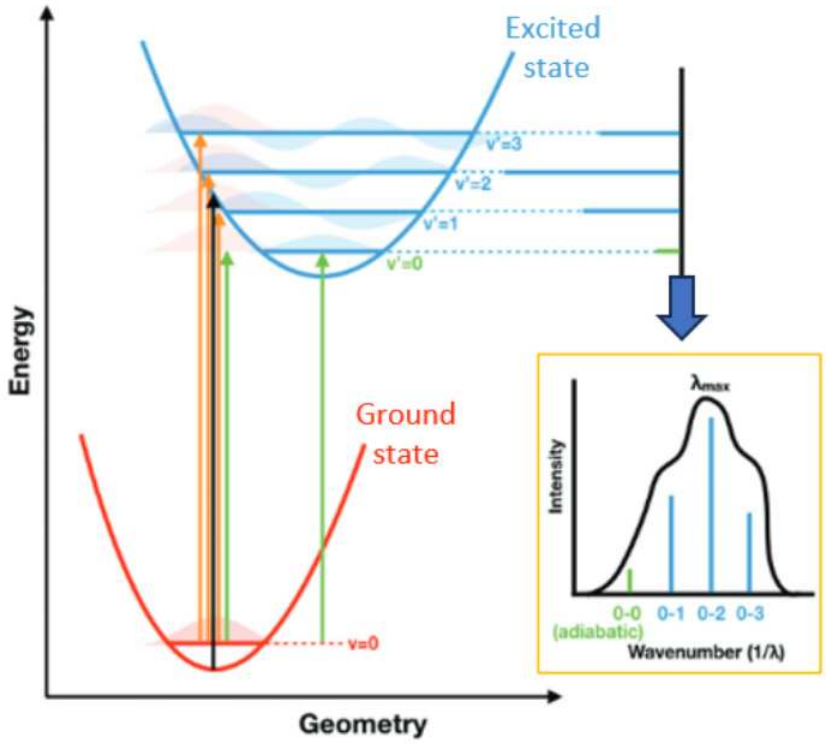

Figure 2.1: Schematic figure showing the physical basis of UV/Vis spectroscopy. The absorption of light at a specific wavelength by electrons within a chromophore facilitates their excitation (depicted by a theoretical black arrow) from the electronic ground state (depicted in red) to an excited state (depicted in blue). Both electronic energy states are characterized by various vibrational states (v = 0, 1, 2, etc.). For simplification, under the assumption that the ground state is always in the lowest vibrational state (at 0 K, v = 0), discrete energy differences (orange arrows) between this lowest vibrational state of the ground state to any vibrational state of the excited electronic states causes absorbances thus resulting in the characteristic UV/Vis absorbance spectra (in yellow box). The intensities of vibronic transitions are determined by the degree of overlap of the ground state vibrational wave function (in light red) and excited state vibrational wave functions (in light blue). Figure adapted from Kabir *et al.*(2019) [108].

are anti-parallel (S_{AP}, $m_s = +½$) to the applied magnetic field. The energy difference (ΔE) between the two energy levels (S_P & S_{AP}) depends linearly on the magnetic field strength (B_0), according to the Zeeman principle (see figure 2.2). Electrons in the parallel S_P spin state can absorb energy, which allows them to transition to the energetically higher, anti-parallel S_{AP} spin state. The energy required for this transition corresponds to the microwave region of the electromagnetic spectrum ($\nu \sim$ GHz), and the absorption of this energy is recorded as an EPR signal [85].

In the Continuous Wave EPR (CW-EPR) experimental design, due to the limited availability of an adjustable microwave sources, the microwave frequency (ν) is kept constant (most commonly 9 GHz "X-band") while the magnetic field (B_0) strength is swept. An increase in the absorption will occur when the magnetic field splits the two spin states in a way that their energy difference (ΔE) exactly matches the energy of the microwave radiation ($h \cdot \nu$) leading to an absorption (resonance condition). Since the magnetic field is swept with an additional modulation, which allows for an increased signal-to-noise ratio, the first derivative of the absorption signal is recorded (see figure2.2).

Since the frequency (ν) of the utilized microwave radiation varies slightly between different ex-

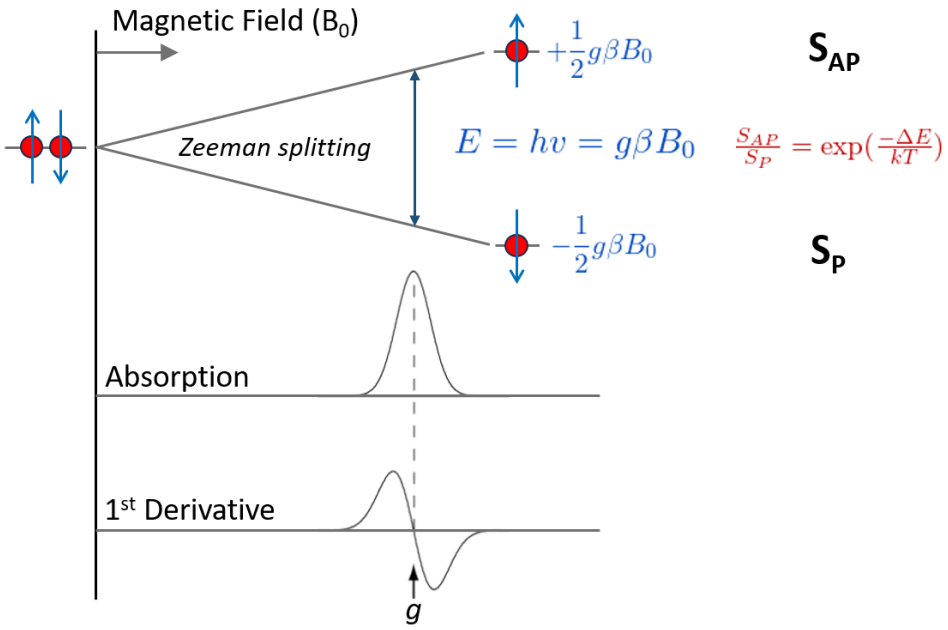

Figure 2.2: Schematic figure showing the theoretical basis of EPR spectroscopy. The external magnetic field (B_0) causes the electrons of the paramagnetic species to adopt two energy states of parallel (S_P) and anti-parallel (S_{AP}) spin (Zeeman splitting). At a given magnetic field, if the difference in energy (ΔE) between the two states equals the frequency of the microwave radiation (ν), an (in this case isotropic) EPR-signal is detected. In the equations, h is Planck's constant ($h = 4.136 \times 10^{-15}$ eV · s) and β is the Bohr magneton ($\beta = 5.788 \times 10^{-5}$ eV · T^{-1}), two fundamental physical constants. The constant of magnetization (g) is obtained by dividing the energy of the microwave frequency by the magnetic field strength and the Bohr magneton. Figure adapted from Ohnishi (1999) [172] under a Creative Commons Attribution License.

periments the position of the obtained EPR-signal is expressed in terms of a "magnetization constant" (commonly known as "g-value"), that contains both the magnetic field strength and the microwave frequency and thus describes a compound-specific property via 2.1 [172]:

$$g = \frac{h \cdot \nu}{\beta \cdot B_0} \tag{2.1}$$

With the fundamental physical constants, h (Planck's constant $= 4.136 \times 10^{-15}$ eV·s) and β (Bohr magneton $= 5.788 \times 10^{-5}$ eV · T^{-1}). For a free electron, the g-value is equal to 2.0023 [85].

2.2.1 The influence of Temperature, Spin Relaxation and Power-Saturation

The energy difference (ΔE) between the two energy levels, S_{AP} & S_P inside the magnetic field around $g = 2.000$ (i.e., in X-band at a magnetic field strength around 350 mT) is relatively low. This energy corresponds to the energy of microwave quanta which are therefore used to excite the electron spins to the energetically higher spin state. The occupation or population of these two energy levels is temperature-dependent. At room temperature in many biologically relevant cofactors such as FeS-clusters, ΔE can easily be overcome by thermal activation according to the Boltzmann factor kT (with the Boltzmann constant $k = 1.380649 \times 10^{-23}$ J · K^{-1}), resulting in a roughly equal occupation of S_P and S_{AP}. At thermal equilibrium, the absorption of microwaves equals emission, and there is no

net EPR signal.

As the temperature is lowered, the energetically lower S_P becomes more populated relative to S_{AP}. The ratio of the occupation of the two energy levels follows a Boltzmann distribution according to $\frac{S_{AP}}{S_P} = \exp\left(-\frac{\Delta E}{kT}\right)$. As a consequence, the EPR-signal grows linearly with decreasing values of $\frac{S_{AP}}{S_P}$ and thus follows the Curie Law[85].

Spin relaxation describes the process of the energy-dissipating return of the excited spin back to the thermal equilibrium. This process is primarily governed by spin-lattice relaxation, which involves interactions of the excited spin with the external surrounding. The detection of an EPR-signal depends on the interplay between the rate of spin relaxation and the absorption of incoming microwave quanta.

When spin relaxation occurs more rapidly than the absorption of microwave quanta, it leads to the generation of a substantial signal, proportional to the intensity of the incoming microwave radiation. Conversely, if spin-lattice relaxation is slow, the observed signal becomes broadened with increasing microwave intensity. In this scenario, the spin system reaches a state of saturation, where both the anti-parallel aligned electron spins (S_{AP}) and parallel aligned spins (S_P) are equally populated. This equality results in microwave quanta having an equal probability of being absorbed by both spin states.

A distinctive phenomenon known as “stimulated emission” occurs when a microwave quanta interacts with an anti-parallel aligned spin (S_{AP}). This interaction triggers the emission of a microwave quanta of the same wavelength, effectively doubling the quanta output (since the “stimulating” quanta is not absorbed). This phenomenon offsets the equal-probable absorption of a single quanta by the energetically lower S_P state, ultimately resulting in the cancellation of the EPR signal[11].

The phenomenon of spin saturation can be amplified through the application of microwave power, which regulates the flow of microwave quanta to which the spin system is subjected. When high microwave power is applied to a spin system with slow relaxation characteristics, it leads to the complete broadening of the signal, a condition referred to as power saturation. Therefore, each spin system has a certain set of parameters that allows a maximal signal detection[185]. Primarily, the temperature at which the EPR scan is performed therefore allows to distinguish different paramagnetic species: [4Fe-4S]-clusters generally exhibit fast relaxation rates, with discernibly sharp lines at 15 K, which begin to broaden around 25 K and become undetectable above 50 K. Conversely, [2Fe-2S]-clusters typically display slightly slower relaxation rates and therefore exhibit saturation behavior at low temperatures, but are characterized by sharp non-saturated lines around 50 K that start to broaden at approximately 90 K but remain readily detectable above 100 K. Organic radicals exhibit exceptionally slow relaxation rates, enabling their detection at high temperatures. Due to

strong saturation at low temperatures these radicals are generally non-detectable below 20 K, often even below 50 K.

2.2.2 g-value anisotropy

The paramagnetic nature of the semi-reduced radical species of the flavin renders an EPR signal at X-band that is characterized by one resonance line of almost Gaussian shape. Such an apparent "isotropic" signal (as shown in figure 2.2) near the g-value of a free electron ($g = 2.0023$) is typical for organic radicals[105]. However, the unpaired electron in the molecular spin system of FeS-clusters is subject to electromagnetic interactions with the surrounding, resulting in more convoluted EPR-signals (figure 2.3).

This gives rise to g-value anisotropy of a paramagnetic center which can be described by a g-tensor composed of up to 3 g-values (g_x, g_y, g_z), each corresponding to the interaction of the magnetic field with one of the spatial directions of spin-system[172]. Due to the 3-dimensional electronic structure of FeS-clusters, they generally exhibit axial or rhombic signals (figure 2.3).

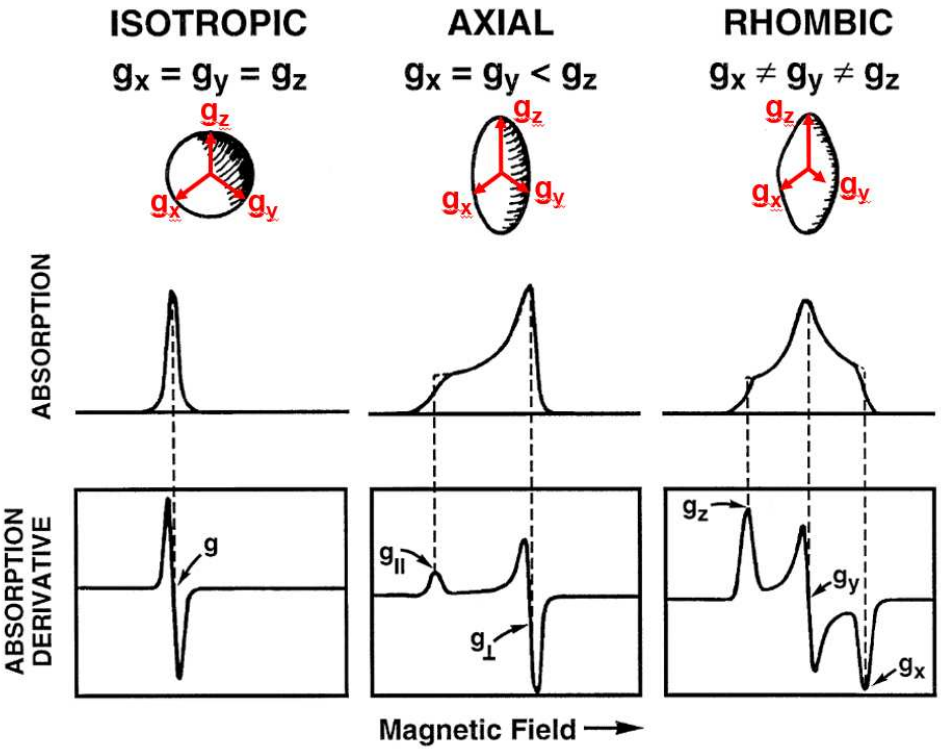

Figure 2.3: Schematic presentation of the relationship between g-value anisotropy and the EPR spectral line shapes. Geometric shapes of isotropic, axial and rhombic magnetic moments are simplified as a sphere, a rugby ball, and a rugby ball compressed toward the equator, respectively. Schematic shape of the absorption curves as "powder spectra" and the corresponding EPR derivative curves are shown below. Figure adapted from Ohnishi (1999)[172] under a Creative Commons License.

It should be noted that for organic radicals such as semi-reduced radical state of flavins, the g-value anisotropy is often indiscernible at X-band microwave frequencies, whereas under high-field

conditions, axial or rhombic patterns of the radical signal will emerge.

2.2.3 X-band EPR-signals and characteristics of FeS-clusters

Besides organic cofactors such as flavins that are bound as prosthetic groups inside proteins, life employs inorganic cofactors, such as clusters made up of iron (Fe) and sulfur (S) to catalyze a wide range of reactions[14;15]. Fe and S assemble most commonly to form cubic [4Fe-4S]- or [3Fe-4S]-clusters, or planar rhombic [2Fe-2S]-clusters, ligated by cysteine residues, whereas also alternative ligands exist[10]. The Fe atoms of FeS-clusters are tetrahedrally coordinated through the inorganic sulfur (S) and by the surrounding cysteines. The molecular basis of the redox activity are the two oxidation states of iron (Fe) in the oxidized form as ferric (Fe^{3+}) and in the reduced form as ferrous (Fe^{2+}). The individual irons inside FeS-clusters exhibit a high spin state with Fe^{3+} characterized by five unpaired d-orbital electrons and Fe^{2+} has six d-orbital electrons, four of which are unpaired. Since electrons have a spin (S) of S = ½, the two iron redox states Fe^{3+} and Fe^{2+} show S = $\frac{5}{2}$ and S = 2, respectively. Due to the paramagnetic character of the unpaired electrons, most FeS-clusters are studied by continuous wave EPR (CW-EPR) at least in one redox state, either oxidized (for [3Fe4S]-cluster) or reduced ([2Fe-2S]- and [4Fe-4S]-clusters)[36;90;93]. Anti-ferromagnetic coupling between the interacting Fe in the considered [2Fe-2S]- and [4Fe-4S]-clusters cause an overall diamagnetic character in the oxidized state and are paramagnetic in the reduced state.

HydABC from *T.maritima* contains a total of 10 iron-sulfur clusters, six cubane [4Fe-4S]-clusters and four [2Fe-2S]-clusters. These types of FeS-clusters exhibit a net spin of ½ in their reduced states and can thus be detected by CW-EPR. Differences in the saturation properties of these FeS-clusters were exploited to distinguish them from another. The oxidized state with S = 1 is undetectable by the here employed perpendicular mode EPR. However, degradation of [4Fe-4S]-clusters can give rise to [3Fe-4S] cluster with S = ½ in the oxidized state.

2.3 Equilibrium Redox titrations

The distinctive spectral characteristics of flavins and iron-sulfur clusters in their different redox states, as observed through UV/Vis- and EPR-spectroscopy, form the experimental basis for the investigation of their redox properties via redox potentiometric titrations[125]. The basic principle of this technique consists of sequentially bringing a protein solution to a specific redox potential (E_h) through different means (as further elaborated below), and the observation of the spectral changes associated with each change in redox potential. Here, the enzyme is placed in a defined buffer solution fixed at a certain pH, inside an oxygen-free environment. Besides the redox enzyme of interest, a mix of redox mediators is added to ensure an efficient transfer of electrons between the enzyme, the measuring

electrode, and the electron donor or electron acceptor, depending on whether the experiment is carried out in the reducing or oxidizing direction, respectively. In addition, mediators act as "redox buffers" in chemical titration setups (see below).

Equilibrium redox titration experiments allow for the assignment of three parameters regarding the redox compound of interest:

1. the standard redox midpoint potential at a specific pH ($E_{m,pH}$), which under standard conditions defines the standard redox potential, E°,

2. the number of electrons (n) associated with this redox transition derived from the slope of the titration curve, i.e., the degree of change around the E_m, and

3. spectral characteristics of the individual redox species hold information on the nature of the underlying cofactor and its concentration, if the extinction coefficient of the species in UV/Vis is known, or the signal is integrated in EPR.

Equilibrium redox titrations determine, by definition, the redox potential (E_m) at equilibrium conditions, i.e., while the ΔG° of the entire system is zero, and thus forward and backward redox reactions occur to the same degree. Such measurements thus describe the redox potential of a specific cofactor in the presence of all the other cofactors in a specific microstate. As a consequence, the redox potential of the highest-potential cofactor is determined with all other remaining cofactors in the oxidized state, whereas the redox-active cofactor with the apparent lowest redox potential is measured with all other redox cofactors already reduced. Two different techniques of tuning the redox potential of the entire system (E_h) will be presented. Both of these approaches can be combined with any form of spectroscopy or method of following the redox change. I will discuss them in the context of how they were mainly employed over the course of this thesis.

2.3.1 Chemical redox titrations monitored by EPR-spectroscopy

The redox potential can be poised by the addition of chemical reductant or oxidant to the solution. Most commonly used are freshly-prepared sodium dithionite ($E^\circ = -502$ mV, at 0.1 mM, pH 7) [139] or potassium ferricyanide ($E^\circ = +530$ mV) [125], due to their function as strong reductant or oxidant, respectively and their controllable spectroscopic contributions. The range of redox potentials to be tested during a chemical titration is limited by these redox potentials of reductant and oxidant. The stepwise addition of these chemical titrants adjusts the systems redox potential E_h in a roughly 1 V span. Low amounts of highly concentrated titrant solutions should be added to minimize dilution effects. Once a desired redox potential is reached, a sample (~ 200 μL) is withdrawn from the titration vessel, immediately frozen in a cold bath, and measured individually in EPR (see Setup figure 2.4).

High protein concentration (> 15 μM) and a high titration volume (multiple mL, depending on the number of samples) are thus required for this type of titration. Current developments of new EPR-techniques will potentially require much less protein sample[232].

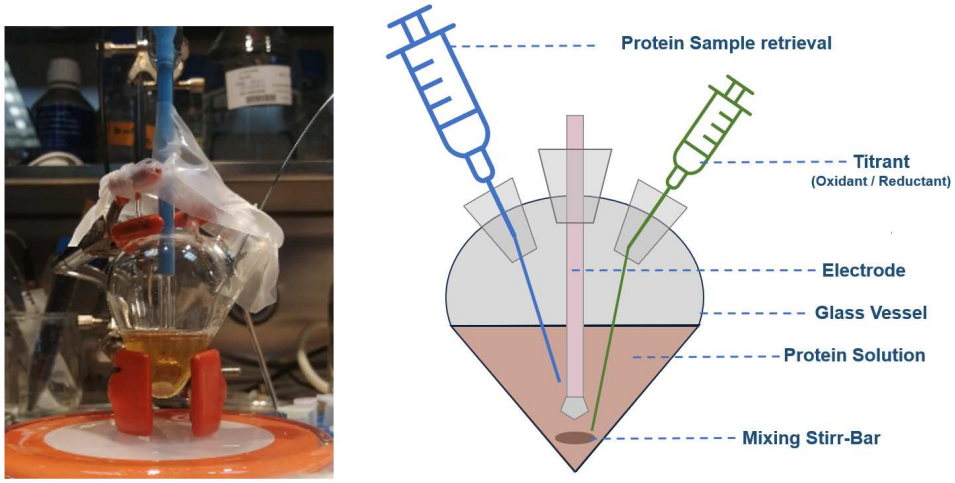

Figure 2.4: Picture and schematic setup of a chemical redox titration setup for the preparation of redox-poised EPR samples. *Left* Image of the redox titration setup employed at the BIP laboratory inside a Jacomex glove box. *Right* Analogous scheme of the main elements for this redox titration setup.

2.3.2 Electrochemical redox titrations followed by UV/Vis-Spectroscopy

The application of an electrochemical system allows the redox potential of the solution (E_h) to be established through the application of an electric current controlled by a potentiostat via a three-electrode system, consisting of a working electrode (WE), counter electrode (CE) and a reference electrode (RE)[43;170]. Thereby, the enzyme solution exchanges electrons (by the action of redox mediators) within an electrically closed circuit consisting of WE and CE, whereas the calibrated RE measures its potential difference to the WE and adjusts in a feedback loop the effectively applied potential at the WE to be at the desired value. During a reductive potentiometric titration, the content of the electrochemical cell is stepwise reduced by bulk electrolysis, effectively by performing a coulometry, where in each step a constant, more negative potential at the WE is applied and electrons are consumed, by reducing the entire sample solution, which is monitored over time as a change in current. Near-equilibrium between all redox components in the enzyme and the redox mediators is reached as the applied current asymptotically approaches a constant value. This equilibrium can also be verified by means of the associated UV/Vis-spectral changes of the components over time. The equilibrium is thereby characterized by the time point at which all spectral changes cease, which is assessed by difference spectra between different time points.

Multiple setups have been developed that allow electrochemical redox titration in various bioenergetic proteins to be monitored by UV/Vis-Spectroscopy (short Spectro-electrochemical redox titra-

tion). Gold capillary electrodes in conjunction with fiber optic spectrometry allowed for a miniaturization of spectro-electrochemical setups using low sample volumes ($\sim$ 150 μL) , while maintaining an optical pathlength of 5 mm as used in this thesis. In this setup, the protein solution is located in the center of a thin gold capillary WE through which the light is guided directly via optical fibers (figure 2.5). The electric circuit is closed via the CE at a larger distance from the light beam to minimize erroneous spectral changes caused by the opposite potential applied on the CE. Good conductivity between both electrodes and the RE must be ensured by higher ionic strength in the buffer solution. As compared to the chemical titration, the redox potential range to be scanned during these electrochemical setups is primarily constrained by the stability of the protein and the physical properties of aqueous solutions, i.e., the electrolysis of water at high redox potentials and the reduction of protons at low redox potentials. However along this wide redox range, suitable redox mediators for a particular redox span which show good electron exchange with the cofactors and minimized interaction with the electrode material still need to be employed.

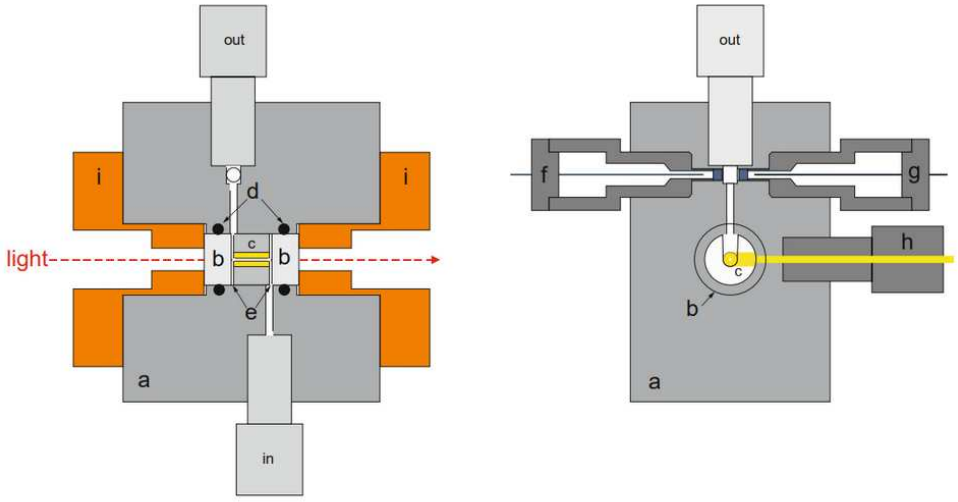

a) PEEK-body
b) Quartz-windows
c) Gold capillary
d) O-ring
e) Spacer
f) Reference electrode
g) Counter electrode
h) Connector working electrode
i) Plug-in optical fibers

Figure 2.5: Technical drawing of the spectro-electrochemical cell using a gold capillary working electrode (WE) primarily used in this thesis. Design, construction and drawing by Christoph Laurich. Figure taken with permission from Birrell *et al.* (2016) [18]. Copyright 2016 American Chemical Society.

Chapter

3

The dyad of the Y-junction- and a flavin module unites diverse redox enzymes

(published in BBA - Bioenergetics, 2021, 1862 (6), 148401)

BBA - Bioenergetics 1862 (2021) 148401

Contents lists available at ScienceDirect

BBA - Bioenergetics

journal homepage: www.elsevier.com/locate/bbabio

The dyad of the Y-junction- and a flavin module unites diverse redox enzymes

Kilian Zuchan, Frauke Baymann, Carole Baffert, Myriam Brugna *, Wolfgang Nitschke

Aix Marseille Univ, CNRS, BIP, 31 Chemin Joseph Aiguier, 13402 Marseille Cedex 09, France

ARTICLE INFO

Keywords:
Hydrogenase
Complex I
Formate dehydrogenase
Electron bifurcation
Evolution
Flavin

ABSTRACT

The concomitant presence of two distinctive polypeptide modules, which we have chosen to denominate as the "Y-junction" and the "flavin" module, is observed in 3D structures of enzymes as functionally diverse as complex I, NAD(P)-dependent [NiFe]-hydrogenases and NAD(P)-dependent formate dehydrogenases. Amino acid sequence conservation furthermore suggests that both modules are also part of NAD(P)-dependent [FeFe]-hydrogenases for which no 3D structure model is available yet. The flavin module harbours the site of interaction with the substrate NAD(P) which exchanges two electrons with a strictly conserved flavin moiety. The Y-junction module typically contains four iron-sulphur centres arranged to form a Y-shaped electron transfer conduit and mediates electron transfer between the flavin module and the catalytic units of the respective enzymes. The Y-junction module represents an electron transfer hub with three potential electron entry/exit sites. The pattern of specific redox centres present both in the Y-junction and the flavin module is correlated to present knowledge of these enzymes' functional properties. We have searched publicly accessible genomes for gene clusters containing both the Y-junction and the flavin module to assemble a comprehensive picture of the diversity of enzymes harbouring this dyad of modules and to reconstruct their phylogenetic relationships. These analyses indicate the presence of the dyad already in the last universal common ancestor and the emergence of complex I's EFG-module out of a subgroup of NAD(P)- dependent formate dehydrogenases.

1. Introduction

Enzyme subunits (or N- and C-terminal subunit-extensions thereof) rich in iron-sulphur centres are found in a plethora of redox enzymes. Such [Fe-S]-cluster-bearing units frequently are variations on one of the widespread structural themes referred to as dicubane- (or bacterial [8Fe-8S]-), tetracubane- ([16Fe-16S]-, [1]) or plant-type ([2Fe-2S]-) ferredoxins or feature more divergent architectures (*e.g.* the proximal cluster of the O_2-tolerant [NiFe]-hydrogenases [2]). They are in general considered to play the role of simple electron transfer relays. The [FeFe]-hydrogenase from *Clostridium (C.) pasteurianum* contains such an iron-sulphur-centre rich domain as an N-terminal extension to the actual catalytic domain [3,4]. The high-resolution structure of this enzyme showed that the set of [Fe-S]-clusters in this domain are arranged in a Y-shaped geometry [3]. Intriguingly, [Fe-S]-cluster-domains with strikingly similar molecular architecture have turned up in several 3D structure models of very diverse enzymes, such as complex I [5] or specific types of [NiFe]-hydrogenases [6] and most recently in a subgroup of formate dehydrogenases [7]. The simultaneous occurrence of this peculiar structural motif in so diverse enzymes begs the question of its functional significance. To advance our understanding of its role we have searched genome databases for further homologs. The results described below strongly suggest a role for this domain which significantly exceeds that of a simple electron wire building block. As emerging from our survey and already from the smaller sample of available 3D-structures, this [Fe-S]-domain occurs in most enzymes together with another functional unit which uses a flavin moiety and one or two iron sulphur centres to interface 1- and 2-electron redox events. Interestingly, many enzymes containing those two structural units were described as performing electron bifurcation [8–15]. The analysis of the pattern of occurrence of these modules in distinct enzymes, their likely molecular make-up and their phylogenetic grouping provides insights into their functional roles and suggests unexpected evolutionary relationships.

Abbreviations: NAD(P), nicotinamide adenine dinucleotide (phosphate); FMN, flavin mononucleotide; *bis*PGD, *bis* pyranopterin guanosine dinucleotide; ETF, electron transfer flavoprotein; Nfn, NADH-dependent reduced ferredoxin:$NADP^+$ oxidoreductase.

* Corresponding author.
E-mail address: mbrugna@imm.cnrs.fr (M. Brugna).

https://doi.org/10.1016/j.bbabio.2021.148401
Received 27 August 2020; Received in revised form 9 February 2021; Accepted 16 February 2021
Available online 6 March 2021
0005-2728/© 2021 Elsevier B.V. All rights reserved.

2. Methods

2.1. Database searches

The protein sequences of the Y-junction module from the structurally known proteins for complex I (NuoG/Nqo3 of *Thermus thermophilus HB8*: WP_011227701.1), the bidirectional [NiFe]-hydrogenase (HoxU of *Hydrogenophilus thermoluteolus TH-1*: WP_119335399.1) and [FeFe]-hydrogenase (CpI of *Clostridium pasteurianum DSM 525*: WP_004455619.1) were used as BLASTp and tBLASTn queries under default settings (BLOSUM62, gap opening penalty = 11, gap extension penalty = 1, word size = 6) to identify homologs in organisms with publicly available complete RefSeq genomes from NCBI until May 2020. Homologous sequences from phylogenetically disperse, representative sequences with e-values below e^{-10} and operon structures that contain a neighboring flavin-binding protein to ensure a functioning of the protein complex as described in the literature were selected [5,6,8].

Trimeric and tetrameric [FeFe]-hydrogenases were selected, when all proteins could be found in one operon, optionally followed by genes coding for hydrogenase maturase proteins (*hydE*, *hydF*, *hydG*) [16]. [NiFe]-hydrogenases were selected when all proteins could be found in one operon optionally with hydrogenase maturase (*hoxW*) factors present alongside [17]. Complex I sequences were selected based on the presence of all 14 genes specifying the minimal structural framework of the mitochondrial type enzyme (*nuoA-nuoN*) encoded in the same operon (to the exception of sequences from the family of Aquificales, where the genes are scattered over the genome, the gene products, however, were shown to assemble [18]). Trimeric and tetrameric formate dehydrogenases were selected provided all proteins could be found in one operon and the catalytic subunit contained a cysteine or selenocysteine at the molybdopterin/tungstopterin binding site, optionally also containing molybdopterin maturation factors (*moaA*, *mobB*, *fdhD*) alongside [19]. Supplementary Table 1 contains a list of specific binding/ligating motifs for each of these cofactors, on which the presence or absence of that cofactor was determined. From this initial dataset genes of biochemically characterised representatives from a wide phylogenetic variety that also fulfilled this criterion were selected and used as queries in a second round of data mining [7,20–24].

2.2. Structure-informed protein alignment and phylogenetic analysis

Structure image preparation was done in the open-source version of PyMOL (v1.8.4, Schrödinger, LLC). Structural alignment of the Y-junction modules (n = 160) were initially performed by the align function in PyMOL and Swiss PDB Viewer, successively constructed using MAFFT-DASH by employing the iterative refinement algorithm, E-INS-i at default settings (BLOSUM62, gap opening penalty = 1.53, offset = 0; as shown in Supplementary Fig. 1) [25,26]. For tree reconstruction the alignment of the Y-junction module was trimmed 15 aa before the first coordinating cysteine residue and 15 aa after the last coordinating cysteine residue of the highly conserved iron-sulphur clusters resulting in contiguous sequence stretches of 186–228 amino acids. The alignment of the sequences from the Y-junction modules from representatives sequences for which 3D structure models have been determined is shown in Supplementary Fig. 1.

Structure-informed alignments of the RefSeq sequences from the flavin-binding subunit and NuoE/Nqo1 homologs (n = 154, 6 [FeFe]-hydrogenases without flavin module excluded) were constructed based on the structural alignments described above and subsequently manually adjusted. Homologous sequences corresponding to NuoE/Nqo1 and NuoF/Nqo2 of the above mentioned structurally known proteins were separately aligned using MAFFT-DASH and trimmed to the last conserved residues. Due to the overall agreement in the architecture of the trees in these two sets of aligned sequences (see Results and discussion section), the trimmed alignments were concatenated (as shown in Supplementary Fig. 2).

Neighbor-joining clustering of both, the alignments of the Y-junction module (n = 160) and the flavin module (n = 154) was conducted in ClustalX2.1 under correction for multiple substitutions by including all gaps. Bootstrap values correspond to the frequency of occurrence of nodes in 1000 bootstrap-replicates. Tree representation for the figures were prepared in ITOL v5 and manually annotated [27].

3. Results and discussion

3.1. An [Fe-S]-cluster-bearing module with a conserved structural layout is common to [FeFe]-hydrogenases, NAD-dependent complex I, NAD-dependent [NiFe]-hydrogenases and NAD(P)-dependent formate dehydrogenases

The minimal core of [FeFe]-hydrogenases as exemplified by the enzyme from *Chlamydomonas (C.) reinhardtii* corresponds to a protein harbouring only the catalytic H-cluster, which is formed by a [4Fe-4S]-cluster together with a 2Fe subcluster, the latter containing non-protein ligands such as azadithiolate, carbon monoxide and cyanide groups (PDB: 3LX4, *nota bene*: this structure lacks the 2Fe subcluster [28]). In numerous prokaryotic [FeFe]-hydrogenases, however, this catalytic domain is supplemented by additional N-terminal domains carrying between two (PDB: 1HFE [29]) and four (PDB: 6N59 [4]) iron-sulphur centres which serve as electron wires connecting the H-cluster to physiological electron donors and acceptors. The earliest crystal structure of an [FeFe]-hydrogenase, *i.e.* that of the *Clostridium (C.) pasteurianum* enzyme (Fig. 1C, in blue), revealed that the four iron-sulphur clusters present in this enzyme form a puzzling Y-shaped, *i.e.* branched chain of redox centres (Fig. 1A and B, [3]) rather than a linear one as usually observed in electron wire modules [3,30,31]. This geometric arrangement suggested the possible existence of two distinct patches on the enzyme surface where electrons may enter or exit. Mutagenesis approaches designed to probe the pertinence of either of the two possible exit/entry pathways found that they both could mediate electron transfer between the ferredoxin and the H-cluster corroborating the idea that the central iron-sulphur cluster acts as a branching point for electron transfer within this module [32]. The polypeptide harbouring these four electron transfer clusters forms a compact (N-terminal) subdomain within the *C. pasteurianum* enzyme. In line with the notion of a Y-shaped arrangement of cofactors discussed for the *C. pasteurianum* hydrogenase, we will in the following refer to this electron transfer unit as the "Y-junction module".

A surprisingly similar structural unit (Fig. 1E) was early on identified to form the N-terminal domain of the NuoG (Nqo3) subunit of the NADH:quinone oxidoreductase or NAD-dependent version of complex I (Fig. 1F, in red; for a discussion of the intricacies of the complex I nomenclature, see the Supplementary Section 1) [33]. The C-terminal part of NuoG, however, is fully unrelated to [FeFe]-hydrogenases but belongs to the superfamily of Mo/W-*bis*PGD enzymes (*alias* the DMSO-reductase superfamily) [34,35]. Fig. 1B and E illustrate the close similarity of the polypeptide fold and iron-sulphur cluster positioning between the module in [FeFe]-hydrogenases and in NAD-dependent complex I, respectively [36]. One iron-sulphur cluster is missing in the latter enzyme, the protein chain harbouring this cluster in the clostridial [FeFe]-hydrogenase, however, is still present. In NAD-dependent complex I the remaining clusters are part of the electron transfer pathway from the NADH-oxidising site to the quinone-reducing one (Fig. 1D).

In the crystal structure of the NAD-reducing [NiFe]-hydrogenase (frequently referred to as "Hox"-type hydrogenase) from *Hydrogenophilus (H.) thermoluteolus* a separate protein subunit bearing [Fe-S]-clusters was found which strongly resembles the Y-junction module (Fig. 1I, in cyan). Like in the NAD-dependent complex I, this module lacks the "C-terminal" (see Section 3.1.1) iron-sulphur cluster as depicted in Fig. 1H. Again, the 3D architectures of the [NiFe]-hydrogenase's catalytic HoxH and HoxY subunits are unrelated to that of [FeFe]-hydrogenases, but share structural features with the NuoD

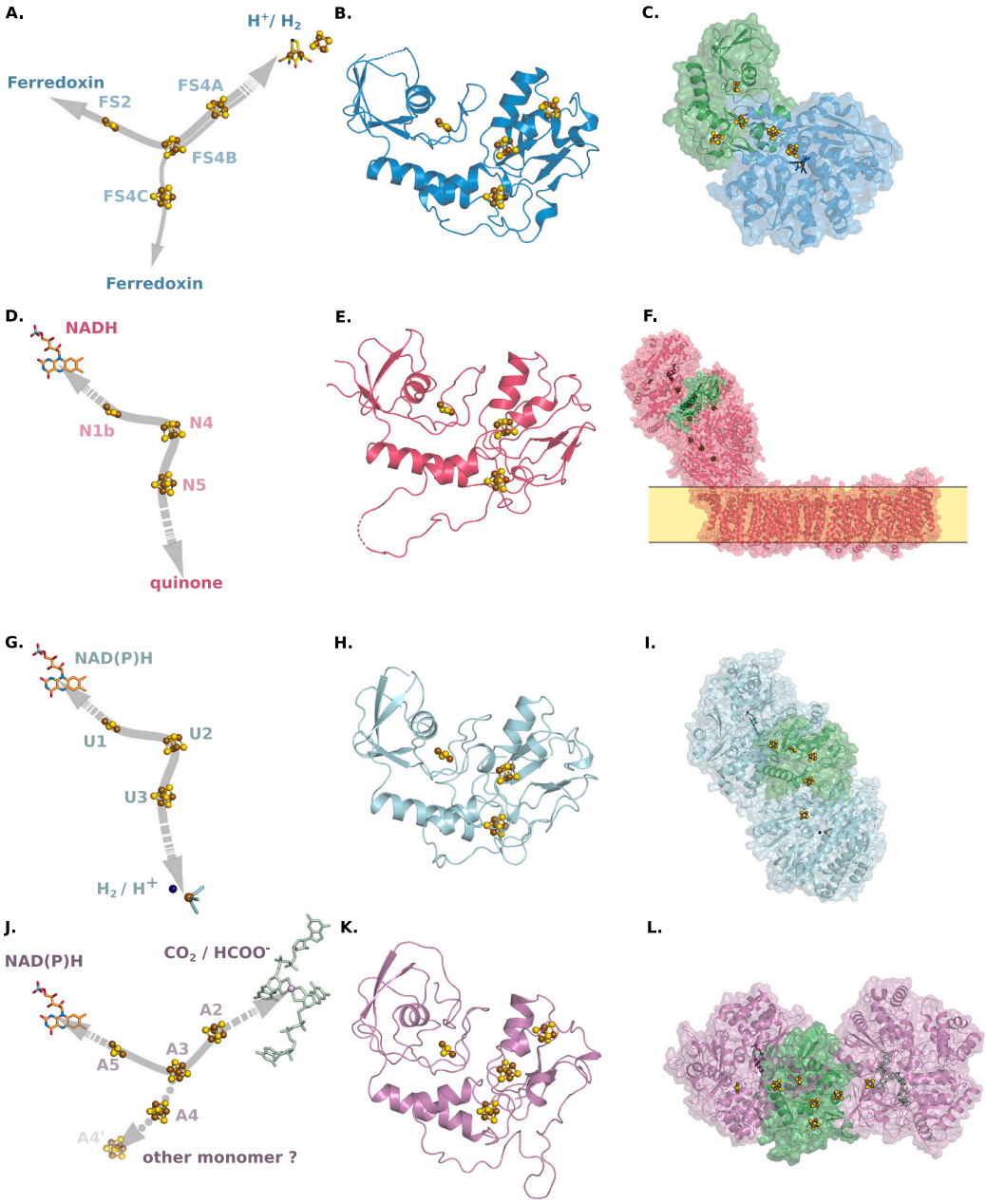

Fig. 1. Electron-transfer pathways through the Y-junction modules from different enzymes.
Comparison of the electron-transfer pathways in the first column (A., D., G. and J. with donor/acceptor location not to scale) enabled by the structurally conserved Y-junction module in the second column (B., E., H. and K., color of Y-junction module according to the general coloring scheme for each of these four protein complexes will be used throughout this article) from 4 bioenergetic proteins. Location of the Y-junction module (in green) in the structural representatives of the prototypical [FeFe]-hydrogenase (C., in blue, PDB: 6N59, Y-junction module in residue 1–209), of membrane-bound complex I (F., in red, PDB: 4HEA, membrane in beige, Y-junction module in residue 1–239 of NuoG), bidirectional [NiFe]-hydrogenase (I., in cyan, PDB: 5XF9, Y-junction module is hoxU) and in formate dehydrogenase (L., in purple, PDB: 6TG9, Y-junction module in residue 1–248 of FdhA) in the last column (relative protein sizes not to scale). The denomination of the iron-sulphur clusters in the first column (as in Table 1) follows Peters et al. [3] for [FeFe]-hydrogenase in A., Sazanov and Hinchliffe [33] for complex I in D., Shomura et al. [6] for [NiFe]-hydrogenase in G. and Radon et al. [7] for formate dehydrogenase in J. The same color coding for each of these four protein complexes will be used throughout this article.

(Nqo4) and NuoB (Nqo6) proteins of NAD-dependent complex I, respectively, although their redox substrates are completely different [6]. The physiological electron transfer pathway in this class of [NiFe]-hydrogenases is shown in Fig. 1G.

Finally, the recently published Cryo-EM structure of the NAD-dependent formate dehydrogenase from *Rhodobacter (R.) capsulatus* again features, as anticipated from sequence similarities, the presence of the Y-junction module, in this case containing the full set of iron-sulphur clusters just as in the *C. pasteurianum* enzyme [7]. Following the scheme of the previous three cases mentioned above, Fig. 1 shows the electron transfer (Fig. 1J), the structure of the Y-junction module (Fig. 1K) and its positioning within the parent enzyme (Fig. 1L) in purple. The color coding for the specific enzymes as introduced in Fig. 1 right column will be used throughout the manuscript.

Most interestingly, the structure of the entire NAD-dependent formate dehydrogenase from *R. capsulatus* also informs on the mutual spatial arrangement of individual monomers in the physiological dimeric state of the enzyme. This enzyme indeed forms a homodimer of heterotetramers wherein the interaction between individual enzymes occurs mainly *via* the surface of the Y-junction module. This arrangement positions the two histidine-coordinated clusters in sufficiently close proximity (edge-to-edge distance of about 10 Å [7]) to allow facile and rapid inter-monomer electron transfer [37]. We have indicated the position of the histidine cluster in the second half of the functional dimer as A4′ in Fig. 1J. Such an organisation of potentially cross-talking electron transfer chains is reminiscent of what is observed in the Rieske/cyt*b* complexes (where inter-enzyme electron transfer may occur through the b_L hemes at an edge-to-edge distance of about 11 Å [38,39]) or heterodisulfide reductases (over a distance of again about 11 Å [40]). However, while in these latter cases, inter-monomer communication may be afforded by redox centres which are part of the intrinsic electron transfer chain of each monomer, the formate dehydrogenase enzyme from *R. capsulatus* recruits the "out-of-line" clusters to electrically connect the two individual monomers. It is noteworthy that cross-dimer electron transfer in the formate dehydrogenase from *R. capsulatus* only is a theoretical possibility (albeit extremely likely) and no experimental evidence for this phenomenon has been obtained so far. For the Rieske/cyt*b* complex, by contrast, inter-monomer electron transfer has been shown to occur, albeit at slow rates [39]. A physiological organisation as a dimer was observed in several further NAD(P)-dependent formate dehydrogenases and, intriguingly (as further discussed below) also in electron bifurcating NAD(P)-dependent [FeFe]-hydrogenases [8,10,13].

3.1.1. *Structural features of the Y-junction module*

As illustrated in Fig. 2A, the entire Y-junction module (always shown in green shades hereafter) is itself composed from three distinct submodules, that is, an N-terminal plant-type [2Fe-2S]-ferredoxin domain (in olive) followed by a median domain (in mint) ligating a single [4Fe-4S]-cluster and finally a C-terminal bacterial-ferredoxin-type domain (in lime) featuring 2 cubane [4Fe-4S]-centres one of which may be absent in certain cases as mentioned above and described in more detail below [34,41]. The cubane cluster harboured by the median domain features a histidine ligand in addition to the three canonical cysteine ligands (in the following denoted as "histidine-[4Fe-4S]") in all enzymes shown in Fig. 1. Interesting structural and sequence features of this ligating histidine are discussed in the Supplementary Section 2 (see also Supplementary Fig. 3). For the sake of annotating the phylogenetic trees which we will present below (Section 3.5), we have represented each of the four individual iron-sulphur clusters by a specific symbol and the resulting electron transfer pathways in an iconographic way as defined in Fig. 2B. This depiction is used throughout the article in order to more abstractly present the genomic organisation and structural layouts of the above mentioned protein complexes.

The histidine-[4Fe-4S]-cluster and the C-terminal [4Fe-4S]-centre were found to be missing in certain enzymes. However, most representatives of all enzyme families dealt with in this work contain all four clusters. This and the fact that all four structures shown in Fig. 1 contain the full complement of the polypeptide chain with or without harbouring all four clusters seen in the *C. pasteurianum* structure leads us to conclude that the four-cluster domain represents the archetypal version of the module and that either the histidine-ligated or the C-terminal [4Fe-4S] cluster have been lost in certain cases.

A modular make-up of electron transfer proteins has been pointed out repeatedly over the last two decades [1,35,42–44] and it is by itself therefore not astonishing to find an electron transfer module built-up from more basic components. The strictly conserved succession of subdomains and the astonishingly similar global architecture of the module, however, render the possibility that this structure emerged four times independently in the above considered enzymes from the described more basic building blocks extremely unlikely. The Y-junction module

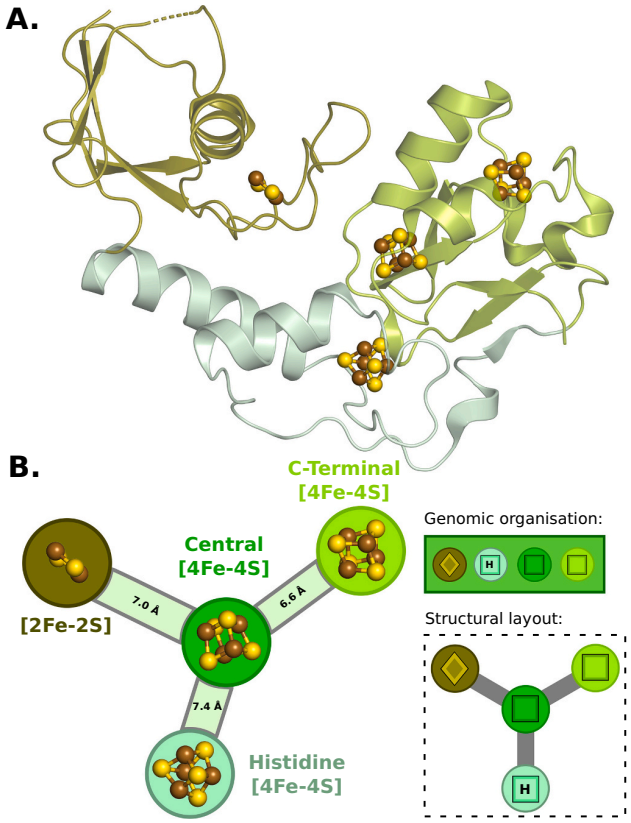

Fig. 2. Domain-architecture of the Y-junction module.
A. The Y-junction module is constructed of a plant-type-[2Fe-2S]-ferredoxin domain (in olive), a histidine-[4Fe-4S]-binding domain (in mint) and a regular 2x[4Fe-4S]-ferredoxin domain (in lime) [41].
B. Nomenclature of the 4 electron-conducting iron-sulphur clusters in the Y-junction module and subsequent representation of the genomic organisation and structural layout of this protein module as symbols and pictograms. Numbers on the edges between the clusters show averaged edge-to-edge distances (in Å) that include the ligating residues. PDB-structure used for this module, [FeFe]-hydrogenase from *C. pasteurianum* (CpI): 6N59.

therefore almost certainly originated only once and was then docked *en bloc* onto different catalytic protein units.

3.1.2. *The Y-junction module at the crossroads of electron transfer chains*

The variability of electron transfer pathways through the 4-cluster domain seen in the left column of Fig. 1 exceeds even that identified for the *C. pasteurianum* [FeFe]-hydrogenase. Redox communication with catalytic subunits are seen to occur either *via* the C-terminal [4Fe-4S]-cluster (Fig. 1A and J) or the histidine cluster (Fig. 1D and G). Both the histidine cluster and the [2Fe-2S]-centre can interact with soluble electron carriers such as ferredoxins and likely also flavodoxins (Fig. 1A) [32]. Alternatively, the histidine cluster is seen to mediate inter-monomer communication (Fig. 1J) and the [2Fe-2S]-centre can talk to an additional flavin-bearing subunit (Fig. 1D, G and J; see below). The comparison of the cases depicted in the left column of Fig. 1 thus shows that the 4-cluster domain fully merits to be called the Y-junction module.

3.1.3. *Inter-enzyme similarities exceed the Y-junction module and include a flavin-bearing protein module*

While similarity between the *Clostridium* hydrogenase and the other three systems is limited to the Y-junction module, common elements of NAD-dependent complex I, NAD(P)-dependent [NiFe]-hydrogenases and NAD(P)-dependent formate dehydrogenases furthermore comprise

a structural module binding a flavin together with two additional iron-sulphur centres, more specifically a [2Fe-2S] and a [4Fe-4S] cluster. In the NAD-dependent [NiFe]-hydrogenase from *H. thermoluteolus*, this unit is contained within a single polypeptide, the HoxF protein, while in the NAD-dependent complex I and NAD(P)-dependent formate dehydrogenase of Fig. 1 it is made up from two subunits (NuoE and NuoF for complex I) which structurally correspond to N-and C-terminal domains of the HoxF protein, respectively (Fig. 3). The N-terminal part of HoxF thus contains the [2Fe-2S] cluster domain (without the Fe-S cluster in this particular structure) and the C-terminal domain corresponds to the flavin/[4Fe-4S]-bearing subunit of the other enzymes. Whereas this [4Fe-4S]-cluster is present in all systems and connects the flavin to the Y-junction module, the [2Fe-2S]-cluster is found in many, but not all representatives of the diverse enzyme families as will be elaborated below. The polypeptide chain harbouring the cluster in the other discussed cases, by contrast, is present, again arguing for a selective loss of this Fe-S cluster in certain enzyme representatives.

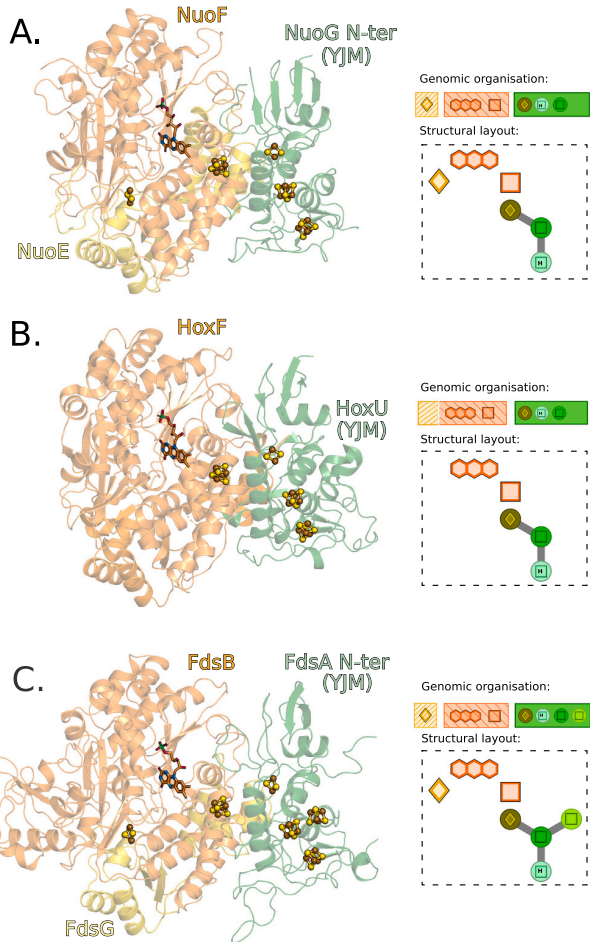

Fig. 3. Structural comparison of the "flavin module" from different complexes. Structural juxtaposition of the "flavin module" of the respiratory complex I from *Thermus thermophilus* (A., PDB: 4HEA), the NAD-dependent [NiFe]-hydrogenase from *Hydrogenophilus thermoluteolus* (B., PDB: 5XF9) and the NAD-dependent formate dehydrogenase from *Rhodobacter capsulatus* (C., PDB: 6TG9). Subunits are colored according to homology with the flavin-binding subunit in orange, the [2Fe-2S]-cluster-containing subunit in yellow and the Y-junction module in green. Iron-sulphur clusters are brown and yellow for iron and sulphur, respectively. Carbons in the flavin are orange. General genomic organisation and structural layout in accordance with Figs. 4, and 5a and b, where the pictograms for the operon depictions and structural arrangements are given.

This structural unit couples the 2-electron redox conversion of NAD(P)$^+$/NAD(P)H to electron transfer chains which perform only 1-electron redox reactions. It therefore serves the function of a 2- to 1-electron gate. Since the functionally pivotal cofactor in this unit is a flavin, we will refer to it as the "flavin-module".

3.2. The link to NAD(P)-dependent, electron bifurcating [FeFe]-hydrogenases

The larger segment containing both the flavin- and the Y-junction-module is suggested *via* sequence similarities to also be present in NAD(P)-dependent, electron bifurcating [FeFe]-hydrogenases [8,16]. These enzymes are generally classed into tri- and tetrameric representatives, while rare monomeric and dimeric enzymes due to subunit fusion exist as well [24] (see below). Two of the common subunits constitute the above described flavin module while the third is closely related to the *C. pasteurianum* [FeFe]-hydrogenase. Similar to the *C. pasteurianum* enzyme, the hydrogenase catalytic subunit of these enzymes features the Y-junction module as its N-terminal part followed by the core domain of [FeFe]-hydrogenases [16]. The Y-junction module therefore exists in all four enzymes shown in Fig. 1. These similarities indicate that bifurcating [FeFe]-type hydrogenases employ structural components of NAD-dependent complex I, NAD(P)-dependent [NiFe]-hydrogenases and NAD(P)-dependent formate dehydrogenases on one side and of the *C. pasteurianum* [FeFe] hydrogenase on the other side. The structural element common to both sides is the Y-junction module and it can therefore serve as a cornerstone for building a homology model of the entire bifurcating [FeFe]-hydrogenase by merging the structural features depicted in Figs. 1 and 3. Such a model using the NuoEFG (Nqo213) part of complex I as a template has recently been presented by Chongdar et al. (2019) for the trimeric hydrogenase of *Thermotoga (T.) maritima* [45]. Still, judging from sequence comparisons, this structural segment of complex I differs from both trimeric and tetrameric electron bifurcating [FeFe]-hydrogenases in several aspects (see Fig. 4). (i) The C-terminal cluster of the Y-junction module is generally absent in complex I. (ii) An N-terminal extension in the flavin/[4Fe-4S] subunit of the flavin module is absent in complex I and also in the structures of the NAD(P)-dependent [NiFe]-hydrogenases. This domain, found to be present in most [FeFe]-hydrogenases and formate dehydrogenases, was even proposed to ligate an additional iron-sulphur cluster [15]. In between the genes encoding the [2Fe-2S]-ligating and the flavin/[4Fe-4S]-bearing subunits and in rare cases in other gene cluster positions, a gene coding for an additional subunit is present in tetrameric [FeFe]-hydrogenases and certain formate dehydrogenases [16]. Sequence analysis indicates homology to the [2Fe-2S]-domain and, more generally, to thioredoxin-like [2Fe-2S]-ferredoxins [46] but the [2Fe-2S] cofactor likely is absent (for a more detailed discussion, see Section 3.4.1). (iii) The flavin/[4Fe-4S]-carrying protein features an additional [8Fe-8S]-ferredoxin-like domain as C-terminal extension. Again, neither complex I nor NAD(P)-dependent [NiFe]-hydrogenases possess this domain (see below and Fig. 4).

Since Chongdar et al. (2019) proposed their homology model, the above discussed (and shown in Fig. 1) 3D-structures of NAD(P)-dependent formate dehydrogenases have come out [7,47]. These structures remedy two of the three above mentioned shortcomings entailed by using complex I or NAD(P)-dependent [NiFe]-hydrogenases as templates since both formate dehydrogenase structures contain all four iron sulphur cluster of the Y-junction module and furthermore possess the equivalent of the small subunit/domain in the flavin module. Unfortunately, the C-terminal [8Fe-8S]-extension does not occur in the NAD-dependent formate dehydrogenase enzymes for which structures are now available, although other representatives of this enzyme family contain this domain (see Section 3.5.4). While positioning at molecular detail of the C-terminal [8Fe-8S] domain in the flavin/[4Fe-4S] subunit is thus not yet possible, a rough estimate of its approximate configuration with respect to the core of the enzyme formed by the three main

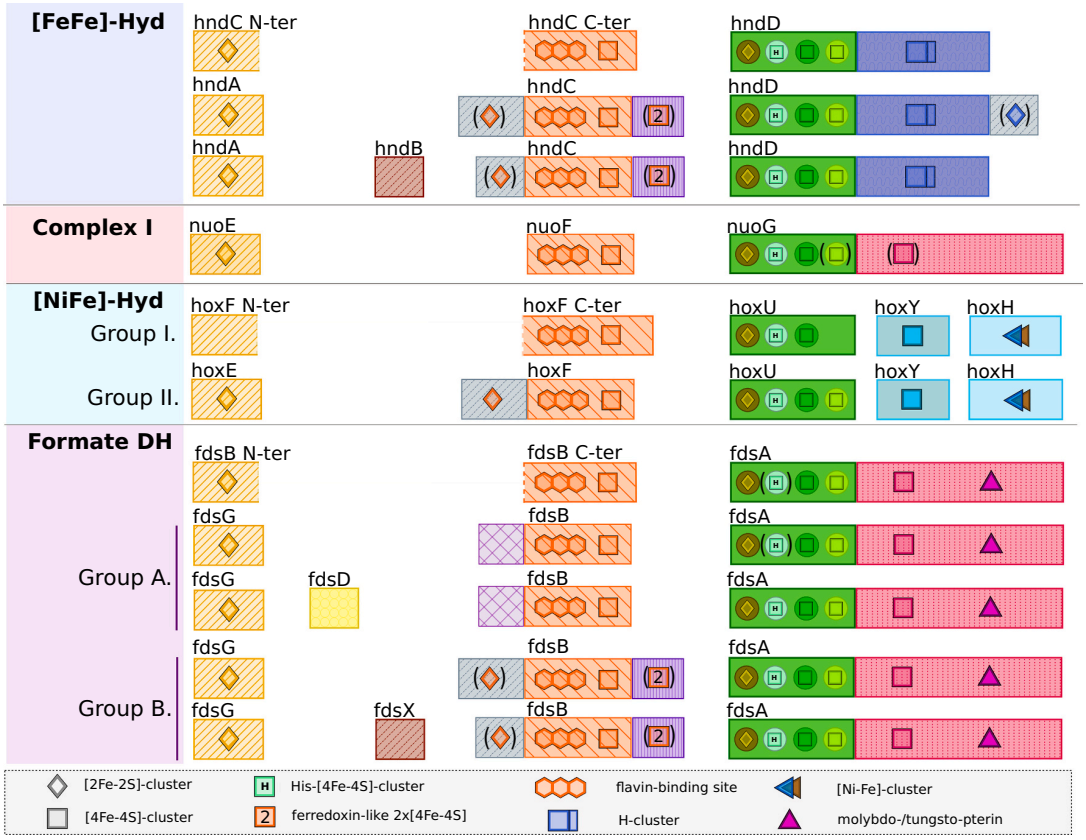

Fig. 4. Operon organisation for the bioenergetic proteins containing the Y-junction module.
Gene cluster organisation in [FeFe]-hydrogenase (in blue), complex I (in red), bidirectional [NiFe]-hydrogenase (in cyan) and the formate dehydrogenase (in purple). Sequence motifs for the coordination of cofactors are depicted by colored symbols in accordance with the pictograms used in Figs. 2, 3, 5a and b and summarised in Table 1. Symbols enclosed by parenthesis indicate the presence of the cofactor and/or binding domain of that cofactor in a majority of considered sequences. Identical colors and underlying patterns of the sequence stretches indicate homologous regions. Y-junction module is shown in green. Group definitions follow compositional and functional differences of proteins belonging the same protein complex. Coloring of the iron-sulphur clusters corresponds to its location in the operon analogously as in the Figs. 2, 3, 5a and b. Sequence lengths not to scale.

subunits can be derived from the spatial localisation of the C-terminus of the flavin/[4Fe-4S]-subunit. Since the [8Fe-8S]-domain represents the C-terminal extension of this subunit, it must be positioned close to where the flavin/[4Fe-4S]-subunits of the enzymes of Fig. 3 have their C-termini.

We have in this work surveyed prokaryotic genomes for homologs of the characterised bifurcating [FeFe]-hydrogenases (to be detailed in Section 3.5.2) and the retrieved data set suggests that the structural unit encompassing the NAD-redox-converting flavin module and the Y-junction module is indeed common to NAD-dependent complex I, NAD(P)-dependent [NiFe]-hydrogenases, NAD(P)-dependent formate dehydrogenases and ferredoxin-dependent (also called electron bifurcating) [FeFe]-hydrogenases.

3.3. NAD(P)-dependent [FeFe]-hydrogenases and NAD(P)-dependent formate dehydrogenases: two manifestations of the same electron bifurcating enzyme?

As discussed in Section 3.2 and further detailed below (Section 3.5 and Fig. 4), the molecular make-up of NAD(P)-dependent [FeFe]-hydrogenases most closely resembles that of NAD(P)-dependent formate dehydrogenases. These two enzymes families share the flavin and the Y-junction module and communicate reducing equivalents (*via* the C-terminal [4Fe-4S]-cluster of the Y-junction module) to and from a catalytic unit which redox-converts either the CO_2/formate or the H^+/H_2 couple.

We emphasise that the apparent standard electrochemical potentials of these two redox couples are virtually indistinguishable (−414 mV *vs.* −420 mV at pH 7, respectively) suggesting a facile interchangeability without needing to adapt the redox properties of the cofactors in the Y-junction- and the flavin-module [48].

The similarities in functional properties between these two enzymes are indeed striking. In 2013, the Thauer group reported the biochemical and functional characterisation of a formate dehydrogenase purified from *Gottschalkia (G.) acidurici* which couples NAD^+-reduction by electrons derived from the oxidation of formate to the concomitant reduction of ferredoxin [11]. This reaction scheme closely resembles the process carried out by electron bifurcating [FeFe]-hydrogenases. It is noteworthy that other representatives of this family have been characterised previously, such as the enzymes from *Methylosinos trichosporium* [49], *Cupriavidus necator* [41] and *Rhodobacter capsulatus* [50] but their potential ferredoxin-dependent reactions weren't analysed, even if Jollie and Lipscomb [49] found characteristics which in retrospect may be interpreted to suggest electron bifurcating properties of the enzyme. For the two NAD(P)-dependent formate dehydrogenases for which 3D structure models recently became available [7,51], the implication of ferredoxins hasn't been studied in detail. We deem worth noting that the coupling of NAD(P)- and ferredoxin-redox conversions in the formate dehydrogenase from *G. acidurici* was observed as early as 1972 [52], that is, almost contemporary with the development of the Q-cycle scheme by Peter Mitchell, which rationalised the redox processes in Rieske/cyt*b*

complexes through electron bifurcation [53,54]. However, the conceptual association of the reactions in NAD(P)-dependent [FeFe]-hydrogenases and formate dehydrogenases to that of the Rieske/cyt*b* complex was only made four decades later [36,55,56].

The pioneering work on the *G. acidurici* enzyme [11,52] therefore revealed that selected representatives from the NAD(P)-dependent formate dehydrogenase family can indeed couple ferredoxin reductions/oxidations to their overall redox reactions just as ferredoxin-dependent [FeFe]-hydrogenases do. Both the [FeFe]-hydrogenase [24,57] and the formate dehydrogenase families [50], however, also seem to include cases which redox convert NAD(P) without implicating redox reactions of ferredoxins.

3.4. Functional significance of the Y-junction - flavin module dyad

3.4.1. On the number and roles of the iron-sulphur centres in the flavin module

The 3D-structure model of the flavin module is known for representatives from three out of the four described families. The spatial positioning of the flavin moiety and the cubane iron-sulphur cluster located in between the flavin and the Y-junction module is well-conserved between all these three cases (Fig. 3). However, the [2Fe-2S]-cluster in NuoE (Nqo2) of NAD-dependent complex I-type enzymes (denoted N1a) positioned on the opposite side of the flavin [33], is also seen in the structures of NAD(P)-dependant formate dehydrogenases but is absent in the NAD-reducing [NiFe]-hydrogenase from *H. thermoluteolus*. This latter structure nonetheless exhibits the protein fold ligating this cluster in complex I and formate dehydrogenases (see Fig. 3). However, this cluster is present in phylogenetically close sister enzymes of the *H. thermoluteolus* one as we will show below (Section 3.5.3). Indeed, in all four enzyme-families, this [2Fe-2S]-cluster is present in the majority of considered cases as suggested by the conservation of its respective cysteine ligands (Supplementary Table 1).

In many NAD-dependent complex I-enzymes studied so far, the N1a cluster is seen to become transiently reduced upon addition of NADH [58]. Deleting the N1a cluster results in an inactive enzyme [59], showing that the presence of N1a and N3 clusters is essential for the function of that complex. A similar observation has been made for the homologous [2Fe-2S]-cluster-bearing HoxE subunit in the [NiFe]-hydrogenase of *Synechocystis* sp. *PCC 6803*. Deleting this subunit from the complex causes all NAD-related functionality to cease [60]. The reduction of complex I by NADH (just like that of cyanobacterial [NiFe]-hydrogenase) therefore very likely involves an initial bifurcated 2-electron transfer from the flavin to its flanking clusters and the electron "parked" on the [2Fe-2S] centre eventually follows the path of the first electron through the Y-junction module towards the quinone reduction site [61]. As we have argued before, this reaction scheme may allow NAD-dependent complex I to optimize electron transfer from the 2-electron compound NADH towards the 1-electron redox conduit constituted solely from iron-sulphur clusters by striking a compromise between the conflicting requirements of 2- and 1-electron transfer events [62].

Many flavin modules in all families except NAD-dependent complex I harbour one to several additional iron-sulphur centres, the function of which is not known so far. Several of these additional centres are most likely positioned close to the [2Fe-2S]-cluster. It seems inevitable to us that for those cases the scenario of "parking" the second electron involved in flavin redox reactions cannot be applicable. Rather, these clusters almost certainly provide a conduit for shuttling the electron to/from other electron acceptors such as for example soluble ferredoxins [8].

We therefore consider that presence/absence of the [2Fe-2S]-cluster next to the flavin as well as of an additional electron transfer pathway in contact with the [2Fe-2S]-cluster is of prominent importance for the catalytic and kinetic abilities of the respective enzymes in communicating with soluble electron shuttles.

In many hydrogenases and formate dehydrogenases, an additional domain is fused to the N-terminus of the flavin/[4Fe-4S] subunit as is the case in the two formate dehydrogenase enzymes for which a structure is available (Fig. 3). Tetrameric versions of NAD(P)-dependent [FeFe]-hydrogenases (see Section 3.2) and of NAD(P)-dependent formate dehydrogenases contain a further small subunit. In most cases, the gene encoding this protein is flanked upstream by that coding for the [2Fe-2S]-bearing subunit of the flavin-module and downstream by that encoding the flavin/[4Fe-4S] subunit. The gene cluster disposition of these cases and those discussed below are summarised in Fig. 4. As noticed previously [16,46], sequence comparisons indicate that the small subunit/N-terminal-domain and the [2Fe-2S]-binding domain most likely arose from gene duplications and that they therefore are likely to exhibit a common fold. Meyer et al. pointed out that this fold corresponds to the structure of thioredoxin-like [2Fe-2S]-ferredoxins [46]. The recently obtained structures validate these sequence-based predictions (see Fig. 3). The presence of cysteine residues in the small subunit/N-terminal-domain has led to the proposal that this subunit may add a further iron-sulphur-centre to the cluster inventory of the flavin module [16,63]. Our multiple alignments of a large sample of small subunit/N-terminal-domain sequences in both hydrogenases and formate dehydrogenases showed that the first cysteine ligating the cluster in thioredoxin-like ferredoxins and in the [2Fe-2S]-domains of the flavin module is absent in these polypeptides. The second one is only sporadically conserved and only the third and forth cysteines are present in appropriate positions in the majority of sequences from NAD(P)-dependent [FeFe]-hydrogenases. Since only two potential cluster ligands are conserved and since furthermore mutagenesis studies on thioredoxin-like ferredoxins [46,64] have demonstrated the first cysteine (absent in these sequences) to be indispensable for stabilising an iron-sulphur cluster, we tend to consider it highly unlikely that these domains contribute a further cluster to the inventory of redox centres in the flavin module. In the homologous subunits/domains of NAD(P)-dependent formate dehydrogenases (such as for example the enzyme depicted in Figs. 1J–L and 3C), cysteine residues are fully absent furthering our doubts on the existence of additional [Fe-S]-clusters afforded by these polypeptide chains.

Remarkably, in a specific group of formate dehydrogenases, the gene encoding the thioredoxin-like protein and flanked in the gene cluster by ORFs for the [2Fe-2S]-subunit (upstream) and the flavin/[4Fe-4S]-protein (downstream) is replaced by an unrelated gene the product of which is located in the enzyme on the surface of the catalytic subunit [7], that is, in a spatial position completely different from that of the thioredoxin-related small subunit (Fig. 4). We will come back to this observation below (Section 3.5.4).

In a few tetrameric versions of NAD(P)-dependent [FeFe]-hydrogenases, a gene coding for a thioredoxin-like protein is additionally found at the end of the gene cluster downstream of the ORF encoding the catalytic subunit. This gene can also be found fused to the 5′-end of the catalytic subunit's gene as is for example the case for the biochemically characterised enzyme from *Thermotoga maritima* [65]. In contrast to what is the case for the above discussed subunit/domain, the sequences of the thioredoxin-like proteins/domains encoded at the end of the gene cluster contain all four canonical cysteines of thioredoxin-like [2Fe-2S]-ferredoxins [46] and they are generally assumed to indeed provide an additional redox centre to the enzyme [45,65] (see Fig. 4).

3.4.2. Branched electron transfer, electron bifurcation and energy-converting electron bifurcation: a specification of meanings

Branching of electron transfer occurs when single reducing equivalents can take either of two distinct paths leading away from the branchpoint redox centre. Which pathway or to which extent each of the two pathways is taken will depend on relative redox potentials of the involved redox centres, their distances and/or on congesting either pathway by downstream kinetic limitations. The inverse reaction would in this definition be the "merging" of distinct electron transfer chains

and the branchpoint redox centre would become the merging cofactor. Electron transfer reactions through this module are exergonic and all individual redox transitions are 1-electron reactions. This type of processes obviously is what the Y-junction module can mediate, since the edge-to-edge distances between each of the surface-oriented clusters, *i.e.* the [2Fe-2S], the histidine-[4Fe-4S] and the C-terminal [4Fe-4S], to the central [4Fe-4S] are around 7 Å (Fig. 2). Such a branching behavior of the Y-junction module has indeed been demonstrated *via* mutational studies for the [FeFe]-hydrogenase from *C. pasteurianum* [32].

Bifurcation in colloquial language may appear quite synonymous to branching. In the field of bioenergetics, however, the term has originally been introduced to describe the quinol oxidation reaction in mitochondrial complex III (a member of the Rieske/cyt*b* family of enzymes) by Peter Mitchell [53,54] and in particular to rationalise the phenomenon that low potential hemes were seen to be reduced by quinones in a reaction triggered by the addition of oxidants (the so-called "oxidant-induced reduction" [66]). This concept was later expanded by Buckel and Thauer [36,55,56,67,68] towards flavin-containing enzymes in the aim to explain the observed reduction of low potential ferredoxins concomitant with and coupled to the reduction of oxidants such as NAD(P) or crotonyl-CoA. The phenomenon of the reduction of low potential acceptors is presently understood on the basis of an interfacing of 2-electron redox compounds (such as quinones or flavins) with two distinct 1-electron redox chains. It is this interfacing process which we regard as the actual electron bifurcation/confurcation reaction. The immediate redox partners of the bifurcating centre within these two distinct 1-electron redox chains, however, can be (and mostly are) intra-enzyme redox centres, rather than ferredoxins or flavodoxins.

Quinones and flavins are known to the organic chemists since almost a century as displaying intriguingly versatile redox properties [69,70] and in particular variable strengths of what is called redox cooperativity between their individual 1-electron redox transitions (for a more detailed discussion, see [62]). While intuitively the loss of the first electron from a fully reduced 2-electron compound should disadvantage departure of the second one (due to loss of electrostatic repulsion), redox cooperativity denotes cases when, by contrast, the first redox transition favours occurrence of the second one. Redox cooperativity thus results in lowering of the difference in redox potentials of the two individual 1-electron transitions and can even lead to so-called "inverted" redox potentials where the first redox transition generates a highly reactive semi-reduced state and thereby triggers the immediate occurrence of the second one, yielding an apparent concomitant 2-electron redox event [71]. The strong reactivity of the semi-reduced state and appropriate tuning of electrochemical potentials of all redox centres involved in the "$2e^-/2 \times 1e^-$" -interfacing reaction allows the reduction of low potential acceptors, the hallmark phenomenon of electron bifurcation, to naturally emerge from the energetic landscape of the process [72,73]. The reaction schemes observed in the Rieske/cyt*b* complexes, in Electron Transfer Flavoproteins (ETFs) and in the NADH-dependent reduced ferredoxin:$NADP^+$ oxidoreductase (Nfn) enzyme nicely fit this electrochemical scheme [36,55,56,62,73].

However, as we have argued before [62,74], the extent of redox inequivalence (resulting from varying strength of redox cooperativity of the 2-electron compound) was found to be variable and likely represents a continuum reaching up to a virtual equivalence as may for example be the case in certain types of complex I (discussed in Baymann et al. [62]). Electron bifurcation defined as $2e^-/2 \times 1e^-$-interfacing thus is not equivalent to the process of reducing low potential acceptors, since the two electrons could be forwarded to two roughly equipotential 1-electron acceptors. Ferredoxin-dependent electron bifurcation is therefore a special case of the wider scheme of electron bifurcation.

To integrate the empirically observed redox reactions performed by the NAD(P)-dependent [FeFe]-hydrogenases and formate dehydrogenases dealt with in this work into the above described conceptual framework, Buckel and Thauer have realised that the most straightforward way implied assuming the presence of two distinct flavin moieties in these enzymes [36]. One of these flavins would represent the $2e^-/2 \times 1e^-$ bifurcating site while the second one would consecutively accumulate two electrons to eventually be able to reduce NAD(P) in a 2-electron redox reaction. Unfortunately, the ensemble of structural information accumulated over the last few years and summarised in Section 3.1 renders the two-flavin model extremely unlikely. The previous mechanistic rationalisation of what is observed experimentally has thereby lost its basis. To remedy this problem, several alternative mechanistic models have been proposed. For example, Peters et al. [75] considered the possibility that electron bifurcation actually occurs on the H-cluster of the hydrogenase catalytic subunit while Chongdar et al. [45] proposed the Y-junction module to perform this function.

The definitions detailed above make it clear that the Y-junction module in the bifurcating [FeFe]-hydrogenases cannot perform electron bifurcation as defined by NAD-dependent ferredoxin reduction but only electron branching. Such a branching pathway has been proposed to result in redox equilibration with the ferredoxin pool in an attempt to rationalise the observed substochiometric reduction of ferredoxin by hydrogen [8]. The recent structure model of NAD-dependent formate dehydrogenase from *R. capsulatus*, however, showed that the branching in the Y-junction module might connect individual enzymes of the functional dimer. Assuming that the dimeric forms of electron bifurcating, NAD(P)-dependent [FeFe]-hydrogenases resemble their formate dehydrogenase sister enzymes, an equilibration with the ferredoxin pool through the Y-junction module's histidine cluster is thus precluded. We are also reluctant to consider the H-cluster as the electron bifurcating site. Since NAD(P)-dependent formate dehydrogenases were shown to operate pretty much the same way as the [FeFe]-hydrogenases do, this would imply that the molybdopterin cofactor performs the same redox reaction as the H-cluster is proposed to do in this scheme. While molybdopterins have been shown to feature the crucial electrochemical properties allowing also quinones and flavins to bifurcate electrons [76], it seems difficult to imagine the reduction of soluble ferredoxins at the molybdopterin site in the light of the known 3D-structures of this class of enzymes [7,77]. To our minds the only potentially electron bifurcating site needs to be the flavin within the flavin module. We admit that an adequate mechanistic theory so far is sorely missing. However, we suspect that the single flavin must somehow integrate the distinct redox functions of the two electrochemically differing flavins hypothesised previously. To accomplish this feat, the electrochemical properties of this single flavin may be more malleable and tunable by external parameters than previously thought. Recent studies pinpointing sequence stretches in the flavin module which distinguish ferredoxin-dependent [FeFe]-hydrogenases from ferredoxin-independent ones [24] or unraveling conformational changes within this module which potentially alter the energetic landscape of the entire bifurcating reaction [78] may provide first clues into how the single flavin can be coaxed into acting in two electrochemically different ways to fulfill the roles of both previously proposed flavin entities.

It is worth restating that the above definition of electron bifurcation thus differs from that frequently used in the literature on [FeFe]-hydrogenases and formate dehydrogenases which calls an enzyme from this group electron bifurcating/confurcating if it reduces/oxidises ferredoxins while it redox-connects the NAD(P)H/$NAD(P)^+$ couple to the H^+/H_2 or CO_2/formate couples. The ferredoxin-reducing process, however, appears as a special case in our definition of electron bifurcation which, by contrast, also considers situations where reducing equivalents on a 2-electron compound are bi-/confurcated to/from two individual 1-electron centres and none of the two electrons goes to or derives from a ferredoxin. Rather than "bifurcating" or "non-bifurcating" [24] we suggest to refer to these enzymes as "ferredoxin-dependent" or "ferredoxin-independent". Distinguishing the bifurcating $2e^-/2 \times 1e^-$-reaction from the generation of reduced low potential acceptors allows to integrate the cases of the ferredoxin-independent [FeFe]-hydrogenases [57] and formate dehydrogenases (which may

both operate in a way related to complex I, that is, bifurcate electrons towards two distinct 1-electron chains, however without reducing ferredoxins). This distinction may also help to provide insights for understanding the observation of less-than-strict coupling of ferredoxin reduction in certain [FeFe]-hydrogenases [8,12,13].

3.5. Phylogenetic relationships between and within the four families of NAD(P)-dependent enzymes and mapping of structural/functional particularities onto the tree

We have used sequences of the Y-junction module as queries against complete RefSeq genomes available in NCBI databases to search for the presence of gene clusters containing this module. In the majority of cases where the sequence of the Y-junction module was detected, the surrounding gene cluster (see Fig. 4) also featured ORFs coding for the flavin module and the individual clusters could be attributed to one of the four enzyme families introduced above plus an additional enzyme family to be discussed below (Section 3.5.6) *via* their dissimilar catalytic subunits/domains. However, significant variability in the detailed make-up of these gene clusters was observed resulting in corresponding variability in the structural layout of these individual enzymes (see Figs. 4 and 5a, b). Rare examples of gene clusters which include the Y-

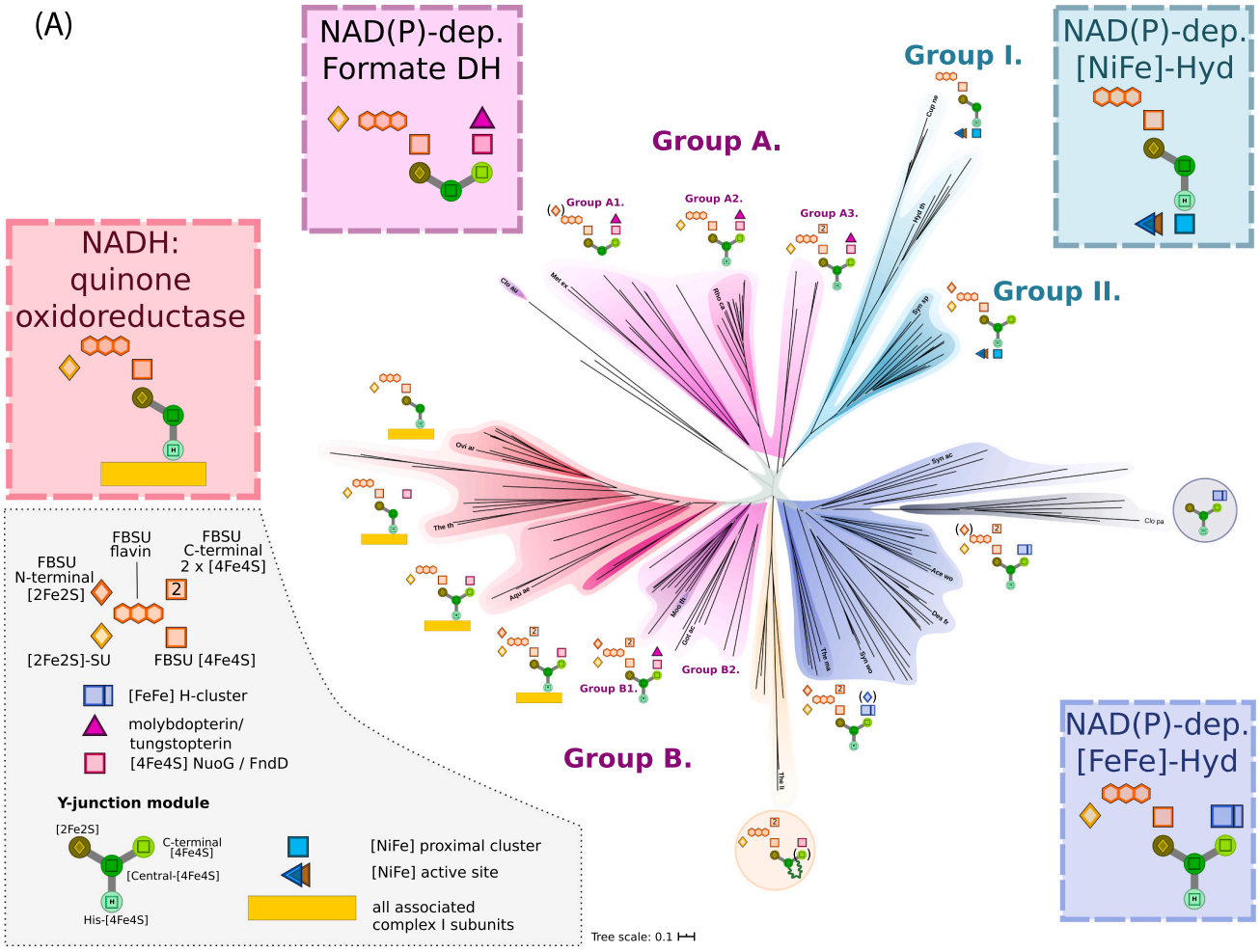

Fig. 5. a: Neighbor-Joining Tree of the Y-junction module in representative sequences.
Similarity clustering of the sequences belonging to the [FeFe]-hydrogenase (in blue), complex I (in red), [NiFe]-hydrogenase (in cyan) and formate dehydrogenase (in purple). Minimal subunit and cofactor composition of the proteins including the [2Fe-2S]-containing subunit ([2Fe-2S]-SU), flavin/[4Fe4S]-binding subunit (FBSU), as well as specific subunits for all members of each protein family are shown as pictograms in the colored square. Additional specific cofactors characterising a specific group inside each protein family can be found as small pictograms at the representive leaves of the tree. Symbols enclosed by parentheses indicate the presence of the cofactor and/or the binding domain of that cofactor in the majority of sequences of the respective group. The symbols used are the same throughout all figures and tables. Grey clouds and grey-colored branches indicate bootstrap values below 50%. Species name abbreviations are shown for selected characterised enzyme complexes. Fully annotated tree can be found in Supplementary Fig. 4a.

b: Neighbor-Joining Tree of the flavin module in representative sequences.
Similarity clustering of the sequences belonging to the [FeFe]-hydrogenase (in blue), complex I (in red), [NiFe]-hydrogenase (in cyan) and formate dehydrogenase (in purple). Cofactor composition of the enzymes are shown as pictograms as in panel a. Additional specific cofactors characterising a specific group inside each protein family can be found as small pictograms at the representive leaves of the tree. Symbols enclosed by parentheses indicate the presence of the cofactor and/or the binding domain of that cofactor in the majority of sequences of the respective group. The symbols used are the same throughout all figures and tables. Grey clouds and grey-colored branches indicate bootstrap values below 50%. Species name abbreviations are shown for selected characterised enzyme complexes. Fully annotated tree can be found in Supplementary Fig. 4b.

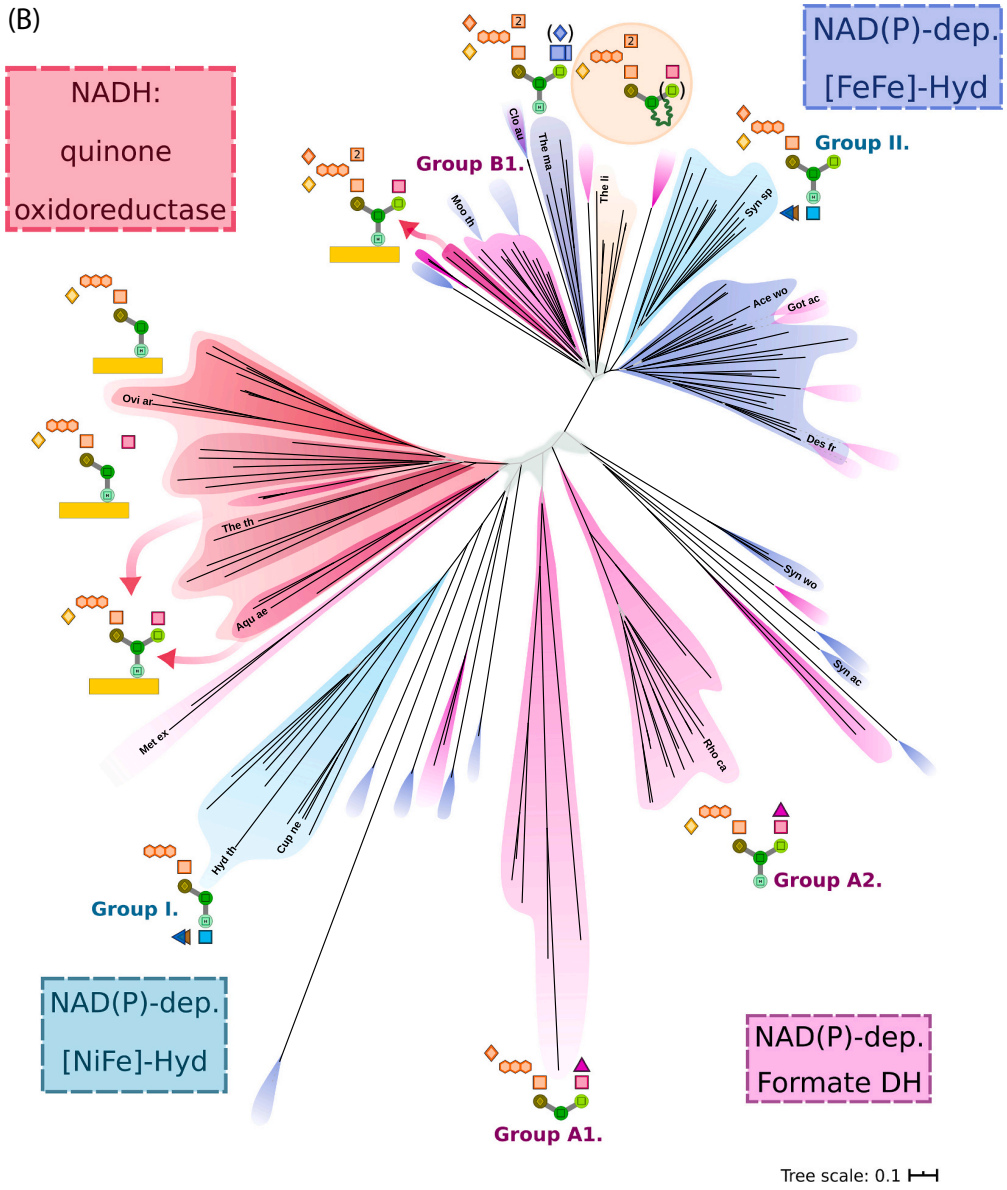

Fig. 5. (*continued*).

junction module but not the flavin module were excluded from the present analysis which focuses on the NAD(P)-dependent enzymes. These rare cases likely correspond to so far unknown enzymes.

Phylogenies of both the Y-junction and the flavin modules were reconstructed and are shown in Fig. 5a and b, respectively. Sequences of the Y-junction module are contiguous with no significant indels (the only exception shall be discussed in Section 3.5.6) and contain amino acid residues ligating between three and four iron-sulphur clusters. The 12–16 conserved residues are evenly distributed over the entire sequence and therefore substantially facilitate the alignment. The sequence stretch considered for tree reconstruction amounts to 200 amino acid residues on average (alignment of the Y-junction module can be found in Supplementary Fig. 1). In addition to these functionally conserved residues, sequences of the Y-junction module exhibit several stretches of high conservation. The flavin module, by contrast, is frequently split into two to three subunits requiring concatenation for tree reconstruction. We restricted the concatenation procedure to the two ubiquitously present domains as discussed above and highlighted in Fig. 3 (Section 3.1.3 and Supplementary Fig. 2). The concatenated sequences of the flavin module contain on average 510 amino acid residues. Neither the Y-junction nor the flavin module therefore correspond to very large molecules and the number of phylogenetically informative sequence sites therefore is limited. This resulted in low bootstrap values (visualized by grey shaded branches in the phylogenetic trees in Fig. 5a and b) for some of the lowest nodes connecting the individual enzyme families. These low bootstrap values preclude firm inferences on the sequence of evolutionary events during emergence of the entire superfamily of these NAD(P)-dependent enzymes. However, individual clades were strongly bootstrap-supported.

The phylogenetic tree of the Y-junction module shown in Fig. 5a clearly distinguishes the four groups of enzymes discussed above, that is, the NAD(P)-dependent subfamilies of [FeFe]-hydrogenases (on a dark blue background shading), [NiFe]-hydrogenases (cyan background), formate dehydrogenases (purple background) and complexes I (red background). The molecular layout of the enzymes and the presence or absence of specific redox cofactors were deduced from the organisation

of the observed gene clusters and the presence/absence of conserved motifs (as shown in Supplementary Table 1). The conserved general outline of the gene clusters in the various families is schematically presented in Fig. 4.

The schematic pictograms drawn within the boxes of Fig. 5a indicate the respective minimal cofactor composition for each of the four main enzyme families. When individual clusters within a family subtree share common setups with additional redox centres, these arrangements are shown in smaller pictograms drawn at the representive leaves of the tree in Fig. 5a and b. For branches which don't feature pictograms, their specific additional cofactor complement varies too much to be explicitly displayed without overloading the figure. Fully-annotated trees can be found in the Supplementary Fig. 4a and b, for Fig. 5a and b, respectively. The exact layout of each enzyme considered in this study is specified in the Supplementary Table 3.

3.5.1. *Did the Y-junction- and the flavin-module coevolve?*

A detailed inspection of the well-defined clades in Fig. 5a and b shows that the phylogenies reconstructed from the Y-junction- and the flavin module feature very similar clusterings. However, the general layout of these trees, that is, the ordering of low-branching nodes, differs substantially between Fig. 5a and b. This may in part be due to poor reliability of the deep branchings mentioned above. By contrast, several discrepancies between the two trees cannot be rationalised by low bootstrap support. The tree of the flavin module in fact shows a pronounced and strongly bootstrap-supported (99.6%) cleavage into two subtrees which notably tears apart the two individual clades of [NiFe]-hydrogenases (denoted as Group I and II, respectively, see Section 3.5.3) as well as numerous [FeFe]-hydrogenases and formate dehydrogenases, all of which are grouped together in the tree of the Y-junction module.

A second indisputable discrepancy consists in the fact that in the tree of the flavin module, formate dehydrogenases are interspersed within [FeFe]-hydrogenases and *vice versa*. Even in the absence of any tree reconstruction, the multiple alignments by themselves already show that the respective sequences are much more closely related to those of neighboring branches corresponding to dissimilar enzymes than to those of their genuine family.

We consider that the following observations show a lead to a possible and quite parsimonious rationalisation of the above described discrepancies: (a) The Y-junction module almost perfectly clusters individual enzyme families. (b) The Y-junction module is fused to the catalytic domain in all representatives of NAD(P)-dependent [FeFe]-hydrogenases and formate dehydrogenases hindering shuffling of genes encoding these two protein domains between different gene clusters in the same species or even inter-species. (c) As already touched upon in Section 3.3, from an electrochemical point of view the CO_2/formate and the H^+/H_2 couples are basically indistinguishable. Interchanging flavin modules between these two families therefore does not require redox adaptations and resulting hybrids would be instantly fully functional. (d) The split in the flavin tree of Fig. 5b reflects a dichotomy which has recently been proposed by Losey et al.(2020) to be linked to the ability/disability of [FeFe]-hydrogenases and formate dehydrogenases to exchange electrons derived from the flavin-based bifurcation/confurcation reactions with the pool of low potential ferredoxins/flavodoxins as defined in Section 3.4.2 [24].

The ensemble of these findings suggest the following scenario: The Y-junction module almost strictly coevolved with the catalytic domains of the respective enzyme families rationalising the at first sight puzzling observation that a tree based solely on sequences of the Y-junction module manages to reproduce the grouping of the diverse enzyme families. The flavin module, by contrast, can be interchanged between (particularly [FeFe]-hydrogenase and formate dehydrogenase) families which explains the occurrence of hybrid enzymes. The equivalence of the formate and hydrogen redox reactions furthermore may rationalise the emergence of more exotic cases such as that characterised in *Clostridium autoethanogenum* [14,48] which merges [FeFe]-hydrogenase, formate dehydrogenase, the Y-junction and the flavin module into a super-enzyme (see Supplementary Section 3). Finally, if the proposal by Losey et al. [24] that the major dichotomy of the flavin module tree corresponds to its ability/disability to reduce low potential ferredoxins/flavodoxins (see Section 3.4.2), should weather the challenges of an increasing number of characterised enzymes, this would point towards very early divergence of the flavin module into two groups involving or excluding ferredoxin/flavodoxin redox reactions in/from the bifurcation/confurcation process. According to the metabolic needs of each organism it may then have plugged either of these functionally different modules onto their respective enzymes.

The molecular layout of the two clades (denoted as Group I and Group II) of [NiFe]-hydrogenases appears to be in line with this hypothesis. While these two clades appear as close sisters in the tree of the Y-junction module, they are pulled apart into the distinct regions of the flavin tree. The 3D-structure of the characterised enzyme (Fig. 3B) as well as the predicted molecular makeup of the other representatives in this clade (Group I in Fig. 5a) show that the flavin module lacks the [2Fe-2S] centre, a redox cofactor which most likely is indispensable for electron transfer between the flavin and soluble ferredoxins/flavodoxins. Characterised [NiFe]-hydrogenases from this clade do not exchange electrons with the low potential soluble carriers. In line with these structural considerations, these enzymes are found within the ferredoxin-independent part (according to [24]) of the tree. The representatives of the Group II clade (located within the presumed ferredoxin/flavodoxin-dependent part of the flavin tree), by contrast, have the full complement of redox centres also found in ferredoxin-dependent [FeFe]-hydrogenases and formate dehydrogenases at their disposition. Biochemically studied cases from Group II have been shown to exchange electrons both with $NAD(P)^+$/NAD(P)H and ferredoxins or flavodoxins, although a potential coupling of these two reactions could not be conclusively assessed so far [79,80]. We will present more speculative assessments of the very early evolutionary pathways of the enzyme families towards the end of this article. In the following we will first discuss both the fine structure of the tree and the pertinence of the observed structural and functional idiosyncrasies.

3.5.2. *NAD(P)-dependent [FeFe]-hydrogenases*

3.5.2.1. Phylogenetic distribution and molecular layout. As suggested by the tree of the Y-junction module in Fig. 5a, the NAD(P)-dependent [FeFe]-hydrogenases form a compact clade with several deep-branching subclades. The gene cluster compositions of the enzymes representing this clade strongly resemble each other (Fig. 4) to the exception of the subclade clustering around the *C. pasteurianum* enzyme (see Section 3.5.2.2). The clade of NAD(P)-dependent [FeFe]-hydrogenases comprise sequences encoded by genes which are annotated in their respective genomes as either "hnd", "hyd", "hyt" or "hym". These dissimilar naming schemes do not coincide with phylogenetic clustering but are purely historical. The alphabetical numbering of subunits, despite substantial homologies and strongly conserved succession in gene clusters (Fig. 4), furthermore differs between the Hnd-, Hyd- *etc.* naming schemes. To avoid confusion when discussing the molecular makeup of enzymes in this clade, we have adopted the Hnd-type nomenclature throughout and provide in Supplementary Table 2, the correlation between all these naming schemes. The introduction of the term Hnd was originally motivated by the fact that these hydrogenases are NAD(P)-dependent and, in the light of the fact that all cases treated in this work contain the flavin module, we consider this nomenclature as the most appropriate.

So far in prokaryotes, Hnd-type enzymes are exclusively found in Bacteria. They share this trait with their NAD(P)-independent relatives further corroborating the picture that [FeFe]-hydrogenases are absent from the archaeal domain [81].

Hnd-type enzymes generally occur as tetrameric, trimeric or in rare

occasions as dimeric versions. In the ciliate *N. ovalis*, a eukaryote, even a monomeric Hnd has been found [82,83]. It has been proposed previously that the small HndB subunit of the tetrameric form corresponds to an N-terminal domain of the flavin containing HndC subunit in trimeric manifestations of the enzyme and that therefore the molecular layouts of tri- and tetrameric versions are virtually the same [12,16]. Mono- and dimeric forms represent more extensive fusions of subunits [24]. Our genome survey corroborates this view since in all trimeric cases we retrieved, the N-terminal domain of the HndC subunit, when it exists, shows intriguing sequence similarities with the HndB proteins (Such homology is illustrated by same color and shade in Fig. 4). HndB, just as the [2Fe-2S]-domain of HndA, have been predicted to feature the fold of Trx-like [2Fe-2S]-ferredoxins as discussed in Section 3.4.1.

We furthermore found four trimeric sequences (also discussed in Section 3.4.1), with a domain homologous to HndB fused to the C-terminal end of the catalytic [FeFe]-hydrogenase subunit HndD (see Fig. 4). A clustering of these four cases is observed both in the Y-junction- and the flavin-module-tree. No clustering into tri- and tetrameric clades can be observed on these trees (in accordance with [16]). While the lower nodes on the tree aren't supported by high bootstrap values, higher level branchings come close to 100% bootstrap support and in several cases such nodes separate tri- from tetrameric representatives. We therefore conclude that the gene fusion/fission of the DNA-stretch coding for the HndB subunit has occurred several times independently during [FeFe]-hydrogenases' evolutionary history from their emergence to the present day.

3.5.2.2. The C. pasteurianum-type monomeric, NAD(P)-independent enzymes possibly derive from NAD(P)-dependent hydrogenase ancestors. As mentioned above we restricted this analysis to enzymes that contain both the Y-junction and the flavine module. As the only exception to this rule we included the monomeric enzymes resembling the *C. pasteurianum* [FeFe]-hydrogenase (denoted by a dark-grey background within the tree of [FeFe]-Hydrogenase in Fig. 5a). Since this entire work was initially triggered by the observation of a structural module conserved between the *C. pasteurianum* (*i.e.* NAD(P)-independent!) [FeFe]-hydrogenase and the three NAD(P)-dependent enzymes shown in Fig. 1, we found it indispensable to include the *C. pasteurianum* sequence into our phylogenetic analysis (as it also guided the structure model informed alignments, Supplementary Fig. 1). To increase the reliability of nodes, we searched genomes for further cases related to the *C. pasteurianum* enzyme, that is, featuring the Y-junction module as N-terminal (F-) domain with a [FeFe]-catalytic (H-) domain but lacking genes coding for the flavin module. The resulting tree topology draws an intriguing evolutionary picture. All *C. pasteurianum*-type enzymes cluster together and emerge as a subclade from within the tree of NAD(P)-dependent [FeFe]-hydrogenase (Fig. 5a). The most parsimonious interpretation of this topology is that *C. pasteurianum*-type enzymes derive from NAD(P)-dependent precursors which still contained the flavin module. The Y-shaped form of the electron entry/exit pathways to and from the catalytic H-cluster thus would find its *raison d'être* as an evolutionary relic from an NAD(P)-dependent past. This of course does not necessarily mean that the two distinct electron transfer pathways aren't physiologically relevant in the extant *C. pasteurianum* enzyme and its relatives [32]. However, rather than having specifically emerged to perform such physiological functions, they derive from a different kind of process, that is, branched electron transfer as in the Hnd-type enzymes, and have been attributed novel functions when the flavin module got lost. The low bootstrap support at the base of this clade cannot strictly rule out alternative scenarios which would have in common that they consider an [FeFe]-hydrogenase devoid of the flavin module as the ancestor of the Hnd family. However, such scenarios would entail the necessity for extensive lateral transfer of both the flavin and the Y-junction module across all families rendering them significantly less parsimonious than the above proposed one.

3.5.3. NAD(P)-dependent [NiFe]-hydrogenases

As mentioned above, this family features a deep branching into two clades (Group I and Group II in Fig. 5a and b). The first group shows a further, more recent divergence into two subclusters of sequences. The structurally and biochemically known enzyme from *H. thermoluteolus* (Fig. 1G–I [6,84]) and the biochemically best characterised complex from *Cupriavidus necator* (formerly called *Alcaligenes eutrophus*) belong to Group I and represent relatively typical members of their particular subclade [21,22,85]. They contain only three iron-sulphur clusters in the Y-junction module (missing the C-terminal cluster as indicated in Fig. 1G and H) and furthermore lack the [2Fe-2S]-centre from the pair of clusters flanking the flavin (Fig. 3). This implies that (a) the Y-junction module cannot mediate branching into two distinct electron transfer pathways and (b) the reduction of the flavin cannot occur in a confurcating 2-electron process but the electrons must reach the flavin one-by-one on their way from the H_2-oxidising catalytic site of the [NiFe]-hydrogenase or *vice versa*. Electron transfer in the enzymes from this clade therefore necessarily is linear as indicated in Fig. 1G. Consequently, we predict that in these enzymes the flavin features a relatively high stability constant for its semi-reduced form to facilitate one-by-one reduction [62].

By contrast, the second clade forms a single radiation (Group II in Fig. 5a and b). All members of Group II not only seem to contain the [2Fe-2S]-cluster next to the flavin but their Y-junction modules contain the full set of all four iron-sulphur centres and their Y-junction/flavin-module dyad therefore strongly resembles that of ferredoxin/flavodoxin-dependent and NAD(P)-dependent [FeFe]-hydrogenases and formate dehydrogenase. It hence is tempting to assume corresponding functional properties. Experimental evidences gathered on the cyanobacterium *Synechocystis* sp. *PCC 6803* give credence to this assumption. *In vitro* tests in cell-free extracts have shown a significant increase in hydrogen production upon addition of ferredoxin or flavodoxin, indicating a potential second donor/acceptor [79]. These experimental results may indicate a less-than-strict coupling of NAD(P) and ferredoxin redox reactions as also observed in the Hnd-enzyme from *D. fructosovorans* [8]. While we would suggest a bifurcating ability in these enzymes, to our knowledge a coupling of the reductions of ferredoxin and of NAD^+ by electrons derived from hydrogen has not been unambiguously demonstrated so far (however, see Artz et al. [86]).

We were unable to detect any archaeal representatives of this enzyme family and the detailed structure of its subtree shows only little resemblance to species trees. At the present state of available genome data, it therefore seems likely that this enzyme emerged in Bacteria and was subsequently distributed largely *via* horizontal gene transfer over the bacterial domain. As a caveat to these conclusions, it is worth mentioning that heterotetrameric, soluble NADP-dependent [NiFe]-hydrogenases can be found in the euryarchaeal family of Thermococcaceae with characterised proteins from *Thermococcus litoralis* [87], *Thermococcus kodakarensis* [88] and *Pyrococcus furiosus* [89]. Besides a certain degree of similarity in the catalytic hydrogenase subunits, we were unable to identify a Y-junction module nor could we find similarities in the sequences of the respective flavin subunits (the flavin can occur either as FAD or as FMN in these cases). While they have been called "Hox-type" hydrogenases by some authors [90], we have not considered them here since they are extremely divergent with respect to those dealt with in our phylogenetic analysis. Whether archaeal enzymes of this type will ultimately modify the tentative conclusions on the ancestrality of this clade remains to be seen.

3.5.4. NAD(P)-dependent formate dehydrogenases

A few isolated cases of this type of enzyme have been dealt with in the literature [7,11,41,47,49–51,91,92] and phylogenetic investigations are scarce [93]. In the phylogenetic tree reconstructed from sequences of the Y-junction module (Fig. 5a), all cases containing a formate-

dehydrogenase of the Mo/W-*bis*PGD-type cluster into five groups, well-separated from the NAD(P)-dependent versions of both [FeFe]- and [NiFe]-hydrogenases. Three of these groupings are also seen in the tree based on flavin module sequences (Fig. 5b).

The common presence of the flavin module in all formate dehydrogenases in the tree implies that all these enzymes are indeed NAD(P)-dependent and belong to a homogeneous group. Similar to what we discussed in Section 3.5.2 for [FeFe]-Hydrogenases, several naming schemes are in use for this enzyme family (*e.g.* Fds [41,94], Fdh [91,93,95] or Fno [96]). To avoid confusion, we will apply the "Fds"-scheme to all these enzymes and specify nomenclature correspondences with Table 1 and Supplementary Table 2.

In the depicted phylogeny of the Y-junction module, the subtree of NAD-dependent complexes I grows out of one of the clades of the NAD(P)-dependent formate dehydrogenases. This intriguing observation will be discussed at length in the following section (Section 3.5.5) dealing with the complex I subtree.

In striking contrast to NAD-dependent [FeFe]- and [NiFe]-hydrogenases, a few clusters of NAD(P)-dependent formate dehydrogenase-type enzymes show deep splittings into archaeal and bacterial subgroups. Group A3 in Fig. 5a, for example, is characterised by a deep (Eury-)Archaea/Bacteria divergence but unfortunately this clade so far contains only two representatives for each prokaryotic domain. In enzymes from this clade the Y-junction module retains all four clusters and the flavin module is equipped with both clusters flanking the flavin. All representatives are trimeric, *i.e.* their small subunit is fused to the flavin-binding FdsB subunit. Since the complement of redox cofactors is equivalent to that of Hnd- and Fds-type enzymes for which ferredoxin reduction *via* electron bifurcation (see Sections 3.2 and 3.3) has been experimentally observed, it seems tempting to assume that the enzymes in Group A3 are able to fulfill similar functions. However, while the flavin modules of the two archaeal representatives indeed cluster within the "ferredoxin/flavodoxin-dependent" domain (see Section 3.5.1) of the tree shown in Fig. 5b, the two bacterial sequences are part of the lower, ferredoxin-independent subtree and biochemical information on the respective enzymes will be required to settle this question.

Enzymes from a further archaeal cluster (denoted as Group A1 in Fig. 5a) differ significantly from the above mentioned euryarchaeal examples. This group encompasses both Cren- and Euryarchaea as well as two additional bacterial species. They all lack the histidine cluster in the Y-junction module and most of them don't possess a flavin-flanking [2Fe-2S]-cluster. Only the enzymes from the *Aciduliprofundum* genus retain this cluster. Again to the exception of these two euryarchaeal cases, all members of the group are dimeric enzymes with one polypeptide encompassing the entire flavin module. The absence of two crucial [Fe-S]-clusters makes the possibility of a communication with soluble ferredoxins in these enzymes doubtful. Two proteobacterial

Table 1
Subunit and cofactor nomenclature.

Subunit nomenclature used in this article	Multimeric [FeFe]-hydrogenase[a]		Complex I[b]		Bidirectional [NiFe]-hydrogenase[c]		Formate dehydrogenase[d]		Symbol	Cofactor
YJM-subunit	**HndD** (HydA)	FS2	**NuoG** (Nqo3 75 kDa SU)	N1b	**HoxU**	U1	**FdsA** (alpha SU)	A5		[2Fe-2S]
		FS4C		N5		U3		A4		[4Fe-4S]
		FS4B		N4		U2		A3		[4Fe-4S]
		FS4A		n.n.		n.n.		A2		[4Fe-4S]
		n.a.		N7		n.a.		A1		[4Fe-4S]
		n.a.		n.a.		n.a.		Mo/W-pterin		
		H-cluster		n.a.		n.a.		n.a.		
flavin/[4Fe-4S] subunit	**HndC** (HydB)		**NuoF** (Nqo1, 51 kDa SU)		C-terminal **HoxF**		**FdsB** (beta SU)			[2Fe-2S]
										flavin
		n.n.		N3		F1		B6		[4Fe-4S]
									2	2 [4Fe-4S]
[2Fe-2S]-binding subunit	**HndA** (HydC)	n.n.	**NuoE** (Nqo2, 24 kDa SU)	N1a	**HoxE** or N-terminal **HoxF**	n.n.	**FdsG** (gamma SU)	G7		[2Fe-2S]
small subunit	**HndB** (HydD)		n.a.		n.a.		**FdsX**			
			n.a.		n.a.		**FdsD** (delta SU)			

Subunit and cofactor composition of the characterised protein complexes containing the Y-junction module. Coloring scheme for each protein complex and symbols used to denote the presence of specific cofactor binding sites same throughout the paper. Subunits in the same rows (from left to right) are homologous to each other. Cofactor binding sites in the same row (from right to left) are homologous to each other. Bold names are used throughout the publication to refer back to specific subunits. A more extensive nomenclature table specifically for [FeFe]-Hydrogenases and Formate Dehydrogenase is given in Supplementary Table 2.
n.a. - not available, *i.e.* cofactor not present.
n.n. - no naming convention.
SU - subunit.
[a]Nomenclature according to Peters et al. (1998) for [FeFe]-hydrogenase (in blue) [3].
[b]Nomenclature according to Sazanov and Hinchliffe (2006) for complex I (in red) [33].
[c]Nomenclature according to Shomura et al. (2017) for bidirectional [NiFe]-hydrogenase (in cyan) [6].
[d]Nomenclature according to Radon et al. (2020) for formate dehydrogenase (in purple) [7].

representatives, *Methylorubrum extorquens* (Met ex) and *Cupriavidus oxalaticus* (Cup ox), are associated with this archaeal clade (see Supplementary Fig. 3a). Notably, these two bacterial sequences do not cluster with archaeal ones in the tree of the flavin module. Their Y-junction module lacks the histidine-cluster, a feature not found in other bacterial NAD(P)-dependent formate dehydrogenases but characteristic for the mentioned archaeal clade. The low bootstrap support for the nodes of these two bacterial sequences favours the assumption that pulling them into the archaeal clade is driven by the common absence of the residues ligating the histidine cluster and therefore a tree-building artefact. This effect likely also explains the positioning of the sequence of the dimeric enzyme from the Archaeon *Methanothermobacter methylutens* (Met me) basal to the bacterial cluster Group A2 next to the archaeal Group A1. This sequence contains the histidine-ligating residues (just as all bacterial members of this clade) which likely drags its branch over from the archaeal clade. In the tree of the flavin module its branch is indeed part of the corresponding archaeal clade. We therefore consider it highly likely that the groups A1 and A2 in Fig. 5a in fact correspond to well-separated archaeal and bacterial clades, respectively. Potential evolutionary consequences of such a clustering will be discussed below.

Members of Group A2 contain both tri- and tetrameric manifestations of the enzyme in a strongly mingled manner. However, the 3D structure model of the A2-type enzyme from *Rhodobacter capsulatus* (Rho ca) [7] indicates that, in stark contrast to NAD(P)-dependent [FeFe]-hydrogenases, the fourth subunit (denoted FdsD, see Fig. 4) in the tetrameric versions (a) does not resemble thioredoxin-like [2Fe-2S]-proteins (see Section 3.4.1) and (b) is located on the surface of the catalytic molybdopterin-subunit. Like the enzymes from Group A3, the members of this group feature the full set of cofactors required to bifurcate electrons and to connect to the ferredoxin pool. In fact, for the tetrameric enzyme from *Methylosinus trichosporium* (Met tr) the absence of an observable flavin semiquinone species [49], indicative for inverted redox potentials, supports this scenario. Further biochemically characterised members of Group A2 are the Fds enzymes from *Rhodobacter capsulatus* (Rho ca) [50] and *Cupriavidus (C.) necator* (Cup ne) [41] for which the structural models of the entire protein [7] or the flavin module [47] have been recently obtained. In addition, the latter study regarding the enzyme of *C. necator* observed a neutral semiquinone species by EPR, thereby suggesting a ferredoxin-independence of the reaction. Such a ferredoxin-independent reduction of CO_2 by NADH could also be shown for its relative *C. oxalaticus* (Cup ox) [97].

The cluster denoted as Group B again contains tri-and tetrameric enzymes exclusively from the bacterial kingdom. In contrast to the above mentioned Group A2, the fourth subunit in the tetrameric versions in this group is a homolog of the HndB protein of [FeFe]-hydrogenases. Since the name FdsB is already taken by the flavin/[4Fe-4S]-subunit of the flavin module, we have chosen to denote the gene coding for this subunit as fdsX in Fig. 4.

We have organised Group B into a larger group B2 encompassing a second enzymes cluster denoted as group B1, which homogeneously display the full complement of redox centres involved in electron bifurcation and in branched electron transfer. Members of the enclosing Group B2, by contrast, show more heterogeneous layouts of subunits and cofactors (specific information for each individual representative can be found in the Supplementary Table 3). Group B2 contains the only Fds-enzyme for which electron bifurcation involving reduction of ferredoxins has been demonstrated experimentally, *i.e.* the Fds from *Gottschalkia acidurici* [11]. Unfortunately, the gene cluster organisation of this very case deviates somewhat from that of the bulk of cases situated in this group. Its gene cluster features a Y-junction module (with the FdsA specific A1 cluster, see Table 1) as separate ORF together with two distinct catalytic formate dehydrogenase subunits, each of which contains its own Y-junction module as an N-terminal extension. The two latter Y-junction module sequences cluster together (not shown since difficult to discern on the scale of the tree), indicating relatively recent gene duplication events. However, the Y-junction module encoded by a separate gene located in between the duplicated catalytic subunits and the flavin module, is of yet indetermined origin (and not included in the trees). A traditional flavin module is also present. While the global conformation of all other enzymes can be reasonably well predicted based on the 3D-structure models shown in Fig. 1, imagining the spatial layout of this specific enzyme appears more challenging to us. For the more abundant cases, however, a similar cofactor arrangement as for Hnd-type enzymes is likely as already proposed by Hille et al. [94].

The representatives making up Group B1 in Fig. 5a are found to also cluster together in the tree of the flavin module (Fig. 5b) and more precisely in the subtree suggested to represent ferredoxin/flavodoxin-dependent cases [24]. By contrast, members of Group B2 as defined by the tree based on the Y-junction module do not cluster in the flavin module tree but interestingly are interspersed either within clades representing Hnd-type enzymes or in between Hnds, [NiFe]-hydrogenases and "glutamate-synthase-insertion" (see below, Section 3.5.6) clades. Nevertheless, all these latter disperse branches (to the sole exception of *Desulfobacca acetoxidans*) are still part of the "upper" subtree, possibly indicating ferredoxin/flavodoxin-dependent enzymes in line with the biochemical characterisation of the *G. acidurici* enzyme [11]. This indicates that their flavin modules do not derive *via* vertical inheritance from their counterparts in the ancestral enzymes but rather from genes transferred from diverse sources into the respective operons to replace the original flavin modules of these ancestors.

These enzymes therefore all represent "reassembled" forms merging genuine "Y-junction-module/formate-dehydrogenase" subunits with flavin modules from other enzyme systems as already mentioned in Section 3.5.1. All enzymes but one from both Group B1 and B2 share the trait of belonging to the putatively ferredoxin/flavodoxin-dependent [24] subtree of Fig. 5b.

A small number of cases do not follow the gene cluster scheme for NAD(P)-dependent formate dehydrogenases as outlined in Fig. 4. These cases are further discussed in the Supplementary Section 3.

3.5.5. NAD-dependent complex I

We again emphasise that we here deal only with a subgroup of what is frequently referred to as complex I, *i.e.* those complexes I which contain the NuoEFG module and thus certainly redox-convert NAD during their catalytic cycle (as discussed in Supplementary Section 1). More specifically, the evolutionary conclusions we will draw below only pertain to this EFG-module and do not inform on the evolutionary history of the remaining modules of the enzyme, that is, the quinone-module and the actual ion-pumping subunits.

Rather than appearing as a separate family, the phylogenetic tree shown in Fig. 5a features complex I's Y-junction module as emanating from within the B1-Group of NAD(P)-dependent formate dehydrogenses. While the bootstrap values supporting this topology are respectable (48%), they are certainly far from suggesting infallible reliability. However, a range of structural features which can be deduced from the amino acid sequences of the relevant protein subunits both of true NAD(P)-dependent formate dehydrogenase- and complex I-gene clusters corroborate a gradual transitioning from an NAD(P)-dependent formate dehydrogenase enzyme towards the NuoEFG module of complex I.

Members of Group B of the Fds therefore show the following features: (1) The presence of the Mo/W-*bis*Pterin centre which catalyses the CO_2/formate redox conversion. The distinguishing amino acid sequence motif for the presence of this cofactor is the conservation of a specific cysteine/selenocysteine residue in addition to a conserved histidine and an arginine which together form a catalytic triad in these enzymes [19]. (2) A Y-junction module which contains all four iron-sulphur clusters. (3) A flavin module which possesses the FMN binding motif as well as conserved cysteines for the two iron-sulphur centres flanking the flavin and which is located within the subtree of Fig. 5b which putatively corresponds to ferredoxin/flavodoxin-dependent enzymes. By contrast,

none of the further subunits characterising complex I are found in their respective gene clusters to the exception of *Pelobacter propionicus*, which is discussed in the Supplementary Section 3. The set of enzymes forming early branching clusters of genuine complex I still retain all iron-sulphur centres and the flavin but they additionally feature the complex I-specific membrane subunits as well as the NuoB/D genes in their gene clusters.

Intriguingly, the lowest-branching complex I cluster (made up from two Geobacter sequences in Fig. 5a) furthermore maintains a conserved cysteine at the sequence position where the 5th Mo/W-ligand is found in formate dehydrogenases (all later-branching complex I enzymes in our tree lack this crucial cysteine/selenocysteine residue). However, the sequence stretch surrounding these cysteines diverges very strongly from those observed in all NAD(P)-dependent formate dehydrogenases.

The flavin-modules of these two enzymes cluster in the ferredoxin/flavodoxin-dependent subtree neighboring those of the B-type formate dehydrogenases. Sequence information thus suggests the tantalising possibility that these two complex I-type enzymes may still contain the Mo/W-*bis*Pterin cofactor and possibly even CO_2/formate redox activity as well as involve ferredoxin/flavodoxin redox reactions in their catalytic processes. Biochemical characterisations of these enzymes will be required to assess the validity of the respective sequence-based functional predictions. The cluster formed by the two Geobacter sequences in Fig. 5b furthermore encompasses a complex I-type enzyme from the Planctomycetes *Kuenenia stuttgartensis*. The bootstrap value of the node for this enzyme's Y-junction module (Fig. 5a) is too low to allow conclusions on positioning within the evolutionary history of complex I.

All complex I representatives branching higher than the two Geobacter sequences in Fig. 5a feature flavin modules which are located in the lower subtree of Fig. 5b, possibly indicating ferredoxin/flavodoxin-independence, as would indeed be expected based on functional characterisations of canonical complex I enzymes. This may imply that the ancestor of all these higher-branching enzymes has replaced its originally ferredoxin-dependent flavin-module by a ferredoxin-independent one, a process which likely has occurred in many NAD(P)-dependent [FeFe]-hydrogenases and formate dehydrogenases (see Section 3.5.4).

When moving up the tree towards more and more recent branchings, a progressive loss of the iron-sulphur centres not involved in the electron transfer chain connecting the flavin module to the quinone binding subunit is observed. Over the evolutionary journey from its inception out of an NAD(P)-dependent formate dehydrogenase up until its form in the mitochondrial complex I, the unit formed by the flavin module and the Y-junction module, obviously has successively lost all the dispensable iron-sulphur centres and individual transition states are still with us as living fossils in the species indicated on the tree of Fig. 5a [33]. In the light of this evolutionary offloading, it is intriguing that the [2Fe-2*S*] centre flanking the flavin, *alias* the N1a cluster, is still present even in the mitochondrial enzyme. The example of the NAD-reducing [NiFe]-hydrogenase of *H. thermoluteolus* (see Section 3.4.1) demonstrates that redox conversions of NAD can be mediated by a flavin module lacking this cluster [84]. A scenario assuming that cluster N1a may be on its way out and disappear in the evolutionary future similar to the other out-of-line clusters, however, seems highly questionable to us. Site-directed mutations eliminating this cluster were seen to entail significant loss of NADH-oxidase activity in *E. coli* [59]. In humans, absence of the subunit harbouring cluster N1a was observed to be associated with debilitating conditions such as Alzheimer's and Parkinson's disease [98]. As outlined above, we suspect that kinetic optimization of the 2-electron oxidation of the flavin in complex I requires the presence of both flanking clusters.

3.5.5.1. Repercussions on the debate of complex I's evolutionary origins. A plethora of scenarios attempting to retrace the evolutionary whereabouts of complex I have been proposed [5,35,99–105]. While they all agree that complex I was assembled from a range of functional units with differing enzyme ancestors, the specific evolutionary roots of particularly the membrane-extrinsic parts, that is, the NAD- and the quinone-redox-converting entities, are controversial. While some models proposed [FeFe]-hydrogenases or formate dehydrogenases as precursors of the NAD-redox converting module [105], others involve NAD-dependent [NiFe]-hydrogenases and formate hydrogenlyase (FHL) as ancestors of both the NAD- and the quinone-binding modules [5,106]. FHL is indeed an intriguing enzyme since it features the presence of a Mo/W-*bis*Pterin subunit together with the two [NiFe]-hydrogenase subunits known to share substantial sequence similarity with NuoB and NuoD, the subunits involved in redox conversion of the quinone in complex I. To top up these similarities, one or more of the proton-pumping membrane subunits are also found to be part of FHL. However, the formate dehydrogenase subunit in FHL is a standard Mo/W-*bis*Pterin protein containing only the canonical adjacent [4Fe-4S] cluster but lacking the N-terminal Y-junction module domain. The small iron-sulphur protein (HycB) of FHLs proposed as homolog of the Y-junction module clearly has a different architecture since no significant conservation of cluster-ligating residues is observed [5]. The flavin module is also absent in FHL. Despite the intriguing overall structural similarities of FHL and complex I, the devil is in the above mentioned details which differ substantially between these two enzymes. Claims of direct evolutionary relationships between these two [107] may therefore have been premature.

The second oft-discussed candidate [100,101,103], the NAD(P)-dependent [NiFe]-hydrogenase, by contrast, contains the Y-junction module, the flavin module and the NuoB and NuoD homologs. It misses the Mo/W-subunit and the membrane subunits together with a few further small subunits. However, the tree of Fig. 5a suggests that the NAD(P)-dependent [NiFe]-hydrogenase is not the phylogenetically closest relative of the respective proteins in NAD-dependent complex I. Instead, the so far only relatively scantly studied NAD(P)-dependent formate dehydrogenase is! This enzyme family featured as the poor cousin among all the evolutionary precursor candidates of NAD-dependent complex I until the characterisation of the *G. acidurici* enzyme by the Thauer group [11] managed to appreciate the catalytic feats performed by this enzyme. The tree of Fig. 5a thus indicates that the NuoEFG module in NAD-dependent complex I directly derives from an NAD(P)-dependent formate dehydrogenase. The ultimate ancestor to complex I's EFG-module may have been the putative ancestral ferredoxin/flavodoxin-dependent version (Section 3.5.4) with a subsequent exchange of the type of flavin-module leading to canonical reaction scheme of complex I. During the evolutionary conversion from a Group B formate dehydrogenase to the NAD-redox converting unit of complex I, the histidine cluster of the Y-junction module saw its function of either connecting the two halves of a dimeric assembly or of mediating electron transfer to or from a ferredoxin in putative monomeric forms of NAD(P)-dependent formate dehydrogenases morphed into being part of the chain of redox cofactors leading "down" towards the quinone binding site of the ancestral, NAD-independent form of complex I. The CO_2/formate converting function of the Mo/W-*bis*Pterin subunit was shut down, initially *via* elimination of the protein ligands to the molybdenum/tungsten and then step-by-step *via* the taking out of further iron-sulphur centres connecting the central cluster of the Y-junction module to the Mo/W-*bis*Pterin subunit. While our data have no bearing on the question of how EFG-less forms of complex I may have arisen, they very strongly indicate that it was a previously overlooked subgroup of NAD(P)-dependent formate dehydrogenases which gave birth to the membrane-extrinsic part of the NADH-oxidising version found in many respiratory chains and eventually in mitochondria.

Astonishingly, the three rhizobial representatives show molecular architectures that deviate from that of other Alphaproteobacteria since they retain both all four clusters in the Y-junction module and the FS0 cluster of the formate dehydrogenase-derived domain similar to what is found in the much lower branching enzymes from the Aquificales. They furthermore branch substantially earlier than Alphaproteobacteria in

the complex I clade of both the Y-junction module and the flavin module trees. It therefore seems likely that these Rhizobia acquired their complex I *via* lateral gene transfer.

3.5.6. The "glutamate-synthase-insertion"-clade

In 2008, Toth et al. [20] reported the characterisation of an enzyme from the Euryarchaeon *Thermococcus litoralis* which features puzzling similarities to Hnd-type enzymes but which stands out by the presence of a long insertion showing substantial sequence similarities to the small subunit of the enzyme glutamate synthase, within the Y-junction module sequence. Toth et al. determined that this enzyme might represent an NAD(P)-dependent polysulphide reductase. Sequences related to this enzyme popped up during our genome surveys and are denoted in the trees of Fig. 5a and b by a beige area. They cluster together and apart from the rest of the tree. Intriguingly, these sequences show a deep Archaea/Bacteria split and therefore potentially diverged from the bulk of other families already in the last universal common ancestor (LUCA). Together with the NAD(P)-dependent formate dehydrogenase enzymes, this clade therefore supports the notion that the functional dyad constituted from the Y-junction- and the flavin-module is evolutionarily ancient and represents a pre-LUCA entity. Enzymes belonging to the glutamate-synthase-insertion-clade certainly are tantalising and to our mind merit further scrutiny. Most recently, a NAD/NADP-transhydrogenase was characterised from the acetogenic *Clostridium Sporomusa ovata* which features a Y-junction module containing this glutamate-synthase-related insertion sequence [108].

4. Conclusions

4.1. The functional unit formed by the Y-junction-/flavin-module dyad likely pre-dates the last universal common ancestor

As mentioned earlier, firm inferences on the evolutionary emergence of the Y-junction-/flavin-module dyad and its earliest diversifications are hampered by low bootstrap support for the deepest nodes of the trees in Fig. 5a and b. However, a few leads can be extracted from these phylogenies. At the time of writing, neither Hnd-type nor NAD(P)-dependent [NiFe]-hydrogenases appear to contain archaeal representatives and therefore do not qualify as potentially present in the last universal common ancestor (LUCA). By contrast, deep Archaea/Bacteria cleavages are observed for NAD(P)-dependent formate dehydrogenase as well as for the "insertion-type" enzymes. The Y-junction/flavin-unit may therefore have emerged already in the LUCA as a functional part of one of these two enzymes. Phylogenies of further representatives and/or of further subunits in their parent enzymes may help to progress in our understanding of the earliest events during spawning of the superfamily of enzymes shown in Fig. 5a and b. For example, the NAD(P)-dependent formate dehydrogenases are a subgroup of a much larger superfamily of formate dehydrogenases which do not contain the dyad, such as the enzymes denoted as Fdh-H, Fdh-N, Fwd *etc*. The composite phylogeny of their molybdopterin-binding catalytic subunits will provide a means of rooting of the NAD(P)-dependent subtee and thus will help to decide whether the NAD(P)-dependent enzymes indeed may have been present in LUCA.

4.2. Lessons to be drawn from the comparative analysis of the enzymes containing the dyad

4.2.1. The Y-junction module is a versatile 3-way redox hub with a poorly understood function

The structural peculiarity of the Y-junction module to provide electron transfer connectivity between 3 distinct electron entry/exit sites on its surface is exploited by diverse enzymes for building a range of dissimilar architectures. Some of these enzymes appear to have shut down one of these pathways by eliminating either the histidine- or the C-terminal iron-sulphur cluster. Others, by contrast, seem to take advantage of the crossroad-functionality in still poorly understood ways. For example, an inter-dimer redox-connection *via* the two respective histidine clusters appears inevitable in the light of the oligomerization arrangement seen in the 3D-structure of an NAD(P)-dependent formate dehydrogenase. The mechanistic implications of such inter-dimer connections have not been explored so far. However, the scarcity of data with respect to oligomerization properties in the vast majority of enzymes considered in this work leaves room for speculations that in some enzymes the 3rd redox pathway may be used to connect soluble carriers to the main electron transfer chain from the main redox substrate to NAD(P). The precise functional role of the peculiar electron transfer crossroad in the Y-junction module thus clearly deserves further exploration.

4.2.2. The electron bifurcating site is located within the Y-junction-/flavin-module dyad

Electron bifurcation-based reduction of low potential ferredoxins or flavodoxins was experimentally observed in NAD(P)-dependent [FeFe]-hydrogenases and NAD(P)-dependent formate dehydrogenases [8,10–13,15,45]. Complex I was shown to bifurcate electrons in its corresponding functional unit (the EFG-module) albeit without relaying to low potential soluble acceptors [58]. As we have discussed in Section 3.5.3, selected NAD(P)-dependent [NiFe]-hydrogenases also couple ferredoxin redox reactions to their canonical catalytic activities, although the strength of coupling has not been explored so far. The only element common to these 4 distinct enzyme families is the Y-junction-/flavin-module dyad. We therefore find it ineluctable that it is this structural unit which confers the ability to perform electron bifurcation. In none of the remaining, extremely diverse protein subunits has electron bifurcation ever been observed. As argued in Section 3.4.2, the Y-junction module lacks the electrochemical properties conducive to electron bifurcation and we therefore favour the flavin module as the actual electron bifurcating entity.

4.2.3. The strong conservation of the dyad between all families renders the presence of a second flavin in Hnd-type [FeFe]-hydrogenases unlikely

The absence of a 3D-structure for Hnd-type enzymes together with conceptual difficulties to rationalise the observed reaction patterns using only a single flavin led to the proposal that Hnd-type enzymes actually contain two distinct flavins [8,36], one dedicated to the bifurcation of electrons and the second one performing the 2 × 1-electron-to-2-electron gating function for NAD(P)H oxidoreduction (as for example observed for the flavin moiety located on the small subunit of Nfn) [8,36]. For NAD-dependent complex I, NAD(P)-dependent formate dehydrogenase and NAD(P)-dependent [NiFe]-hydrogenase, 3D-structures are now available [6,7,33,47,109,110]. In all these structures only one flavin is found in a strictly conserved location. The high similarity of the amino acid sequences in the subunits constituting the Y-junction-/flavin-module dyad between the diverse enzymes and in particular between formate dehydrogenase and Hnd-type [FeFe]-hydrogenase families to our minds leaves no leeway for the presence of a second flavin in the Hnd-type enzymes. The observed mode of functioning thus must almost certainly be explained on the basis of only a single flavin moiety. The difficulties to come up with a straightforward rationalisation using only one flavin precisely was the reason for postulating the two-flavin models and the comparative analysis of the diverse enzymes dealt with here unfortunately takes us back to the initial mechanistic riddle. Novel ideas for solving this enigmatic process are thus required.

4.2.4. The electron bifurcating site occurs in a range of electrochemical layouts

As discussed in this article, various enzymes from the described superfamilies behave in substantially different ways with respect to the electron bifurcating reaction. Some of them strongly couple the reduction of low potential ferredoxins or flavodoxins to the electron bifurcating processes. Others, such as for example complex I, perform the

electron bifurcating reaction without involving these low potential soluble electron shuttle proteins. When characterised, the electrochemical properties of the flavin in these latter enzymes do not indicate strongly cooperative redox transitions as considered crucial for truly energy conserving electron bifurcation [55,56,62,71–73]. Still others even manage to interface the 2-electron redox conversion of NAD(P) to the intramolecular 1-electron transfer chain without bifurcating electrons as evidenced by the absence of the [2Fe-2S]-cluster next to the flavin. In these cases, the flavin must feature reasonably stable semireduced states as discussed previously [62]. The ensemble of these observations suggest that the flavin moiety in the flavin module present in the enzymes we dealt with in this article comes in electrochemically quite diverse forms. As suggested by simulations recently reported by Yuly et al. [73], such variability of cooperativity will result in variable strength of coupling between the exergonic and the endergonic 1-electron transfer steps. It will be interesting to use the above described cases to experimentally test the predictions that the ability to involve low potential electron donors/acceptors is correlated to the degree of redox cooperativity of the bifurcating 2-electron centre.

4.3. Perspective: towards an understanding of the structural determinants which tune the flavin cofactor's redox cooperativity

As discussed previously [62,73], the precise type of redox reactions occurring within flavin-based electron bifurcation is likely correlated to the electrochemical properties of the flavin moiety and in particular to the strength of its redox cooperativity. These properties are necessarily pre-set by the flavin's immediate protein environment [111] but the type of influence the flavin's surroundings exerts on its electrochemical properties are only badly understood so far. As transpires from the previous sections, the reaction schemes performed by the flavin module vary substantially over the ensemble of enzymes discussed. So far, only a handful of high resolution 3D structure models are available. The set of cases for which comprehensive measurements of redox parameters of the involved cofactors and in particular of the flavin have been reported is even smaller. However, the possibility of confronting the close surroundings of flavins from enzymes cases with dissimilar coupling strengths in the electron bifurcating process would go a long way towards unraveling the molecular underpinnings of the electron bifurcating reaction. We therefore argue that the integration of the diverse enzymes into a common scheme, as attempted by our article, may allow valuable cross-fertilisations between so far rather distinct research communities and, in particular, may be key to understanding of what allows a 2-electron compound to act as an electron bifurcating agent. The development of a unified naming scheme for enzymes and subunits thereof, possibly arrived at *via* a community-wide concertation as for example achieved for arsenics-dependent molybdoenzymes [112] would certainly facilitate such cross-fertilisations.

Supplementary data to this article can be found online at https://doi.org/10.1016/j.bbabio.2021.148401.

Declaration of competing interest

The authors declare that they have no known competing financial interests or personal relationships that could have appeared to influence the work reported in this paper.

Acknowledgements

We thank Barbara Schoepp-Cothenet (BIP/CNRS Marseille/France) for help with the formate dehydrogenase family of enzymes and Wolfgang Buckel (MPI Marburg/Germany) for many stimulating discussions and critical reading of the manuscript. Thanks are also due to Kirsten Gutekunst (Christian-Albrechts-Universität zu Kiel/Germany) for providing the pdf-file of an article in a monograph. We are furthermore grateful to Jacques Meyer (Grenoble/France) for his willingness to extensively discuss and benefit from his expertise concerning ligation patterns of thioredoxin-like [2Fe-2S]-ferredoxins. The first author would also like to acknowledge the Studienstiftung des deutschen Volkes (Germany) for its funding.

References

[1] F. Baymann, E. Lebrun, M. Brugna, B. Schoepp-Cothenet, M.T. Giudici-Orticoni, et al., The redox protein construction kit: pre-last universal common ancestor evolution of energy-conserving enzymes, Philos. Trans. R. Soc. Lond. B Biol. Sci. 358 (2003) 267–274.

[2] Y. Higuchi, H. Ogata, K. Miki, N. Yasuoka, T. Yagi, Removal of the bridging ligand atom at the Ni–Fe active site of [NiFe] hydrogenase upon reduction with H_2, as revealed by X-ray structure analysis at 1.4 Å resolution, Structure 7 (1999) 549–556.

[3] J.W. Peters, W.N. Lanzilotta, B.J. Lemon, L.C. Seefeldt, X-ray crystal structure of the Fe-only hydrogenase (CpI) from *Clostridium pasteurianum* to 1.8 Angstrom resolution, Science 282 (1998) 1853–1858.

[4] J.H. Artz, O.A. Zadvornyy, D.W. Mulder, S.M. Keable, A.E. Cohen, et al., Tuning catalytic bias of hydrogen gas producing hydrogenases, J. Am. Chem. Soc. 142 (2019) 1227–1235.

[5] R.G. Efremov, L.A. Sazanov, The coupling mechanism of respiratory complex I – a structural and evolutionary perspective, Biochimica et Biophysica Acta (BBA)-Bioenergetics 1817 (2012) 1785–1795.

[6] Y. Shomura, M. Taketa, H. Nakashima, H. Tai, H. Nakagawa, et al., Structural basis of the redox switches in the NAD^+-reducing soluble [NiFe]-hydrogenase, Science 357 (2017) 928–932.

[7] C. Radon, G. Mittelstädt, B.R. Duffus, J. Bürger, T. Hartmann, et al., Cryo-EM structures reveal intricate Fe-S cluster arrangement and charging in *Rhodobacter capsulatus* formate dehydrogenase, Nat. Commun. 11 (2020) 1–9.

[8] A. Kpebe, M. Benvenuti, C. Guendon, A. Rebai, V. Fernandez, et al., A new mechanistic model for an O_2-protected electron-bifurcating hydrogenase, Hnd from *Desulfovibrio fructosovorans*, Biochimica et Biophysica Acta (BBA)-Bioenergetics 1859 (2018) 1302–1312.

[9] S. Wang, H. Huang, J. Moll, R.K. Thauer, $NADP^+$ reduction with reduced ferredoxin and $NADP^+$ reduction with NADH are coupled via an electron-bifurcating enzyme complex in *Clostridium kluyveri*, J. Bacteriol. 192 (2010) 5115–5123.

[10] K. Schuchmann, V. Müller, A bacterial electron-bifurcating hydrogenase, J. Biol. Chem. 287 (2012) 31165–31171.

[11] S. Wang, H. Huang, J. Kahnt, R.K. Thauer, *Clostridium acidurici* electron-bifurcating formate dehydrogenase, Appl. Environ. Microbiol. 79 (2013) 6176–6179.

[12] Y. Zheng, J. Kahnt, I.H. Kwon, R.I. Mackie, R.K. Thauer, Hydrogen formation and its regulation in *Ruminococcus albus*: involvement of an electron-bifurcating [FeFe]-hydrogenase, of a non-electron-bifurcating [FeFe]-hydrogenase, and of a putative hydrogen-sensing [FeFe]-hydrogenase, J. Bacteriol. 196 (2014) 3840–3852.

[13] S. Wang, H. Huang, J. Kahnt, R.K. Thauer, A reversible electron-bifurcating ferredoxin-and NAD-dependent [FeFe]-hydrogenase (HydABC) in *Moorella thermoacetica*, J. Bacteriol. 195 (2013) 1267–1275.

[14] S. Wang, H. Huang, J. Kahnt, A.P. Mueller, M. Kopke, et al., NADP-specific electron-bifurcating [FeFe]-hydrogenase in a functional complex with formate dehydrogenase in *Clostridium autoethanogenum* grown on CO, J. Bacteriol. 195 (2013) 4373–4386.

[15] G.J. Schut, M.W.W. Adams, The Iron-Hydrogenase of *Thermotoga maritima* utilizes ferredoxin and NADH synergistically: a new perspective on anaerobic hydrogen production, J. Bacteriol. 191 (2009) 4451–4457.

[16] S. Poudel, M. Tokmina-Lukaszewska, D.R. Colman, M. Refai, G.J. Schut, et al., Unification of [FeFe]-hydrogenases into three structural and functional groups, Biochimica et Biophysica Acta (BBA)-General Subjects 1860 (2016) 1910–1921.

[17] S. Thiemermann, J. Dernedde, M. Bernhard, W. Schroeder, C. Massanz, et al., Carboxyl-terminal processing of the cytoplasmic NAD-reducing hydrogenase of *Alcaligenes eutrophus* requires the hoxW gene product, J. Bacteriol. 178 (1996) 2368–2374.

[18] M. Guiral, L. Prunetti, S. Lignon, R. Lebrun, D. Moinier, et al., New insights into the respiratory chains of the chemolithoautotrophic and hyperthermophilic bacterium *Aquifex aeolicus*, J. Proteome Res. 8 (2009) 1717–1730.

[19] T. Hartmann, P. Schrapers, T. Utesch, M. Nimtz, Y. Rippers, et al., The molybdenum active site of formate dehydrogenase is capable of catalyzing C–H bond cleavage and oxygen atom transfer reactions, Biochemistry 55 (2016) 2381–2389.

[20] A. Tóth, M. Takács, G. Groma, G. Rákhely, K.L. Kovács, A novel NADPH-dependent oxidoreductase with a unique domain structure in the hyperthermophilic archaeon, *Thermococcus litoralis*, FEMS Microbiol. Lett. 282 (2008) 8–14.

[21] Lauterbach L, Idris Z, Vincent KA, Lenz O (2011) Catalytic properties of the isolated diaphorase fragment of the NAD^+-reducing [NiFe]-hydrogenase from *Ralstonia eutropha*. PloS one 6.

[22] L. Lauterbach, J. Liu, M. Horch, P. Hummel, A. Schwarze, et al., The hydrogenase subcomplex of the NAD^+-reducing [NiFe] hydrogenase from *Ralstonia eutropha* – insights into catalysis and redox interconversions, Eur. J. Inorg. Chem. 2011 (2011) 1067–1079.

[23] G. Peng, B. Meyer, L. Sokolova, W. Liu, S. Bornemann, et al., Identification and characterization two isoforms of NADH: ubiquinone oxidoreductase from the hyperthermophilic eubacterium *Aquifex aeolicus*, Biochimica et Biophysica Acta (BBA)-Bioenergetics 1859 (2018) 366–373.
[24] N.A. Losey, S. Poudel, E.S. Boyd, M.J. McInerney, The beta subunit of non-bifurcating NADH-dependent [FeFe]-hydrogenases differs from those of multimeric electron-bifurcating [FeFe]-hydrogenases, Front. Microbiol. 11 (2020) 1109.
[25] Guex N, Peitsch MC (1997) SWISS-MODEL and the Swiss-PDB Viewer: an environment for comparative protein modeling. electrophoresis 18: 2714–2723.
[26] J. Rozewicki, S. Li, K.M. Amada, D.M. Standley, K. Katoh, MAFFT-DASH: integrated protein sequence and structural alignment, Nucleic Acids Res. 47 (2019) W5–W10.
[27] I. Letunic, P. Bork, Interactive Tree Of Life (iTOL) v4: recent updates and new developments, Nucleic Acids Res. 47 (2019) W256–W259.
[28] D.W. Mulder, E.S. Boyd, R. Sarma, R.K. Lange, J.A. Endrizzi, et al., Stepwise [FeFe]-hydrogenase H-cluster assembly revealed in the structure of HydA ΔEFG, Nature 465 (2010) 248–251.
[29] Y. Nicolet, C. Piras, P. Legrand, C.E. Hatchikian, J.C. Fontecilla-Camps, *Desulfovibrio desulfuricans* iron hydrogenase: the structure shows unusual coordination to an active site Fe binuclear center, Structure 7 (1999) 13–23.
[30] J. Alric, J. Lavergne, F. Rappaport, A. Verméglio, K. Matsuura, et al., Kinetic performance and energy profile in a roller coaster electron transfer chain: a study of modified tetraheme-reaction center constructs, J. Am. Chem. Soc. 128 (2006) 4136–4145.
[31] M.G. Bertero, R.A. Rothery, M. Palak, C. Hou, D. Lim, et al., Insights into the respiratory electron transfer pathway from the structure of nitrate reductase A, Nat. Struct. Mol. Biol. 10 (2003) 681–687.
[32] C. Gauquelin, C. Baffert, P. Richaud, E. Kamionka, E. Etienne, et al., Roles of the F-domain in [FeFe] hydrogenase, Biochimica et Biophysica Acta (BBA)-Bioenergetics 1859 (2018) 69–77.
[33] L.A. Sazanov, P. Hinchliffe, Structure of the hydrophilic domain of respiratory complex I from *Thermus thermophilus*, Science 311 (2006) 1430–1436.
[34] M. Finel, Organization and evolution of structural elements within complex I, Biochimica et Biophysica Acta (BBA)-Bioenergetics 1364 (1998) 112–121.
[35] T. Friedrich, B. Böttcher, The gross structure of the respiratory complex I: a Lego System, Biochimica et Biophysica Acta (BBA)-Bioenergetics 1608 (2004) 1–9.
[36] W. Buckel, R.K. Thauer, Energy conservation via electron bifurcating ferredoxin reduction and proton/Na^+ translocating ferredoxin oxidation, Biochimica et Biophysica Acta (BBA) - Bioenergetics 1827 (2013) 94–113.
[37] C.C. Page, C.C. Moser, X. Chen, P.L. Dutton, Natural engineering principles of electron tunnelling in biological oxidation–reduction, Nature 402 (1999) 47–52.
[38] M. Świerczek, E. Cieluch, M. Sarewicz, A. Borek, C.C. Moser, et al., An electronic bus bar lies in the core of cytochrome bc1, Science 329 (2010) 451–454.
[39] S. Hong, D. Victoria, A.R. Crofts, Inter-monomer electron transfer is too slow to compete with monomeric turnover in bc1 complex, Biochimica et Biophysica Acta (BBA)-Bioenergetics 1817 (2012) 1053–1062.
[40] T. Wagner, J. Koch, U. Ermler, S. Shima, Methanogenic heterodisulfide reductase (HdrABC-MvhAGD) uses two noncubane [4Fe-4S] clusters for reduction, Science 357 (2017) 699–703.
[41] J.I. Oh, B. Bowien, Structural analysis of the Fds operon encoding the NAD^+-linked formate dehydrogenase of *Ralstonia eutropha*, J. Biol. Chem. 273 (1998) 26349–26360.
[42] B. Schoepp-Cothenet, R. Van Lis, A. Atteia, F. Baymann, L. Capowiez, et al., On the universal core of bioenergetics, Biochimica et Biophysica Acta (BBA)-Bioenergetics 1827 (2013) 79–93.
[43] F. Grein, A.R. Ramos, S.S. Venceslau, I.A. Pereira, Unifying concepts in anaerobic respiration: insights from dissimilatory sulfur metabolism, Biochimica et Biophysica Acta (BBA)-Bioenergetics 1827 (2013) 145–160.
[44] P.M. Vignais, B. Billoud, Occurrence, classification, and biological function of hydrogenases: an overview, Chem. Rev. 107 (2007) 4206–4272.
[45] N. Chongdar, K. Pawlak, O. Rüdiger, E.J. Reijerse, P. Rodríguez-Maciá, et al., Spectroscopic and biochemical insight into an electron-bifurcating [FeFe] hydrogenase, JBIC Journal of Biological Inorganic Chemistry (2019) 1–15.
[46] J. Meyer, S.L. Andrade, O. Einsle, Thioredoxin-like [2Fe-2S] ferredoxin, Encyclopedia of Inorganic and Bioinorganic Chemistry, Online © 2011, John Wiley & Sons, Ltd., 2011, https://doi.org/10.1002/9781119951438.eibc0652.
[47] T. Young, D. Niks, S. Hakopian, T.K. Tam, X. Yu, et al., Crystallographic and kinetic analyses of the FdsBG subcomplex of the cytosolic formate dehydrogenase FdsABG from *Cupriavidus necator*, J. Biol. Chem. 295 (2020) 6570–6585.
[48] K. Schuchmann, N.P. Chowdhury, V. Müller, Complex multimeric [FeFe] hydrogenases: biochemistry, physiology and new opportunities for the hydrogen economy, Front. Microbiol. 9 (2018) 2911.
[49] D.R. Jollie, J.D. Lipscomb, Formate dehydrogenase from *Methylosinus trichosporium OB3b*. Purification and spectroscopic characterization of the cofactors, J. Biol. Chem. 266 (1991) 21853–21863.
[50] T. Hartmann, S. Leimkühler, The oxygen-tolerant and NAD^+-dependent formate dehydrogenase from *Rhodobacter capsulatus* is able to catalyze the reduction of CO_2 to formate, FEBS J. 280 (2013) 6083–6096.
[51] R. Hille, T. Young, D. Niks, S. Hakopian, T.K. Tam, et al., Structure: function studies of the cytosolic, Mo-and NAD^+-dependent formate dehydrogenase from *Cupriavidus necator*, Inorganics 8 (2020) 41.
[52] J.J. Kearny, R.D. Sagers, Formate dehydrogenase from *Clostridium acidiurici*, J. Bacteriol. 109 (1972) 152–161.
[53] P. Mitchell, Protonmotive redox mechanism of the cytochrome bc complex in the respiratory chain: Protonmotive ubiquinone cycle, FEBS Lett. 56 (1975) 1–6.
[54] P. Mitchell, The protonmotive Q cycle: a general formulation, FEBS Lett. 59 (1975) 137–139.
[55] W. Buckel, R.K. Thauer, Flavin-based electron bifurcation, a new mechanism of biological energy coupling, Chem. Rev. 118 (2018) 3862–3886.
[56] W. Buckel, R.K. Thauer, Flavin-based electron bifurcation, ferredoxin, flavodoxin and anaerobic respiration with protons (Ech) or NAD^+ (Rnf) as electron acceptors: a historical review, Frontiers in Microbiology 9 (2018).
[57] N.A. Losey, F. Mus, J.W. Peters, H.M. Le, M.J. McInerney, *Syntrophomonas wolfei* uses an NADH-dependent, ferredoxin-independent [FeFe]-hydrogenase to reoxidize NADH, Applied and Environmental Microbiology 83 (2017).
[58] E. Gnandt, J. Schimpf, C. Harter, J. Hoeser, T. Friedrich, Reduction of the off-pathway iron-sulphur cluster N1a of *Escherichia coli* respiratory complex I restrains NAD^+ dissociation, Sci. Rep. 7 (2017) 1–10.
[59] K. Dörner, M. Vranas, J. Schimpf, I.R. Straub, J. Hoeser, et al., Significance of [2Fe-2S] cluster N1a for electron transfer and assembly of *Escherichia coli* respiratory complex I, Biochemistry 56 (2017) 2770–2778.
[60] E. Aubert-Jousset, M. Cano, G. Guedeney, P. Richaud, L. Cournac, Role of HoxE subunit in *Synechocystis sp. PCC 6803* hydrogenase, FEBS J. 278 (2011) 4035–4043.
[61] L.A. Sazanov, Respiratory complex I: mechanistic and structural insights provided by the crystal structure of the hydrophilic domain, Biochemistry 46 (2007) 2275–2288.
[62] F. Baymann, B. Schoepp-Cothenet, S. Duval, M. Guiral, M. Brugna, et al., On the natural history of flavin-based electron bifurcation. Frontiers in Microbiology (2018) 9.
[63] S. Malki, I. Saimmaime, G. De Luca, M. Rousset, Z. Dermoun, et al., Characterization of an operon encoding an NADP-reducing hydrogenase in *Desulfovibrio fructosovorans*, J. Bacteriol. 177 (1995) 2628–2636.
[64] M.P. Golinelli, C. Chatelet, E.C. Duin, M.K. Johnson, J. Meyer, Extensive ligand rearrangements around the [2Fe-2S] cluster of *Clostridium pasteurianum* ferredoxin, Biochemistry 37 (1998) 10429–10437.
[65] M.F. Verhagen, T. O'Rourke, M.W. Adams, The hyperthermophilic bacterium, *Thermotoga maritima*, contains an unusually complex iron-hydrogenase: amino acid sequence analyses versus biochemical characterization, Biochimica et Biophysica Acta (BBA)-Bioenergetics 1412 (1999) 212–229.
[66] M.K. Wikström, J.A. Berden, Oxidoreduction of cytochrome b in the presence of antimycin, Biochimica et Biophysica Acta (BBA)-Bioenergetics 283 (1972) 403–420.
[67] G. Herrmann, E. Jayamani, G. Mai, W. Buckel, Energy conservation via electron-transferring flavoprotein in anaerobic bacteria, J. Bacteriol. 190 (2007) 784–791.
[68] F. Li, J. Hinderberger, H. Seedorf, J. Zhang, W. Buckel, et al., Coupled ferredoxin and crotonyl coenzyme A (CoA) reduction with NADH catalyzed by the butyryl-CoA dehydrogenase/Etf complex from *Clostridium kluyveri*, J. Bacteriol. 190 (2008) 843–850.
[69] L. Michaelis, Theory of the reversible two-step oxidation, J. Biol. Chem. 96 (1932) 703–715.
[70] W.M. Clark, et al., Oxidation-reduction potentials of organic systems, 1960.
[71] W. Nitschke, M.J. Russell, Redox bifurcations: mechanisms and importance to life now, and at its origin, BioEssays 34 (2011) 106–109.
[72] A.R. Crofts, S. Hong, C. Wilson, R. Burton, D. Victoria, et al., The mechanism of ubihydroquinone oxidation at the Q_o-site of the cytochrome bc_1 complex, Biochimica et Biophysica Acta (BBA)-Bioenergetics 1827 (2013) 1362–1377.
[73] J.L. Yuly, P. Zhang, C.E. Lubner, J.W. Peters, D.N. Beratan, Universal free energy landscape produces efficient and reversible electron bifurcation. arXiv preprint arXiv:200514052, 2020.
[74] L. Bergdoll, F. ten Brink, W. Nitschke, D. Picot, F. Baymann, From low- to high-potential bioenergetic chains: thermodynamic constraints of Q-cycle function, Biochimica et Biophysica Acta (BBA) - Bioenergetics 1857 (2016) 1569–1579.
[75] J.W. Peters, D.N. Beratan, G.J. Schut, M.W.W. Adams, On the nature of organic and inorganic centers that bifurcate electrons, coupling exergonic and endergonic oxidation–reduction reactions, Chem. Commun. 54 (2018) 4091–4099.
[76] S. Duval, J.M. Santini, D. Lemaire, F. Chaspoul, M.J. Russell, et al., The H-bond network surrounding the pyranopterins modulates redox cooperativity in the molybdenum-*bis*PGD cofactor in arsenite oxidase, Biochimica et Biophysica Acta (BBA)-Bioenergetics 1857 (2016) 1353–1362.
[77] S. Grimaldi, B. Schoepp-Cothenet, P. Ceccaldi, B. Guigliarelli, A. Magalon, The prokaryotic Mo/W-*bis*PGD enzymes family: a catalytic workhorse in bioenergetic, Biochimica et Biophysica Acta (BBA)-Bioenergetics 1827 (2013) 1048–1085.
[78] M. Schulte, K. Frick, E. Gnandt, S. Jurkovic, S. Burschel, et al., A mechanism to prevent production of reactive oxygen species by *Escherichia coli* respiratory complex I, Nat. Commun. 10 (2019) 1–9.
[79] K. Gutekunst, X. Chen, K. Schreiber, U. Kaspar, S. Makam, et al., The bidirectional NiFe-hydrogenase in *Synechocystis* sp. *PCC 6803* is reduced by flavodoxin and ferredoxin and is essential under mixotrophic, nitrate-limiting conditions, J. Biol. Chem. 289 (2014) 1930–1937.
[80] K. Gutekunst, R. Schulz, The physiology of the bidirectional NiFe-hydrogenase in cyanobacteria and the role of hydrogen throughout the evolution of life, Microalgal Hydrogen Production, European Society for Photobiology, In, 2018, pp. 107–138.
[81] J. Meyer, [fefe] hydrogenases and their evolution: a genomic perspective, Cellular and Molecular Life Sciences 64 (2007) 1063.
[82] B. Boxma, R.M. de Graaf, G.W. van der Staay, T.A. van Alen, G. Ricard, et al., An anaerobic mitochondrion that produces hydrogen, Nature 434 (2005) 74–79.

[83] B. Boxma, G. Ricard, A.H. van Hoek, E. Severing, S.Y. Moon-van der Staay, et al., The [FeFe] hydrogenase of *Nyctotherus ovalis* has a chimeric origin, BMC Evol. Biol. 7 (2007) 1–12.

[84] Preissler J, Wahlefeld S, Lorent C, Teutloff C, Horch M, et al. (2018) Enzymatic and spectroscopic properties of a thermostable [NiFe]-hydrogenase performing H_2-driven NAD^+-reduction in the presence of O_2. Biochimica et Biophysica Acta (BBA)-Bioenergetics 1859: 8–18.

[85] A. Tran-Betcke, U. Warnecke, C. Böcker, C. Zaborosch, B. Friedrich, Cloning and nucleotide sequences of the genes for the subunits of NAD-reducing hydrogenase of *Alcaligenes eutrophus H16*, J. Bacteriol. 172 (1990) 2920–2929.

[86] J.H. Artz, M. Tokmina-Lukaszewska, D.W. Mulder, C.E. Lubner, K. Gutekunst, et al., The structure and reactivity of the HoxEFU complex from the cyanobacterium *Synechocystis* sp. *PCC 6803*, Journal of Biological Chemistry 295 (2020) 9445–9454.

[87] G. Rákhely, Z.H. Zhou, M.W. Adams, K.L. Kovács, Biochemical and molecular characterization of the [NiFe] hydrogenase from the hyperthermophilic archaeon, *Thermococcus litoralis*, Eur. J. Biochem. 266 (1999) 1158–1165.

[88] T. Kanai, S. Ito, T. Imanaka, Characterization of a cytosolic NiFe-hydrogenase from the hyperthermophilic archaeon *Thermococcus kodakaraensis KOD1*, J. Bacteriol. 185 (2003) 1705–1711.

[89] K. Ma, R. Weiss, M.W. Adams, Characterization of hydrogenase ii from the hyperthermophilic archaeon *Pyrococcus furiosus* and assessment of its role in sulfur reduction, J. Bacteriol. 182 (2000) 1864–1871.

[90] J. Maróti, A. Farkas, I.K. Nagy, G. Maróti, É. Kondorosi, et al., A second soluble hox-type NiFe enzyme completes the hydrogenase set in *Thiocapsa roseopersicina BBS*, Appl. Environ. Microbiol. 76 (2010) 5113–5123.

[91] M. Laukel, L. Chistoserdova, M.E. Lidstrom, J.A. Vorholt, The tungsten-containing formate dehydrogenase from *Methylobacterium extorquens AM1*: purification and properties, Eur. J. Biochem. 270 (2003) 325–333.

[92] A. Graentzdoerffer, D. Rauh, A. Pich, J.R. Andreesen, Molecular and biochemical characterization of two tungsten-and selenium-containing formate dehydrogenases from *Eubacterium acidaminophilum* that are associated with components of an iron-only hydrogenase, Arch. Microbiol. 179 (2003) 116–130.

[93] C.F. Nielsen, L. Lange, A.S. Meyer, Classification and enzyme kinetics of formate dehydrogenases for biomanufacturing via CO_2 utilization, Biotechnol. Adv. 37 (2019), 107408, https://doi.org/10.1016/j.biotechadv.2019.06.007.

[94] R. Hille, J. Hall, P. Basu, The mononuclear molybdenum enzymes, Chem. Rev. 114 (2014) 3963–4038.

[95] D. Niks, R. Hille, Molybdenum-and tungsten-containing formate dehydrogenases and formylmethanofuran dehydrogenases: structure, mechanism, and cofactor insertion, Protein Sci. 28 (2019) 111–122.

[96] L.G. Ljungdahl, J.R. Andreesen, Formate dehydrogenase, a selenium-tungsten enzyme from Clostridium thermoaceticum. In: Methods in Enzymology, Elsevier 53 (1978) 360–372.

[97] U. Ruschig, U. Müller, P. Willow, T. Höpner, CO_2 reduction to formate by NADH catalysed by formate dehydrogenase from *Pseudomonas oxalaticus*, Eur. J. Biochem. 70 (1976) 325–330.

[98] H.Y. Liu, P.C. Liao, K.T. Chuang, M.C. Kao, Mitochondrial targeting of human NADH dehydrogenase (ubiquinone) flavoprotein 2 (NDUFV2) and its association with early-onset hypertrophic cardiomyopathy and encephalopathy, J. Biomed. Sci. 18 (2011) 1–17.

[99] U. Weidner, S. Geier, A. Ptock, T. Friedrich, H. Leif, et al., The gene locus of the proton-translocating NADH: ubiquinone oxidoreductase in *Escherichia coli*: organization of the 14 genes and relationship between the derived proteins and subunits of mitochondrial complex I, J. Mol. Biol. 233 (1993) 109–122.

[100] T. Friedrich, D. Scheide, The respiratory complex I of bacteria, archaea and eukarya and its module common with membrane-bound multisubunit hydrogenases, FEBS Lett. 479 (2000) 1–5.

[101] R. Hedderich, Energy-converting [NiFe] hydrogenases from archaea and extremophiles: ancestors of complex I, J. Bioenerg. Biomembr. 36 (2004) 65–75.

[102] P.J. Castro, A.F. Silva, B.C. Marreiros, A.P. Batista, M.M. Pereira, Respiratory complex I: a dual relation with H^+ and Na^+? Biochimica et Biophysica Acta (BBA)-bioenergetics 1857 (2016) 928–937.

[103] H. Yu, C.H. Wu, G.J. Schut, D.K. Haja, G. Zhao, et al., Structure of an ancient respiratory system, Cell 173 (2018) 1636–1649.

[104] K. Parey, C. Wirth, J. Vonck, V. Zickermann, Respiratory complex I—structure, mechanism and evolution, Curr. Opin. Struct. Biol. 63 (2020) 1–9.

[105] W. Chow, I. Ragan, B.H. Robinson, Determination of the cDNA sequence for the human mitochondrial 75-kDa Fe–S protein of NADH-coenzyme Q reductase, Eur. J. Biochem. 201 (1991) 547–550.

[106] F. Sargent, The model [NiFe]-hydrogenases of *Escherichia coli*, Advances in microbial physiology, Elsevier 68 (2016) 433–507.

[107] W. Nitschke, Carbon fixation: "let things flow naturally forward in whatever way they like", Curr. Biol. 28 (2018) R110–R112.

[108] F. Kremp, J. Roth, V. Müller, The Sporomusa type Nfn is a novel type of electron-bifurcating transhydrogenase that links the redox pools in acetogenic bacteria, Sci. Rep. 10 (2020) 1–14.

[109] R. Baradaran, J.M. Berrisford, G.S. Minhas, L.A. Sazanov, Crystal structure of the entire respiratory complex I, Nature 494 (2013) 443–448.

[110] J.A. Letts, K. Fiedorczuk, G. Degliesposti, M. Skehel, L.A. Sazanov, Structures of respiratory supercomplex I+III2 reveal functional and conformational crosstalk, Mol. Cell 75 (2019) 1131–1146.

[111] K. Kayastha, S. Vitt, W. Buckel, U. Ermler, Flavins in the Electron Bifurcation Process, Archives of Biochemistry and Biophysics in press, 2021.

[112] M.C. Lett, D. Muller, D. Lièvremont, S. Silver, J. Santini, Unified nomenclature for genes involved in prokaryotic aerobic arsenite oxidation, J. Bacteriol. 194 (2012) 207–208.

Supplementary - The dyad of the Y-junction- and a flavin module unites diverse redox enzymes

Kilian Zuchan[a], Frauke Baymann[a], Carole Baffert[a], Myriam Brugna[a,*], Wolfgang Nitschke[a]

[a] *Aix Marseille Univ, CNRS, BIP, 31 Chemin Joseph Aiguier, 13402, Marseille Cedex 09, France*

Supplementary Table 3 containing all sequences considered in this study are given as a seperate file: `SupplementaryTable3.ods`

1. Complex I, an enzyme with a somewhat ambiguous naming scheme

The name complex I historically derives from the fact that it is the first in a chain of membrane-integral enzymes through which electrons pass in mitochondrial respiration on their way to the terminal electron acceptor, O_2. This enzyme couples the redox conversions of NAD^+/NADH and quinone/quinol to the translocation of protons across energy converting membranes and is frequently also referred to as "type 1 NADH dehydrogenase" or "NDH-1" (NDH-2's are structurally much simpler enzymes which perform the exactly same redox conversions but without pumping protons [10]).

We contend that the term "type 1 NAD:quinone oxidoreductase" is more appropriate since (a) the enzyme is known to operate in both directions and (b) the second redox substrate always is a quinone [11]. By contrast, the NAD^+/NADH couple can be substituted by other substrates. Several enzymes have in fact been characterized which lack the subunits involved in the redox conversion of NAD but which retain the full remaining complement of subunits, e.g. in cyanobacteria [12, 13]. These enzymes are sometimes also referred to as complex I but they aren't "NAD-dependent" but transfer electrons between other redox compounds and the quinol/quinone couple. The terms complex I and NDH-1 therefore cannot be used interchangeably.

Part of the evolutionary analyses detailed in section *XXX* pertains to the evolutionary origins of precisely that subgroup of complexes I which truly can operate with NAD^+/NADH and, *a fortiori*, to the evolutionary history of the NuoEFG-module.

We therefore refer throughout this article to this subgroup as "NAD-dependent" complex I to distinguish it from the wider family of proton-translocating complexes I, which may use a range of other redox compounds instead of NAD, such as for example ferredoxins or coenzyme F_{420} [14, 15]. To address the different subunits of NAD-dependant complex I we will furthermore use the older "Nuo"-nomenclature originally referring to NAD:ubiquinone oxidoreductase. However, since complex I also functions with menaquinones, the naming of

*Corresponding author
Email address: `mbrugna@imm.cnrs.fr` (Myriam Brugna)

subunits introduced from the enzyme from *Thermus thermophilus* (Nqo) would rigorously be the more appropriate one [16]. For readers used to these alternative nomenclatures we compiled currently used abbreviations for concerned subunits of this and the other enzymes discussed in this article in Table 1.

2. The Histidine-[4Fe-4S] cluster - a case for structure informed alignments

Multiple sequence alignments can be guided by the available 3D structures depicted in Fig. 1 and improvements in reliability of trees (as judged by their bootstrap values) are observed upon correcting algorithm-based alignments by structure-based ones [17, 18]. An intriguing example of deviation between these two methods is provided by the position of the histidine residue ligating the "histidine-[4Fe-4S]" cluster in Fig. 2. The full conservation of a histidine as ligand biases algorithm-based alignment methods into aligning all these histidines by generating indels shortly before and after the histidine residue to compensate for the fact that in NAD-dependent [NiFe]-hydrogenases the histidine doesn't align straightforwardly with those of all the other enzymes. The structural alignment of the known protein models (Suppl. Fig. 3A), however, shows that the polypeptide chains overlap perfectly and without any indels and that the histidine in the Y-junction module of the NAD-reducing [NiFe]-hydrogenase is indeed at a sequence and structural position that differs from that of the other cases (Fig. 3B). To still be able to serve as a ligand to the cluster, coordination of the iron-atom is achieved by the N_{δ}-atom of the imidazole moiety in the NAD-dependent [NiFe]-hydrogenases rather than by the ϵ-nitrogen in all other cases (Fig. 3A). This particularity of the NAD-dependent [NiFe]-hydrogenase seen in the *H. thermoluteolus* structure was found to be conserved in all other members of this family detected in genomes as described below. However, we also detected a few cases of enzymes with histidines simultaneously present in both positions (e.g. the case of the complex I enzyme in *Escherichia coli* shown in Fig. 3B) suggesting a likely pathway for the evolutionary transition from one position to the other. Whether the strict conservation of the deviant histidine position in NAD-dependent [NiFe]-hydrogenases is a mere phylogenetic trait or whether it plays a functional role (e.g. by tuning the redox midpoint potential of the cluster) remains to be elucidated.

3. Cases of NAD(P)-dependent formate dehydrogenases which appear as structural and possibly functional outliers

A specific member of Group B2 displays an intriguing architecture. In addition to having exchanged its proper flavin module against one from an NAD(P)-dependent [FeFe]-hydrogenase, the gene cluster encoding a putative NAD(P)-dependent formate dehydrogenase in *Pelobacter propionicus DSM 2379* (Seq. Num. 107 Fig. 4a and Fig. 4b) contains all subunits required for the assembly of a complex I. Albeit this complex harbours a NuoD-like subunit featuring the binding motif (CxxC-CxxC) for the [NiFe]-catalytic centre and a NuoG subunit predicted to harbour all four [Fe-S]-clusters in the Y-junction module, the FS0-cluster of the formate dehydrogenase catalytic domain and a cysteine residue in the canonical position of the protein-ligand to the molybdenum. The first few features were

already noticed by Marreiros *et al.* (2013), whereas the additional occurence of a CO_2-reducing site would allow the Y-junction module to function as a three-way electron conduit between these different reaction sites [19]. The assembled genome of this organism, however, features several strictly identical (with respect to sequences of ORFs) gene clusters coding for bona fide complexes I. Such a situation being extremely unlikely, a further verification of the reliability of this genome sequence might be required before firm conclusions can be drawn.

Three formate dehydrogenase sequences (to the left of Group A1 in Fig. 4a) retrieved in our genomic survey do not cluster with any of the above delineated Fds-groups as mentioned in the main text (nor with any other group in Fig.Fig. 4a and Fig. 4b). They furthermore strongly diverge among each other with respect to their structural layout. Future expansion of genomic databases may yield the emergence of further classes encompassing these cases or else they may represent phylogenetic artifacts resulting from long-branch attraction, a common pitfall in phylogenetic analyses . Excessively long branches may be due to rapid evolution entailed by the emergence of uncommon functional roles. The enzymatically characterised enzyme from *Clostridium autoethanogenum* [6, 20] might favour the latter explanation. This enzyme actually represents a chimera between an NAD(P)-dependent formate dehydrogenase and an NAD(P)-dependent [FeFe]-hydrogenase and probably serves as a "ferredoxin- and hydrogen-dependent CO_2-reductase" as discussed by Schuchmann *et al.*(2018). Its gene cluster as well as its biochemically verified subunit composition suggests the presence of the flavin module, a Y-junction module (again represented by a separate protein and lacking not only the histidine-cluster but also the entire histidine-cluster subdomain) as well as formate dehydrogenase (lacking an N-terminal Y-junction module) and [FeFe]-hydrogenase catalytic subunits (with two cubane iron-sulphur clusters N-terminal domain to the H-domain of the hydrogenase), supplemented by two additional tetracubane [16Fe-16S]-ferredoxin subunits [21]. Neither the formate dehydrogenase subunit nor the [FeFe]-hydrogenase one contain a complete Y-junction module as N-terminal domain. A straightforward deduction of the architecture of this enzyme based on known 3D-structures is thus not possible.

3

Supplementary Table 1: **Sequence motifes used for the identification of cofactors in the respective proteins.**

Pictogram	Respective cofactor	Motif	Reference
	[2Fe-2S]-cluster in [2Fe-2S] binding SU	**CxxxxC-...-CxxxC**	Meyer *et al.*(2011)
	[2Fe-2S]-cluster in flavin/[4Fe-4S]-SU	**CxxxxC-...-CxxxC**	Meyer *et al.*(2011)
	NAD(P)-binding site in flavin/[4Fe-4S]-SU	**GxGxx[GA]xxx[GA]x{6}[G]**	Scrutton *et al.*(1990)
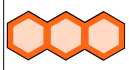	flavin-binding site in flavin/[4Fe-4S]-SU	**[GSA]xxG[ASR][FY]CG[ED]**	Hanukoglu & Gutfinger (1989)
	[4Fe-4S] in flavin/[4Fe-4S]-SU	**CxxCxxC-...-C**	Baradaran *et al.*(1990)
	2x[4Fe-4S] in flavin/[4Fe-4S]-SU	**CxxCxxCxxxC-...-CxxCxxCxxxC**	Poudel *et al.* (2016)
	[4Fe-4S]-proximal cluster in [NiFe] Hydrogenases	**CxxC-...-C-...-C**	Shomura *et al.* (2017)
	[NiFe] catalytic cluster in [NiFe] Hydrogenases	**CxxC-...-CxxC**	Shomura *et al.* (2017)
	H-cluster in [FeFe] Hydrogenases	**C-...-C-...-CxxxC**	Poudel *et al.* (2016)
	N1/A7 [4Fe-4S]-cluster in complex I/Fds	**CxxCxxxC-...-C**	Radon *et al.* (2020)
	molybdopterin/ tungstopterin in Fds	**[CU]-…-H-…-R**	Hartmann *et al.*(2016)
	YJM [2Fe-2S]-cluster	**Cx{10}CxxCx{10-13}C**	
	YJM His-[4Fe-4S]-cluster	**see Supplementary Fig.2**	
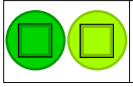	YJM Central and C-Terminal [4Fe-4S]-cluster	**CxxCxxCxxxC-...-CxxCxxCxxxC**	

Supplementary Table 2: **Overview subunit nomenclature of [FeFe]-Hydrogenase and Formate dehydrogenase.**
Recently used subunit nomenclature for homologous subunits in [FeFe]-Hydrogenase and formate dehydrogenase. Additional non-homologous subunits characterizing specific protein complexes not shown.

Organism	Oligo-merization state	Name	[2Fe-2S] subunit	Flavin/ [4Fe-4S] subunit	YJM containing subunit	H-cluster containing subunit	Mo-/W-containing subunit	
Desulfovibrio fructosovorans	Tetrameric	***Hnd***	**HndA**	**HndC**	**HndD**	**HndD**	-	**Kpebe et al. (2018)**
Desulfovibrio fructosovorans	Trimeric	*Hnt*	HntA	HntC	HntD	HntD	-	**Baffert et al. (2019)**
Thermotoga maritima	Trimeric	*Hyd*	HydC	HydB	HydA	HydA	-	**Chongdar et al. (2019)**
Acetobacterium woodii	Tetrameric	*Hyd*	HydC	HydB	HydA	HydA	-	**Schuchmann & Müller (2012)**
Eubacterium acidaminophilum	Tetrameric	*Hym*	HymA	HymB	HymC	HymC	-	**Graentzdoerffer et al. (2002)**
Clostridium autoethanogenum	Heptameric	*Hyt*	HytC	HytB	HytD	HytA	FdhA	**Wang et al. (2013)**
Clostridium acidiurici	Tetrameric	*Hyl*	HylC	HylB	HylA, FdhF2, FdhF1	-	FdhF2, FdhF1	**Wang et al. (2013)**
Cuprividus necator	Trimeric	*Fds*	FdsG	FdsB	FdsA	-	FdsA	**Hille et al. (2020)**
Rhodobacter capsulatus	Tetrameric	*Fds*	FdsG	FdsB	FdsA	-	FdsA	**Radon et al. (2020)**
Methylobacterium extorquens	Dimeric	*Fdh*	Fdh1B	Fdh1B	Fdh1A	-	Fdh1A	**Laukel et al. (2003)**

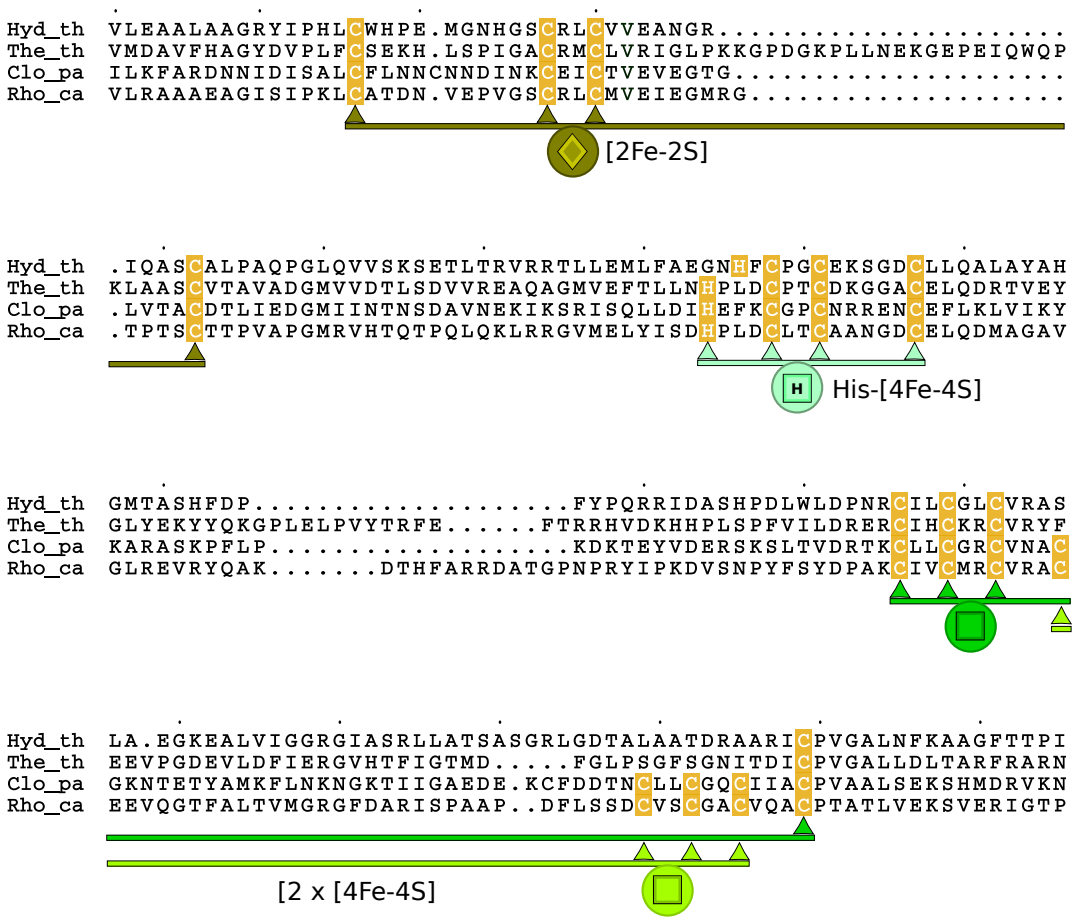

Supplementary Figure 1: **Structural alignment of the Y-junction module.**
Structural alignment of the four structurally known template sequences of the Y-junction module were constructed using MAFFT-DASH by employing the iterative refinement algorithm as described in the methods section [18]. Multiple sequence alignment initially visualized with the ESPript 3.0 Server [22]. Cofactor annotation according to specified motifs in Supplementary Table 1. Functional cluster annotation congruent with the pictograms used throughout the article.
Hyd th - hoxU subunit, [NiFe]-Hydrogenase of *Hydrogenophilus thermoluteolus TH-1*
Clo pa - N-terminal [FeFe]-Hydrogenase of *Clostridium pasteurianum DSM 525*
The th - N-terminal nuoG subunit, complex I of *Thermus thermophilus HB8*
Rho ca - N-terminal fdsA subunit, Formate dehydrogenase of *Rhodobacter capsulatus YW2*

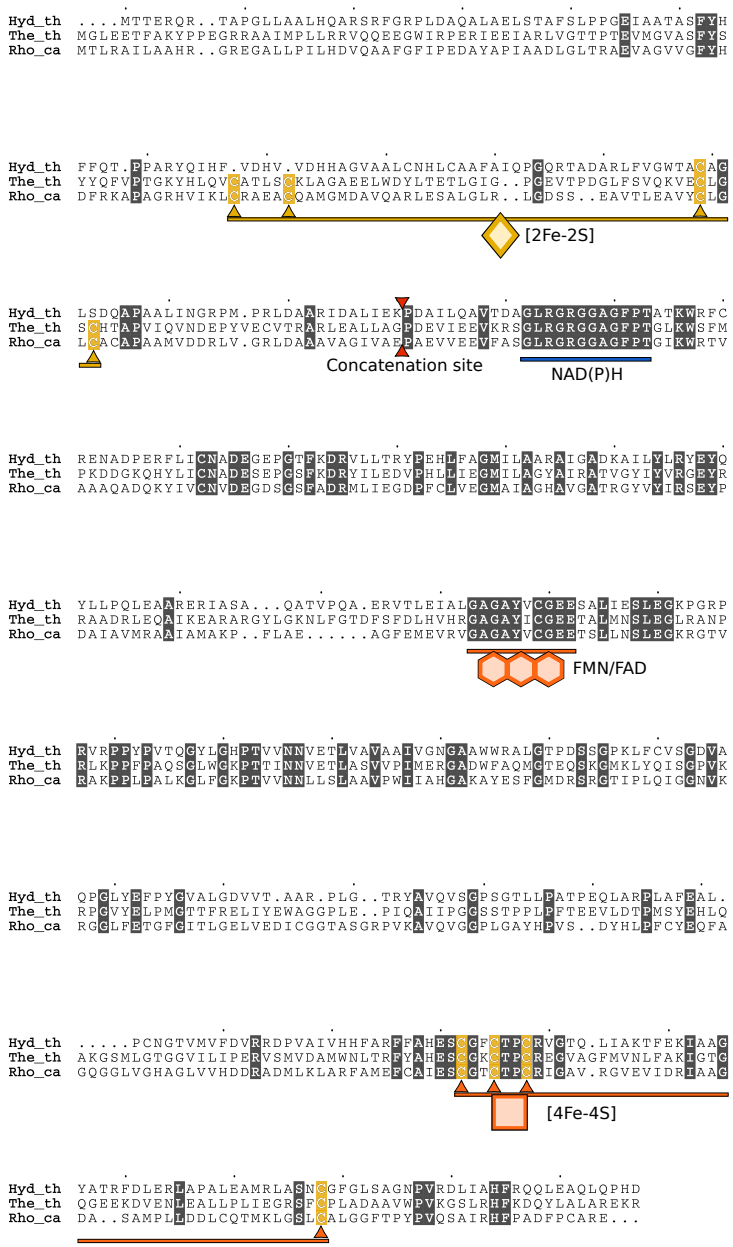

Supplementary Figure 2: **Structural alignment of the flavin module.**
Structural alignment of the three structurally characterized template sequences of the "flavin module" as shown in Figure 3 were constructed using MAFFT-DASH by employing the iterative refinement algorithm as described in the methods section [18]. Multiple sequence alignment initially visualized with the ESPript 3.0 Server [22]. Cofactor annotation according to specified motifs in Supplementary Table 1. Functional cluster annotation congruent with the pictograms used throughout the article.
Hyd th - hoxF subunit, [NiFe]-Hydrogenase - *Hydrogenophilus thermoluteolus TH-1*
The th - concatenated nuoE and nuoF subunit, complex I - *Thermus thermophilus HB8*
Rho ca - concatenated fdsG and fdsB subunit, Formate dehydrogenase - *Rhodobacter capsulatus YW2*

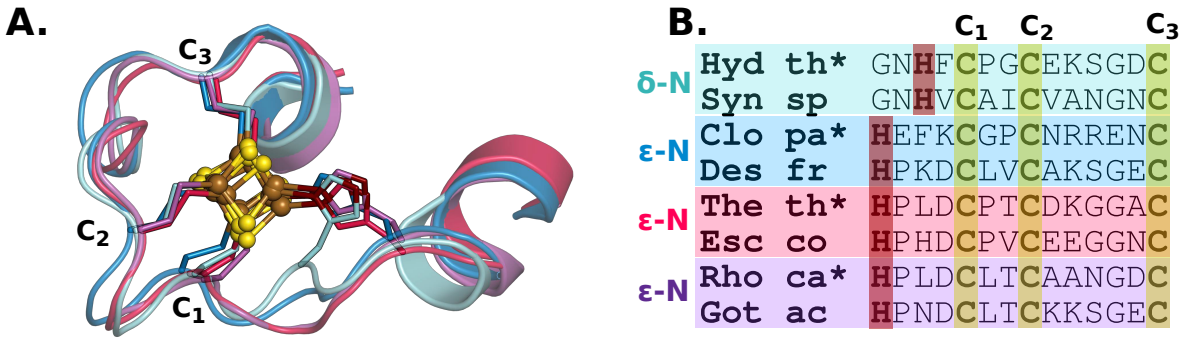

Supplementary Figure 3: **Coordination of the Histidine-[4Fe4S]-cluster of the examined bioenergetic proteins.**
Structural (A.) and sequence (B.) comparison of the coordination of the histidine-[4Fe-4S]-cluster (iron in brown, sulphur in yellow) from the bidirectional [NiFe]-hydrogenase (in cyan, PDB: 5XF9), [FeFe]-hydrogenase (in blue, PDB: 6N59), Complex I (in red, PDB: 4HEA) and formate dehydrogenase (in purple, PDB: 6TG9) indicate a specific coordination through the δ-nitrogen (in maroon) for the [NiFe]-hydrogenases. All other examined bioenergetic proteins exhibit coordination through the ϵ-nitrogen.
Asterisk (*) denotes the sequences of the structural representative:
Hyd th - *Hydrogenophilus thermoluteolus TH-1*
Syn sp - *Synechocystis sp. PCC 6803*
Clo pa - *Clostridium pasteurianum DSM 525*
Des fr - *Desulfovibrio fructosovorans DSM 3604*
The th - *Thermus thermophilus HB8*
Esc co - *Escherichia coli strain M19*
Rho ca - *Rhodobacter capsulatus YW2*
Got ac - *Gottschalkia acidurici 9a*

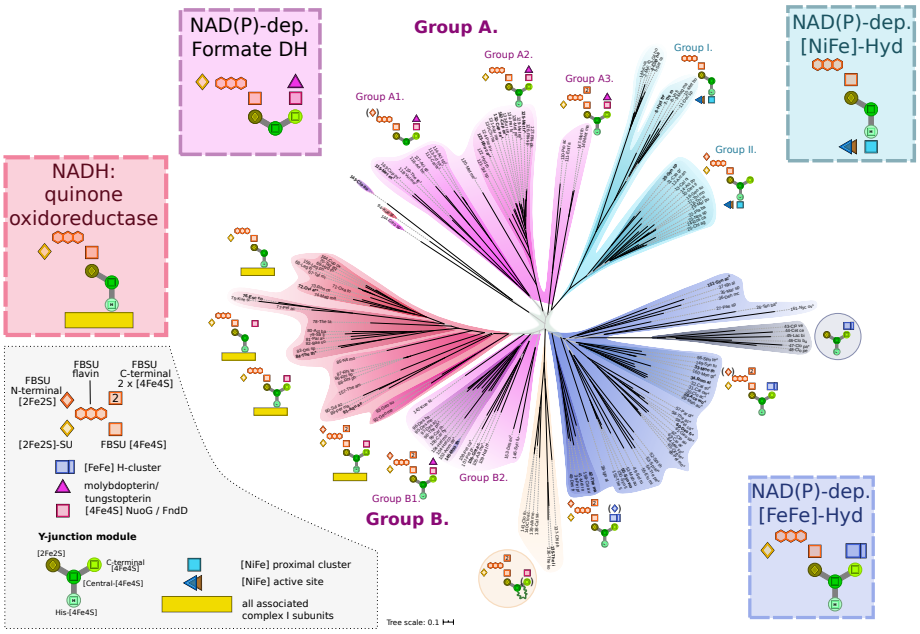

Supplementary Figure 4a: **Fully annotated Neighbor-Joining Tree of the Y-junction module in representative sequences.** Similarity clustering of the sequences belonging to the [FeFe]-hydrogenase (in blue), complex I (in red), [NiFe]-hydrogenase (in cyan) and formate dehydrogenase (in purple) as in Figure 5a. Minimal subunit and cofactor composition of the proteins including the [2Fe-2S]-containing subunit ([2Fe-2S]-SU), flavin/[4Fe4S]-binding subunit (FBSU), as well as specific subunits for all members of each protein family are shown as pictograms in the colored square. Additional specific cofactors characterizing a specific group inside each protein family can be found as small pictograms at the representive leaves of the tree. Symbols enclosed by parentheses indicate the presence of the cofactor and/or the binding domain of that cofactor in the majority of sequences of the respective group. The symbols used are the same throughout figures and tables. Numbers in front of each species name refer to Supplementary Table 3, where RefSeq accessions and additional information to each sequence are given. Grey clouds and grey-colored branches indicate bootstrap values below 50%. Additional information include:
* - representative sequences that were used for the structural alignment
4 - tetrameric Hnd/Fds
2 - dimeric Hnd/Fds

Experimentally studied protein complexes as indicated in bold in Supplementary Fig. 4a and 4b:

[NiFe]-hydrogenase (in cyan)

Cupriavidus necator H16 (**4-Cup ne**) [23, 24, 25]
Hydrogenophilus thermoluteolus TH-1 (**6-Hyd th***) [26, 27]
Thiocapsa roseopersicina strain DSM 217 (**7-Thi ro**) [28]
Synechocystis sp. PCC 6803 (**20-Syn sp***) [29, 30, 31]

[FeFe]-hydrogenase(in blue)

Acetobacterium woodii DSM 1030 (**28-Ace wo**^{4}) [4]
Moorella thermoacetica ATCC 39073 (**33-Mor th**) [32]
Ruminococcus albus DSM 20455 (**34-Rum al**) [33]
Thermotoga maritima DSM 3109 (**42-The ma**) [34, 3]
Syntrophomonas wolfei subsp. wolfei str. Goettingen G311 (**50-Syn wo**) [35]
Desulfovibrio fructosovorans DSM3604 (**60-Des fr**^{4}) [2]
Syntrophus aciditrophicus SB (**151-Syn ac**^{2}) [36]

Complex I (in red)

Ovis aries (**72-Ovi ar***) [37, 38]
Escherichia coli strain M9 (**76-Esc co**) [39]
Thermus thermophilus DSM 579 (**84-The th***) [40, 41, 16, 42, 43]
Aquifex aeolicus VF5 (**91-Aqu ae**) [44, 45]

Formate Dehydrogenase (in purple)

Gottschalkia acidurici 9a (**106-Got ac**) [7]
Methylorubrum extorquens AM1 (**115-Met ex**^{2}) [46]
Rhodobacter capsulatus YW2 (**123-Rho ca***^{4}) [47, 9]
Methylosinus trichosporium OB3b (**125-Met tr**^{4}) [48]
Cupriavidus necator N-1 (**132-Cup ne**^{4}) [49, 50, 8]
Cupriavidus oxalaticus strain T2 (**162-Cup ox**^{4}) [51]

Other proteins

Thermococcus litoralis DSM 5473 (**135-The li**) [52]
Clostridium autoethanogenum DSM 10061 (**143-Clo au**) [6]
Moorella thermoacetica ATCC 39073 (**145-Moo th**) [53]

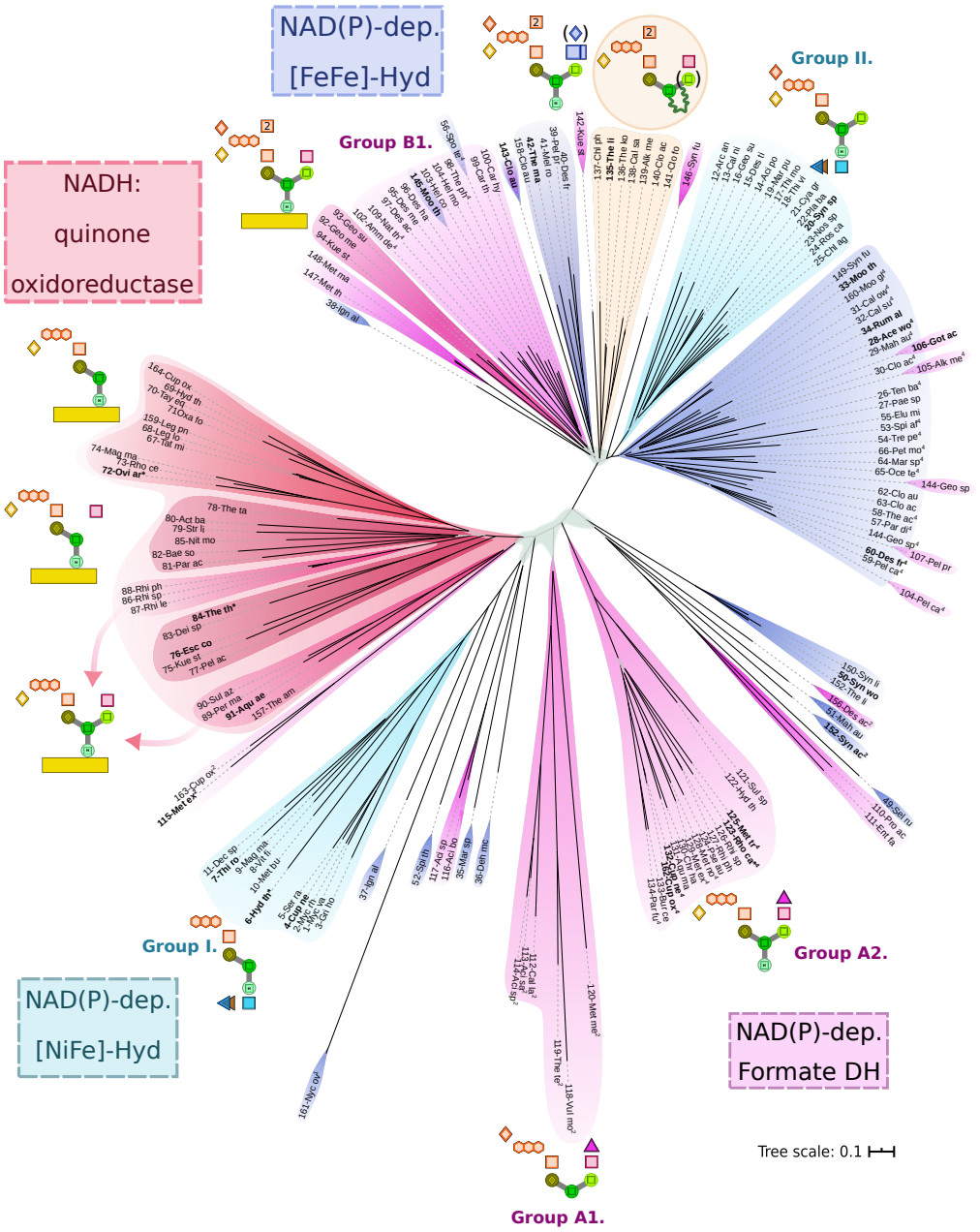

Supplementary Figure 4b: **Fully annotated Neighbor-Joining Tree of the flavin module in representative sequences.**
Similarity clustering of the sequences belonging to the [FeFe]-hydrogenase (in blue), complex I (in red), [NiFe]-hydrogenase (in cyan) and formate dehydrogenase (in purple) as in Figure 5b. Cofactor composition of the enzymes are shown as pictograms as in Figure 4a. Additional specific cofactors characterizing a specific group inside each protein family can be found as small pictograms at the representive leaves of the tree. Symbols enclosed by parentheses indicate the presence of the cofactor and/or the binding domain of that cofactor in the majority of sequences of the respective group. The symbols used are the same throughout figures and tables. Numbers in front of each species name refer to Supplementary Table 3, where RefSeq accessions and additional information to each sequence are given. Grey clouds and grey-colored branches indicate bootstrap values below 50%. Additional information include:
* - representative sequences that were used for the structural alignment
[4] - tetrameric Hnd/Fds
[2] - dimeric Hnd/Fds

References

[1] C. Baffert, A. Kpebe, L. Avilan & M. Brugna (2019); 'Hydrogenases and H_2 metabolism in sulfate-reducing bacteria of the *Desulfovibrio* genus'. In Advances in microbial physiology, vol. 74, pp. 143–189 (Elsevier).

[2] A. Kpebe, M. Benvenuti, C. Guendon, A. Rebai, V. Fernandez et al. (2018); 'A new mechanistic model for an O_2-protected electron-bifurcating hydrogenase, Hnd from *Desulfovibrio fructosovorans*'. Biochimica et Biophysica Acta (BBA)-Bioenergetics, vol. 1859(12):pp. 1302–1312.

[3] N. Chongdar, K. Pawlak, O. Rüdiger, E. J. Reijerse, P. Rodríguez-Maciá et al. (2019); 'Spectroscopic and biochemical insight into an electron-bifurcating [FeFe] hydrogenase'. JBIC Journal of Biological Inorganic Chemistry, pp. 1–15.

[4] K. Schuchmann & V. Müller (2012); 'A bacterial electron-bifurcating hydrogenase'. Journal of Biological Chemistry, vol. 287(37):pp. 31165–31171.

[5] A. Graentzdoerffer, D. Rauh, A. Pich & J. R. Andreesen (2003); 'Molecular and biochemical characterization of two tungsten-and selenium-containing formate dehydrogenases from *Eubacterium acidaminophilum* that are associated with components of an iron-only hydrogenase'. Archives of microbiology, vol. 179(2):pp. 116–130.

[6] S. Wang, H. Huang, J. Kahnt, A. P. Mueller, M. Kopke et al. (2013); 'NADP-specific electron-bifurcating [FeFe]-hydrogenase in a functional complex with formate dehydrogenase in *Clostridium autoethanogenum* grown on CO'. Journal of Bacteriology, vol. 195(19):pp. 4373–4386.

[7] S. Wang, H. Huang, J. Kahnt & R. K. Thauer (2013); '*Clostridium acidurici* electron-bifurcating formate dehydrogenase'. Appl. Environ. Microbiol., vol. 79(19):pp. 6176–6179.

[8] R. Hille, T. Young, D. Niks, S. Hakopian, T. K. Tam et al. (2020); 'Structure: Function studies of the cytosolic, Mo-and NAD^+-dependent formate dehydrogenase from *Cupriavidus necator*'. Inorganics, vol. 8(7):p. 41.

[9] C. Radon, G. Mittelstädt, B. R. Duffus, J. Bürger, T. Hartmann et al. (2020); 'Cryo-EM structures reveal intricate Fe-S cluster arrangement and charging in *Rhodobacter capsulatus* formate dehydrogenase'. Nature communications, vol. 11(1):pp. 1–9.

[10] K. Björklöf, V. Zickermann & M. Finel (2000); 'Purification of the 45 kDa, membrane bound NADH dehydrogenase of *Escherichia coli* (NDH-2) and analysis of its interaction with ubiquinone analogues'. Febs Letters, vol. 467(1):pp. 105–110.

[11] T. Friedrich & B. Böttcher (2004); 'The gross structure of the respiratory complex I: a Lego System'. Biochimica et Biophysica Acta (BBA)-Bioenergetics, vol. 1608(1):pp. 1–9.

[12] T. Friedrich & D. Scheide (2000); 'The respiratory complex I of bacteria, archaea and eukarya and its module common with membrane-bound multisubunit hydrogenases'. FEBS letters, vol. 479(1-2):pp. 1–5.

[13] T. G. Laughlin, D. F. Savage & K. M. Davies (2018); 'Revealing the subunit architecture of NAD(P)H dehydrogenase type-1 from cyanobacteria through Cryo-EM'. Biophysical Journal, vol. 114(3):p. 424a.

[14] J. M. Schuller, J. A. Birrell, H. Tanaka, T. Konuma, H. Wulfhorst et al. (2019); 'Structural adaptations of photosynthetic complex I enable ferredoxin-dependent electron transfer'. Science, vol. 363(6424):pp. 257–260.

[15] H. Brüggemann, F. Falinski & U. Deppenmeier (2000); 'Structure of the $F_{420}H_2$: quinone oxidoreductase of *Archaeoglobus fulgidus*: Identification and overproduction of the $F_{420}H_2$-oxidizing subunit'. European Journal of Biochemistry, vol. 267(18):pp. 5810–5814.

[16] R. Baradaran, J. M. Berrisford, G. S. Minhas & L. A. Sazanov (2013); 'Crystal structure of the entire respiratory complex I'. Nature, vol. 494(7438):pp. 443–448.

[17] B. Schoepp-Cothenet, R. Van Lis, P. Philippot, A. Magalon, M. J. Russell et al. (2012); 'The ineluctable requirement for the trans-iron elements molybdenum and/or tungsten in the origin of life'. Scientific reports, vol. 2:p. 263.

[18] J. Rozewicki, S. Li, K. M. Amada, D. M. Standley & K. Katoh (2019); 'MAFFT-DASH: integrated protein sequence and structural alignment'. Nucleic acids research, vol. 47(W1):pp. W5–W10.

[19] B. C. Marreiros, A. P. Batista, A. M. Duarte & M. M. Pereira (2013); 'A missing link between com-

plex I and group 4 membrane-bound [NiFe] hydrogenases'. Biochimica et Biophysica Acta (BBA)-Bioenergetics, vol. 1827(2):pp. 198–209.

[20] J. Mock, Y. Zheng, A. P. Mueller, S. Ly, L. Tran et al. (2015); 'Energy conservation associated with ethanol formation from h2 and co2 in clostridium autoethanogenum involving electron bifurcation'. Journal of bacteriology, vol. 197(18):pp. 2965–2980.

[21] K. Schuchmann, N. P. Chowdhury & V. Müller (2018); 'Complex multimeric [FeFe] hydrogenases: biochemistry, physiology and new opportunities for the hydrogen economy'. Frontiers in microbiology, vol. 9:p. 2911.

[22] X. Robert & P. Gouet (2014); 'Deciphering key features in protein structures with the new endscript server'. Nucleic acids research, vol. 42(W1):pp. W320–W324.

[23] A. Tran-Betcke, U. Warnecke, C. Böcker, C. Zaborosch & B. Friedrich (1990); 'Cloning and nucleotide sequences of the genes for the subunits of NAD-reducing hydrogenase of *Alcaligenes eutrophus H16*.' Journal of bacteriology, vol. 172(6):pp. 2920–2929.

[24] L. Lauterbach, Z. Idris, K. A. Vincent & O. Lenz (2011); 'Catalytic properties of the isolated diaphorase fragment of the NAD^+-reducing [NiFe]-hydrogenase from *Ralstonia eutropha*'. PloS one, vol. 6(10).

[25] L. Lauterbach, J. Liu, M. Horch, P. Hummel, A. Schwarze et al. (2011); 'The hydrogenase subcomplex of the NAD^+-reducing [NiFe] hydrogenase from *Ralstonia eutropha* – insights into catalysis and redox interconversions'. European Journal of Inorganic Chemistry, vol. 2011(7):pp. 1067–1079.

[26] Y. Shomura, M. Taketa, H. Nakashima, H. Tai, H. Nakagawa et al. (2017); 'Structural basis of the redox switches in the NAD^+-reducing soluble [NiFe]-hydrogenase'. Science, vol. 357(6354):pp. 928–932.

[27] J. Preissler, S. Wahlefeld, C. Lorent, C. Teutloff, M. Horch et al. (2018); 'Enzymatic and spectroscopic properties of a thermostable [NiFe]-hydrogenase performing H_2-driven NAD^+-reduction in the presence of O_2'. Biochimica et Biophysica Acta (BBA)-Bioenergetics, vol. 1859(1):pp. 8–18.

[28] G. Rákhely, A. T. Kovács, G. Maróti, B. D. Fodor, G. Csanádi et al. (2004); 'Cyanobacterial-type, heteropentameric, NAD^+-reducing NiFe hydrogenase in the purple sulfur photosynthetic bacterium *Thiocapsa roseopersicina*'. Appl. Environ. Microbiol., vol. 70(2):pp. 722–728.

[29] O. Schmitz, G. Boison, H. Salzmann, H. Bothe, K. Schütz et al. (2002); 'HoxE—a subunit specific for the pentameric bidirectional hydrogenase complex (HoxEFUYH) of cyanobacteria'. Biochimica et Biophysica Acta (BBA)-Bioenergetics, vol. 1554(1-2):pp. 66–74.

[30] F. Germer, I. Zebger, M. Saggu, F. Lendzian, R. Schulz et al. (2009); 'Overexpression, isolation, and spectroscopic characterization of the bidirectional [NiFe] hydrogenase from *Synechocystis sp. PCC 6803*'. Journal of Biological Chemistry, vol. 284(52):pp. 36462–36472.

[31] K. Gutekunst, X. Chen, K. Schreiber, U. Kaspar, S. Makam et al. (2014); 'The bidirectional NiFe-hydrogenase in *Synechocystis sp. PCC 6803* is reduced by flavodoxin and ferredoxin and is essential under mixotrophic, nitrate-limiting conditions'. Journal of Biological Chemistry, vol. 289(4):pp. 1930–1937.

[32] S. Wang, H. Huang, J. Kahnt & R. K. Thauer (2013); 'A reversible electron-bifurcating ferredoxin-and NAD-dependent [FeFe]-hydrogenase (HydABC) in *Moorella thermoacetica*'. Journal of bacteriology, vol. 195(6):pp. 1267–1275.

[33] Y. Zheng, J. Kahnt, I. H. Kwon, R. I. Mackie & R. K. Thauer (2014); 'Hydrogen formation and its regulation in *Ruminococcus albus*: involvement of an electron-bifurcating [FeFe]-hydrogenase, of a non-electron-bifurcating [FeFe]-hydrogenase, and of a putative hydrogen-sensing [FeFe]-hydrogenase'. Journal of bacteriology, vol. 196(22):pp. 3840–3852.

[34] G. J. Schut & M. W. W. Adams (2009); 'The Iron-Hydrogenase of *Thermotoga maritima* utilizes ferredoxin and NADH synergistically: a new perspective on anaerobic hydrogen production'. Journal of Bacteriology, vol. 191(13):pp. 4451–4457.

[35] N. A. Losey, F. Mus, J. W. Peters, H. M. Le & M. J. McInerney (2017); '*Syntrophomonas wolfei* uses an NADH-dependent, ferredoxin-independent [FeFe]-hydrogenase to reoxidize NADH'. Applied and environmental microbiology, vol. 83(20).

[36] N. A. Losey, S. Poudel, E. S. Boyd & M. J. McInerney (2020); 'The beta subunit of non-bifurcating NADH-dependent [FeFe]-hydrogenases differs from those of multimeric electron-bifurcating [FeFe]-

hydrogenases'. Frontiers in microbiology, vol. 11:p. 1109.
[37] J. A. Letts, G. Degliesposti, K. Fiedorczuk, M. Skehel & L. A. Sazanov (2016); 'Purification of ovine respiratory complex I results in a highly active and stable preparation'. Journal of Biological Chemistry, vol. 291(47):pp. 24657–24675.
[38] J. A. Letts, K. Fiedorczuk, G. Degliesposti, M. Skehel & L. A. Sazanov (2019); 'Structures of respiratory supercomplex I+III2 reveal functional and conformational crosstalk'. Molecular cell, vol. 75(6):pp. 1131–1146.
[39] T. Friedrich (1998); 'The NADH: ubiquinone oxidoreductase (complex I) from *Escherichia coli*'. Biochimica et Biophysica Acta (BBA)-Bioenergetics, vol. 1364(2):pp. 134–146.
[40] T. Yagi, K. Hon-Nami & T. Ohnishi (1988); 'Purification and characterization of two types of NADH-quinone reductase from *Thermus thermophilus HB-8*'. Biochemistry, vol. 27(6):pp. 2008–2013.
[41] L. A. Sazanov & P. Hinchliffe (2006); 'Structure of the hydrophilic domain of respiratory complex I from *Thermus thermophilus*'. science, vol. 311(5766):pp. 1430–1436.
[42] R. G. Efremov, R. Baradaran & L. A. Sazanov (2010); 'The architecture of respiratory complex I'. Nature, vol. 465(7297):pp. 441–445.
[43] R. G. Efremov & L. A. Sazanov (2012); 'The coupling mechanism of respiratory complex I – a structural and evolutionary perspective'. Biochimica et Biophysica Acta (BBA)-Bioenergetics, vol. 1817(10):pp. 1785–1795.
[44] M. Guiral, L. Prunetti, S. Lignon, R. Lebrun, D. Moinier et al. (2009); 'New insights into the respiratory chains of the chemolithoautotrophic and hyperthermophilic bacterium *Aquifex aeolicus*'. Journal of proteome research, vol. 8(4):pp. 1717–1730.
[45] G. Peng, B. Meyer, L. Sokolova, W. Liu, S. Bornemann et al. (2018); 'Identification and characterization two isoforms of NADH: ubiquinone oxidoreductase from the hyperthermophilic eubacterium *Aquifex aeolicus*'. Biochimica et Biophysica Acta (BBA)-Bioenergetics, vol. 1859(5):pp. 366–373.
[46] M. Laukel, L. Chistoserdova, M. E. Lidstrom & J. A. Vorholt (2003); 'The tungsten-containing formate dehydrogenase from *Methylobacterium extorquens AM1*: Purification and properties'. European journal of biochemistry, vol. 270(2):pp. 325–333.
[47] T. Hartmann & S. Leimkühler (2013); 'The oxygen-tolerant and NAD^+-dependent formate dehydrogenase from *Rhodobacter capsulatus* is able to catalyze the reduction of CO_2 to formate'. The FEBS journal, vol. 280(23):pp. 6083–6096.
[48] D. R. Jollie & J. D. Lipscomb (1991); 'Formate dehydrogenase from *Methylosinus trichosporium OB3b*. purification and spectroscopic characterization of the cofactors.' Journal of Biological Chemistry, vol. 266(32):pp. 21853–21863.
[49] J.-I. Oh & B. Bowien (1998); 'Structural analysis of the Fds operon encoding the NAD^+-linked formate dehydrogenase of *Ralstonia eutropha*'. Journal of Biological Chemistry, vol. 273(41):pp. 26349–26360.
[50] T. Young, D. Niks, S. Hakopian, T. K. Tam, X. Yu et al. (2020); 'Crystallographic and kinetic analyses of the FdsBG subcomplex of the cytosolic formate dehydrogenase FdsABG from *Cupriavidus necator*'. Journal of Biological Chemistry, vol. 295(19):pp. 6570–6585.
[51] U. Rusching, U. Müller, P. Willow & T. Höpner (1976); 'CO_2 reduction to formate by NADH catalysed by formate dehydrogenase from *Pseudomonas oxalaticus*'. European journal of biochemistry, vol. 70(2):pp. 325–330.
[52] A. Tóth, M. Takács, G. Groma, G. Rákhely & K. L. Kovács (2008); 'A novel NADPH-dependent oxidoreductase with a unique domain structure in the hyperthermophilic archaeon, *Thermococcus litoralis*'. FEMS microbiology letters, vol. 282(1):pp. 8–14.
[53] J. R. Andreesen & L. G. Ljungdahl (1974); 'Nicotinamide adenine dinucleotide phosphate-dependent formate dehydrogenase from *Clostridium thermoaceticum*: purification and properties'. Journal of bacteriology, vol. 120(1):pp. 6–14.

Chapter

Thermodynamic landscape of the redox-centres in the electron-confurcating [FeFe]-Hydrogenase (HydABC) of *Thermotoga maritima*

4

(in preparation)

Thermodynamic landscape of the redox-centers in the electron-confurcating [FeFe]-Hydrogenase (HydABC) of *Thermotoga maritima*

Kilian Zuchan[1], Nina Breuer[2], Christoph Laurich[2], Wolfgang Nitschke[1], Frauke Baymann[1], James Birrell[2,3]

1. *Aix-Marseille Université, CNRS, BIP UMR 7281, IMM, 13402, Marseille, France*.

2. *Department Inorganic Spectroscopy, Max Planck Institute for Chemical Energy Conversion, 45470, Mülheim an der Ruhr, Germany*.

3. School of Life Sciences, University of Essex, UK.

Abstract

The [FeFe]-hydrogenase from *Thermotoga maritima*, HydABC, physiologically catalyzes the evolution of hydrogen (H_2) from NADH and reduced ferredoxin during glucose fermentation. Recent structural HydABC models show 10 iron-sulfur (FeS) clusters in addition to the two catalytic sites, the H-cluster for proton reduction and the flavin mononucleotide (FMN) for oxidizing NADH and electron confurcation. Half of the FeS clusters are arranged to form a chain between the two catalytic sites, the remaining FeS clusters are in mobile domains, with three thioredoxin-like [2Fe-2S]-clusters, one in each subunit and two [4Fe-4S]-clusters in a bacterial ferredoxin-like C-terminal domain of HydB.

In this work, redox titrations in monitored by electron paramagnetic resonance- (EPR) and UV/Visible-spectroscopy allowed to assign a redox midpoint potential to all but one of the FeS clusters and the flavin of the apoprotein and its constituting subunits. HydABC features an overall low redox potential landscape (below -400 mV vs SHE) with the three thioredoxin-like [2Fe-2S]-clusters, A5, B1, C1 demonstrating radically different redox potentials from each other, with -270 mV, -550 mV and -400 mV, respectively. The central FMN in the isolated HydB subunit shows a strongly stabilized semi-reduced state with -160 mV and -540 mV for the individual redox transitions at pH 6.5. The redox properties of the FMN in HydABC were inconclusive between the two employed experimental setups.

Keywords: hydrogenase, FeS-cluster, flavin, electron bifurcation, redox midpoint potential

Introduction

Electron bifurcation/confurcation is the coupled redox reaction of a two-electron redox compound with two individual one-electron redox centers of differing nature and electrochemical potential, one of them usually featuring more negative redox midpoint potentials than the two-electron compound while the second one has a more positive midpoint potential (Buckel & Thauer (2013), (2018)) The phenomenon of electron bifurcation was first observed in mitochondrial Complex III (Wikström and Berden (1972)) and later interpreted within an electrochemical framework by Mitchell (Mitchell (1975a), (1975b)). In Complex III, a quinone reduces in a coupled manner a lower potential heme b_L and a higher potential Rieske iron-sulfur center. A more in-depth functional model for this process was presented by Crofts *et al.* (2013).

In 2008, an analogous reaction scheme was proposed to explain the endergonic reduction of ferredoxin by the Electron transferring flavoprotein (Etf) (Li *et al.* (2008), Herrmann *et al*. (2008)). The role of the quinone as pivotal two-electron redox compound in electron bifurcation/confurcation may thus also be played by the flavin cofactor (Nitschke & Russell (2012)).

Since its first discovery in 2008, flavin-based electron bifurcation (FBEB) and -confurcation (FBEB) was proposed to occur in a wide variety of different enzymes (Lubner *et al.* (2017), Schut *et al.* (2009), Wagner *et al.* (2017)). While the majority of these flavoenzymes seem to perform electron bifurcation/confurcation reactions resembling those described for Complex III and its various prokaryotic homologs (summarily referred to as the "Rieske/cyt*b* complexes", Schütz *et al.* (2000)), a subgroup of FBEB-enzymes stands out by virtue of the fact that one of the redox partners of the bifurcating flavin is itself an obligatory two-electron redox compound, i.e., NAD(H) or NADP(H), hampering straightforward transposition of the functional models previously developed to rationalize EB processes (Crofts et al. (2013), Bergdoll et al. (2016), Nitschke and Russel et al. (2012)).

This subgroup of "NAD(P)-dependent" FBEB-enzymes has recently been recognized to constitute a large NAD(P)H dehydrogenase family comprising [FeFe]- and [NiFe]-hydrogenases, formate dehydrogenases as well as respiratory Complex I (Buckel & Thauer (2018), Zuchan *et al.* (2021), Losey *et al.* (2020)). Some of them however are not thought to be bifurcating in the above-described manner.

The unifying features of all representatives in this group are the presence of a structurally well-conserved (flavin-containing) module catalyzing the redox conversion of NAD(P) and of an iron-sulfur-

center-rich module mediating charge transfer between the NAD(P)-binding module and the respective catalytic centers in the diverse enzymes. The aforementioned fact that in this group electrons are bifurcated/confurcated towards/from one-electron redox substrates (mostly ferredoxins) in one branch and the two-electron compound NAD(P) in the other branch substantially complicates the elaboration of functional models. A very promising approach to rationalize this process initially involved the presence of two rather than one flavin cofactor in these enzymes (Buckel & Thauer (2013), (2018)). Crystallographic and Cryo-EM structure models of proteins from this family of enzymes resolved during recent years did not confirm this hypothesis, sending the respective community back to the drawing boards (Efremov and Sazanov (2012), Feng *et al*. (2022), Radon *et al.* (2020), Furlan *et al.* (2022), Katsyv *et al.* (2023)).

In order to develop mechanistic models for the electron bifurcating/confurcating process in this group of enzymes, two crucial parameters need to be known: (a) the structural arrangement of the involved cofactors including an assessment of potential domain movements/conformational changes modulating this arrangement and (b) the electrochemical parameters (i.e., redox midpoint potentials) of the redox centers participating in the bifurcating/confurcating reaction together with an assessment of potential variations thereof in response to conformational changes.

Over the last two years, multiple 3D-structure models of three major representatives of the NAD(P)-dependent bifurcating/confurcating enzymes belonging to this NAD(P)H dehydrogenase family have been reported and, although a number of structural/conformational details are still controversial, our knowledge of the architecture of these complexes has improved substantially (Feng *et al.* (2022), Furlan *et al.* (2022), Katsyv *et al.* (2023), Kumar *et al.* (2022)).

By contrast, to the exception of Complex I, the electrochemical characterization of these enzymes remains rudimentary at best. Although in Complex I the initial electron transfer from the flavin follows the bifurcation scheme (Buckel & Thauer (2018), Baymann *et al.* (2016), Zuchan *et al.* (2021)), the enzyme has evolved to carry out significantly differing catalytic processes shuttling all electrons to quinone and coupling this electron transfer to transmembrane proton pumping (Verkhovskaya *et al.* (2008), de Vries *et al.* (2015), Dörner *et al.* (2017)). Transposability of results obtained on Complex I towards the remainder of the enzyme superfamily therefore remains doubtful.

To remediate this lack of information, we have in this work tried to obtain for the first time a comprehensive catalogue of the redox properties of the relevant cofactors in the electron confurcating, NADH-dependent [FeFe]-hydrogenase (HydABC) from the hyperthermophilic bacterium *Thermotoga*

maritima.

Recent structural efforts using Cryo-EM have elucidated that the trimeric HydABC in *T. maritima* functionally forms a multimer of heterotrimers (Furlan *et al.* (2022)). The detailed molecular model clearly features 10 FeS clusters per heterotrimer, four of the binuclear [2Fe-2S]- and six of the cubic, tetranuclear [4Fe-4S]-type (Figure 1).

Interestingly, the well-resolved central core of HydABC only features half of these FeS (B2, A1, A2, A3, A4) forming a chain that connect the two active sites, the essential prosthetic flavin-molecule, FMN as the binding site of NADH and bifurcating site in the HydB subunit and the proton-reducing H-cluster in the HydA subunit.

The other five FeS clusters (A5, B1, B3, B4, C1) in HydABC are arranged outside of this chain and seem to be in more dynamic or flexible regions (Figure 1). Three of these, one in each subunit (A5, B1& C1) are [2Fe-2S]-clusters, that are coordinated by cysteinyl-residues inside a thioredoxin-like protein fold exhibiting well characterized UV/Vis and EPR-signals (Meyer, Andrade, Einsle (2011)).
The two remaining FeS clusters, B3 and B4 outside of the “main wire” are [4Fe-4S]-clusters that can be found inside a flexible 8Fe ferredoxin domain as a C-terminal extension of the flavin-containing HydB subunit (Furlan *et al.* (2022)).
Here, the assignment of redox potentials and magnetic interactions of most FeS clusters in HydABC are presented. The thermodynamic parameters of this enzyme complex together with their spectroscopic characteristics have been obtained by means of electron paramagnetic resonance (EPR) spectroscopy and UV/Vis spectroscopy in the entire HydABC complex, as well as its separate subunits.
We have hereby emphasized our interest on the characterization of the FeS clusters closest to and inside the flavin-bearing HydB subunit in order to gain initial insights into the confurcating mechanism.

Materials and Methods

Protein expression and purification
Themotoga maritima bifurcating Hydrogenase apo-HydABC, the “apo”-HydA subunit and the HydB subunit were expressed and purified as described in Chongdar *et al.* (2020) with minor modifications: to ensure maximal FMN occupation, 50 µg/mL riboflavin was added to the culture medium of *E. coli* and 10-fold molar excess FMN were added to the sample prior to the gel-filtration column. The HydC subunit

was recovered during HydABC purification. The genes encoding HydABC without the ferredoxin domain of HydB (TmHydABC Δ571-626), the separate C-terminal 8Fe-ferredoxin domain of Hyd B (TmHydBCTD) and the C-terminal thioredoxin domain of HydA (TmHydACTD) were amplified by PCR from *Thermotoga maritima* MSB8 genomic DNA (ATCC, 43589D-2) using the following primers: TmHydB Δ571-626 5'-TGAGGAGGGAAGAAAAATGAAAATTTACG -3' (forward) and TmHydB Δ571-626 5'-TTTCTTGAACGCCGTGCACATTC-3' (reverse), TmHydBCTD 5'- AAGAAATACGTCATCAATCCAG -3' (forward) and TmHydBCTD 5'- GCCCTGAAAATAAAGATTCTCAC -3' (reverse) and HydA-CT 5'-AAAGATGTGGAAATACTGCCC -3' (forward) and HydA-CT 5'- GCCCTGAAAATAAAGATTCTCAC 3' (reverse) and expressed and purified following the same protocol as apo-HydA (Chongdar *et al.* 2020). The Strep-tag remained uncleaved in all samples. Concentrated proteins were stored, frozen and shipped in 100 mM Tris-HCl, 150 mM NaCl, pH 8. Protein concentration was determined by absorbance at 280 nm using our experimentally determined extinction coefficient of 250 mM^{-1} cm^{-1} for HydABC, 108 mM^{-1} cm^{-1} for HydA, 20 mM^{-1} cm^{-1} for HydC and 112 mM^{-1} cm^{-1} for HydB. FMN concentration in HydB samples was determined by absorbance at 450 nm (FMN 12.2 $mM^{-1}cm^{-1}$(Hinkson 1968)) of the supernatant after protein denaturation in 2.25 M KCl, in 50 mM $NaPO_4$ Buffer, pH 7 at 100°C for 30 min and centrifugation at 1400g for 30 min. Protein concentration was corrected for the contribution of the FMN at 280 nm and the protein:FMN ratio determined to be close to 1 for HydB samples. Flavin content of apo-HydABC was determined to be at about 0.6 FMN/protein.

Optical spectroscopy

UV/Vis spectra were recorded on a Cary 5E or Cary 4000 spectrophotometer. Samples were prepared anaerobically in a glovebox and measured in rubber-capped Quartz cuvettes.

Mediator spectra were recorded on a diode array spectrometer (Ocean Optics,DH-2000-BAL light source, USB2000+UV-Vis-ES detector) in a glove box (MBraun LabMaster SP) purged constantly with a 100% nitrogen atmosphere. 177.5 µM AQ1 S ($E_m^{0'}$ = -228 mV, ThermoFisher, CAS: 131-08-8) and 2.75 µM BV ($E_m^{0'}$ = -350/540 mV, Merck, CAS: 1102-19-8) were prepared in buffer mix A with 80mM KCl and 50 mM each of sodium acetate (Merck, CAS: 127-09-3, pK_a = 4.54), MES (ROTH, CAS: 4432-31-9, pK_a = 6.15), HEPES (ROTH, CAS: 7365-45-9, pK_a = 7.5), Tris (ROTH, CAS: 77-86-1, pK_a = 8.07) and glycine (ROTH, CAS: 56-40-6, pK_a = 9.6), adjusted to pH 7. The mediator mix (10 µM AQ1 Q-1-, 1 µM BV and 16 µM MV ($E_m^{0'}$ = -440/-772 mV, Acros Organics, CAS: 1910-42-5) in buffer mix A as used for redox titrations was also measured.

Electrochemical redox titrations followed by optical spectroscopy

Sample preparations and measurements were carried out in a glove box. 150 µL protein sample (containing 15 to 30 µM HydB or 8.5 to 15 µM HydABC) in buffer mix A adjusted to pH values in the range of 5.2 to 9.2 and with mediator mix was injected into the electrochemical setup (Birrell et al.2020, SI). The setup consists of a capillary non-modified gold working electrode (WE), an $Ag/AgCl_2$ reference electrode (RE) in 3 M KCl (WPI, Ref: DRIREF-2SH) and a platinum counter electrode (CE). The setup was calibrated before and after each measurement by Cyclic Voltammetry with Ferrocene methanol (E = 233 mV vs $Ag/AgCl_2$ in 3 M KCl, 97%, Sigma-Aldrich, CAS: 1273-86-5) in 0.5 M KCl (Zheng *et al.* 2017). Experiments were started by initial reduction of the sample after which potentials were incremented in steps of 20 mV for two complete oxidation/reduction cycles (Metrohm potentiostat, Autolab/ PGSTAT101). After 10 min equilibration spectra were recorded on a diode array spectrometer (Ocean Optics,DH-2000-BAL light source, USB2000+UV-Vis-ES detector), connected to the cell by optical fibers (QP-600-2-SR) via a 320 nm cutoff filter to avoid photo damage of FMN. The potentiostat together with the spectrometer are controlled by a LABVIEW script (Version 2021).

Chemical redox titrations followed by EPR spectroscopy

Redox titrations were performed in a Jacomex glove box under nitrogen atmosphere in a conic vessel with an Ag/AgCl reference electrode, calibrated before and after each experiment against a saturated quinhydrone solution ($E_m^{0'}$ = +280 mV vs SHE, Sigma Aldrich, CAS: 106-34-3) in MOPS buffer, pH 7, at RT. Titrations were performed in buffer mix B: MES (Sigma, CAS: 4432-31-9, pK_a = 6.15), HEPES (ROTH, CAS: 7365-45-9, pK_a = 7.5), Tricine (ROTH, CAS: 5704-04-1, pK_a = 8.15), AMPSO (Sigma, CAS: 68399-79-1, pK_a = 8.9) and KCl at 50 mM each, adjusted to pH values between 6 and 9. 3ml of 10-30 µM protein in buffer mix B was stirred for 1h with mediators (depending on experiments 10 µM or 100 µM each AQ-1-S, BV, MV and AQ-2-S ($E_m^{0'}$ = -184 mV, TCI Chemicals, CAS: 853-35-0)). Aliquots of 200mM sodium dithionite and 10mM potassium ferricyanide (III) solutions were added to shift the potential. After equilibration, 200µl sample were transferred to an EPR tube and frozen inside the glove box in a cold-finger in ethanol cooled to -50°C to -60°C.

EPR spectroscopy

EPR spectra were recorded on a Bruker Elexsys E-500 EPR spectrometer equipped with an ER4012ST rectangular cavity and an ESR900 helium flow cryostat (Oxford Instruments). Experimental parameters are given in the Figure legends.

Protein film voltammetry

1ul protein solution in 100 mM TRIS/HCl (no salts) was applied to a glassy carbon electrode in a glove box. Reference electrode was Standard Calomel. Cyclic voltammetry was conducted at room temperature without rotation at a scan rate of 50 mV min^{-1}.

Results

The high number of iron-sulfur clusters in HydABC from *Thermotoga maritima* substantially hampers identification and characterization of individual redox centers due to spectral superposition both in optical and in EPR spectroscopy. We have therefore assisted the examination of the native enzyme complex by a parallel study of the individually expressed protein subunits HydA, HydB and HydC as well as of selected cofactor-carrying domains thereof. While at cryogenic temperatures below 20K, all types of iron sulfur centers generally are well-detectable, cubane [4Fe-4S]-centers rapidly broaden to beyond detection at higher temperatures. We therefore ran EPR spectra at 8K, 15K, 50K and 120K. As shown below, in HydABC as well as in all studied subunits and fragments of the enzyme, this procedure allowed to tease apart the contributions arising from [2Fe-2S]-clusters which were selectively visible at T ≥ 50K, devoid of appreciable spectral overlap from the cubane clusters. We will in the following first present the results gathered on these individual subunits and fragments of the whole enzyme and then try to integrate the obtained spectral and redox parameters into the dataset measured on the entire enzyme.

HydA and its C-terminal [2Fe-2S]-domain

As mentioned above, the HydA protein corresponds to a fusion of a *Chlamydomonas-type* [Fe-Fe]-hydrogenase (Mulder *et al.* (2010)) with an (N-terminal) Y-junction module and a (C-terminal) thioredoxin-like [2Fe-2S]-domain (see also Zuchan *et al.* (2021)). The catalytic H-cluster is not matured in the samples studied in this work permitting equilibrium redox titrations to be performed even at ambient potentials conducive to redox conversion of protons to H_2.

An initial spectroscopic characterization the isolated HydA protein was reported previously (Chondgar *et al*. (2020)). However, individual redox potentials of the ensemble of its iron sulfur centers have not yet been determined. A stepwise reduction of the HydA-subunit showed that in the spectra run at 50K, the thioredoxin-like [2Fe-2S] cluster A5 became observable at less reducing potentials than the plant-type [2Fe-2S]-cluster A1. Furthermore, the A5 cluster appeared also earlier than the bulk of the [4Fe-4S]-

clusters A2, A3 and A4, identifying cluster A5 as the highest potential iron sulfur center of the HydA subunit. Since the available amount of HydA as well as of its separately expressed C-terminal domain were insufficient for bulk redox titrations (both in EPR and in UV/Vis spectroscopy), the redox potential of the A5 cluster was determined by protein film voltammetry (PFV) to -270 mV (Figure 3, 3rd row, 2nd column). For the sake of assigning individual thioredoxin-like clusters in the entire enzyme (see below), we recorded the EPR-spectrum of cluster A5 in the heterologously, separately expressed C-terminal domain which exclusively contains the A5 cluster (Figure 2). Further characterization of the remaining iron sulfur centers was achieved on the entire enzyme HydABC, for which sufficient amounts of sample were available.

The HydC-subunit

HydC has been examined previously and both its spectral and redox parameters have been reported (Birrell *et al*. (2016)). Since EPR spectra presented therein have been obtained on an X-band EPR spectrometer different from the one used here, we recorded well-resolved spectra of the single thioredoxin-like cluster C1 present in this subunit under the instrumental conditions of the present study. As will be discussed below, this allowed attribution of each of the individual thioredoxin-like present in HydA, HydB and HydC to the electrochemical species observed in the entire HydABC enzyme. The corresponding EPR spectrum is shown in Figure 3 (row 8, column 2). The redox midpoint potential of cluster C1 of -377 mV at pH 8 was adopted from (Birrell *et al*. (2016)) and is represented in Figure 3 (8th row, 3rd column).

The HydB-subunit and its C-terminal 2x[4Fe-4S]-domain

HydB harbors the FMN moiety together with four iron sulfur centers, that is, the thioredoxin-like cluster B1, the cubane [4Fe-4S]-cluster B2 (in close vicinity of the flavin) as well as the bacterial ferredoxin-like (double-cubane) protein carrying clusters B3 and B4. We performed redox titrations on the HydB subunit at pH values in the range of 6.5 to 9, monitored in EPR- and 5.2 to 9.2 in UV/Vis-spectroscopy. Due the very low redox midpoint potentials of the redox cofactors in the Hyd enzyme, in chemical redox titrations high pH values were required to attain near-full reduction of the cofactors. To avoid spectral contributions from mediators, samples were also stepwise reduced by addition of sodium dithionite, in the absence of mediators and a measuring electrode.

EPR redox titrations monitored at 50 K and higher demonstrated the presence of a single redox species featuring the spectral characteristics of a thioredoxin-like [2Fe-2S] center and titrating at -460 mV. This spectral and redox species was therefore attributed to cluster B1.

The data recorded at 15K during the titration (Suppl. Figure 1) featured the appearance of an iron sulfur center below -300 mV. No iron sulfur-type signal was visible at these potentials in spectra recorded at 50K and above, identifying this center as arising from a [4Fe-4S]-cluster. On progressive reduction, additional signal amplitude severely distorting the spectral shape of the above-mentioned center was observed indicating reduction of a spectrally different redox component (Suppl. Figure 1). Intriguingly, while this second paramagnetic center came up, the g_Z-signal of the first center decreased (Suppl. Figure 1 and see the negative contribution in the difference spectrum shown in Figure 3, 7th row, 2nd column). This behavior is characteristic of bacterial-type ferredoxins, where paramagnetic interactions between the two neighboring cubane clusters frequently induce shifts of g-tensor components and hence the disappearance of spectral features arising from the non-interacting species (Bentrop *et al.* (1997), Vassiliev *et al.* (2001), Cammack and MacMillan (2010)). Figure 3 (7th row, 3rd column) shows the dependence on ambient potential of the g_z-signal of the first cluster to become reduced. Fitting the depicted data to the expected dependence for sequential reduction of two interacting centers yields very close ($\Delta E_m \approx 50$ mV) redox midpoint potentials for the individual redox species. While the higher potential component can be observed in relatively pure form at less reducing potentials, determining the spectrum of the second cluster in its non-interacting state is impossible and even the spectrum of the cluster in the interacting state, devoid of contributions from the first one, is difficult to obtain. The top spectrum in the respective panel of Figure 3 (7th row, 2nd column, and Suppl. Fig. S5) represents our best approximation (*via* subtraction of consecutive spectra during the reducing and oxidizing directions of the redox titration) of the spectral shape of this cluster. Its g_y-line lies at substantially lower magnetic fields than that of the 1st cluster and its entire spectrum features near-axial symmetry (since the small g_x-trough visible in this spectrum belongs to the 1st cluster as evidenced by its dependence on ambient potential). The g-values of all EPR species observed in this study are summarized in Table 1.

Since the C-terminal domain of the HydB protein structurally corresponds to a bacterial-type ferredoxin, we attribute the [4Fe-4S]-clusters with the highest and second highest redox midpoint potentials observed in our titration to clusters B3/B4 within this domain. This attribution is supported by protein film (cyclic) voltammetry-experiments on the heterologously expressed C-terminal domain of HydB, which find a single redox species nicely corresponding to the average of the midpoint potentials, at -400 mV (at pH 8), seen in EPR. Given the very close spacing of the individual redox potentials seen in

EPR, it seems plausible that PFV would not be able to differentiate these two redox species. It is in fact due to the EPR-spectral differences as well as to the interaction-induced features that individual potentials could be inferred in the EPR experiments. We were able to obtain high enough quantities of this separately expressed C-terminal domain to record EPR spectra at increasing reduction states, generated by stepwise addition of sodium dithionite. The obtained spectra further corroborate the attribution outlined above, although their spectral features were broader than those measured on the HydB subunit (see Figure S5). This observation mirrors the findings on other bacterial-ferredoxin-like proteins or domains which frequently show higher g-strains than their native, enzyme-bound, counterparts (*e.g.* PsaC, Aasa *et al*. (1981)). Obviously, the question which of the two spectral/redox species belongs to structural cluster B3 and which one to B4 remains open.

At potentials below -400 mV, the reduction of a new [4Fe-4S]-cluster became visible which clearly stood out by a well-defined g_z-peak at g = 2.02 together with an additional contribution to the g_x-region at 1.87. Calculating difference spectra and subtracting the contribution of the [2Fe-2S]-cluster B1 yielded the spectral shape of this additional redox species, which, for lack of other candidates in the structure, was attributed to center B2. Its redox titration behavior was analyzed on the mentioned g_z-peak since the spectral convolution of the remaining EPR spectral features hampered evaluation of the g_y- and g_x-lines. Furthermore, strong contributions from mediators appearing below -500 mV drowned out center B2's g_z-peak below these redox potentials. From the limited set of data points, we estimate a redox midpoint potential for center B2 in the range of -460 to -500 mV.

No significant pH-dependence between pH 6 and pH 9 was detected for any of the above discussed iron sulfur centers in the HydB subunit.

At ambient potentials of -500 mV and lower, the field positions of basically all observed lines started to slightly shift in different directions, resulting in redox difference spectra with a wave-like, higher-order derivative, character over the whole spectral range of the iron sulfur centers. This phenomenon was consistently observed in redox titrations on HydB at all pH-values. We were unable to attribute these spectral signatures to new paramagnetic centers but found, as mentioned above, that they can be most parsimoniously explained by wholesale shifts of the g-tensor lines of several distinct iron sulfur centers. We will propose a tentative interpretation of this phenomenon in the discussion section. In UV/Vis-monitored redox titrations between pH 7 and pH 9, we were could not distinguish individual iron sulfur centers and found a single redox wave at around -375 mV, the spectrum of which corresponds to a superposition of thioredoxin-like [2Fe-2S]- and cubane-type [4Fe-4S]-clusters. However, simulating the ensemble of redox centers in EPR into a convoluted titration curve in UV/Vis (where spectral features

arising from the different centers overlap much more than in EPR) yielded curves which are substantially wider than the observed, apparently n = 1 Nernst-type, titration wave. Under the conditions of the electrochemical titration monitored by UV/Vis, the HydB redox centers therefore display a substantially more homogeneous redox behavior than when observed via the EPR redox setup.

In EPR redox titrations, the presence of mediators precludes the observation of enzyme-associated radical species. We have therefore gradually reduced HydB samples via addition of increasing amounts of sodium dithionite in the absence of mediators and therefore a measuring electrode. After the disappearance of spurious amounts of a [3Fe-4S]-cluster spectrum (visible also in the redox titrations and which we interpret to arise from a small fraction of degraded [4Fe-4S]-clusters) in the region of -100 mV, an isotropic, radical-type, signal became observable at g = 2 at all applied temperatures and remained visible down to the highest reduction states achieved with dithionite. An EPR spectrum of this radical species is shown in Figure 3 (4th row, 2nd column and Supp. Mat. Figure S2). The width of the isotropic g = 2 feature was 1.9 mT, which corresponds well to that of a neutral semi-reduced flavin radical (Murataliev (1999)). While this coincidence was intriguing, g = 2 signals are much less characteristic for specific free radicals than are for example the signatures of iron sulfur centers. We therefore decided to perform optical redox titrations on the HydB protein. We tried both chemical and electrochemical titrations but, due to the very reducing conditions required to cover the entire redox range of cofactors, the electrochemical titrations proved superior, and all data shown in this work were consequently gathered by using this method. The UV/Vis spectra of flavins (in all redox and protonation states) are expected to be strongly convoluted with those of the iron sulfur centers. However, since in the mediator-free EPR experiments described above, the radical signal appeared well before reduction of iron sulfur centers, the corresponding redox region should also in UV/Vis spectroscopy be free from contaminating spectral contributions of these clusters. Indeed, UV/Vis difference spectra below -100 mV and above -250 mV turned out to feature spectra as expected for a transition from the oxidized flavin to its neutral, semi-reduced, form, that is, a decrease of the broad 450 nm-peak arising from the oxidized form of FMN and the appearance of features at higher wavelengths (500-625 nm region) belonging to the neutral (blue) semi-reduced species (Murataliev (1999)). A representative UV/Vis spectrum of this transition is shown in Figure 3 (4th row, 4th column). Figure 3 (4th row, 3rd column) depicts the dependence of this spectral form on ambient potentials at the two extreme pH-values examined. The full pH-dependence is separately shown in Figure 4).

The potentials for the second transition towards the fully reduced flavin and the pH-dependence thereof is shown in Figure 3, 4th row, 3rd column and in Figure 4.

To further corroborate that the radical feature in EPR and the flavin-type UV/Vis difference spectra belong to the same redox species, we have performed a redox titration on HydB using significantly higher protein concentrations and lowering the amount of mediators present. Under these conditions, the radical species could be directly observed in EPR. Due to sample limitations, we performed these titrations only at two representative pH-values, the results whereof are shown in Figure 4. The EPR data correspond reasonably well to those obtained in UV/Vis-spectroscopy, confirming that the observed radical species indeed represents the neutral semi-reduced flavin.

While the appearance of the radical signal between -100 mV and -300 mV (Figure S3) corresponded well with the optical titration curve of the neutral flavin signal, we observed a so-far unexplained further increase in radical signal between -350 and -450 mV. No semi-reduced flavin-feature was detected in the corresponding range of ambient potentials in UV/Vis-monitored titrations. We will further discuss this effect below in the paragraph dealing with the relaxation properties of the flavin radical.

The entire HydABC enzyme

HydABC was subjected to redox titrations in the range of pH 6.5 to 9, monitored both by EPR (at 8K, 15K, 50K and 120K) and UV/Vis spectroscopy. In EPR at 50K and 120K, only [2Fe-2S]-centers were detected and contributions from the cubane clusters were negligible. Due to the different relaxation properties of the thioredoxin-like and the plat-type [2Fe-2S]-centers (see SI Figure S3) the former could selectively be observed at 120K. Figure 2 shows the dependence of the amplitude of the thioredoxin-like [2Fe-2S]-centers' g_x-trough on ambient potential. The dotted Nernst-curves in the bottom off the figure represent the midpoint potentials as determined on the isolated subunits. Redox difference spectra for the three distinguishable redox waves are indicated next to these individual transitions and compared to the spectral characteristics of the thioredoxin-like centers observed on the individual subunits. As shown in the inset of Figure 2, these centers (also depicted in Figure 3, second column) differ slightly by the position of their g_x-troughs and the position of the g_y signal. The thioredoxin-like centers observed in HydA (cluster A5) and in HydC (cluster C1) feature virtually identical g-tensors while that seen in HydB (cluster B1) has its g_x-trough and g_y signal shifted to higher g-values (indicated by dotted vertical lines in the inset to Figure 2). The positions of the two distinguishable g_x-troughs shown in the inset were reproduced in the spectra of the individual redox waves (dotted vertical lines). The respective spectrum obtained for the highest potential wave corresponds thus to that of either HydA or HydC. Since the determined redox dependence in the HydABC enzyme for the highest potential wave corresponds well

to that of the thioredoxin-center in the HydA protein (green dashed Nernst curve in Figure 2), we consider that this redox wave corresponds to the titration of HydA's thioredoxin center. The second thioredoxin-like redox wave in HydABC lies at slightly lower midpoint potentials (-410 to -420 mV) than that of the center in the HydC protein (-390 mV, blue dashed Nernst curve) while the redox difference spectrum of this redox component is found halfways between those of HydA/C and of HydB. However, the middle wave of the thioredoxin-like center titrates roughly together with that of the plant-type [2Fe-2S]-cluster also present in the higher temperature EPR spectra and the wing of the plant-types strongly axial (see Figure 3, 1st row, 2nd column) g// line may have pulled the thioredoxin-likes g_x-trough slightly to the left. For this reason and in particular for lack of an alternative interpretation (see below), we consider it very likely that the middle redox wave observed in HydABC at higher temperatures, that is, 50 K and 120 K, arises from the HydC cluster C1. The redox difference spectrum corresponding to the lowest potential wave indeed closely matches that recorded in the HydB subunit and, from its spectral features, therefore must arise from the thioredoxin-like center B1. In contrast to the other two thioredoxin-like [2Fe-2S]-clusters, this center's redox midpoint potential was strongly shifted towards lower potentials, to about -550 mV, in the entire HydABC enzyme as compared to the titration data on the HydB protein (red dashed Nernst curve). This effect is most straightforwardly attributed to electrostatic interaction with the reduced center C1 on HydC, in close vicinity to center B1 in the HydABC complex while absent in the isolated HydB subunit. In the isolated HydB subunit, center B1 is predicted to be surface-exposed from the cryoEM structure of the HydABC enzyme in the case where HydC is absent.

[4Fe-4S]-centers (observed at 15K and 8K) only began to titrate below about -300 mV and the highest potential [2Fe-2S]-thioredoxin-like center therefore represents the highest potential iron sulfur cluster of the entire enzyme. In line with these EPR results, the highest potential redox species observed in UV/Vis spectroscopy showed the typical spectral features of a thioredoxin-like [2Fe-2S]-center and its potential was determined to -270 mV, similar to the EPR data. At low redox potentials a thioredoxin-like spectrum could be resolved in UV/Vis, too. Its amplitude is three times bigger than the amplitude of the signal attributed to A5. This is in line with the observation made in EPR, where the high potential wave was systematically of smaller amplitude that the two other redox changes attributed to the reduction of C1 and B1 (Figure 2). We attribute this to a substoichiometric presence of the mobile thioredoxin domain in HydA in the heterologously expressed complex due to partial proteolytic digest.

The plant-type [2Fe-2S]-center (center A1) distorts the EPR spectral form of the thioredoxin-like clusters as measured at 50K in the redox region between – 350 mV and -500 mV. It notably features a g_z-peak (at g = 2.018) which is positioned outside the magnetic field range of the thioredoxin-like clusters.

Its ambient potential dependence can therefore be conveniently monitored by following the intensity of this line. The obtained Nernst-curve with an E_m of -415 mV is represented in Figure 3 (1st row, 3rd column). As mentioned, the HydA protein harboring the plant-type ferredoxin cluster A1 within its Y-junction module could not be redox-titrated due to sample limitations and we therefore cannot assess whether the E_m-value of this center may be influenced by the assembly of the individual subunits into the entire enzyme, such as for example center B1 is (see above). The surface-exposed localization of center A1 in the Y-junction module (discussed in Zuchan *et al.* (2021)) renders respective redox shift upon complex formation conceivable.

The bulk of the [4Fe-4S]-centers, whereof there is a total of six in the entire HydABC enzyme proved more challenging to deconvolute, both in EPR and in UV/Vis spectroscopy. The spectral features attributed to the C-terminal ferredoxin domain of HydB, including the bell-shaped titration curve of the g_z-peak at 2.06 of the higher potential center were observed at the same potentials in the HydABC complex as in HydB and represent the highest potential pair of [4Fe-4S]-clusters. The dependence of the g_z-peak on ambient potential is depicted in Figure 3 (7th row, 3rd column, open symbols) and corresponds well to that observed in the HydB protein. By contrast, a similar phenomenon, i.e., an appearing and then disappearing g_z-peak (at g = 2.045) is observed at much lower potentials (below -420 mV) in the HydABC titrations while being absent in HydB. The paramagnetic centers responsible for this effect therefore need to reside in the HydA protein and, more specifically, its Y-junction module (which carries all the matured iron sulfur clusters). As discussed in Zuchan *et al*. (2021), the Y-junction module is made up from three distinct domains, that is, a plant-type [2Fe-2S]-ferredoxin, a single [4Fe-4S]-cluster domain and a bacteria-type 2x[4Fe-4S]-ferredoxin. This latter domain is structurally related to the C-terminal ferredoxin domain of HydB and it therefore seems very likely to us that the observed bell-shaped titration behavior of the g_z=2.045 peak at potentials between -400 mV and -500 mV arises from paramagnetic interactions of the two [4Fe-4S]-clusters in the bacterial ferredoxin domain of the Y-junction module. We therefore tentatively ascribe the redox potentials deduced from the titration curve shown in Figure 3 (2nd row, 3rd column) to clusters A2 and A3. We were not able to reliable deconvolute cluster B2 (identified in the HydB-titration beneath the multitude of [4Fe-4S]- and [2Fe-2S]-clusters titrating in the respective redox region and contributing to spectra recorded at 15K and at 8K). However, while this cluster B2 could be well-characterized in the HydB subunit, cluster A4 of the Y-junction module, that is, the cluster in the mono-cubane domain and standing out from all other cubane clusters of the enzyme by featuring a histidine ligand to the cluster (see Zuchan *et al.* (2021)), could not be

isolated from beneath the bulk of centers titrating below -400 mV. A4 therefore remains the sole iron sulfur center of the HydABC enzyme for which only an upper limit can be proposed for E_m.

No radical signal attributable to semi-reduced forms of the FMN moiety was detected in HydABC in EPR, even under the specific conditions used to monitor the neutral semi-reduced flavin in HydB (as described above). This would indicate that the flavin features crossed-over potentials for the individual redox transitions and therefore behaves as an n = 2 component in equilibrium redox titrations. Surprisingly, however, the dependence of the flavin absorption band at 450 nm as observed in UV/Vis-spectroscopy followed an n = 1 Nernst curve at almost all pH-values between pH 5.2 and 9.2 and only at pH 8, an n = 2-behavior was seen (data not shown). While below pH 6, small spectral contributions of a putative neutral semi-reduced flavin species were observed, no such features could be detected at and above pH 7. The data with respect to a semi-reduced flavin radical in HydABC therefore are inconsistent between the EPR- and the UV/Vis-monitored redox titrations and also within the optical experiments themselves. At the time being, we therefore refrain from drawing conclusions as to whether the flavin features crossed-over or uncrossed potentials for the individual redox waves in the entire HydABC enzyme.

Discussion

In this work, we have determined a first, almost comprehensive, data set for the thermodynamic characteristics of redox cofactors in the confurcating [FeFe]-hydrogenase from *Thermotoga maritima*. In this enzyme a H_2/H^+ converting catalytic center on one side of the protein complex is connected to an $NADH/NAD^+$ and Fd^{red}/Fd^{ox} converting unit on the other side via a chain of iron sulfur clusters (i.e., centers A1, A2, A3 and B2) all featuring redox midpoint potentials around and below -400 mV. Since the enzyme, in its natural cellular host, must be expected to operate at dissolved H_2-concentrations well below those corresponding to 1 atm H_2 in the gas phase, the effective redox midpoint potential of the H_2/H^+ couple will be substantially more oxidizing than -400 mV. The thermodynamic bias of the electron transfer chain between the flavin module and the hydrogenase center therefore is slightly skewed towards delivering electrons to the reduction of protons to H_2. While we cannot attribute a precise Em-value to center A4, that is, the histidine-ligand-containing cubane custer of the Y-junction module, is redox midpoint potential must be comprised within those of the bulk of clusters titrating below -400 mV, since otherwise the center would have been detectable at 8K and 15K in the higher potential range during our redox titrations. Incidentally, the cryoEM structure shows that this cluster is not part of the direct path of electron transfer from the flavin module to the hydrogenase center but resides at the interface of the dimeric enzyme. Even so the distance of 8.8Å as measured in the structure (Furlan et al.(2022)) is in line with inter-monomer electron transfer mediated by this clusters, deletion of this cluster by site-directed mutagenesis in HydABC of *Thermoanaerobacter kivui* does not influence bifurcating activity (Katsyv *et al.* (2022)) as measured *in vitro*.

The redox centers surrounding the flavin moiety show more electrochemical heterogeneity than those in the above mentioned electron wire. Three of the centers (C1, B3 and B4) were found to titrate higher than -400 mV while centers B1 and B2 are substantially more reducing. Notably, the redox transition of center B1 was observed to occur at more than a hundred millivolts more negative ambient potentials in the entire enzyme complex than in the isolated HydB subunit. In the structure of the HydABC complex, the surface-exposed B1 cluster of HydB in fact directly faces the HydC subunit while it is solvent-exposed in the isolated HydC protein. Intriguingly, in the cryoEM structure of *Acetobacterium woodii* (Katsyv *et al.* (2022)), the Trx-like [2Fe-2S]-cluster domain of the HydC subunit (or its equivalent in homologous enzymes) was seen mobile and not always occupying its binding pocket at the HydB subunit. Our data together with these structural findings suggest the possibility of conformation-dependent substantial alterations of cluster B1's redox parameters, a property potentially important for the mode of functioning of the flavin module.

We were able to characterize the FMN's redox properties in the isolated HydB subunit. In this sample, the flavin was consistently (that is, via all experimental approaches) found to feature strongly uncrossed potentials for its two individual redox transitions. The transition from the oxidized to the semi-reduced form was determined to occur between -160 and -220 mV (depending on pH, see below), which makes it by far the least reducing redox center of the entire enzyme. Both optical and EPR properties provide evidence that the semi-reduced form is in the neutral, i.e., protonated, state. The second transition from this neutral semi-reduced state to the two-electron, fully-reduced FMN was observed at around -550 to -600 mV, that is, roughly on par with the B1-cluster when measured in the entire enzyme. Therefore both the overall redox midpoint potential of the two electron transition of the flavin and the stability constant of the semi-reduced species are drastically shifted with respect to FMN in aqueous solution (Mayhew (1999)).

While this second transition therefore fits into the ensemble of redox potentials determined for the iron sulfur clusters, the very high E_m of the first transition is puzzling from a functional perspective. Since no potential oxidant for this form is obvious from our data, a continued turnover of the flavin site is difficult to envisage. We have in the past (for other reasons) discussed the possibility that the flavin moiety in this enzyme (and related ones) may shuttle between two (or more) different types of redox behavior (Zuchan *et al*. (2021)), which might resolve some of the outlined functional problems. The pH-dependences of the FMN's individual redox potentials on pH observed in the isolated HydB subunit strongly resemble those reported for flavodoxins (Ludwig *et al*. (1990), (1997), where also a neutral semiquinone form is observed, albeit without a observable pK_a in the examined pH-range. Since UV/Vis and EPR spectral parameters off this neutral semiquinone are indicative for protonation of the N_5-nitrogen atom of the isoalloxazine moiety (Müller *et al*. (1970)), our observed pH-dependence is most straightforwardly rationalized as shown in Figure 4. Similar to flavodoxins, the recorded pH-dependence would then result from an upshift (as compared to flavin in aqueous solution) of the $pK_{a,ox}$ value of the N_5-proton by about 6-7 units to roughly pH 7. While in the structures of flavodoxins, there is clear evidence for a stabilizing effect on N_5-protonation by the protein environment of the flavin (Watt *et al.* 1991, Ludwig, *et al.* 1997), unfortunately there is no 3D structure of the isolated HydB subunit available. In the structure of the entire HydABC enzyme, no obvious candidate for such a stabilization of the N_5-proton is seen, which would predict a redox behavior of the flavin more closely resembling that of the moiety in aqueous solution, that is, compatible with our results obtained by EPR but not by UV/Vis spectroscopy on the HydABC-enzyme.

Both, in Hyd B and in Hyd ABC the EPR signal of the one-electron reduced flavin was visible over the entire temperature range from 8K to 180K without any change in spectral shape. Saturation experiments showed that the signal was saturated over a broad range of conditions and out of saturation at 50K below a microwave power of 0.01mW (Figure S4) or above 180K at a microwave power below 6.54mW (see SI). We carried out most of the experiments on the flavin signal at 50K 6.54mW and the observed increase in signal amplitude in HydB at low redox potentials may therefore well stem from a change in saturation behavior of the semi-reduced flavin upon reduction of a neighboring iron-sulfur cluster. Spectral changes of the iron-sulfur clusters observed at low redox potentials occurring in a potential range where the flavin becomes fully reduced may result from the disappearance of a spin/spin interaction between the semi-reduced flavin and one or several of the reduced iron-sulfur centers.

Structural data on the isolated HydB subunit as well as experimental resolution of the described redox inconsistencies in the HydABC complex will be required to progress on the question of a potential switch in redox behavior of the flavin in th HydABC hydrogenase from *Thermotoga maritima*.

Acknowledgements

This project has been made possible by the MOSBRI European Union's Horizon 2020 research and innovation programme grant (ID MOSBRI: 2021-52 & 2023-156). The first author would like to acknowledge the Studienstiftung des deutschen Volkes (Germany) for its funding.

References

Aasa R, Bergström J, Vänngard T (1981) On the interaction and orientation of the iron sulfur centers A and B in chloroplasts of higher plants, Biochimica et Biophysica Acta (BBA) - Bioenergetics, 637 (1981), 118–123.

Bentrop D, Bertini I, Luchinat C, Nitschke W, Mühlenhoff U (1997) Characterization of the unbound 2[Fe4S4]-ferredoxin-like photosystem I subunit PsaC from the Cyanobacterium *Synechococcus elongatus*. Biochemistry. 36, 13629-13633.

Bergdoll L, ten Brink F, Nitschke W, Picot D, Baymann F (2016) From low- to highpotential bioenergetic chains: Thermodynamic constraints of Q-cycle function. Biochim Biophy Acta 1857, 1569–1579.

Birrell JA, Laurich C, Reijerse EJ, Ogata H, Lubitz W (2016) Importance of Hydrogen Bonding in Fine Tuning the [2Fe-2S] Cluster Redox Potential of HydC from Thermotoga maritima. Biochemistry 55, 4344–4355.

Buckel W, Thauer RK (2013) Energy conservation via electron bifurcating ferredoxin reduction and proton/Na+ translocating ferredoxin oxidation. Biochim Biophys Acta 1827, 94–113.

Buckel W, Thauer RK (2018) Flavin-Based Electron Bifurcation, A New Mechanism of Biological Energy Coupling. Chem Rev 118, 3862–3886.

Cammack R, MacMillan F (2010) Electron Magnetic Resonance of Iron–Sulfur Proteins in Electron-Transfer Chains: Resolving Complexity. In Metals in Biology, G. Hanson and L. Berliner, eds., Vol. 29, Springer New York, New York, NY,pp. 11–44.

Chongdar N, Pawlak K, Rüdiger O, Reijerse EJ, Rodriguez-Macia P, Lubitz W Birrell JA, Ogata H (2020) Spectroscopic and biochemical insight into an electron-bifurcating [FeFe] hydrogenase. J Biol Inorg Chem 25, 135–149.

Crofts AR, Hong S, Wilson C, Burton R, Victoria D, Harrison C, Schulten K (2013) The mechanism of ubihydroquinone oxidation at the Qo-site of the cytochrome bc1 complex. Biochim Biophys Acta 1827, 1362–1377.

de Vries S, Dörner K, Strampraad MJ, Friedrich T (2015) Electron tunneling rates in respiratory complex I are tuned for efficient energy conversion. Angew Chem Int Ed Engl. 54, 2844-2848.

Dörner K, Vranas M, Schimpf J, Straub IR, Hoeser J, Friedrich T (2017) Significance of [2Fe-2S] Cluster N1a for Electron Transfer and Assembly of Escherichia coli Respiratory Complex I. Biochemistry 56, 2770-2778.

Efremov RG, Sazanov LA. (2012) The coupling mechanism of respiratory complex I - a structural and evolutionary perspective. Biochim Biophys Acta. 1817,1785-95.

Feng X, Schut GJ, Haja DK, Adams MW, Li H (2022) Structure and electron transfer pathways of an electron-bifurcating NiFe-hydrogenase. Science Advances 8, eabm7546

Furlan C, Chongdar N, Gupta P, Lubitz W, Ogata H, Blaza JN, Birrell JA (2022) Structural insight on the mechanism of an electron-bifurcating [FeFe] hydrogenase, eLife 11, e79361.

Grzybek, S., Baymann, F., Müller, K.-H., Mäntele, W. (1993) MEH-Fit: A computer Program for the analysis of redox titrtaions. (Theophanides, T., Anastassoupoulou, J, Fotopoulos, N., Eds.) pp25-26, Kluwer Academic Publishers, Dordrecht, The Netherlands.

Herrmann G, Jayamani E, Mai G, Buckel W (2008) Energy Conservation via Electron-Transferring Flavoprotein in Anaerobic Bacteria. J Bacteriol 190,784–791.

Hinkson JW (1968) Azotobacter free-radical flavoprotein. Preparation and properties of the apoprotein. Biochemistry 7,2666-2672.

Katsyv A, Kumar A, Saura P, Pöverlein MC, Freibert SA, Stripp ST, Jain S, Gamiz-Hernandez AP, Kaila VRI, Müller V, Schuller JM (2023) Molecular Basis of the Electron Bifurcation Mechanism in the [FeFe]-Hydrogenase Complex HydABC. J Am Chem Soc 145, 5696–5709.

Kumar A, Kremp F, Roth J, Freibert SA, Müller V, Schuller JM (2023) Molecular architecture and electron transfer pathway of the Stn family transhydrogenase. Nat Commun 14, 5484.

Li F, Hinderberger J, Seedorf H, Zhang J, Buckel W, Thauer RK (2008) Coupled Ferredoxin and Crotonyl Coenzyme A (CoA) Reduction with NADH Catalyzed by the Butyryl-CoA Dehydrogenase/Etf Complex from Clostridium kluyveri. J Bacteriol 190, 843–850.

Losey, NA, Poudel, S, Boyd ES, McInerney MJ (2020) The Beta Subunit of Non-bifurcating NADH-Dependent [FeFe]-Hydrogenases Differs From Those of Multimeric Electron-Bifurcating [FeFe]-Hydrogenases. Front Microbiol 11, 1109.

Lubner CE, Jennings DP, Mulder DW, Schut GJ, Zadvornyy OA, Hoben JP, Tokmina-Lukaszewska M, Berry L, Nguyen DM, Libscomb GL, Bothner B, Jones AK, Miller A-F, King PW, Adams MWW, Peters JW (2017) Mechanistic insights into energy conservation by flavin-based electron bifurcation. Nat Chem Biol 13, 655–659.

Ludwig ML, Pattridge KA, Metzger AL, Dixon MM, Eren M, Feng Y, Swenson RP (1997) Control of Oxidation

Reduction Potentials in Flavodoxin from *Clostridium beijerinckii*: The Role of Conformation Changes. Biochemistry 36, 1259–1280.

Meyer J, Andrade SL, Einsle O (2011) Thioredoxin-Like [2Fe-2S] Ferredoxin. in Encyclopedia of Inorganic and Bioinorganic Chemistry. R. A. Scott, ed. Wiley, 2 ed.

Mitchell P (1975a) The protonmotive Q cycle: A general formulation. FEBS Letters 59, 137–139.

Mitchell P (1975b) Protonmotive redox mechanism of the cytochrome b-c 1 complex in the respiratory chain: Protonmotive ubiquinone cycle. FEBS Letters 56, 1–6.

Mulder D. W., Boyd E. S., Sarma R., Lange R. K., Endrizzi J. A., Broderick J. B., Peters J. W. (2010). Stepwise [FeFe]-hydrogenase H-cluster assembly revealed in the structure of HydAΔEFG. Nature, 465(7295), 248-251.

Müller F, Hemmerich P, Ehrenberg A, Palmer G, Massey V (1970) The Chemical and Electronic

Structure of the Neutral Flavin Radical as Revealed by Electron Spin Resonance Spectroscopy of Chemically and Isotopically Substituted Derivatives. Eur J Biochem 14 , 185–196.

Murataliev MB (1999) Application of Electron Spin Resonance (ESR) for Detection and Characterization of Flavoprotein Semiquinones, in Flavoprotein Protocols, vol. 131, Humana Press, New Jersey, pp. 97–110.

Nitschke W, Russel MJ (2012) Redox bifurcations: Mechanisms and importance to life now, and at its origin: A widespread means of energy conversion in biology unfolds. BioEssays 34, 106–109.

Schopfer L, Ludwig M, Massey V (1990) A working proposal for the role of the apoprotein in determining the redox potential of the flavin in flavoproteins: correlations between potentials and flavin pks, Flavins and Flavoproteins, (1990), pp. 399–404.

Schütz M, Brugna M, Lebrun E, Baymann F, Huber R, Stetter K-O, Hauska, G, Toci R, Lemesle-Meunier D, Tron P, Schmidt C, Nitschke W (2000) Early Evolution of Cytochrome *bc* Complexes. J Mol Biol 300, 663–675.

Schut GJ, Adams MWW (2009) The Iron-Hydrogenase of Thermotoga maritima Utilizes Ferredoxin and NADH Synergistically: a New Perspective on Anaerobic Hydrogen Production. J Bacteriol, 191, 4451–4457.

Radon C, Mittelstädt G, Duffus B R, Bürger J, Hartmann T, Mielke T, Teutloff C, Leimkühler S, Wendler P (2020) Cryo-EM structures reveal intricate Fe-S cluster arrangement and charging in Rhodobacter capsulatus formate dehydrogenase. Nature communications, 11(1), 1912.

Vassiliev IR, Antonkine ML, Golbeck JH (2001) Iron-sulfur clusters in type I reaction centers. Biochim Biophys

Acta. 1507, 139-160.

Verkhovskaya M. L., Belevich N., Euro L., Wikström M., & Verkhovsky M. I. (2008) Real-time electron transfer in respiratory complex I. Proceedings of the National Academy of Sciences, 105(10), 3763-3767.

Wagner T, Koch J, Ermler U, Shima S (2017) Methanogenic heterodisulfide reductase (HdrABC-MvhAGD) uses two noncubane [4Fe-4S] clusters for reduction. Science 357, 699–703.

Watt W, Tulinsky A, Swenson RP, Watenpaugh KD (1991) Comparison of the crystal structures of a Flavodoxin in its three oxidation states at cryogenic temperatures. J Mol Biol 218, 195–208.

Wikström MK, Berden JA (1972) Oxidoreduction of cytochrome *b* in the presence of antimycin. Biochim Biophys Acta 283, 403–420.

Yalloway GN, Mayhew SG, Malthouse JPG, Gallagher ME, Curley GP (1999) pH-Dependent Spectroscopic Changes Associated with the Hydroquinone of FMN in Flavodoxins. Biochemistry 38, 3753–3762.

Zheng Q., Huang X., Liu Y., Fang X., Zhang J., & Shao H. (2017) Electrochemical quantification of intermolecular hydrogen bonding between ferrocenemethanol and 3-mercaptopropanoic acid on gold. The Journal of Physical Chemistry C, 121(40), 22123-22129.

Zuchan K, Baymann F, Baffert C, Brugna M, Nitschke W (2021) The dyad of the Y-junction and a flavin module unites diverse redox enzymes. Biochim Biophys Acta 1862, 148401.

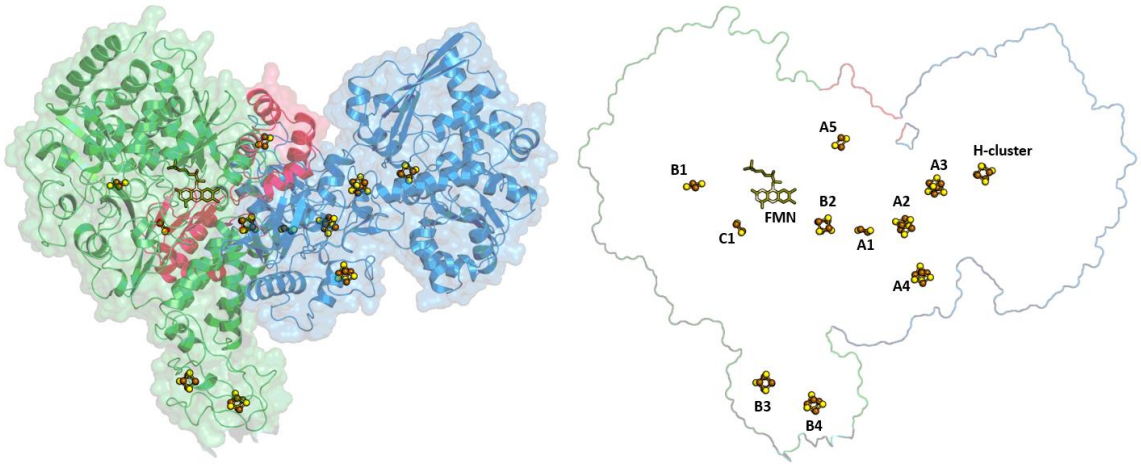

Figure 1: Schematic representation of the redox Cofactors in the Cryo-EM structure model of the [FeFe]-Hydrogenase apo-HydABC complex of *T.maritima* without maturated H-cluster. Nomenclature of redox cofactors according to Furlan *et al.* (2022). FMN cofactor was tilted by 90°C in respect to its position in the enzyme to allow for a better vizualization of all cofactors.

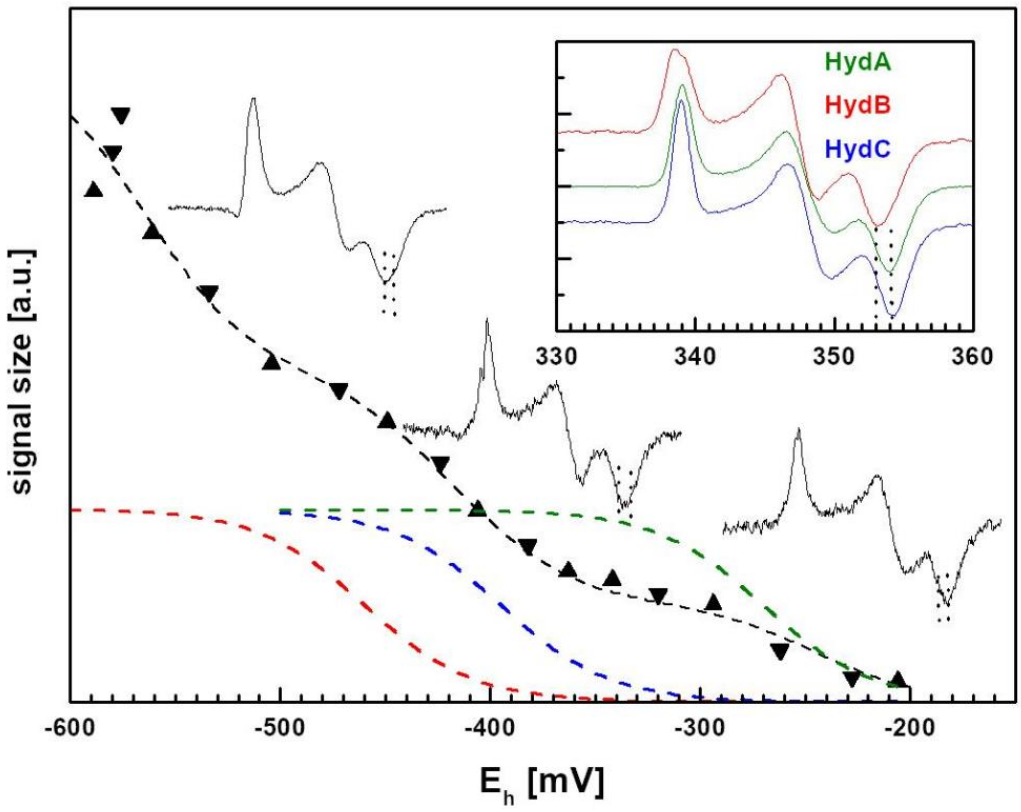

Figure 2 120K EPR redox titration of the three thioredoxin-like [2Fe-2S]-clusters in apo-HydABC. The dependence of the g_x-signal amplitude of the thioredoxin-like [2Fe-2S]-clusters in apo-HydABC on the ambient potential in shown as black dashed curve. Evaluation was done at g = 1.916, where all three [2Fe-2S]-clusters have the same amplitude. Upwards and downwards triangles denote values obtained during reductive and oxidative titration, respectively. A three component Nernst curve yield -270 mV, -420 mV and -550 mV for HydA, HydC and HydB, respectively. Colored dotted lines indicate the redox behavior of the thioredoxin-like [2Fe-2S]-cluster when titrated in the isolated subunits. Spectra obtained from an evaluation of the titration on the apo-HydABC are shown next to the curve. The inset shows the spectra as obtained on the isolated subunits. Recorded EPR spectra at 9.48 GHz, 5 G modulation amplitude, 100 kHz modulation frequency, 82 ms time constant and a receiver gain of 50dB. At each power at least two accumulations were scanned.

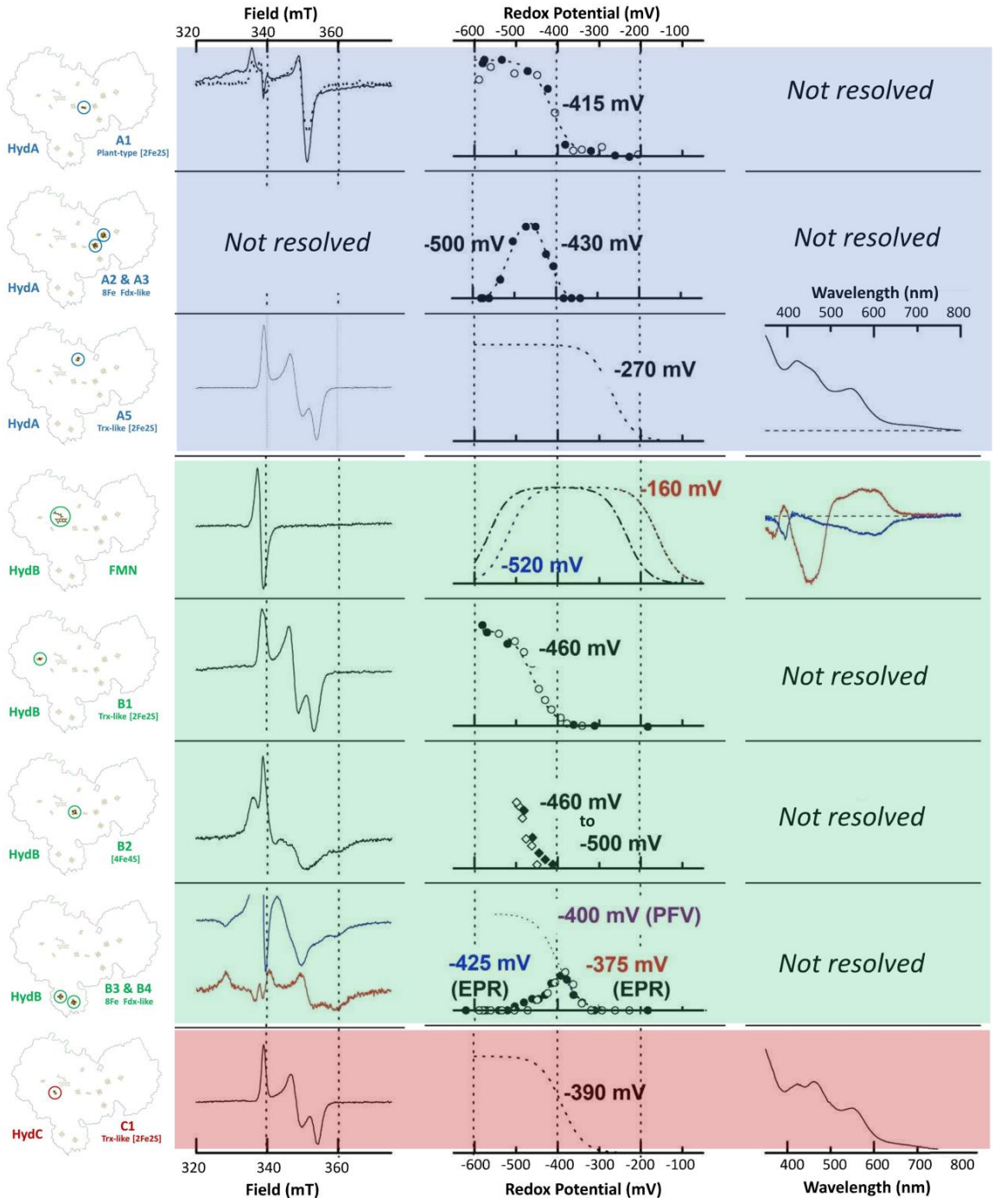

Figure 3: We have condensed in this figure the results on redox cofactors for which we were able to determine UV/Vis and/or EPR spectral species as well as their redox titration behavior (determined either by EPR-, by UV/Vis-spectroscopy or adopted from previous publications as detailed below). The

first column recalls the nomenclature of redox centers as introduced by Furlan *et al.* (2022) and shows their positioning within a sketched outline of the enzyme complex. The second and forth columns depict EPR- and UV/Vis spectra of the individual redox species while the third column present their redox behavior. Spectra and redox titration curves for the individual cofactors were obtained as follows:

A1: the EPR spectrum of the plant-type [2Fe-2S]-cluster was obtained by calculating redox difference spectra at 50K, calculating saturation-difference spectra at 50K and varying microwave powers as well as serendipitously by reoxidizing reduced samples (the plant-type center proved to reoxidize much more slugglishly than the thioredoxin-like clusters). The depicted spectrum corresponds to a redox difference spectrum of a titration at pH 9 and recorded at 50K. The titration curve was measured on the g_z=2.018 peak of this center at 50K (6.32 mW). We were unable to deconvolute the UV/Vis spectrum of cluster A1 from those of the other redox centers.

A2/A3: These two centers present in a bacterial ferredoxin-like fold were identified by the bell-shaped behavior of their g_z=2.045 peak at 15K. We could not resolve complete spectra (neither in EPR nor in UV/Vis-spectroscopy) of these centers.

A5: The EPR spectrum of this center was obtained by reducing the separately expressed HydA subunit with low (stoichiometric) amounts of dithionite or directly on the separately expressed C-terminal domain of HydA. Results of both procedures were identical, and the depicted spectrum corresponds to that of the separate thioredoxin-like domain reduced by dithionite and recorded at 50K. In UV/Vis the spectrum could be calculated by a redox cut between spectra recorded at -180mV and -300mV during a redox titration, after subtraction of contributions of benzyl-viologen, visible at 600 nm, if necessary. The Nernst curve depicted for A5 corresponds to a n = 1 Nernst simulation using E_m= -270 mV as determined by PFV.

FMN: The depicted EPR spectrum of the stabilized NSR state of the FMN is from a HydB sample recorded at 50 K (6.32 mW) at the ambient potential of -303 mV at pH 8.5. The UV/Vis spectra are redox difference spectra calculated during electrochemical titrations at pH 8.34. The blue spectrum corresponds to the redox difference between the fully oxidized and semi-reduced FMN (-268 mV minus -188 mV), the red spectrum shows the redox difference spectrum of the second transition from the semi-

reduced to the fully reduced flavin (-649 mV minus -528 mV). At pH 6.5 spectra and redox midpoint potentials were fitted by a global fit analysis (Grzybek *et al.* (1991)).

The titration curves have been measured on 604 nm of the flavin at pH 6.53 (dotted line) and 8.34 (dash-dotted line). At pH 6.5 spectra and redox midpoint potentials were fitted by a global fit analysis (Grzybek *et al.* (1991)). For clarity, a simulated plot representing both transitions of the FMN in HydB at pH 6.53 is shown to visualize the strongly stabilized NSR, while the original titration curves contain superimposed FeS-cluster signals.

B1: The EPR spectrum of B1 corresponds to an absolute spectrum run on the HydB subunit at 50K (6.32 mW) at -540 mV (pH 9). Its redox behavior was measured on the g_y derivative line (peak minus trough). UV/Vis titrations did not detect iron sulfur centers in this redox region.

B2: The shown EPR spectrum represents a 15K redox difference spectrum (-481 minus -445 mV) during redox titration at pH 9. At these potentials the contributions of clusters B3 and B4 do not vary anymore and only the contribution of the thioredoxin-like cluster B1 had to be subtracted. No iron sulfur clusters were seen to titrate in this redox region during the electrochemical redox titrations monitored by UV/Vis spectroscopy. The titration data represent the dependence of the g_z= 2.02 peak of this center on ambient potential. Due to the overlapping mediator radical signals the determined redox range is rather approximative.

B3/B4: These two clusters present in the C-terminal bacterial-ferredoxin-like domain of HydB were observed as the first two centers visible at 15K to become reduced in redox titrations of HydB and HydABC. The depicted spectra correspond to redox differences of -340 mV minus -270 mV (lower spectrum, first redox species) and -435 mV minus -367 mV (upper spectrum, second redox species) during HydB redox titration at pH 7. The redox titration data represent the dependence of the g_z= 2.06 peak. We furthermore depict the apparent n = 1 Nernst curve as suggested by the results of PFV (with an E_m at -400 mV) on the isolated C-terminal domain of HydB. No iron sulfur clusters were seen to titrate in this redox region in the electrochemical redox titrations monitored by UV/Vis spectroscopy.

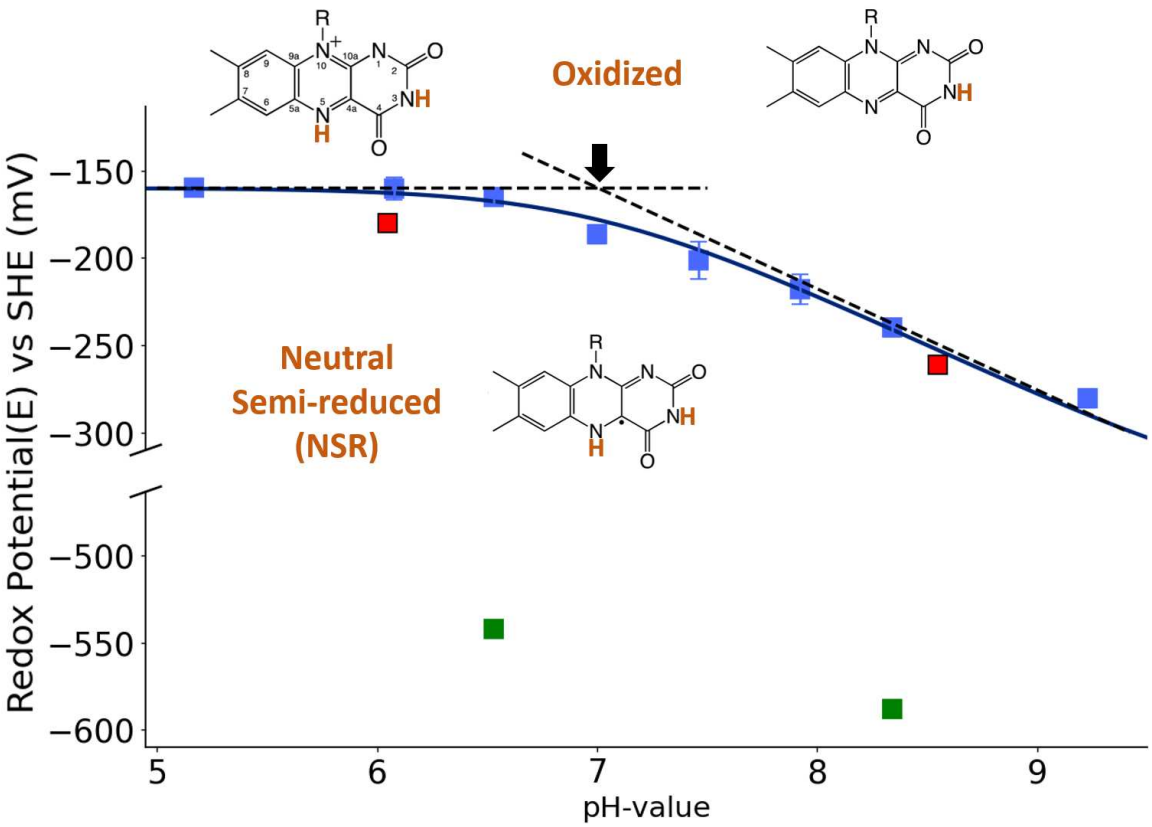

Figure 4: Dependence of FMN $E_{OX\text{-}NSR}$ und $E_{NSR\text{-}RED}$ redox potential in HydB on pH-value.
One-electron redox potentials obtained via Spectro-Electrochmical redox titrations of the Oxidized to Neutral Semi-reduced (NSR) transition ($E_{OX\text{-}NSR}$, blue squares) and to fully-reduced (RED) transition ($E_{NSR\text{-}RED}$, green squares) of the FMN in HydB over a pH range of 5.17 to 9.23. Between pH 5.17 and 6.53, $E_{OX\text{-}NSR}$ is pH-independent and approximates to -160 mV vs SHE. Between pH 7.46 to 9.23, $E_{OX\text{-}NSR}$ decreases linearly with a slope of -60 mV/pH. From these two ranges of pH-dependencies, an apparent pK_a-value of 7 (black arrow) is deduced. The meaning of this pK_a-value is discussed in the main text. Error bars represent standard deviation of the least-square Nernst-fit of multiple (consecutive, not independent) titration datasets (oxidation and reduction were fitted separately) according to Supplementary Table 1. One-electron redox potentials of $E_{OX\text{-}NSR}$ was confirmed via EPR spectroscopy at two pH-values (red squares). The low-potential $E_{NSR\text{-}RED}$ transition (green squares) was only observed once at two pH-values, pH 8.34 and pH 6.53.

Table 1: Nomenclature, type, EPR g-value annotation and redox properties of the FeS-clusters in HydABC of *T.maritima*

Subunit	Cluster	Nature	g_1 / g_z	g_2 / g_y	g_3 / g_x	E_m (mV, pH7)
A	A1	Plant-type [2Fe-2S]	2.018	1.937	1.937	-415 [ABC]
	HP (A2/A3)	8Fe -Fd [4Fe-4S]	~2.045	?	?	-430 [ABC]
	LP (A2/A3)	8Fe -Fd [4Fe-4S]	-	-	-	-505 [ABC]
	A4	His-[4Fe-4S]	-	-	-	-
	A5*	Trx-like [2Fe-2S]	1.998	1.945	1.913	-270 mV [ABC] -270 mV [A(CT)]
B	B1	Trx-like [2Fe-2S]	1.999	1.949	1.917	-460 [B] -550 [ABC]
	B2	[4Fe-4S]	~2.02 ▲	~1.94	1.87	<-460 [B]
	HP (B3/B4)	8Fe -Fd [4Fe-4S]	2.063	1.931	1.886	-375 [B]
	LP (B3/B4)	8Fe -Fd [4Fe-4S]	2.04 > 2.00 ▲	1.96	~1.94	-425 [B]
C	C1	Trx-like [2Fe-2S]	1.998	1.945	1.913	-380 [C] -420 [ABC]

[ABC] redox potential obtained in the entire HydABC complex

[B] redox potential obtained in the isolated HydB subunit only

[C] redox potential obtained in the isolated HydC subunit only (Birrell *et al.* 2016)

▲ g-value close to the radical g = 2 signal during redox titration could not be attributed with certainty

* cluster and domain not conserved in all bifurcating [FeFe]-hydrogenases (Zuchan *et al.* 2021)

Supplementary Information

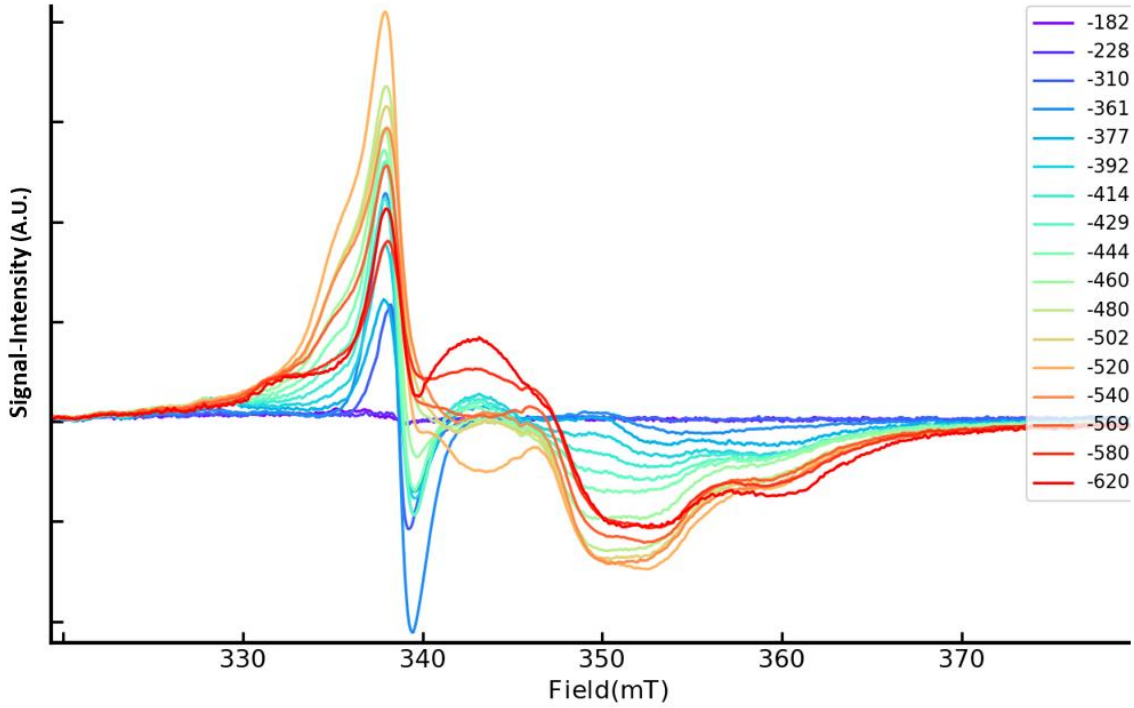

Figure S1: EPR spectra recorded at 15K during a HydB redox titration at pH 9. Recorded EPR spectra at 9.48 GHz, 5 G modulation amplitude, 100 kHz modulation frequency, 82 ms time constant and a receiver gain of 50dB. At each power at least two accumulations were scanned.

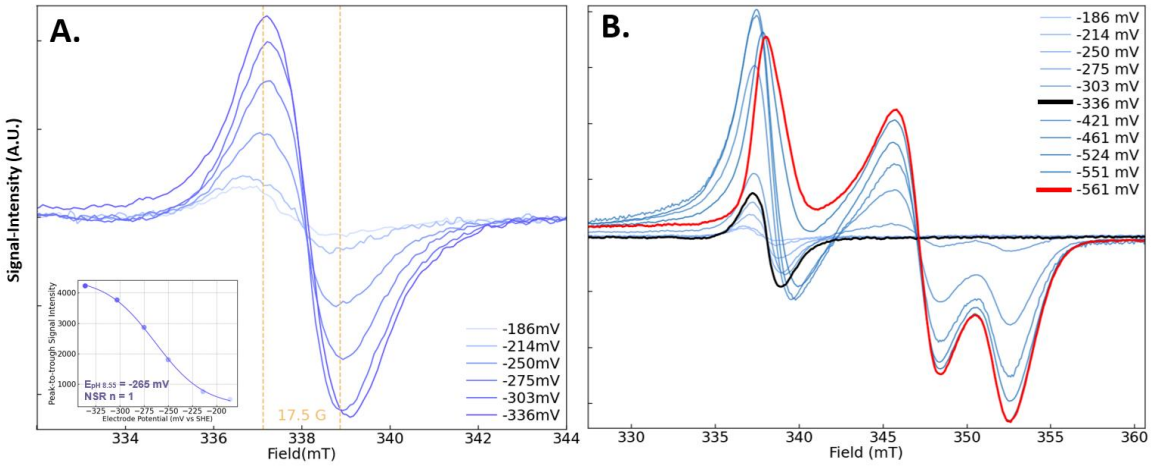

Figure S2: 50K EPR Redox Titration of the FMN neutral semi-reduced species (NSR n = 1) in HydB at pH 8.55. **A.)** Redox Titration of the NSR Radical signal in 60 uM HydB at pH 8.55. Titration was realized at minimal Mediator-concentration and contribution of the B1 Thioredoxin-[2Fe-2S]-cluster was subtracted based on the signal amplitude at the g_x (352.5 mT). Using the peak-2-trough signal intensity (339.2 mT to 336.9 mT) of the Difference Data, a redox potential of -265 mV at this pH-value was determined (see inset). **B.)** After a Nernstian titration behavior of the NSR until -336 mV, a second non-Nernstian increase of the NSR signal intensity was observed. In addition, at strongly reducing ambient potentials the NSR-radical signal fully disappeared as evident by the non-disturbed B1 Trx-like [2Fe-2S]-cluster signal.
All spectra were recorded at 6.32 mW (15 dB Attentuation). Recorded EPR spectra at 9.48 GHz, 5 G modulation amplitude, 100 kHz modulation frequency, 82 ms time constant and a receiver gain of 50dB.

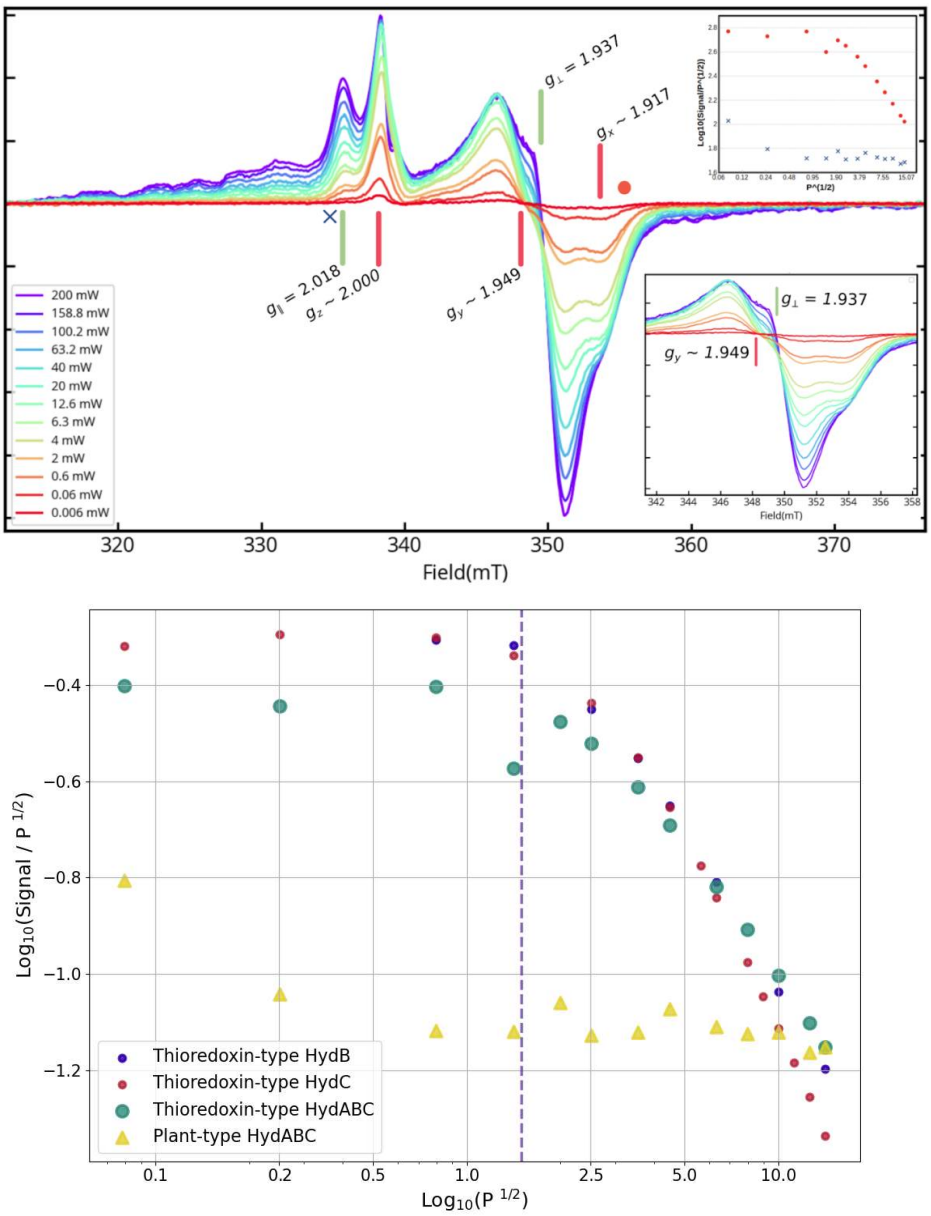

Figure S3a: EPR power saturation series at 40K of a strongly reduced (E_0 = -587 mV vs SHE) 26.6 µM HydABC sample after potentiometric reduction with Dithionite at pH 9. The dataset demonstrates two distinguishable spectra arising from the two types of [2Fe-2S]-clusters; one axial plant-type [2Fe-2S]-cluster ($g_\parallel$ = 2.018, $g_\perp$ = 1.937) and three rhombic thioredoxin-like [2Fe-2S]-cluster (g_z ~ 2.000, g_y ~ 1.949, g_x ~ 1.917). g = 2.000 region is altered due to the presence of radical signals by the titration mediators. **Upper Inlet** quantifies the saturation properties of the plant-type [2Fe-2S]-cluster at g = 2.028 (blue cross) and the rhombic thioredoxin-like [2Fe-2S]-clusters at g = 1.907 (orange dot).

Lower Inlet emphasised on the g_y and $g_\perp$ -value distinction between the two types of FeS-clusters. Recorded EPR spectra at 9.48 GHz, 5 G modulation amplitude, 100 kHz modulation frequency, 82 ms time constant and a receiver gain of 50dB. At each power at least two accumulations were scanned.
Figure S3b: EPR power saturation data at 40K of the thioredoxin-like [2Fe-2S]-centers in the separate subunits of HydB (blue dot) and HydC (red dot) as well as all [2Fe-2S]-clusters in the strongly reduced (E = -587 mV vs SHE) HydABC sample after potentiometric reduction with dithionite at pH 9 as in Figure 2. The data shows that the three thioredoxin-like [2Fe-2S]-clusters in HydABC (teal dot) saturate in a comparable manner, as the same clusters in separate subunits HydB and HydC alone around 4 mW, whereas the plant-type [2Fe-2S]-cluster (yellow triangle) does not saturate at that temperature. Saturation curves based on the *g* = 1.907 signal for the thioredoxin-like [2Fe-2S]-clusters and the *g* = 2.028 signal for the plant-type [2Fe-2S]-cluster. Recorded EPR spectra at 9.48 GHz, 5 G modulation amplitude, 100 kHz modulation frequency, 82 ms time constant and a receiver gain of 50dB. At each power at least two accumulations were scanned.

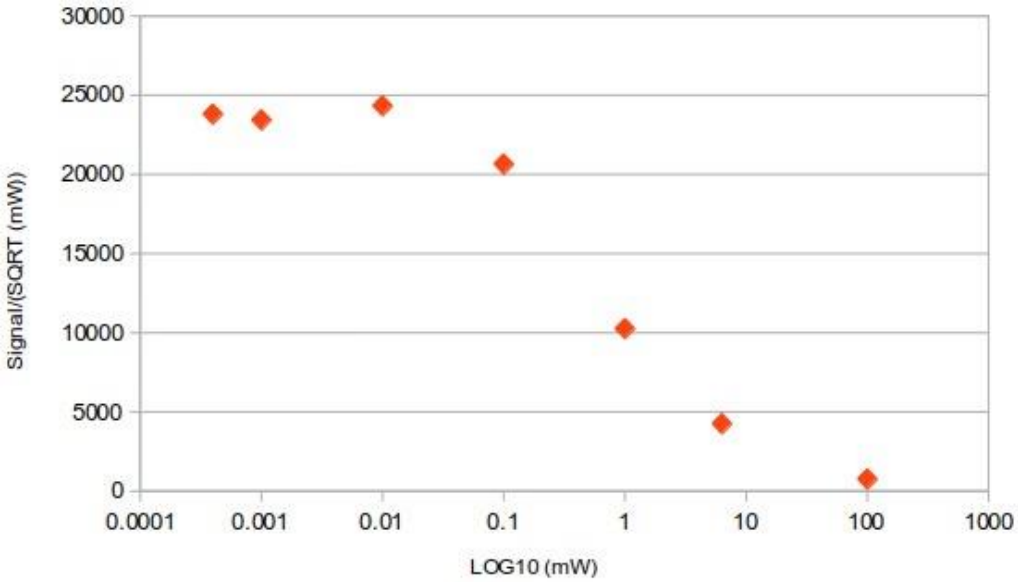

Figure S4: 50 K Saturation Behavior of the FMN NSR in HydB at pH 6 at E = -338 mV.

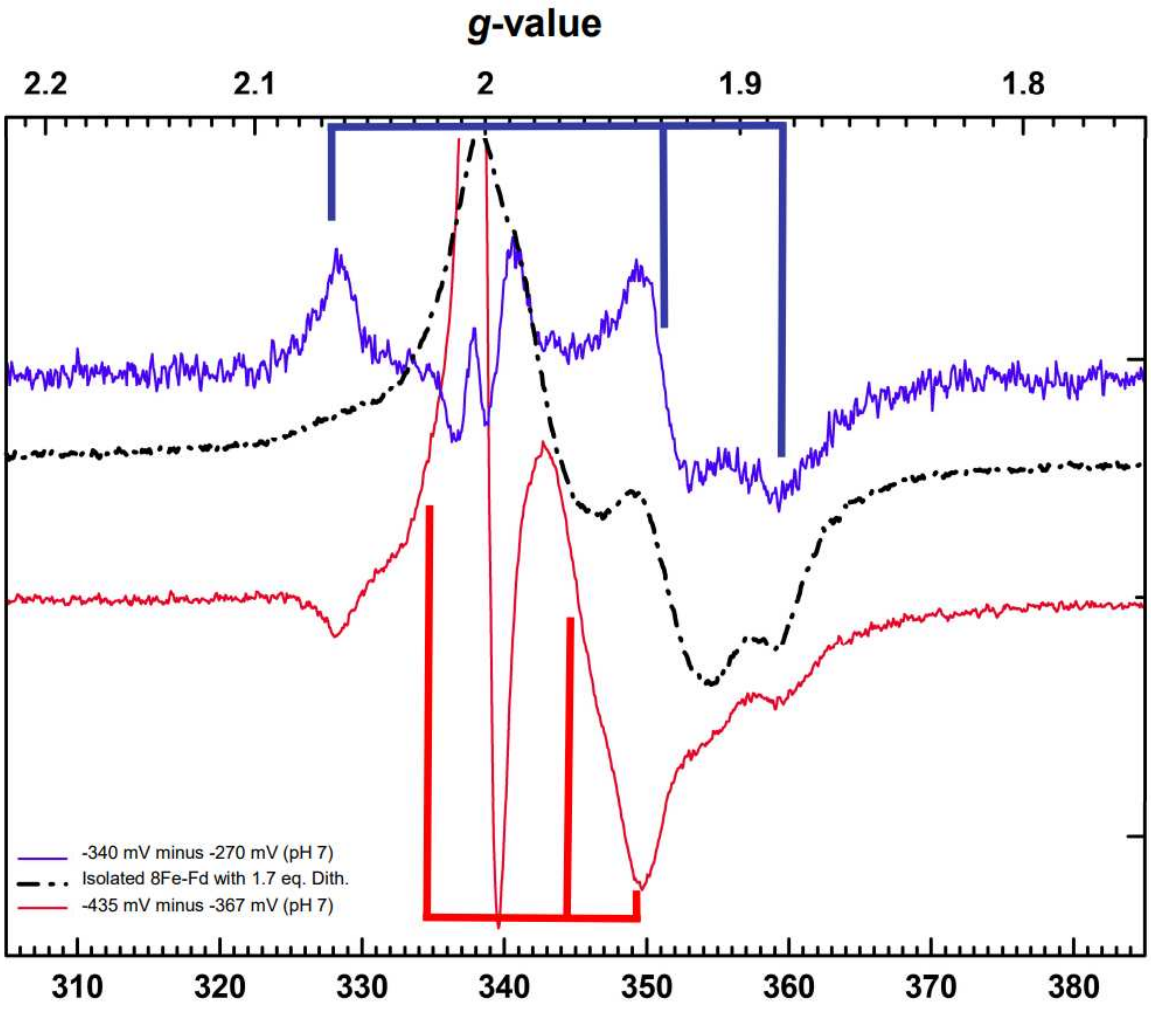

Figure S5: EPR-spectra of the two magnetically interacting [4Fe-4S]-clusters, B3 and B4 in the C-terminal ferredoxin (8Fe-Fd)-like domain in HydB. Redox Difference Spectra of the titration at pH 7 identify a high-potential [4Fe-4S]-cluster which features a clearly rhombic character (in blue, $g_{x,y,z}$ = 1.886, 1.931, 2.063). The second [4Fe-4S]-cluster at more reducing ambient redox potentials demonstrates a more axial character (in red, $g_{x,y,z}$ = ~1.94, ~1.96, ~2.00-2.03). Partial reduction of the separate, heterologously purified 8Fe-Fd domain (in black) confirms the attribution of the high-potential cluster with a broadened g_z. Recorded EPR spectra at 9.48 GHz, 5 G modulation amplitude, 100 kHz modulation frequency, 82 ms time constant and a receiver gain of 50dB. At each power at least two accumulations were scanned.

Table S1: Redox potentials of the FMN_{OX-NSR}, $FMN_{NSR-RED}$ and the Iron-Sulfur (FeS) clusters in HydB at different pH values obtained in electrochemical titrations followed by optical spectroscopy.

Redox potentials obtained during electrochemical redox titrations over a pH range of 5.17 to 9.23. Potential values of the FMN were obtained by Nernst-fit (n = 1) at 604 nm of the difference absorbance data after mediator subtraction. Given deviation arises from the averaged Least-Square-Fit deviation from each fit of the separate (but not independent) oxidation or reduction dataset. Additional error from the experimental setup is not included. Number of separate datasets that were used to obtain these potential values are specified by the number in parenthesis at superscript. The redox titration of a separate $E_{NSR-RED}$ transition (n = 1) at two pH-values, pH 8.34 and pH 6.53 was observed as specified in the main text. Potential values of the FeS were obtained by Nernst-fit (n = 1) at 500 nm, the isosbestic point of the $E_{NSR-RED}$ of the difference absorbance data after mediator subtraction.

	FMN		FeS
pH	E_{OX-NSR} (n=1)	$E_{NSR-RED}$ (n=1)	E_{OX-RED} (n=1)
	mV	*mV*	*mV*
5.17	-160 ± 5 (3)	-	-370 ± 3 (3)
6.08	-160 ± 6 (3)	-	-370 ± 1 (3)
6.53	-165 ± 5 (3)	-542 ± 7 (1)	-365 ± 3 (3)
7.00	-186 ± 6 (2)	-	-379 ± 3 (3)
7.46	-201 ± 11 (3)	-	-371 ± 2 (3)
7.92	-216 ± 6 (3)	-	-376 ± 2 (3)
8.34	-240 ± 5 (3)	-587 ± 4 (1)	-367 ± 6 (3)
8.76	-	-	-378 ± 6 (3)
9.23	-280 ± 5 (3)	-	-382 ± 1 (3)

Chapter 5
Discussion and Perspectives

During this thesis, a phylogenetic and thermodynamic analysis of a [FeFe]-hydrogenase HydABC has been conducted to characterize the thermodynamic landscape of all the redox cofactors and to assess the redox flexibility of the single FMN inside HydABC in pursuit to elucidate the molecular origin of the thermodynamically coupled FBEB/FBEC reaction in this enzyme.

In chapter 3, HydABC has been recognized as a flavoenzyme complex belonging to a NAD(P)H-dehydrogenase family alongside NAD(P)H-dependent formate dehydrogenase and [NiFe]-hydrogenase as well as respiratory complex I. A highly conserved “flavin”-module was identified which harbors a single FMN and two adjacent FeS-clusters in a branching architecture that is proposed as a minimal functional core to catalyze FBEB/FBEC[13]. The "flavin"-module, together with an FeS-cluster containing "Y-junction module" that connects the flavin module to the active sites, is a common feature shared by HydABC and all identified members of this NAD(P)H-dehydrogenase family. In a phylogenetic tree as shown in figure 5.1 based on the flavin-module, these flavoenzymes cluster in a dichotomous manner.

One group is represented by the thermodynamically well-characterized respiratory complex I, which is known to catalyze the two-electron oxidation of NADH to the reduction of quinones in a "ferredoxin-independent" manner. This group also contains some [FeFe]-hydrogenases, but most HydABC flavoenzymes were found in the second group, which is characterized by a dependence on reduced ferredoxin (Fd_{RED}) for the coupled oxidation of NAD(P)H and Fd_{RED} to the reduction of different bioenergetic substrates [a]. For this latter group, which contains additional, conformationally mobile FeS-cluster domains in the flavin-binding HydB subunit, a thermodynamic description was still highly speculative[111] in the absence of experimentally determined redox potentials.

In the work shown in chapter 4, for the first time, the spectral and redox properties of all except one FeS cofactors in HydABC from *T. maritima*, as a representative from the "ferredoxin-dependent" NAD(P)H-dehydrogenase family, were determined. The FMN in the flavin-containing HydB was

[a]The distinction between “ferredoxin-dependent” and “ferredoxin-independent” members correlates with the previously proposed cassification by Losey *et al.* (2020)[128] of “bifurcating” and “non-bifurcating” flavoenzymes. As discussed in chapter 3, the favorable architecture of the ”flavin module” is proposed to allow EB in all representatives of this NAD(P)H dehydrogenase family, with the ability or inability to reduce ferredoxin.

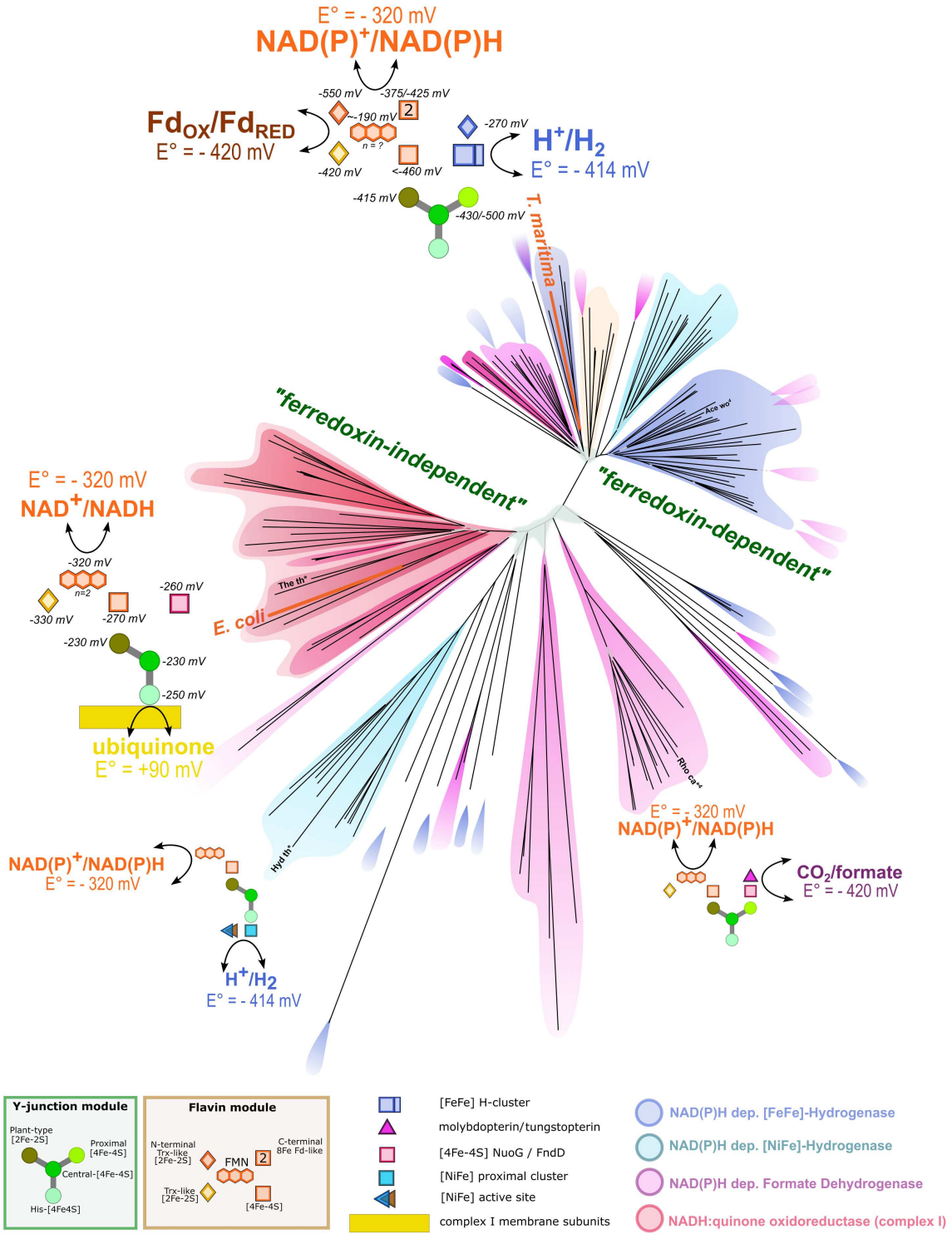

Figure 5.1: Neighborhood-joining tree of the “flavin-module” as elaborated in chapter 3 supplemented with information on the thermodynamic properties of representatives. Similarity clustering of the sequences belonging to the NAD(P)H dehydrogenase family contain [FeFe]-hydrogenase (in blue), complex I (in red), [NiFe]-hydrogenase (in cyan) and formate dehydrogenase (in purple). Structurally characterized species are given at the representative leaves of the tree (abbreviations of the names) together with the only two thermodynamically characterized representatives (names in orange). Complex I (represented in *E. coli*) is the only thermodynamically characterized, ferredoxin-independent NAD(P)H dehydrogenase [78;79;122] and HydABC from *T. maritima* as determined in chapter 4, as the first "ferredoxin-dependent" representative to be characterized during this thesis. Redox potential for the FMN as in HydB at pH 7.

demonstrated to feature a strongly stabilized neutral semi-reduced (NSR) state, whereas the redox properties of the FMN in the apoprotein HydABC seemed to deviate from this. Due to ambiguities in the obtained results from EPR and UV/Vis the redox characteristics of the FMN in HydABC remain elusive.

In this discussion section, I would like to extend on the possible implications of the obtained results from both studies. I will critically interpret the experimental results in a functional view. I will also include additional and the above-mentioned, ambiguous results that did not yet find a way into the main paper in chapter 4 since they require further attention and/or the application of other techniques to confirm or refute the here proposed claims/hypothesis.

This discussion section is subdivided into three parts:

- In section 5.1, as a synthesis of the two employed techniques, phylogeny and thermodynamic characterization, the determined spectral and redox properties of all but one FeS cofactors in HydABC as determined in chapter 4, will be compared to other members of the NAD(P)H-dehydrogenase family which are experimentally characterized. I will show that the homology between members of this enzyme family extends further to the spectral properties of many FeS-cofactors, but not to the thermodynamic realm.

  In particular, the thermodynamic landscape surrounding the FMN in HydABC and the well-characterized electron input module (NuoEFG *E.coli* nomenclature) of the respiratory complex I are clearly distinct and are argued to be primarily determined by the redox potential of the bioenergetic substrate.

  Here, I will also provide an explanation for an approximately 100 mV difference in obtained redox potentials for the Trx-like [2Fe-2S]-cluster B1 and [4Fe-4S]-cluster B2 in the isolated HydB by the two employed techniques, UV/Vis and EPR.

- In section 5.2, the thermodynamic properties of the FMN in the separate HydB subunit and the entire HydABC complex are interpreted in more detail. An in-depth interpretation for the molecular origin of the apparent pK_a-value at pH 7 for the OX-NSR transition of the FMN in HydB is provided. In addition, the degree of redox cooperativity for this flavin is evaluated. In this part, I will also include unpublished and the above-mentioned, ambiguous results that have been obtained for the FMN in HydABC.

- In the final section 5.3, these interpretations are combined for a proposal of mechanistically important intermediate states in HydABC, which would highlight an electron-transferring role of the FMN between the H-cluster and the oxidation/reduction of ferredoxin. I will show that the redox properties of the flavin are variable and that the so far determined redox proper-

ties, obtained during this thesis for the FMN and also the neighboring FeS-clusters in HydB and HydABC, cannot support FBEB/FBEC as elaborated for the quinone in the Q_o-site for the Rieske/cyt*b*-complexes in the introductory section.

5.1 The thermodynamic architecture of the HydABC

The HydABC flavoenzyme contains a single FMN and a string of 8 FeS-clusters which are required for the thermodynamically coupled reduction of Fd_{OX} and $NAD(P)^+$ from the oxidation of H_2 during flavin-based electron bifurcation (FBEB) or oppositely the coupled oxidation of Fd_{RED} and NAD(P)H for H_2-evolution during flavin based electron confurcation (FBEC). Four FeS-clusters, termed B2, A1, A2 and A3 are required to electronically connect the FMN to the proton-reducing/H_2-oxidizing H-cluster, whereas the other 4 FeS-clusters, termed B1, B3, B4 and C1 are found in conformationally dynamic domains and are proposed to interact with the external ferredoxin and the NAD(P)H-interacting FMN site[b].

5.1.1 FeS-cofactor geometries across the NAD(P)H dehydrogenase family

The results in chapter 4 demonstrate for the first time a complete set of a spectral annotation and thermodynamic data for all of the above mentioned 8 FeS-clusters of the HydABC in *T. maritima*. As elaborated in chapter 3 and shown in table 5.1, shared among all members of the NAD(P)H dehydrogenase family are multiple FeS cofactors that exhibit, as confirmed for HydABC in this thesis, comparable spectral characteristics in EPR and UV/Vis.

This observation suggests that the modular homologous domain architecture of these different bioenergetic enzymes transcends via the conserved protein folds to comparable geometric features (such as bond lengths and bond angles) of these functionally essential cofactors, evident by the spectroscopic parameters. In table 5.1, the EPR g-value annotations of the three FeS-clusters closest to the NAD(P)H-oxidizing FMN are compared for all NAD(P)H dehydrogenases.

5.1.2 Comparable geometry doesn't dictate thermodynamics

The phylogenetic tree of the "flavin"-module as shown in figure 5.1 clusters all selected NAD(P)H dehydrogenases in a "ferredoxin-dependent" and "ferredoxin-independent" group. The redox potential landscape of the two thermodynamically characterized representatives, the respiratory complex I from *E.coli*[78;79;122] and the HydABC complex of *T. maritima*, depicted in figure 5.2, exhibits significant differences.

[b] *T. maritima* HydABC contains a total of 10 FeS-clusters in addition to the single FMN and the H-cluster. The Trx-like [2Fe-2S]-cluster A5 in HydA in addition to the His-coordinated [4Fe-4S]-cluster A4 were proposed not to convey an essential contribution to NAD(P)H-oxidizing and electron-confurcating mechanism of the complexes as outlined in detail in the introduction section 1.4 (page 43)

Table 5.1: Comparison of spectral properties (g-values) in electron paramagnetic resonance (EPR) of three FeS-clusters adjacent to the FMN commonly found across NAD(P)H dehydrogenases belonging to different bioenergetic chains: Respiratory complex I from *E.coli*, Hox [NiFe]-hydrogenase from *Synechocystis* sp. PCC 6803, Formate dehydrogenase from *Methylosinus trichosporium OB3b*, and the here determined [FeFe]-hydrogenase HydABC from *T. maritima*. "*n.d.*" denotes a not determined nomenclature of the specific cluster.

NAD(P)H dehydrogenase	**Complex I**	**Hox [NiFe]-Hyd**	**FormateDH**	**[FeFe]-HydABC**
Organism	*E.coli*	*Synechocystis sp.* PCC 6803	*M. trichosporium* OB3b	*T. maritima*
Trx-like [2Fe-2S]	N1a	*n.d.*	*n.d.*	C1
g_x	1.92	1.913	1.909	1.913
g_y	1.95	1.945	1.951	1.948
g_z	1.99	1.998	1.995	1.998
Plant-like [2Fe-2S]	N1b	*n.d.*	*n.d.*	A1
g_x	1.93	1.929	1.933	1.9283
g_y	1.94	1.939	1.94	1.9367
g_z	2.02	2.016	2.014	2.0176
Nearby [4Fe-4S]	N3	*n.d.*	*n.d.*	B2
g_x	1.89	1.875	1.894	1.87
g_y	1.94	1.927	1.94	1.94
g_z	2.044	2.047	2.044	2.02
Reference	[29]	[8]	[106]	this study

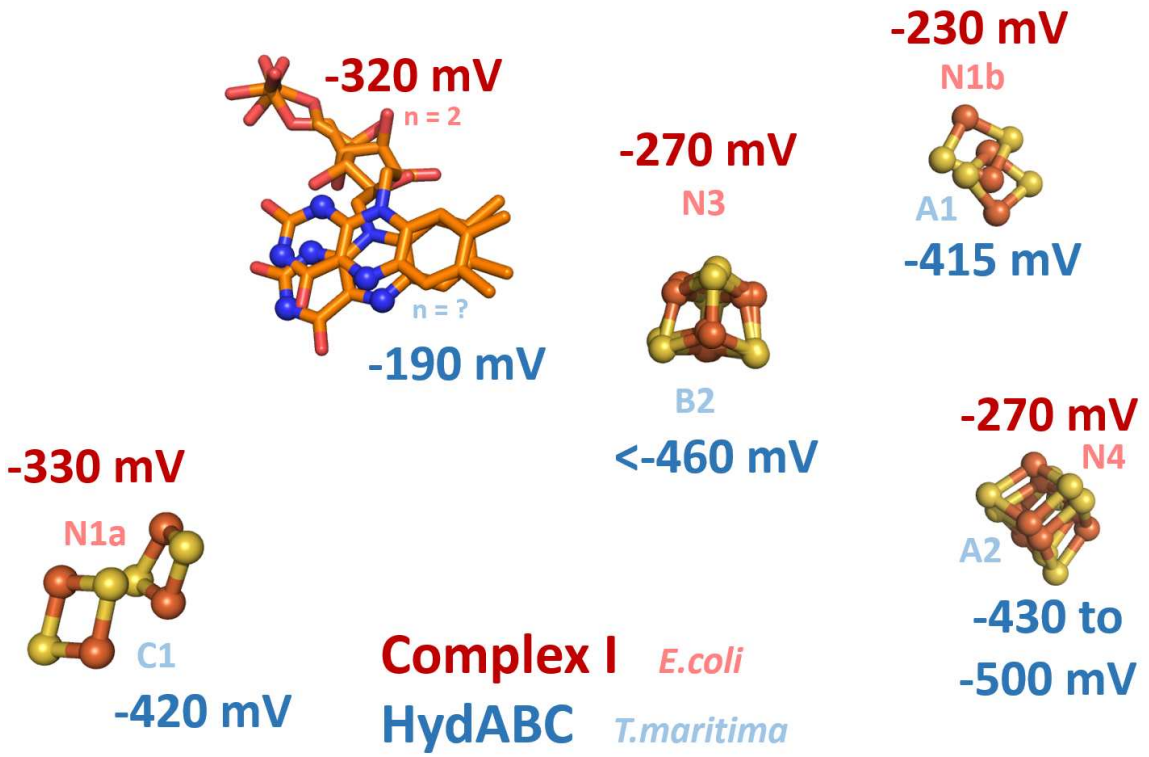

Figure 5.2: Comparison of the redox potential landscape of the FeS-clusters common to both HydABC from *T. maritima* and *E. coli* complex I[78;79;122]. The redox potentials and nomenclature of each cluster is shown for HydABC in blue and complex I in red. Redox potential for the FMN as in HydB at pH 7.

As predicted in chapter 3, the redox potential landscape is largely dictated by the bioenergetic substrate of the enzyme. Complex I of *E.coli* couples the oxidation of NADH to the reduction of ubiquinone, with redox potential of +90 mV[78;79;122;207]. HydABC interacts with ferredoxin ($E_{m,pH8}$ = -420 mV[131]) and H_2 (E° = -414 mV[210]), which thus leads to a roughly 100 to 200 mV lower redox potential of the respective cofactors in HydABC. It's noteworthy that this difference in the redox landscape between complex I and HydABC persists, even when considering the redox potential variation observed during UV/Vis- and EPR spectroscopy for two FeS-clusters in the isolated HydB. Further details on that will be provided in the subsequent section 5.1.3.

This demonstrates that the homologous domain architecture of different members of the NAD(P)H dehydrogenase transcends to comparable spectral properties of its functionally essential cofactors, while the thermodynamic properties align with the bioenergetic substrate, which is largely set by its environmental availability. As HydABC interacts with H^+/H_2 (E° = -414 mV[210]), the closely related "ferredoxin-dependent" formate dehydrogenase with the redox couple CO_2/formate (E° = -420 mV[210]) therefore would be predicted to feature a similarly overall low-potential redox potential landscape. However, as visible in figure 5.1, with the exception of complex I, all other members of the NAD(P)H dehydrogenase family, contain representatives in both the "ferredoxin-dependent" and the "ferredoxin-independent" branch, while sharing the same catalytic redox substrates in addition to NAD(P)H. The presence of [FeFe]-hydrogenases in both groups has been suggested to arise from distinct environmental conditions, where the organism is situated in environments with varying concentrations of dissolved H_2, thereby influencing the overall thermodynamics[128;252].

Given the structural conservation of this flavoenzymes down to the cofactor geometry level, an important implication of this work is that it could facilitate the thermodynamic characterization of these other "ferredoxin-dependent" and "ferredoxin-independent" members of NAD(P)H dehydrogenase family shown in figure 5.1, by providing a "fingerprint"-like spectral signatures to each FeS-cluster.

In regard for the understanding of the catalytic capabilities of the FMN in this enzyme family, the determined EPR-signatures of the neighboring FeS-clusters that surround the FMN in the HydBC-subcomplex (chapter 4 and table 5.1) could be used for the determination of redox properties during equilibrium redox titration experiments in these related enzymes.

Furthermore, kinetic studies such as rapid mixing / freeze quench experiments, monitored by EPR, could help in identifying electron transfer steps which, while being thermodynamically favored, might be constrained by kinetic barriers. Given the suggested extensive conformational changes in the flexible domains housing the FeS-clusters, B1, C1, B3 and B4, within the HydBC-subcomplex (refer to introduction section 1.4.1, page 46 and below), which were proposed to modulate electron

transfers to and from the FMN through a kinetic gating mechanism[72;111], conducting kinetic studies would offer valuable insights. Such studies have been critical in elucidating the QBEB reaction at the Q_o-site in the Rieske/cyt*b* complexes[255] (see introduction section 1.2.4) and were also applied to the respiratory complex I in *E.coli* to deconvolute the electron bifurcating kinetics of the enzyme[55;217].

Besides other electron-bifurcating [FeFe]-hydrogenases[111;115;192;226;252], various enzyme complexes such as the [NiFe]-hydrogenase from *Acetomicrobium mobile*[72] or the formate dehydrogenase-[FeFe]-hydrogenase fusion protein from *Clostridium autoethanogenum*[225] which have both been shown to catalyze FBEB/FBEC would seem interesting candidates to explore their thermodynamic landscape, via the here provided "fingerprint"-toolset. The investigation of the redox potentials of the redox cofactors surrounding the flavin would furthermore enrich our knowledge of the capabilities of the FMN in this enzyme family.

5.1.3 Ambiguities in the redox potential assignment for the Trx-like [2Fe-2S]-cluster B1 in HydB between EPR and UV/Vis

As presented in chapter 4, the spectral and redox potentials of the FeS-clusters assigned by EPR were largely consistent between the two proteins, HydB and HydABC. This feature has been exploited to dissect the thermodynamic properties of all the superposing signals of the FeS-clusters in the apoprotein. A notable exception was observed for the redox properties of the Trx-like [2Fe-2S]-cluster, B1 in HydB. This cluster exhibits distinguishable EPR signatures compared to the other two Trx-like [2Fe-2S]-clusters and is found at approximately 100 mV lower redox potentials in HydABC (E° = -550 mV) compared to HydB (E° = -460 mV). This discrepancy is attributed to an electrostatic effect from the nearby reduced C1-cluster in the HydC subunit, which shifts the redox midpoint potential of B1 to more negative values, and is obviously absent during redox titrations on the isolated HydB subunit.

In the complementary UV/Vis experiments on HydABC, where FeS-clusters are expectedly more challenging to distinguish, Trx-like [2Fe-2S]-clusters were effectively characterized. The assignment was facilitated due to their distinctive absorbance bands around 335 nm, 465 nm, and 550 nm (see introduction section 1.5.2, page 55). These experiments confirmed a strongly reducing redox potential at -550 mV for a Trx-like [2Fe-2S]-clusters attributable to B1 (only in analogy to EPR), alongside a smaller (approximately half amplitude) high-potential Trx-like [2Fe-2S]-cluster wave at -270 mV which was assigned to A5, also in agreement with the results obtained in EPR. The redox potential assignments for the FeS-clusters in HydABC obtained via UV/Vis therefore largely align with the results acquired from EPR.

Meanwhile, during redox titration experiments by EPR and UV/Vis on the isolated HydB subunit, notable differences in the redox potentials of two FeS-clusters, the [2Fe-2S]-cluster B1 and the [4Fe-

4S]-cluster B2, were observed.

As shown in figure 5.4 (see below), a pH-independent redox midpoint potential of the FeS-clusters (evident from the difference spectra) in HydB is observed around -375 mV during spectro-electrochemical redox titrations. Redox cuts, i.e., difference spectra in the high potential and the low potential part of the -375 mV wave as seen in figure 5.3A and figure 5.4, consistently demonstrate a mixture of both Trx-like [2Fe-2S]- and [4Fe-4S]-clusters across the entire -375 mV (n = 1)-wave. A quantification of these FeS-clusters in HydB in UV/Vis was not feasible. In the isolated HydB subunit only a single [2Fe-2S]-cluster, B1, is found, which therefore must be attributed to the Trx-like [2Fe-2S]-like spectral characteristic (red traces in figure 5.3A) of this -375 mV wave.

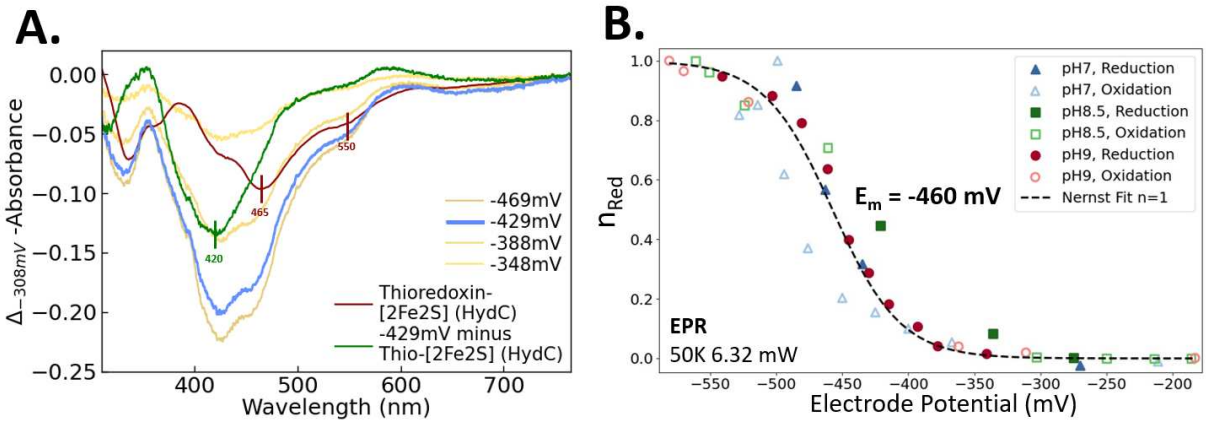

Figure 5.3: Redox Characterization of the B1 Trx-like [2Fe-2S]-cluster by UV/Vis and EPR of the isolated HydB. **A.** UV/Vis spectral deconvolution of the FeS-clusters in HydB at pH 8.55. Δ-308 mV-Absorbance data (in yellow) of the -429 mV spectra (light blue) into a thioredoxin-like [2Fe-2S]-cluster (brown, spectra from HydC) and one or multiple [4Fe-4S]-clusters (green). **B.** Redox titration of B1, the only [2Fe-2S]-cluster in the isolated HydB subunit is selectively titrated by EPR at 50K at pH 7 (blue triangles), pH 8.55 (green squares) and pH 9 (red circles). The normalized total signal amplitude of the g_y and g_x of the entire dataset was fitted to a one-electron Nernst-Fit (n = 1) resulting in a redox midpoint potential of approx. -460 mV.

In EPR, which is better suited for distinguishing the spectral properties of each FeS-cluster, chemical redox titrations attributed to each spectrally unique FeS-cluster in HydB, i.e., the Trx-like [2Fe-2S]-cluster B1 and the [4Fe-4S]-cluster B2, B3 and B4, an individual redox potential in the range from -375 mV to -460 mV was assigned. Thus for some clusters an approximately 100 mV difference between the two spectroscopic techniques is concluded (table 5.2).

The -375 mV FeS-cluster wave from UV/Vis agrees well with the two highest potential [4Fe-4S]-clusters in HydB, which have been assigned to the 8Fe-Ferredoxin domain, containing B3 and B4, with a redox potential of -375 mV and -425 mV in HydB, determined during EPR-monitored titration. Protein film voltammetry (PFV) experiments on the adsorbed, separately expressed C-terminal 8Fe-Fd domain (containing only B3 and B4) from HydB conducted by James Birrell, indicate a indistinguishable redox midpoint potential for both clusters at -400 mV, which is largely in agreement with this interpretation. All three employed techniques, UV/Vis, EPR, PFV on all proteins utilized,

i.e., HydABC, separately expressed HydB subunit and the C-terminal 8Fe-Fd domain of HydB, therefore confirm pH-independent redox potentials of these two [4Fe-4S]-clusters in the -375 to -425 mV range.

Meanwhile, a larger difference between EPR and UV/Vis concerns B1 and B2 in HydB, as shown in table 5.2. The B1 Trx-like [2Fe-2S]-clusters in the isolated HydB subunit distinctively titrates at -460 mV (figure 5.3B) in EPR and is thus at -85 mV lower redox potentials as in UV/Vis. A similar difference arises for the B2 [4Fe-4S]-cluster.

Table 5.2: Comparison of the Redox Midpoint Potential obtained for the FeS-clusters, B1 and B2 in HydB and HydABC, using EPR and UV/Vis-spectroscopy.

	HydB		HydABC	
	B1 [2Fe-2S]	B2 [4Fe-4S]	B1 [2Fe-2S]	B2 [4Fe-4S]
EPR	-460 mV	-470 mV	-550 mV	$\sim$ -450 mV
UV/Vis	-375 mV	-375 mV	-550 mV	Not assigned

The most parsimonious explanation for this difference relates to the state and/or composition of the assembled FeS-clusters in the separate HydB subunit that was used for the respective redox titration experiments.

All UV/Vis-electrochemical redox titration experiments have been carried out on a single batch of HydB protein (483 μM), diluted to a 15 to 30 μM final HydB concentration for the individual experiments at different pH-values. The same HydB batch also contributed approximately 20% (in concentration) to the EPR-titration experiments of HydB at pH 8.55. For the 50K EPR signal of the B1 Trx-like [2Fe-2S]-cluster, during this titration, a partial high-potential wave is identified (green filled squares in figure 5.3B), which, if fitted separately, titrates at slightly higher potentials around -425 mV. This could indicate a slightly variable redox midpoint potential of the B1 cluster from different purified protein batches, which is also evident by the distribution of points in figure 5.3B. The difference in redox potential was not found to be pH-dependent, confirming the observation of a pH-independent redox potential of -375 mV in UV/Vis across the entire assessed pH-range (5.17 to 9.23, figure 5.4). The resulting 50 mV difference between this high-potential wave at -425 mV in EPR and the -375 mV wave in UV/Vis would be at the far edge for the experimental margin of error for these experiments.

The difference in the determined redox potential for different protein batches might be speculatively attributed to a different conformational state of the dynamic HydB subunit (see introduction section 1.4.1, page 46), and/or (more likely) to a slightly different composition of FeS-clusters in the protein. Some [4Fe-4S]-clusters, including B3 and B4 in the 8Fe-Fd domain of HydB (data not shown), are highly sensitive to oxygen, degrading into [3Fe-4S]-clusters, which were commonly observed in HydABC and the isolated HydB as purified in the oxidized state of the protein via EPR

(not shown). [3Fe-4S]-clusters are EPR-silent in the reduced state while paramagnetic and therefore EPR-detectable when oxidized. In HydB, these [3Fe-4S]-clusters could be reversibly redox-titrated with a redox potential of roughly -100 mV (data not shown). It might be speculated that the B2 [4Fe-4S]-cluster in HydB was actually degraded during this UV/Vis-experiments, explaining the absence of any [4Fe-4S]-cluster resembling spectral features (as shown in green traces in figure 5.3A) in a redox range below -460 mV (as assigned in EPR for B2) and thus was assigned to the large -375 mV wave in table 5.2. It shall be re-iterated that the redox properties of the FMN and the other two FeS-clusters B3 and B4 in the ferredoxin-like C-terminal 8Fe domain in the isolated HydB subunit were reproducibly observed in different HydB protein batches in EPR and UV/Vis.

5.2 Thermodynamic properties of the FMN in HydB and HydABC

During this thesis, the thermodynamic properties of the FMN in HydABC and in the isolated flavin-containing HydB subunit were assessed via pH-dependent equilibrium redox titrations. These experiments yielded a clearly distinct redox behavior for the flavin in both proteins. Whereas the FMN in HydB is characterized by a strongly stabilized neutral semi-reduced (NSR) state indicative for a negatively cooperative redox behavior, the FMN in HydABC despite the ambiguous observed results, clearly deviates from the FMN in HydB, with a less strongly stabilized NSR. In this part, an interpretation of the individual results is offered, which will go beyond the obtained thermodynamic parameters, by including information from the structure models of HydABC.

5.2.1 A neutral semi-reduced redox state of the FMN in HydB

As elaborated in chapter 4, pH-dependent redox titrations on the separate HydB subunit evidently distinguished a high-potential, pH-dependent flavin compound from the relatively low-potential, pH-independent FeS-clusters discussed above. Both employed experimental setups, i.e., chemical titration using EPR- and electrochemical titration using UV/Vis-spectroscopy (figure 5.4) confirmed clear spectral indications of a high-potential neutral semi-reduced (NSR) redox state of the FMN across the entire pH-range (5.17 to 9.23). Quantification of the FMN stoichiometry in relation to the protein concentration, indicated a gradual loss of bound FMN over the duration of the experiment, which underlined the common observation in all HydBC-like proteins of a loosely bound flavin[72;115;118;192;194;226]. During electrochemical experiments this loss has been found to be induced by oxidizing conditions above an electrode potential of approximately +100 mV, which were therefore avoided during all titrations (data not shown). A similar loss of the flavin was attributed to the influence of oxygen (data not shown).

The redox dependencies of the absorbance change corresponding to the OX-NSR transition agreed

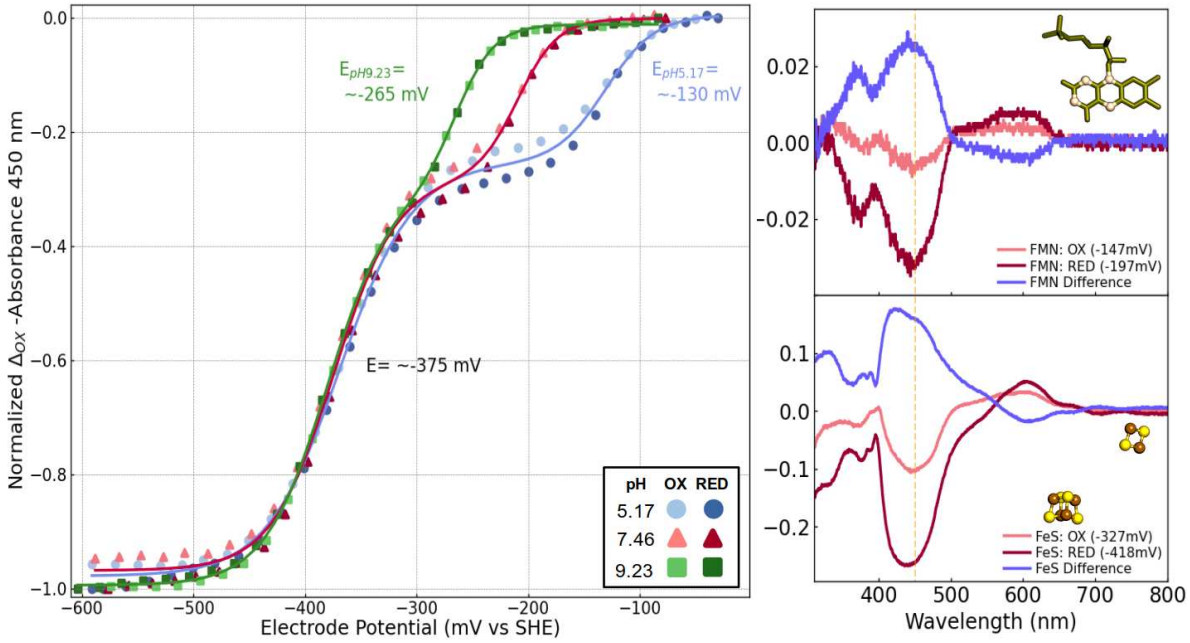

Figure 5.4: Reversible Redox Titration at 450 nm of HydB at different pH-values. Redox Titration Data of the 450 nm signal during the second oxidation/reduction cycle at three pH-values (pH 5.17, 7.46 and 9.23) representative of the sampled pH-range. The absorbance as a difference to the most oxidized spectra (ΔOX) is normalized to the most reduced (largest) signal of the cycle. At 450 nm the mediator-contributions become minimal allowing the redox-components of the HydB protein to be evaluated directly. Data shows minimal hysteresis between oxidation and reduction after 10 min of equilibration between each 20 mV step during the chronoamperometry and is fitted to a 2-component Nernst-fit. A high potential, pH-dependent component contains a mixed FMN population (bound to HydB, n = 1 and free FMN n = 2, see appendix figure 1 and 2) and a low potential, pH-independent component of larger amplitude containing multiple [2Fe-2S]- and [4Fe-4S]-clusters is differentiated. *Right site*: Redox-cuts (in blue) from the pH 7.46 dataset of the FMN component (-147 mV minus -197 mV) and the FeS component (-327 mV minus -418 mV) are shown.

well with the n = 1 - Nernst fitted titration curves for the FMN inside the HydB subunit (chapter 4), whereas a second population of released flavin in solution undergoes a direct oxidized to reduced (n = 2) transition (as specified in the introduction section 1.6, page 58, appendix figure 1 and 2).

Plotting the determined redox potential of the FMN ($E_{OX/SR,\ pH}$) against the pH-value of each experiment (figure 5.5), two distinct regions of pH-dependencies are indicative for an apparent $pK_{a,\ app}$-value near pH 7 for the isoalloxazine of the FMN in HydB. Below $pK_{a,\ app}$ the pH-independent region contains both redox species FMN_{OX} and FMN_{NSR} in their protonated form, thus the electron transfer is not associated with a protonation event. Above pH 7, the formation of the NSR species is thermodynamically coupled to a proton-transfer as indicated by a -60 mV/pH dependence (see introduction section 1.6.2, page 60). The only certain assertion in regard to the pK_a-values of the isoalloxazine in HydB that can be made from these experiments pertains to a shifted $pK_{a,\ SR}$ of the isoalloxazine N(5) from 8.3 in free flavin to above 9.3. The attribution to the $pK_{a,\ SR,\ N(5)}$ is justified by the observed spectral properties of the NSR above and below the apparent pK_a-value, in UV/Vis and EPR, which have been unequivocally assigned to the protonated N(5) in the semi-reduced redox state (refer to introduction section 1.6.5, page 66).

The interpretation of the apparent pK_a-value near 7 therefore unequivocally quantifies the pro-

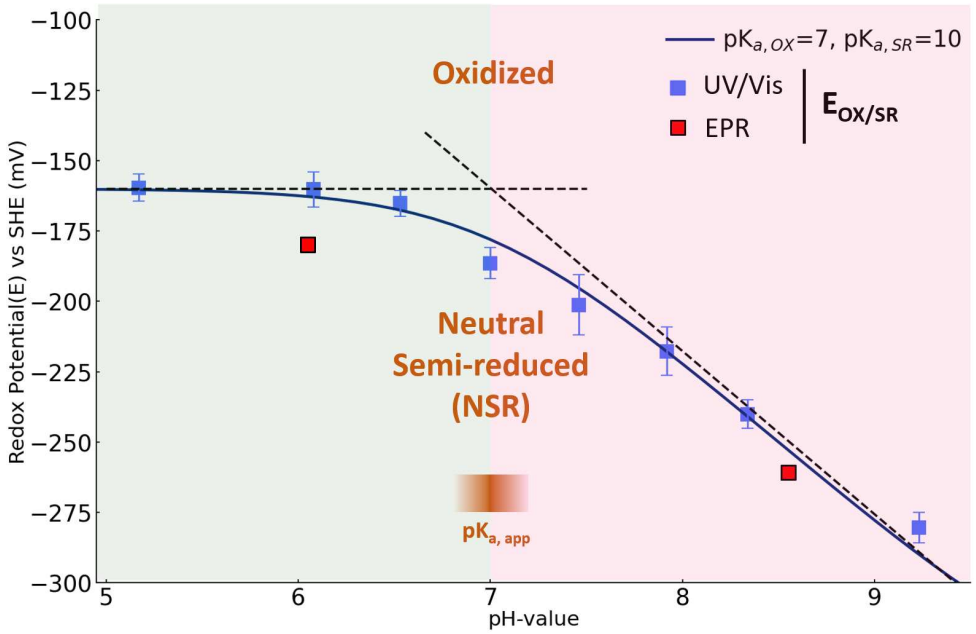

Figure 5.5: Dependence of the FMN $E_{OX\text{-}NSR}$ redox potential in HydB on the pH-value. One-electron redox transition ($E_{OX\text{-}NSR}$) of the oxidized to neutral semi-reduced (NSR) state of the FMN in HydB over a pH range of 5.17 to 9.23. On the intercept of the pH-dependent (-60 mV/pH) and pH-independent region, an apparent pK_a-value ($pK_{a,\,app}$) at pH 7 is deduced. Error bars represent standard deviation of the least-square Nernst-fit of multiple (consecutive) titration datasets (oxidation and reduction were fitted separately) during UV/Vis-monitored electrochemical redox titrations as shown in the supplementary information of chapter 4. The obtained results have been validated by EPR-monitored chemical redox titrations at pH 8.55 and pH 6.05 (red squares). The data was fitted with equation 1.11 (see introduction section 1.6.2, page 60), with $E_{m,\,pH0}$ = -160 mV, $pK_{a,OX}$ = 7 and $pK_{a,SR}$ = 10.

tonation affinity of one of the three nitrogens, N(1), N(3), N(5) of the flavins isoalloxazine in the oxidized state: $pK_{a,\,OX}$. The attribution of the $pK_{a,\,OX}$ to one of the three nitrogens will be discussed below.

5.2.2 The fully-reduced redox state of FMN in HydB

During redox titrations in the oxidizing direction at two pH-values pH 6.53 and 8.34, a minimal mediator contribution permitted both redox transitions of the FMN (RED-NSR and NSR-OX) in HydB to be observed. In figure 5.6 for the titration at pH 8.34 the spectral characteristics of the NSR-RED transitions of the FMN in HydB are compared to the reference spectra of FAD in glucose oxidase (GluOX). The FMN in HydB exhibits three major bands above 400 nm, specifically at 480 nm, 567 nm, and 604 nm, akin to the pattern observed in glucose oxidase. However, the spectra differ in the relative intensities of these bands. A more notable distinction occurs below 400 nm, where HydB lacks the two bands which are found at 345 nm and 380 nm in glucose oxidase. No other spectral components have been identified to explain this variation.

We have therefore interpreted the observed spectral differences by an alteration of the FMN's electronic structure of the reduced and/or semi-reduced state in HydB as compared to the FAD in glucose oxidase. This could be reflected by a change in polarization of the flavin environment or

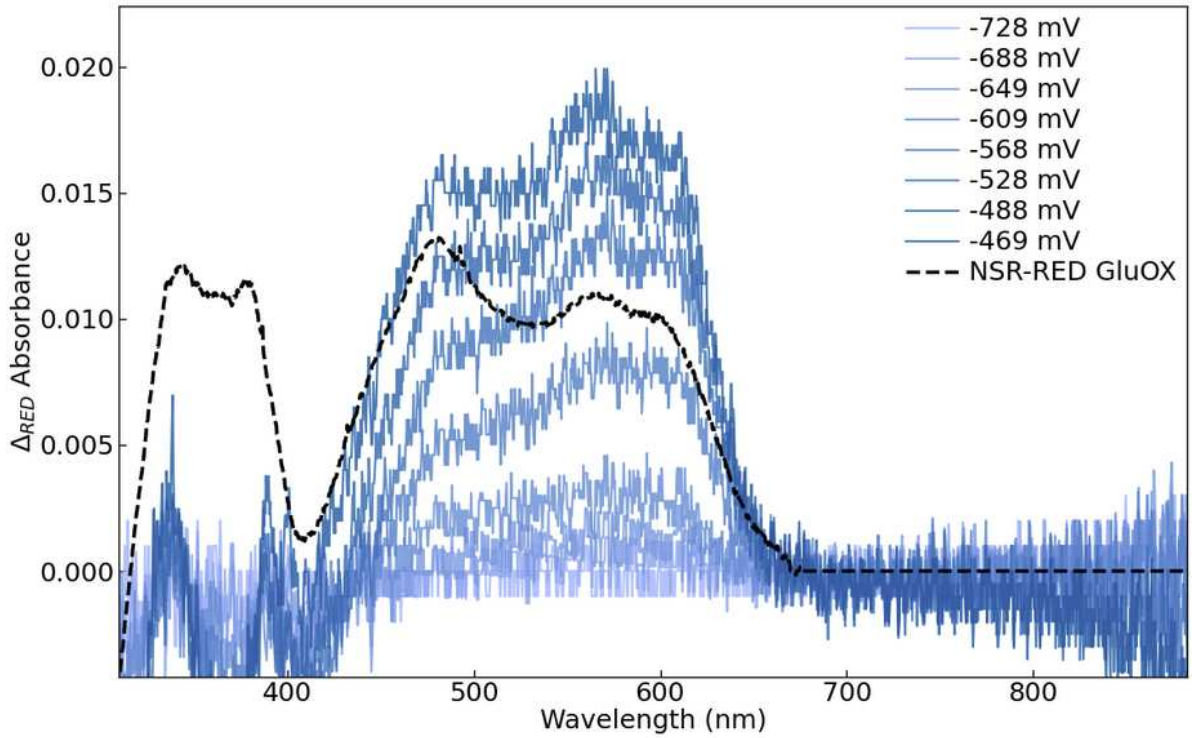

Figure 5.6: UV/Vis (OX-RED)-difference spectra during redox titration of 22 μM HydB at pH 8.34 to the most reduced spectra (-738 mV vs SHE) after Mediator subtraction (blue) compared to a reference (NSR-RED) spectra of 7 μM Glucose oxidase[137] (black dashed).

a different H-bonding network flavin binding pockets[167]. Multiple conserved acidic residues dominate the FMN binding pocket in the HydABC structure models in particular near the O(2), N(3) and O(4) (see figure 5.9 below), whereas GluOx exhibits a rather basic and surface exposed FAD environment[124]. These interactions are dominant parameters that deform the π-electron system of the flavin, which are evident in the differences in the spectra[167].

The observation of the NSR-RED transition during the electrochemical UV/Vis-monitored redox titration, was also confirmed repeatedly by the disappearance of the NSR radical during EPR experiments documented at a similar low redox potential range (see Supplementary Figure 2 in Chapter 4). As shown in figure 5.7, during oxidative redox titrations, the redox potential $E_{NSR\text{-}RED}$ of the FMN in HydB was assigned to -588 mV at pH 8.34 (figure 5.7A/B) and -542 mV at pH 6.53 (figure 5.74C/D). The redox transition from the NSR to RED could only be observed at these two instances due to the larger contribution of the viologen mediators in the other experimental setups. During these two experiments, very reducing electrode potentials (surpassing -700 mV vs SHE, figure 5.7A and C) were reached, which fully reduced the viologens. The fully-reduced viologen undergoes a two-electron transition during oxidation, distinct from the two one-electron transitions observed during reduction. Their property of bypassing the strongly absorbing semi-reduced viologen species during oxidation, allowed the clear observation of the smaller, underlying NSR-RED transition of the FMN. However, while this behavior has been described in the literature for methyl-viologen[236], we couldn't yet find

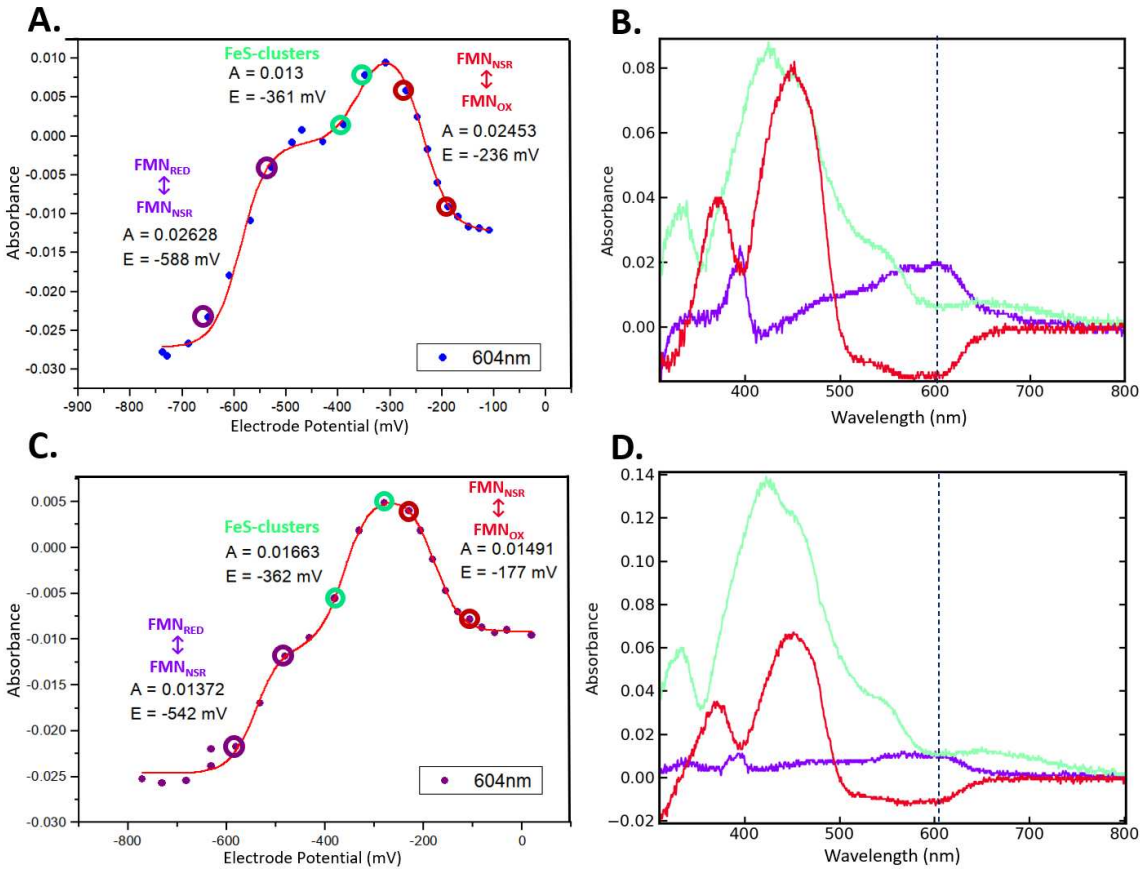

Figure 5.7: Oxidative redox titration of the RED-NSR and NSR-OX redox transitions of the FMN in HydB at two pH values. 604 nm titration curve and difference spectra of individual redox components at pH 8.34 with (**A.** and **B.**) and pH 6.53 (**C.** and **D.**), respectively. The absorbance data was fitted to three one electron (n = 1) component fit. Both redox transitions of the FMN at 22 μM protein concentration are observed in a similar signal amplitude and opposing spectral form at the NSR specific wavelengths around 600 nm. A smaller signal amplitude at pH 6.53 can be explained with a stronger degree of protein denaturation at low pH-values.

it to have been reported for benzyl-viologen.

The pH dependence observed for the evaluated $E_{NSR\text{-}RED}$ redox transitions of the FMN in HydB is approximately -25 mV/pH. This implies a distinct, thermodynamically coupled proton transfer during the NSR-RED redox transition. The deviation from the anticipated -60 mV/pH dependence for these transitions might suggest a pK_a-value between the two assessed pH values. The interpretation of this pK_a-value for the nitrogen on the isoalloxazine will be discussed below. The redox potentials for both redox transitions of the FMN obtained at these two instances allow for an approximation of the stabilization constant (K_s) of the NSR in HydB (figure 5.7). The strongly negative redox cooperativity of the individual electron transfers is quantified by a $\log(K_s) = 6.8$, rendering the observable stabilization of the neutral semi-reduced species comparable to the well-characterized wild-type form of flavodoxin[130] (refer to introduction table 1.3, page 64). It comes to no surprise that in HydB, the strongly stabilized NSR species of the FMN therefore can be induced both by the reduction with dithionite and also by the physiological low-potential electron donor, reduced ferredoxin (not shown).

5.2.3 Assignments of pK_a-values to N(1), N(3) and N(5) to the FMN in HydB

Based on the experimentally obtained pH-dependencies of the two consecutive redox transitions $E_{OX\text{-}NSR}$ and $E_{NSR\text{-}RED}$ from FMN in HydB, the most plausible interpretation would describe the isoalloxazine N(5) as the main target of the enzymes influence on the redox properties of the flavin. The observation of the unique spectral characteristics of the neutral semi-reduced FMN state across the entire sampled pH-range (5.17 to 9.23) must be associated with a shift of the $pK_{a,\,SR}$ of the N(5) above 9.23. The -60 mV/pH dependence, observed at pH values below the apparent pK_a around pH 7 for the OX-NSR transition of the FMN in HydB, imposes additional constraints on the assignment of the other pK_a values.

I will here argue for the most parsimonious assignment of the apparent pK_a around pH 7 to quantify the proton affinity of the N(5) in the oxidized state, $pK_{a,\,OX,\,N(5)}$ of the isoalloxazine. Any alternative assignments of the apparent $pK_{a,\,OX}$ to one of the other nitrogens N(1) or N(3) would require an even stronger shift of the N(5) $pK_{a,\,OX,\,N(5)}$ beyond pH 9.23, due to the above mentioned constraints. As compared to free FMN in aqueous solution the N(5) $pK_{a,\,OX}$ is consequently shifted up by approximately 7.5 pH-units as compared to FMN in aqueous solution (FMN, N(5) $pK_{a,\,OX} = -0.5$, see introduction table 1.2, page 64). This must be accompanied by a simultaneous shift of the N(5) $pK_{a,\,SR}$ from 8.3 (FMN in aqueous solutions) to at least above pH 9.23. Since at this highest pH-value sampled during this study, clear and unchanged NSR species were still documented, the N(5) $pK_{a,\,SR}$ is suggested to be shifted by at least one or two pH-units more (fit in figure 5.5 with N(5) $pK_{a,\,SR} = 10$). The experimental observation of a near perfect -60 mV/pH dependence indicates a strictly coupled 1-proton/1-electron at pH-values above 7. This dependence underlines the involvement of only 1 proton (protonation of N(5)) with the electron transfer, instead of a -120 mV/pH indicative for a 1-electron/2-protons transition when one of the other sites, i.e., N(1) or N(3), were to be involved as well. This indirectly favors a rather unshifted $pK_{a,\,OX}$ of the N(3) compared to free flavin. The $pK_{a,\,OX,\,N(3)}$ is then around 10.3 and remains protonated across the entire sampled pH-range. The interpretation of the obtained pH-dependent redox behavior to the assignment of pK_a-values of the N(5) of the isoalloxazine is summarized as a thermodynamic square (figure 5.8B) and the proposed flavin protonation states as a Pourbaix-like diagram (figure 5.8A).

A -25 mV/pH dependence for the second transition of the FMN ($E_{NSR\text{-}RED}$) between pH 6.53 and 8.34 suggests a proton-coupled redox transition. The deviation from the expected -60 mV/pH dependence for this transition could be explained by a $pK_{a,RED}$ of the N(1) in between the two assessed pH-values. Therefore the N(1) would also remain to be rather unshifted by the protein environment compared to free flavin (as summarized in table 5.3). The here proposed strong stabilization of a protonated N(3)H and N(5)H in the oxidized state (below pH 7), strongly increases the electron

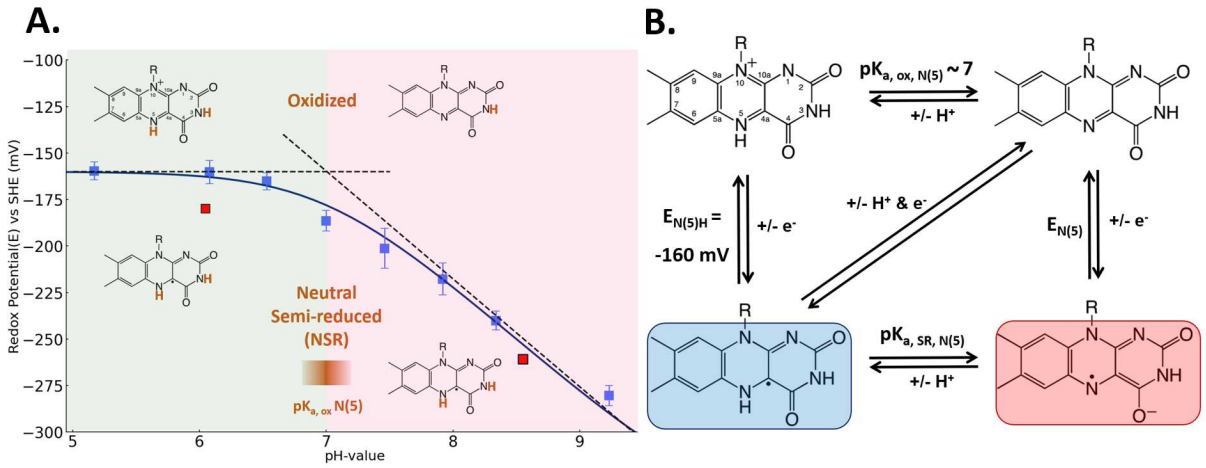

Figure 5.8: Interpretation of the FMN $E_{OX\text{-}NSR}$ pH-dependence in HydB. **A.** Pourboux-like diagram of the interpreted FMN species in HydB dependent on pH and redox potential. The intercept of the two ranges of pH-dependencies, an apparent pK_a-value ($pK_{a,\,app}$) at pH 7 is interpreted as the $pK_{a,\,OX}$ of the N(5) as elaborated in the main text. **B.** Thermodynamic square scheme derived from the interpretation of the pH-dependent redox titration, characterizing the pK_a-value of the FMN in HydB. The blue box shows the isoalloxazine structure of a neutral semi-reduced state (NSR), which was observed across the entire pH-range. The red box indicates the anionic semi-reduced state (ASR), which is not observed.

affinity of the FMN, which effectively leads to the high redox potential of the first reduction ($E_{OX/SR}$). In addition, the hydrogen-bonds to the nitrogens in the oxidized state of the isoalloxazine might also contribute in addition to other factors to a near 100% occupation of the FMN in HydB, whereas roughly 60-70% of FMN are obtained in HydABC (not shown).

5.2.4 The FMN environment in structure models of HydABC

As elaborated in the introductory section 1.6.1(page 59), the redox properties of the flavin are primarily tuned by the pK_a-values of the isoalloxazine nitrogens and the hydrogen-bonding network surrounding it. The here proposed shift in the pK_a-values for the flavin environment of the FMN in HydB, primarily of the $pK_{a,\,OX}$ of the N(5) as elaborated in the previous chapter therefore would predict a strong H-bond interaction of the HydB protein with the N(5). The current lack of a structure model for the isolated HydB subunit prevents testing this prediction. In the HydABC enzyme complex, the FMN in the HydB subunit is closely associated with the adjacent HydC subunit, wherein the C1 Trx-like [2Fe-2S]-cluster is within electron transfer distance of the flavin. A future structure determination of the standalone HydB subunit is essential to comprehend the molecular basis for the observed pH-dependent behavior of the FMN in HydB.

However, this Trx-like C1-domain undergoes extensive domain rearrangement, transitioning from the “HydC-in” state to the “HydC-out” state (see introduction section 1.4.4, page 48). This latter configuration implies a structural state which largely aligns with the proposed structure of the isolated HydB used in this study. In the “HydC-out” state any electrostatic effect that could arise from the Trx-like [2Fe-2S]-cluster C1, would be largely screened by the high dielectric of the aqueous solution.

In the only Cryo-EM structure models from HydABC(D) of *A. woodii*[111] (PDB: 7Q4V), that displays both orientations of the Trx-like C1-domain of HydC, also documents rearrangements around the FMN. The limited structure quality of these structure models however preclude the identification of any pertinent H-bond partners below a 3 Å distance cutoff for a strong hydrogen bonding to the N(5).

The *T. maritima* structures are the highest resolution models featuring the HydBC-like architecture currently available. None of these published structure models of *T. maritima* feature a 'HydC-out' state, although preliminary low-resolution data confirm its existence (personal communication with James Birrell). High-resolution structure models of *T. maritima* HydABC in the "HydC-out" state in addition to the structures of the isolated HydB subunit would therefore be necessary to confirm the above proclaimed resemblance of HydB to the HydABC "HydC-out" state. The currently available *T. maritima* structures feature two potential H-bonds from the peptide backbone to the FMN's isoalloxazine below a 3 Å distance cutoff for a strong hydrogen bonding[52] (figure 5.9). A backbone carbonyl of Asp226 to the N(3) potentially stabilizes the protonated N(3) via a 2.7 Å H-bond. Meanwhile, a backbone amide of the Gly228 over a distance of 2.6 Å to the neighboring O(4) is the closest observable H-bond partner of the flavin. The closest H-bond partner to the N(5) is a carbonyl of a conserved glycine (Gly315) in 3.4 Å distance. In some HydABC structures of *T. maritima*, the N(1) can be observed in 2.7 Å distance to the hydroxyl-group of the ribose-backbone of the FMN (figure 5.9).

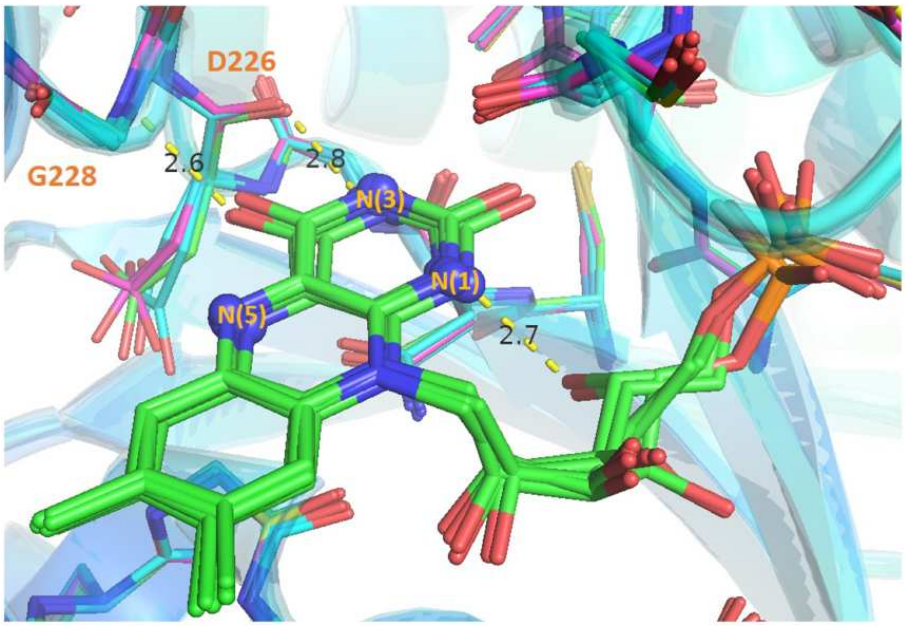

Figure 5.9: H-bonding environment around the FMN of the HydABC inside *T. maritima* at pH 8. All Cryo-EM structure models from the HydABC of *T. maritima* are superimposed (PDB: 7P5H, 7P8N, 7P91, 7P92). Two H-bond interactions (shown as yellow dashed lines) between the nitrogens and oxygens of the isoalloxazine and the protein environment below 3 Å are observed. Distance in Angstrom (Å). The N(1) interaction with one of the ribose hydroxyl-groups is only observed in two PDB-structures (PDB: 7P5H and 7P92).

Both identified H-bond interactions from the surrounding amino acids in HydABC with the isoalloxazine seem to primarily favor a protonated N(3)H. In many flavoenzymes, such as flavodoxin[22] and phenol hydroxylases[51] a protonated N(3)H stabilized by an H-bond interaction with the surrounding residues were proposed to anchor the isoalloxazine to the protein. In addition, the O(4) H-bonding has been proposed to enhance the electron-accepting capacity of the N(5), presumably by increasing the $E_{OX/SR}$ redox potential under a simultaneous downshift of the N(5) $pK_{a,\,SR}$ in other flavoenzymes[94].

The *T. maritima* structure models considered here are " as purified" at pH 8 in the oxidized redox state. According to Furlan *et al.* (2021)[80] the HydABC "apo-protein", i.e., without H-cluster, was heterologously purified in *E.coli* under a 2% H_2 atmosphere, with brief aerobic exposure during Cryo-EM grid preparation. The HydABC and HydB enzymes in this thesis were prepared under the same conditions and showed no or minimal signs of reduction, validating the fully oxidized redox state of the FMN. These conditions therefore provide primarily indication on the $pK_{a,\,OX}$. From the described H-bonds from D226 and G228, a stabilized N(3) protonation in the oxidized state of the FMN in HydABC is suggested. How this quantifies in terms of pK_a-values for the FMN in HydB is rather speculative. Aside from that, the absence of a direct H-bonded protein residue to N(1) or N(5) in HydABC suggests an overall weakly H-bond network surrounding the isoalloxazine in the oxidized state.

Partially resolved waters in the *T. maritima* structure models might mitigate that. Interestingly, in crystal structure models of all other NAD(P)H dehydrogenase members studied in chapter 3, i.e., complex I[193], NAD^+-dependent formate dehydrogenase (FdsBG)[245] and a Hox-type [NiFe]-hydrogenase[197], additional, structurally conserved waters in proximity to the N(3) and the N(5) are observed, which might translate into a common H-bond network.

5.2.5 Summary of the assigned pK_a-values for the FMN in HydB

The assignment of pK_a-values to the three nitrogen N(1), N(3) and N(5) of the isoalloxazine of HydB is entirely based on the experimentally obtained pH-dependencies of the two consecutive redox transitions $E_{OX\text{-}RED}$ and $E_{NSR\text{-}RED}$ and summarized in table 5.3.

Table 5.3: pK_a values of the three nitrogens N(1), N(3), and N(5) in the isoalloxazine of FMN in HydB as compared to FMN in aqueous solution in the different redox states. In parentheses are the values of FMN in aqueous solution as given in the introduction[140] Asterisks denote pK_a-values that are directly (***) or indirectly (**) experimentally observed from figure 5.5, or inferred from the interpretation of the flavin's pH-dependence in association with the structure models (*).

	$\mathbf{pK}_{a,OX}$	$\mathbf{pK}_{a,SR}$	$\mathbf{pK}_{a,RED}$
N(1)	< 2	1.2	$\sim 6.7^{**}$
N(3)	10.3^{*}	> 12	$>> 12$
N(5)	~ 7 (-0.5)***	> 10 (8.3)***	> 12

From the HydABC structures of *T. maritima*, an N(3)H stabilization of the oxidized flavin (via C=O from Asp266, figure 5.9) could anchor the flavin in the protein site which might similarly be translated to the FMN in HydB and be indicative for a rather unshifted $pK_{a,\,OX}$ of the N(3) around 10.3. In the absence of direct and robust H-bonding residues to N(5) of the isoalloxazine, which could elucidate the observed shift in the N(5) $pK_{a,\,OX}$, the possibility of structural alterations in the FMN binding site is suggested. This might be attributed to the absence of the structurally stabilizing HydC subunit. In more definitive terms, the absence of the HydC subunit could potentially induce a collapse of the FMN binding pocket, thereby altering the enzyme's interaction with the FMN and resulting in the observed $pK_{a,\,OX}$ of the N(5). Consequently, the here determined apparent pK_a may be an artifact arising from the independent expression of the HydB subunit.

This interpretation gains support from observations in the homologous complex I. Specifically, the FMN-containing NuoF subunit within the NuoEF subcomplex, homolog to the HydBC subcomplex, has been demonstrated only to be stable in co-expression with NuoE, while separate expressions of NuoF lead to the formation of inclusion bodies[243]. Consequently, NuoE was proposed to play a primary role in stabilizing this subcomplex [19]. However, the parallel with complex I breaks down in the face of the successful over-expression of HydB without the formation of inclusion bodies, hinting at a more stable protein packing, potentially attributable to the presence of additional stabilizing domains in HydB which are absent in NuoF.

In order to distinguish the here proposed claims with the obtained thermodynamic properties of HydB representing a "HydC-out"-like state of HydABC from contrarily being artifactual as a product of the isolated HydB expression, the following results need to be obtained:

In addition to the above suggested structure models of the isolated HydB and a "HydC-out"-like state of HydABC from *T. maritima*, separate experiments on the HydABC with a stabilized "HydC-out" state should be conducted. The stabilization of this state might be realized via site-directed mutagenesis on the flexible HydC loop that connects the mobile Trx-like domain with C1 to the N-terminal four-helical bundle domain, which "anchors" HydC to the HydB subunit. This domain contains a conserved proline residue (^{HydC}P69 in *T. maritima*) surrounded by multiple lysine residues. Prolines are frequently found in loop regions, since its side chain cyclizes back to the backbone amide, making them ideal disrupting residues of secondary structures that correlates with conformational flexibility[117]. Mutating this residue to a much heavier and apolar sidechain such as tryptophan, might abolish the HydC-movement and stabilize a "HydC-out"-like state. If the pH-dependent redox properties of the FMN as observed in HydB, could be reproduced in this state of HydABC, an artifactual nature of the results could be doubted. Preliminary indications from experiments conducted in HydABC during this thesis might be tentatively interpreted in this way. During electrochemical

redox titrations monitored by UV/Vis at low pH, spectral signs of a NSR in a fraction of the total FMN population was obtained.

5.2.6 Characterization of the FMN in HydABC

Spectroelectrochemical redox titration experiments on the apo-enzyme, HydABC revealed distinctive absorbance changes resembling the spectral properties of a flavin occuring at approximately +60 mV higher redox potentials than the OX-NSR transition of the FMN in HydB across the entire pH-range (5.17 to 9.23, appendix figure 3). They suggest an apparent two-electron, oxidized to fully-reduced transition, particularly evident at high pH values (above pH 7), without displaying any spectral indications of an anionic or neutral semi-reduced state (appendix figure 4). Yet, these absorbance changes were exclusively fitted for a single dataset at pH 7.92 with a corresponding n = 2 Nernst curve (see appendix figure 3). Conversely, for the majority of titration curves, these changes aligned best with a one-electron (n = 1) redox transition. At low pH-values, small spectral contributions of a NSR state could be observed (approximating maximally 30% of the FMN concentration), but remained near the detection limit, primarily due to the low protein concentration that could be used (∼8.5 to 15 μM HydABC, with 60% FMN occupation as compared to ∼15 to 30 μM HydB with 100% FMN occupation). As hinted above, this result could also be interpreted as a small population of the enzyme in the HydC-out state, which as suggested above is like HydB and thus stabilizes the spectrally detectable NSR state. EPR samples of HydABC poised to redox potentials that should feature a NSR population according to the spectral changes observed in UV/Vis (-120 mV at pH 6 and -250 mV at pH 9) did not reveal any EPR-detectable, semi-reduced radical signal. The absence of a radical signal in EPR and the spectrally apparent two-electron oxidized to reduced transition in UV/Vis at such high redox potentials would be indicative for crossed-over redox transitions for the FMN in HydABC. However, an n = 1 Nernstian behavior for this spectrally apparently n = 2 transition of the flavin in UV/Vis renders any interpretation rather speculative. Any technical issues that would explain the observed incongruencies between EPR and UV/Vis in the case of the FMN in HydABC are rather unlikely. Both types of spectroscopy were congruent in respect to the redox potential assignment of the low- and high potential wave of the three Trx-like [2Fe-2S]-clusters, which was attributed to A5 in the C-terminal domain of HydA at -270 mV and B1 in the N-terminal domain of HydB at near -550 mV (chapter 4).

5.2.7 Interactions of HydABC and HydB with NAD^+/NADH

According to the above provided interpretation of the isoalloxazine's pK_a-values, the N(5) is the main turning knob which is modulated by the protein environment in order to tune the redox properties of the FMN in HydB. This site is also the protonation site during the hydride transfer from the obligatory

two-electron donor, NAD(P)H (see introduction section 1.6.4, page 64).

Interestingly, the oxidized FMN in HydB is also reducible by NADH under the formation of a NSR state. Upon the 2-electron reduction of the FMN by NADH, the formation of the NSR would need to be accompanied by the reduction of a nearby FeS-cofactor. However, no signs of such a reduction was noted. The highest potential [4Fe-4S]-cluster in HydB is proposed to be located in the Fd-like 8Fe domain, with a redox potential of -375 mV. Whereas a 15x fold excess of NADH (as employed during this experiment) should at least partially reduce this cluster, the distance between the 8Fe domain and the FMN might place it out of reach, as it is not found to be reduced. A possible explanation therefore is the reduction of the above mentioned [3Fe-4S]-clusters, which formed as degraded [4Fe-4S]-clusters and were commonly observed in HydB and HydABC, characterized by rather high potentials approximating -100 mV (data not shown). The observation of a stabilized NSR state and the ability of the FMN to become reduced by excess of NADH, highlights the redox flexibility of the FMN in HydB.

In HydABC, only the addition of NADH or supplying NAD^+ to the pre-reduced complex allows the detection of a NSR state as observed in EPR. While these results lack detailed quantification, the mere presence of an otherwise undetectable NSR radical for the FMN in HydABC in the presence of NADH suggests the influencing effect of NADH on the redox cooperativity of the FMN. These experiments show that the FMN in both HydABC and HydB can be observed in an NADH oxidizing state, under the formation of a NSR.

A prospective avenue for this study involves conducting equilibrium redox titrations on HydABC with varying NAD^+/NADH ratios to quantify the impact of the presumed "high-potential" substrate on the redox potential landscape of HydABC. Leveraging the assigned spectral characteristics, particularly from EPR data, as presented above in section 5.1.1, will facilitate a straightforward assessment of the influence exerted by NAD^+/NADH. Insights from thermodynamic studies on other NADH-dehydrogenases, such as the homologous complex I[182;198], and xanthine-dehydrogenase[101], have demonstrated a notable upshift in the redox potentials of the flavin in the presence of the high-potential substrate couple, NAD^+/NADH. This shift has primarily been attributed to the positively charged nicotinamide head group of the oxidized NAD^+. Moreover, the redox potential of the adjacent FeS-cluster in these proteins have demonstrated susceptibility to the binding state of NAD^+/NADH[101].

5.3 An electron-transferring redox landscape in HydB and HydABC

The minimal requirement for a thermodynamically coupled two-electron transfer via EB/EC demands crossed-over redox potentials of the bifurcating cofactor, alongside the presence of a high- and low-

potential one-electron acceptor in regard to the intermediate-potential, two-electron bifurcating center.

Illustrated in figure 5.2, the redox potential landscape of the FeS-cluster adjacent to the FMN in HydABC is notably more reducing, i.e., below -400 mV, as compared to the FMN. Though uncertainties regarding the precise redox properties of the FMN in HydABC persist, the spectrally observable transitions of the FMN, both in HydABC ($E_{OX\text{-}RED}$, potentially $n = 2$) and HydB ($E_{OX\text{-}NSR}$, $n = 1$), manifest at overall much higher redox potentials (above -280 mV) across the entire pH range. In addition, the strongly uncrossed redox potentials of the FMN in HydB quantified by a $\log(K_s) = 6.8$ are incompatible with the occurrence of FBEB/FBEC.

In absence of a high-potential electron donor to the flavin during the proposed electron-confurcating electron transfer, while excluding the external electron donor NAD(P)H, due to its obligatory two-electron transfer character, renders FBEC in HydABC from *T. maritima* in analogy to the introductory scheme derived from the quinone-based electron bifurcating Rieske/cyt*b*-complexes highly improbable. The thermodynamic architecture sampled during this thesis in HydB and HydABC rather favors a one-by-one electron-transferring function of the FMN. From a purely thermodynamic point of view, the fully-reduced FMN in HydB as documented here ($E = \sim$ -550 mV), could reduce any the two FeS-cluster in electron-transferring distance, C1 and B2, while both FeS-clusters could easily reduce the oxidized FMN to the NSR state.

From the observation of different conformational arrangements in the nearby FeS domains in the HydBC subcomplex (figure 5.10), namely the two Trx-like [2Fe-2S] domains, one in the C-terminus of HydC (containing C1) and the other in the N-terminus of HydB (containing B1) as well as an 8Fe-Fd domain (containing two [4Fe-4S]-clusters, termed B3 and B4) alongside with rearrangements around the FMN binding site are the most likely candidates for driving the accompanied changes required for the fine-tuning of the redox state of the FMN inside the flavin-binding pocket.

I argued in the second part, that the thermodynamic parameters obtained for the isolated HydB subunit and the entire HydABC complex potentially reflect some of these functional states of the HydABC which can be potentially correlated with the observed conformational states (figure 5.10). However, none of these states are shown to represent a functional state conducive for electron confurcation in analogy to the Rieske/cyt*b*-complex.

Under the assumption that long-range electrostatic effects that extend from beyond the HydBC subcomplex have a minimal influence on the thermodynamic properties of the flavin, the redox characteristics of the FMN observed in the separate flavin-containing HydB subunit can be assumed to represent a state of the HydABC complex with the Trx-like C1-cluster domain of HydC being in the “HydC-out” state (figure 5.10 left).

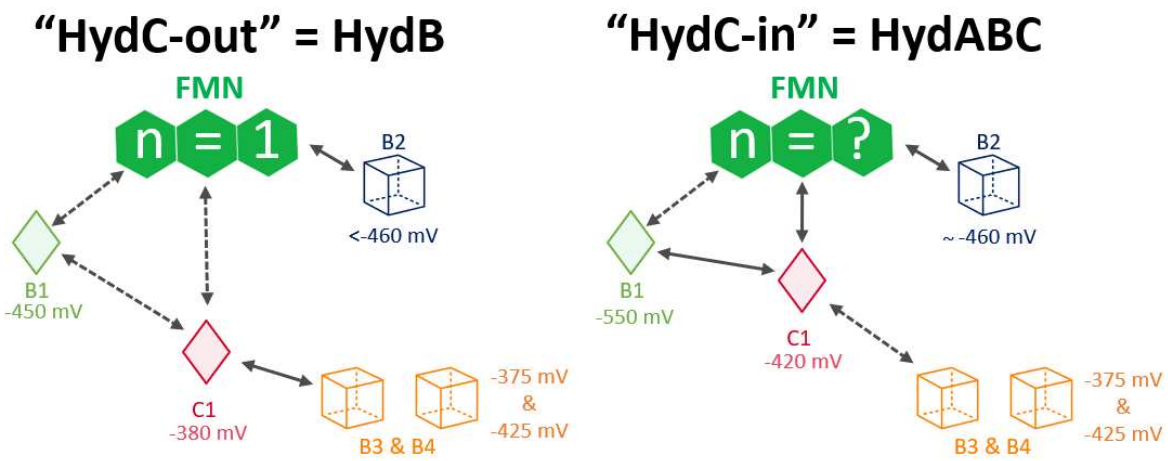

Figure 5.10: Association of the experimentally determined redox-potentials to the conformationally observed states of HydABC. Based on the introduction figure 1.14 , the two proposed conformational states of the Trx-like [2Fe-2S]-cluster domain containing C1 in HydC “HydC-out” (left) and “HydC-in” (right) are associated to the here determined redox-potentials in the isolated HydB and the entire HydABC, respectively. The proposed electron transfer distances in the two states are reflected by straight or dashed lines when below or above 14 Å, respectively. The redox potentials of the three [4Fe-4S]-clusters B2, B3 and B4 are assumed to stay largely unchanged.

Contrarily, a rather speculative assumption includes that the thermodynamically characterized HydABC from *T. maritima* during this thesis has been predominantly in the ”HydC-in” state. In this state, the presence of the Trx-like [2Fe-2S]-cluster domain of HydC near the FMN-binding site is the main factor differentiating the FMN environment in HydABC from the environment in the separate flavin-containing HydB subunit alone (figure 5.10 right). This is suggested by a more destabilized neutral semi-reduced state in HydABC as compared to HydB, as observed by the absence (in EPR) or minimal signs (in UV/Vis) of any semi-reduced spectral characteristics.

The thermodynamic parameters that were determined and attributed to specific cofactors around the FMN in the isolated HydB subunit and the HydABC complex over the course of this thesis are summarized in figure 5.10. The main difference in the redox properties of the FeS-cofactors in the HydBC complex in these two conformations primarily concerns the Trx-like [2Fe-2S]-cluster B1 in HydB and the FMN. The approximately 100 mV difference for the HydB B1 cluster between the two configurations is highly suggestive for an electrostatic influence of the neighboring reduced C1-cluster, the only FeS-cluster in electron-transferring distance to B1. Besides the structural state of the Trx-like [2Fe-2S]-cluster domain in HydC, the presence or absence of the high-potential substrate $NAD(P)^+$/NAD(P)H are suggested to have a significant effect on degree of redox cooperativity of the single FMN.

Chapter 6 Conclusions

6.1 Conclusions

This thesis has embedded the [FeFe]-hydrogenase HydABC in its phylogenetic context and for the first time supplied thermodynamic data (primarily redox potentials) of most FeS-clusters and the central FMN in the HydABC of *Thermotoga maritima*, a representative of the ferredoxin-dependent NAD(P)H dehydrogenase family, in absence of the natural substrates. The determined redox potential landscape of HydABC was demonstrated not to be conducive for flavin-based electron confurcation (FBEC) by following the redox scheme elaborated for quinone-based electron bifurcation (QBEB) of the Rieske/cyt*b* complexes. This requires inverted redox potentials of a two-electron compound and the presence of two distinct one-electron centers with redox potentials substantially higher and lower than the two-electron potential of the electron-bifurcating center.

This concept adequately explains FBEB/FBEC not only for Rieske/cyt*b* complexes but also for the flavoenzymes Etf and Nfn. It has also been suggested to apply to respiratory complex I, a homolog of HydABC.

At variance with all the above cited enzymes, HydABC from *T. maritima* not only catalyzes electron transfer from two distinct electron donors, NADH and ferredoxin, to a single electron acceptor, H^+, but also has to deal with the obligatory two-electron transfer characteristics of one of the electron donors namely NADH and this with the presence of a single catalytic flavin in the enzyme.

We cannot imagine a reaction scheme without variable redox characteristics of the flavin that thereby could fulfill different roles such as NADH oxidation, electron confurcation and one-by-one electron transfer. In this work a variability of the redox characteristics of the flavin was shown, compatible with NADH oxidation and a one-by-one electron transfer. Proof for the electron confurcating capabilities of this FMN or for a different, so far elusive mechanism remains to be found. While the influence of the flavin-binding substrate NAD(P)H on the elaborated thermodynamic landscape of HydABC demands further investigations, an universal application of the inverted redox potential scheme to explain EB/EC is put into question.

Chapter A
Appendix

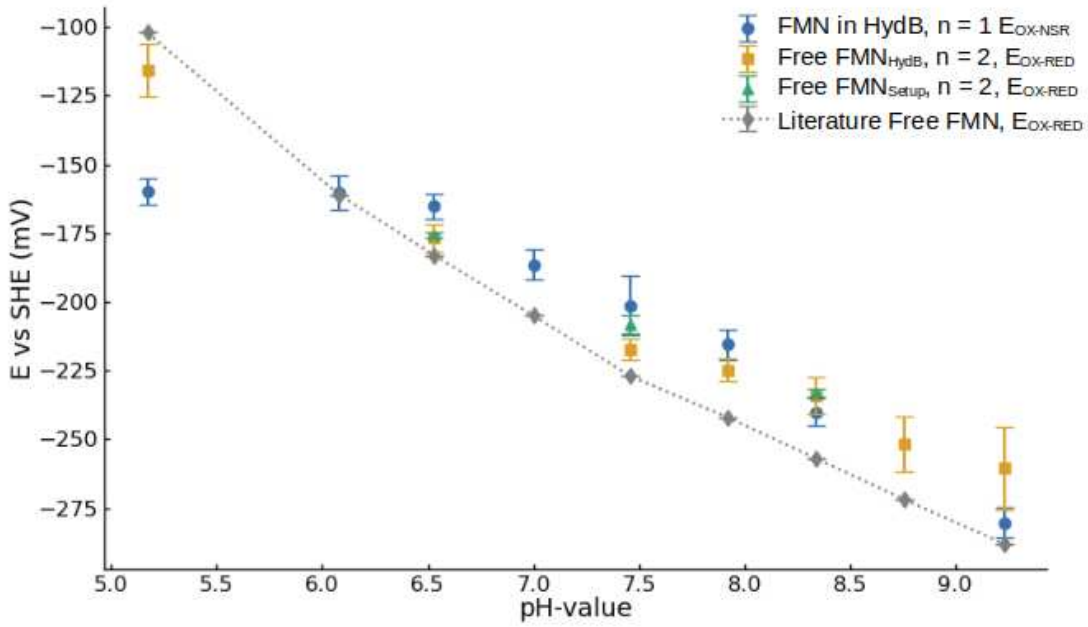

Appendix Figure 1: FMN-related redox potentials obtained during electrochemical redox titrations. In addition to the one-electron redox transition $E_{OX/NSR}$ of the FMN in HydB (blue dots), a gradual release of bound FMN by the HydB was accompanied with an increasing fraction (max. 50%) of free FMN in the buffer, undergoing a characteristic 2-electron transfer (n = 2, yellow squares). The two FMN populations were distinguished by separately analyzing the mediator-corrected absorbance change at 604 nm, sorely indicative for the NSR redox state, i.e., for the FMN in HydB (see Appendix Figure 2). The free FMN population was consequently assessed, by subtracting the OX-NSR contribution contributing to the 450 nm absorbance by multiplying the NSR-absorbance at 604 nm by the 2.66 (Müller *et al*., 1977). The remaining signal titrated was fitted with a n = 2 Nernst fit.
Error bars represent standard deviation of the least-square Nernst-fit of multiple (consecutive) titration datasets (oxidation and reduction were fitted separately) during UV/Vis-monitored electrochemical redox titrations (as specified in the Supplementary Section of Chapter 4). The obtained results for the FMN in the solution were validated by performing the experiment with an FMN solution in the same electrochemical setup with the same buffer at three pH-values (green triangles). The results are compared to the literature free FMN E_{OX-RED} transition potentials (grey diamonds, Mayhew *et al*., 1999).

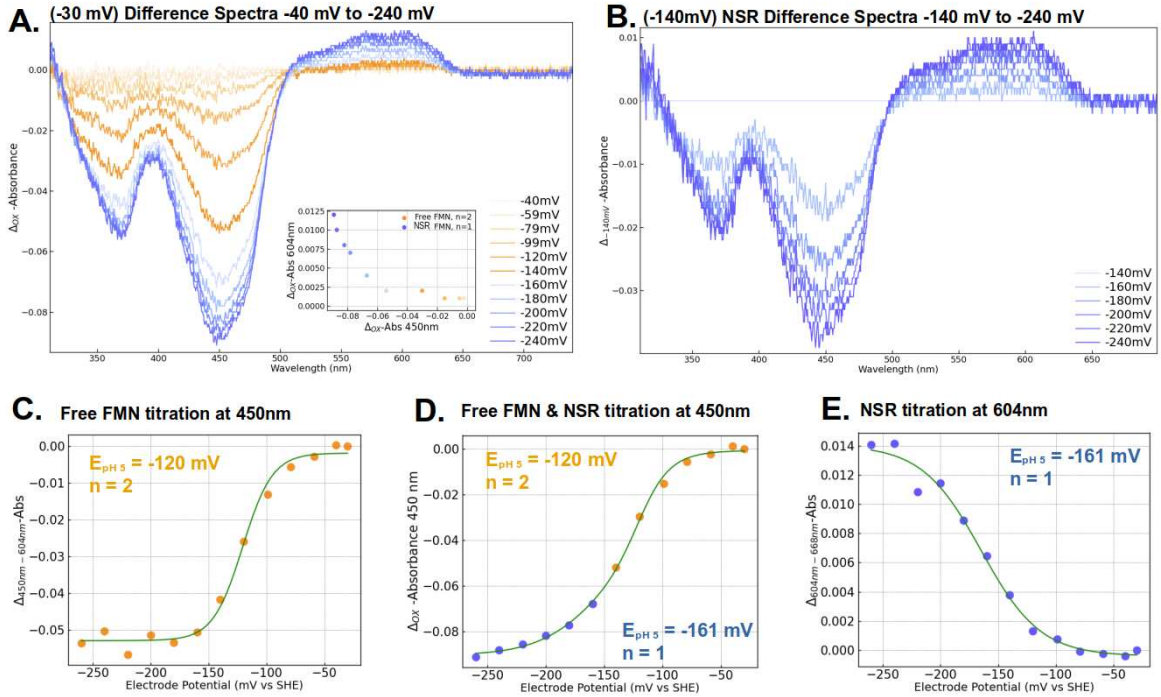

Appendix Figure 2: Free FMN (n = 2) and FMN Neutral Semi-reduced (NSR, n = 1) species during the electrochemical redox titrations of HydB at pH 5.17. **A.** Redox Titration data during reduction of HydB at pH 5.17 is shown as a difference to the most oxidized spectra (at -30 mV vs. SHE) of the second oxidation-reduction cycle. Spectra allows to clearly distinguish two populations of FMN containing free FMN (n = 2, in orange) which was released over the course of the experiment and the remaining bound FMN in HydB that forms NSR (n = 1, in blue). **B.** Difference Spectra to the last clear spectra belonging to the n = 2 FMN population (at -140 mV vs. SHE) highlights the n = 1 FMN NSR population at slightly lower redox potentials. **D.** Both populations can be titrated at 450 nm together without mediator subtraction, giving rise to an n = 2 behavior at high potentials and an n = 1 behavior at low potentials. After subtraction of the mediators (as described in the Chapter 4) both populations can be easily titrated. **E.** Titration curve of the mediator-subtracted NSR follows an n = 1 curve with $E_{pH\,5}$ = -161 mV. **C.** Subtraction of the NSR contribution at 450 nm then allowed an n = 2 fit at 450 nm to account exclusively for the aqueous FMN population undergoing an OX to RED transition at a potential of -120 mV.

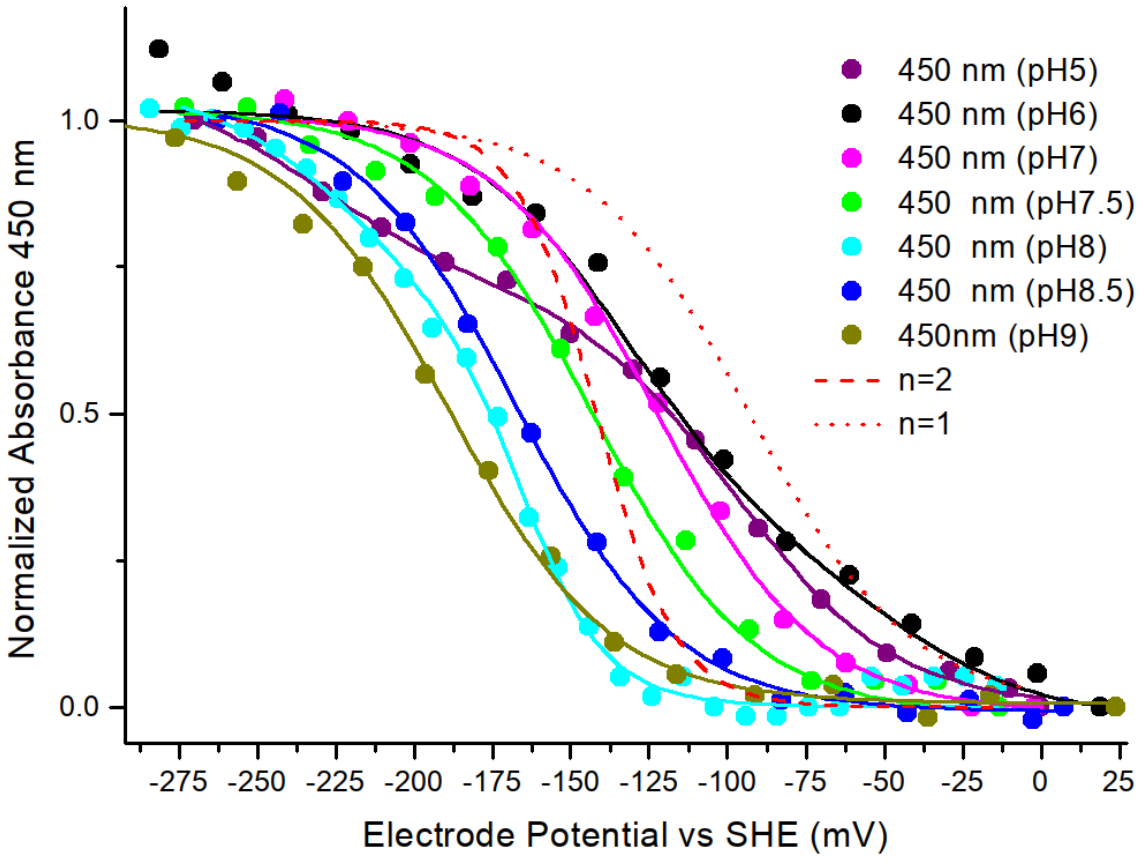

Appendix Figure 3: Redox Titration Behavior of the FMN in HydABC at various pH-values. Spectro-electrochemical redox titration curves assigned to the FMN in HydABC are shown across the sampled redox range from pH 5.17 to 9.23, as for HydB. The normalized, absolute absorbance change at 450 nm, indicative for the FMN in HydABC is best fitted with an n = 1 Nernst-Curve (red, dotted) instead of an n = 2 (red, dashed), with the exception of the dataset at pH 8 (cyan). Contributions of the mediators and the high-potential Trx-like [2Fe-2S]-cluster affect the titration curve below -170 mV.

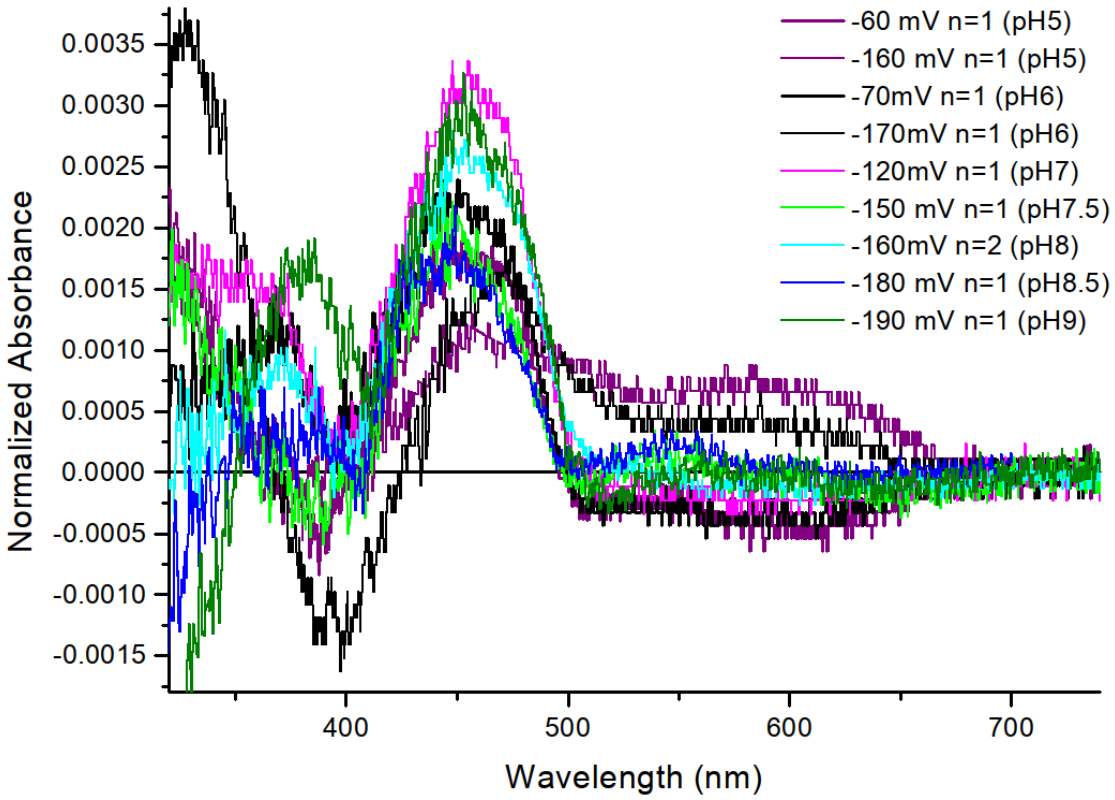

Appendix Figure 4: Difference spectra assigned to the FMN transition in HydABC at various pH-values. Corresponding to the redox titration curves in Appendix Figure 3, the difference spectra for the normalized absorbance of 1 µM protein from the spectro-electrochemical redox titration assigned to the FMN in HydABC are shown across the sampled redox range from pH 5.17 to 9.23, as for HydB. As indicated in the main text, at pH 5 (magenta) and pH 6 (black) indications of a NSR state with characteristic broad bands in the 500 nm to 620 nm regions are observed. Difference spectra for the $E_{OX\text{-}NSR}$ (thin line) and $E_{NSR\text{-}RED}$ (thick line) are given.

!

Chapter Bibliography

[1] R. Aasa, J. Bergström, and T. Vänngård, *On the interaction and orientation of the iron-sulfur centers A and B in chloroplasts of higher plants*, Biochimica et Biophysica Acta (BBA) - Bioenergetics, 637 (1981), pp. 118–123.

[2] M. W. Adams, *The structure and mechanism of iron-hydrogenases*, Biochimica et Biophysica Acta (BBA) - Bioenergetics, 1020 (1990), pp. 115–145.

[3] E. T. Adman, L. C. Sieker, and L. H. Jensen, *The Structure of a Bacterial Ferredoxin*, Journal of Biological Chemistry, 248 (1973), pp. 3987–3996.

[4] R. G. Agarwal, S. C. Coste, B. D. Groff, A. M. Heuer, H. Noh, G. A. Parada, C. F. Wise, E. M. Nichols, J. J. Warren, and J. M. Mayer, *Free Energies of Proton-Coupled Electron Transfer Reagents and Their Applications*, Chem. Rev., 122 (2022), pp. 1–49.

[5] R. F. Anderson, *Energetics of the one-electron steps in the NAD^+/NADH redox couple*, Biochimica et Biophysica Acta (BBA) - Bioenergetics, 590 (1980), pp. 277–281.

[6] ——, *Energetics of the one-electron reduction steps of riboflavin, FMN and FAD to their fully reduced forms*, Biochimica et Biophysica Acta (BBA) - Bioenergetics, 722 (1983), pp. 158–162.

[7] L. Appel, M. Willistein, C. Dahl, U. Ermler, and M. Boll, *Functional diversity of prokaryotic HdrA(BC) modules: Role in flavin-based electron bifurcation processes and beyond*, Biochimica et Biophysica Acta (BBA) - Bioenergetics, 1862 (2021), p. 148379.

[8] J. H. Artz, M. Tokmina-Lukaszewska, D. W. Mulder, C. E. Lubner, K. Gutekunst, J. Appel, B. Bothner, M. Boehm, and P. W. King, *The structure and reactivity of the hoxefu complex from the cyanobacterium Synechocystis sp. PCC 6803*, Journal of Biological Chemistry, 295 (2020), pp. 9445–9454.

[9] M. Asso, O. Mbarki, B. Guigliarelli, T. Yagi, and P. Bertrand, *EPR and Redox Characterization of Ferredoxins I and II from Desulfovibrio vulgaris Miyazaki*, Biochemical and Biophysical Research Communications, 211 (1995), pp. 198–204.

[10] D. W. Bak and S. J. Elliott, *Alternative FeS cluster ligands: tuning redox potentials and chemistry*, Current Opinion in Chemical Biology, 19 (2014), pp. 50–58.

[11] M. G. Bakker, B. Fowler, M. K. Bowman, and G. S. Patience, *Experimental methods in chemical engineering: electron paramagnetic resonance spectroscopy-epr/esr*, The Canadian Journal of Chemical Engineering, 98 (2020), pp. 1668–1681.

[12] F. Baymann, E. Lebrun, M. Brugna, B. Schoepp–Cothenet, M. Giudici–Orticoni, and W. Nitschke, *The redox protein construction kit: pre-last universal common ancestor evolution of energy-conserving enzymes*, Phil. Trans. R. Soc. Lond. B, 358 (2003), pp. 267–274.

[13] F. Baymann, B. Schoepp-Cothenet, S. Duval, M. Guiral, M. Brugna, C. Baffert, M. J. Russell, and W. Nitschke, *On the Natural History of Flavin-Based Electron Bifurcation*, Front. Microbiol., 9 (2018), p. 1357.

[14] H. Beinert, *Erratum to: Iron-sulfur proteins: ancient structures, still full of surprises*, J Biol Inorg Chem, 5 (2000), pp. 409–409.

[15] H. Beinert, R. H. Holm, and E. Münck, *Iron-Sulfur Clusters: Nature's Modular, Multipurpose Structures*, Science, 277 (1997), pp. 653–659.

[16] L. Bergdoll, F. Ten Brink, W. Nitschke, D. Picot, and F. Baymann, *From low- to high-potential bioenergetic chains: Thermodynamic constraints of Q-cycle function*, Biochimica et Biophysica Acta (BBA) - Bioenergetics, 1857 (2016), pp. 1569–1579.

[17] E. A. Berry and L.-s. Huang, *Observations concerning the quinol oxidation site of the cytochrome bc $_1$ complex*, FEBS Letters, 555 (2003), pp. 13–20.

[18] J. A. Birrell, C. Laurich, E. J. Reijerse, H. Ogata, and W. Lubitz, *Importance of Hydrogen Bonding in Fine Tuning the [2Fe-2S] Cluster Redox Potential of HydC from Thermotoga maritima*, Biochemistry, 55 (2016), pp. 4344–4355.

[19] J. A. Birrell, K. Morina, H. R. Bridges, T. Friedrich, and J. Hirst, *Investigating the function of [2Fe–2S] cluster N1a, the off-pathway cluster in complex I, by manipulating its reduction potential*, Biochemical Journal, 456 (2013), pp. 139–146.

[20] G. BLANKENHORN, *Flavin-Nicotinamide Biscoenzymes: Models for the Interaction between NADH (NADPH) and Flavin in Flavoenzymes. Reaction Rates and Physicochemical Properties of Intermediate Species*, Eur J Biochem, 50 (1975), pp. 351–356.

[21] ——, *Nicotinamide-Dependent One-Electron and Two-Electron (Flavin) Oxidoreduction : Thermodynamics, Kinetics, and Mechanism*, Eur J Biochem, 67 (1976), pp. 67–80.

[22] Y. J. BOLLEN, A. H. WESTPHAL, S. LINDHOUD, W. J. VAN BERKEL, AND C. P. VAN MIERLO, *Distant residues mediate picomolar binding affinity of a protein cofactor*, Nature communications, 3 (2012), p. 1010.

[23] A. BOREK, A. WÓJCIK-AUGUSTYN, P. KULETA, R. EKIERT, AND A. OSYCZKA, *Identification of hydrogen bonding network for proton transfer at the quinol oxidation site of Rhodobacter capsulatus cytochrome bc_1*, Journal of Biological Chemistry, 299 (2023), p. 105249.

[24] C. A. BOTTOMS, P. E. SMITH, AND J. J. TANNER, *A structurally conserved water molecule in Rossmann dinucleotide-binding domains*, Protein Science, 11 (2002), pp. 2125–2137.

[25] L. H. BRADLEY AND R. P. SWENSON, *Role of Glutamate-59 hydrogen bonded to N (3) H of the flavin mononucleotide cofactor in the modulation of the redox potentials of the Clostridium beijerinckii flavodoxin. Glutamate-59 is not responsible for the pH dependency but contributes to the stabilization of the flavin semiquinone*, Biochemistry, 38 (1999), pp. 12377–12386.

[26] ——, *Role of hydrogen bonding interactions to N(3)H of the flavin mononucleotide cofactor in the modulation of the redox potentials of the Clostridium beijerinckii flavodoxin*, Biochemistry, 40 (2001), pp. 8686–8695.

[27] E. BRANSCOMB, T. BIANCALANI, N. GOLDENFELD, AND M. RUSSELL, *Escapement mechanisms and the conversion of disequilibria; the engines of creation*, Physics Reports, 677 (2017), pp. 1–60.

[28] E. BRANSCOMB AND M. J. RUSSELL, *Turnstiles and bifurcators: The disequilibrium converting engines that put metabolism on the road*, Biochimica et Biophysica Acta (BBA) - Bioenergetics, 1827 (2013), pp. 62–78.

[29] M. BRAUN, S. BUNGERT, AND T. FRIEDRICH, *Characterization of the overproduced nadh dehydrogenase fragment of the nadh: ubiquinone oxidoreductase (complex i) from escherichia coli*, Biochemistry, 37 (1998), pp. 1861–1867.

[30] W. BUCKEL, *Energy conservation in fermentations of anaerobic bacteria*, Frontiers in Microbiology, 12 (2021).

[31] W. BUCKEL AND R. K. THAUER, *Energy conservation via electron bifurcating ferredoxin reduction and proton/Na^+ translocating ferredoxin oxidation*, Biochimica et Biophysica Acta (BBA) - Bioenergetics, 1827 (2013), pp. 94–113.

[32] ——, *Flavin-Based Electron Bifurcation, A New Mechanism of Biological Energy Coupling*, Chem. Rev., 118 (2018), pp. 3862–3886.

[33] ——, *Flavin-Based Electron Bifurcation, Ferredoxin, Flavodoxin, and Anaerobic Respiration With Protons (Ech) or NAD^+ (Rnf) as Electron Acceptors: A Historical Review*, Front. Microbiol., 9 (2018), p. 401.

[34] R. M. BURNETT, G. D. DARLING, D. S. KENDALL, M. E. LEQUESNE, S. G. MAYHEW, W. W. SMITH, AND M. L. LUDWIG, *The structure of the oxidized form of clostridial flavodoxin at 1.9-Å resolution: Description of the flavin mononucleotide binding site.*, Journal of Biological Chemistry, 249 (1974), pp. 4383–4392.

[35] F. CALISTO, F. M. SOUSA, F. V. SENA, P. N. REFOJO, AND M. M. PEREIRA, *Mechanisms of Energy Transduction by Charge Translocating Membrane Proteins*, Chem. Rev., 121 (2021), pp. 1804–1844.

[36] R. CAMMACK AND F. MACMILLAN, *Electron Magnetic Resonance of Iron–Sulfur Proteins in Electron-Transfer Chains: Resolving Complexity*, in Metals in Biology, G. Hanson and L. Berliner, eds., vol. 29, Springer New York, New York, NY, 2010, pp. 11–44. Series Title: Biological Magnetic Resonance.

[37] J. L. CAPE, M. K. BOWMAN, AND D. M. KRAMER, *Understanding the cytochrome bc complexes by what they don't do. The Q-cycle at 30*, Trends in Plant Science, 11 (2006), pp. 46–55.

[38] G. CECCHINI, I. SCHRÖDER, R. P. GUNSALUS, AND E. MAKLASHINA, *Succinate dehydrogenase and fumarate reductase from Escherichia coli*, Biochimica et Biophysica Acta (BBA)-Bioenergetics, 1553 (2002), pp. 140–157.

[39] F.-C. CHANG AND R. P. SWENSON, *The midpoint potentials for the oxidized-semiquinone couple for Gly57 mutants of the Clostridium beijerinckii flavodoxin correlate with changes in the hydrogen-bonding interaction with the proton on N(5) of the reduced flavin mononucleotide cofactor as measured by NMR chemical shift temperature dependencies*, Biochemistry, 38 (1999), pp. 7168–7176.

[40] C. CHATELET, J. GAILLARD, Y. PÉTILLOT, M. LOUWAGIE, AND J. MEYER, *A [2Fe-2S] protein from*

the hyperthermophilic Bacterium Aquifex aeolicus, Biochemical and Biophysical Research Communications, 261 (1999), pp. 885–889.

[41] N. CHONGDAR, K. PAWLAK, O. RÜDIGER, E. J. REIJERSE, P. RODRÍGUEZ-MACIÁ, W. LUBITZ, J. A. BIRRELL, AND H. OGATA, *Spectroscopic and biochemical insight into an electron-bifurcating [FeFe] hydrogenase*, J Biol Inorg Chem, 25 (2020), pp. 135–149.

[42] N. P. CHOWDHURY, A. M. MOWAFY, J. K. DEMMER, V. UPADHYAY, S. KOELZER, E. JAYAMANI, J. KAHNT, M. HORNUNG, U. DEMMER, U. ERMLER, AND W. BUCKEL, *Studies on the Mechanism of Electron Bifurcation Catalyzed by Electron Transferring Flavoprotein (Etf) and Butyryl-CoA Dehydrogenase (Bcd) of Acidaminococcus fermentans*, Journal of Biological Chemistry, 289 (2014), pp. 5145–5157.

[43] S. L. CHRISTGEN, S. M. BECKER, AND D. F. BECKER, *Methods for determining the reduction potentials of flavin enzymes*, in Methods in Enzymology, vol. 620, Elsevier, 2019, pp. 1–25.

[44] W. M. CLARK, *Modifications of primary equations to account for the formation of intermediate free radicals,* "*semiquinones*", in Oxidation-Reduction Potentials of Organic Systems., Williams & Wilkins, Baltimore, Maryland, 1960.

[45] A. R. CROFTS, *Proton-coupled electron transfer at the Q_o-site of the bc_1 complex controls the rate of ubihydroquinone oxidation*, Biochimica et Biophysica Acta (BBA) - Bioenergetics, 1655 (2004), pp. 77–92.

[46] A. R. CROFTS, M. GUERGOVA-KURAS, L. HUANG, R. KURAS, Z. ZHANG, AND E. A. BERRY, *Mechanism of Ubiquinol Oxidation by the bc_1 Complex: Role of the Iron Sulfur Protein and Its Mobility*, Biochemistry, 38 (1999), pp. 15791–15806.

[47] A. R. CROFTS, S. HONG, N. UGULAVA, B. BARQUERA, R. GENNIS, M. GUERGOVA-KURAS, AND E. A. BERRY, *Pathways for proton release during ubihydroquinone oxidation by the bc_1 complex*, Proc. Natl. Acad. Sci. U.S.A., 96 (1999), pp. 10021–10026.

[48] A. R. CROFTS, S. HONG, C. WILSON, R. BURTON, D. VICTORIA, C. HARRISON, AND K. SCHULTEN, *The mechanism of ubihydroquinone oxidation at the Q_o-site of the cytochrome bc_1 complex*, Biochimica et Biophysica Acta (BBA) - Bioenergetics, 1827 (2013), pp. 1362–1377.

[49] A. R. CROFTS AND S. ROSE, *Marcus treatment of endergonic reactions: A commentary*, Biochimica et Biophysica Acta (BBA) - Bioenergetics, 1767 (2007), pp. 1228–1232.

[50] A. R. Crofts, V. P. Shinkarev, D. R. Kolling, and S. Hong, *The Modified Q-cycle Explains the Apparent Mismatch between the Kinetics of Reduction of Cytochromes c_1 and b_H in the bc_1 Complex*, Journal of Biological Chemistry, 278 (2003), pp. 36191–36201.

[51] K. Crozier-Reabe and G. R. Moran, *Form follows function: structural and catalytic variation in the class a flavoprotein monooxygenases*, International journal of molecular sciences, 13 (2012), pp. 15601–15639.

[52] D. Cui, R. L. Koder Jr, P. L. Dutton, and A.-F. Miller, *15N solid-state NMR as a probe of flavin H-bonding*, The Journal of Physical Chemistry B, 115 (2011), pp. 7788–7798.

[53] E. Davidson, T. Ohnishi, E. Atta-Asafo-Adjei, and F. Daldal, *Potential ligands to the [2Fe-2S] Rieske cluster of the cytochrome bc_1 complex of Rhodobacter capsulatus probed by site-directed mutagenesis*, Biochemistry, 31 (1992), pp. 3342–3351.

[54] S. De Causmaecker, J. S. Douglass, A. Fantuzzi, W. Nitschke, and A. W. Rutherford, *Energetics of the exchangeable quinone, Q_B, in Photosystem II*, Proc. Natl. Acad. Sci. U.S.A., 116 (2019), pp. 19458–19463.

[55] S. de Vries, K. Dörner, M. J. Strampraad, and T. Friedrich, *Electron tunneling rates in respiratory complex i are tuned for efficient energy conversion*, Angewandte Chemie International Edition, 54 (2015), pp. 2844–2848.

[56] J. K. Demmer, J. Bertsch, C. Öppinger, H. Wohlers, K. Kayastha, U. Demmer, U. Ermler, and V. Müller, *Molecular basis of the flavin-based electron-bifurcating caffeyl-CoA reductase reaction*, FEBS Letters, 592 (2018), pp. 332–342.

[57] J. K. Demmer, H. Huang, S. Wang, U. Demmer, R. K. Thauer, and U. Ermler, *Insights into Flavin-based Electron Bifurcation via the NADH-dependent Reduced Ferredoxin:NADP Oxidoreductase Structure*, Journal of Biological Chemistry, 290 (2015), pp. 21985–21995.

[58] J. K. Demmer, N. Pal Chowdhury, T. Selmer, U. Ermler, and W. Buckel, *The semiquinone swing in the bifurcating electron transferring flavoprotein/butyryl-CoA dehydrogenase complex from Clostridium difficile*, Nature Communications, 8 (2017), p. 1577.

[59] J. K. Demmer, F. A. Rupprecht, M. L. Eisinger, U. Ermler, and J. D. Langer, *Ligand binding and conformational dynamics in a flavin-based electron-bifurcating enzyme complex revealed by Hydrogen–Deuterium Exchange Mass Spectrometry*, FEBS Letters, 590 (2016), pp. 4472–4479.

[60] A. DEY, F. E. JENNEY, M. W. W. ADAMS, E. BABINI, Y. TAKAHASHI, K. FUKUYAMA, K. O. HODGSON, B. HEDMAN, AND E. I. SOLOMON, *Solvent Tuning of Electrochemical Potentials in the Active Sites of HiPIP Versus Ferredoxin*, Science, 318 (2007), pp. 1464–1468.

[61] G. DI ROCCO, G. BATTISTUZZI, M. BORSARI, C. A. BORTOLOTTI, A. RANIERI, AND M. SOLA, *The enthalpic and entropic terms of the reduction potential of metalloproteins: Determinants and interplay*, Coordination Chemistry Reviews, 445 (2021), p. 214071.

[62] R. D. DRAPER AND L. L. INGRAHAM, *A potentiometric study of the flavin semiquinone equilibrium*, Archives of Biochemistry and Biophysics, 125 (1968), pp. 802–808.

[63] A.-L. DUCLUZEAU, B. SCHOEPP-COTHENET, R. VAN LIS, F. BAYMANN, M. J. RUSSELL, AND W. NITSCHKE, *The evolution of respiratory O_2 /NO reductases: an out-of-the-phylogenetic-box perspective*, J. R. Soc. Interface., 11 (2014), p. 20140196.

[64] R. V. ECK AND M. O. DAYHOFF, *Evolution of the Structure of Ferredoxin Based on Living Relics of Primitive Amino Acid Sequences*, Science, 152 (1966), pp. 363–366.

[65] D. E. EDMONDSON, *Electron-spin-resonance studies on flavoenzymes*, Biochemical Society Transactions, 13 (1985), pp. 593–600.

[66] A. EHRENBERG, F. MÜLLER, AND P. HEMMERICH, *Basicity, Visible Spectra, and Electron Spin Resonance of Flavosemiquinone Anions*, Eur J Biochem, 2 (1967), pp. 286–293.

[67] B. ENTSCH AND D. P. BALLOU, *Flavins*, Elsevier, 2013, pp. 309–313.

[68] D. H. EVANS, *One-Electron and Two-Electron Transfers in Electrochemistry and Homogeneous Solution Reactions*, Chem. Rev., 108 (2008), pp. 2113–2144.

[69] D. H. EVANS AND K. HU, *Inverted potentials in two-electron processes in organic electrochemistry*, Faraday Trans., 92 (1996), p. 3983.

[70] M. EVANS, *Determination of the oxidation—reduction potential of the bound iron-sulphur proteins of the primary electron acceptor complex of photosystem I in spinach chloroplasts*, FEBS Letters, 49 (1974), pp. 111–114.

[71] J. A. FARRINGTON, E. J. LAND, AND A. SWALLOW, *The one-electron reduction potentials of NAD*, Biochimica et Biophysica Acta (BBA) - Bioenergetics, 590 (1980), pp. 273–276.

[72] X. FENG, G. J. SCHUT, D. K. HAJA, M. W. ADAMS, AND H. LI, *Structure and electron transfer pathways of an electron-bifurcating nife-hydrogenase*, Science Advances, 8 (2022), p. eabm7546.

[73] X. FENG, G. J. SCHUT, G. L. LIPSCOMB, H. LI, AND M. W. W. ADAMS, *Cryoelectron microscopy structure and mechanism of the membrane-associated electron-bifurcating flavoprotein Fix/EtfABCX*, Proc. Natl. Acad. Sci. U.S.A., 118 (2021), p. e2016978118.

[74] N. FISCHER, P. SÉTIF, AND J.-D. ROCHAIX, *Targeted Mutations in the psaC Gene of Chlamydomonas reinhardtii : Preferential Reduction of F_b at Low Temperature Is Not Accompanied by Altered Electron Flow from Photosystem I to Ferredoxin*, Biochemistry, 36 (1997), pp. 93–102.

[75] M. W. FRAAIJE AND A. MATTEVI, *Flavoenzymes: diverse catalysts with recurrent features*, Trends in Biochemical Sciences, 25 (2000), pp. 126–132.

[76] T. FRIEDRICH, *On the mechanism of respiratory complex I*, J Bioenerg Biomembr, 46 (2014), pp. 255–268.

[77] T. FRIEDRICH AND B. BÖTTCHER, *The gross structure of the respiratory complex I: a LEGO system*, Biochimica et Biophysica Acta (BBA)-Bioenergetics, 1608 (2004), pp. 1–9.

[78] T. FRIEDRICH, D. K. DEKOVIC, AND S. BURSCHEL, *Assembly of the escherichia coli nadh: ubiquinone oxidoreductase (respiratory complex i)*, Biochimica Et Biophysica Acta (BBA)-Bioenergetics, 1857 (2016), pp. 214–223.

[79] T. FRIEDRICH AND T. POHL, *Nadh as donor*, EcoSal Plus, 2 (2007), pp. 10–1128.

[80] C. FURLAN, N. CHONGDAR, P. GUPTA, W. LUBITZ, H. OGATA, J. N. BLAZA, AND J. A. BIRRELL, *Structural insight on the mechanism of an electron-bifurcating [FeFe] hydrogenase*, eLife, 11 (2022), p. e79361.

[81] B. G. GALUZZI, A. MIRARCHI, E. L. VIGANÒ, L. DE GIOIA, C. DAMIANI, AND F. ARRIGONI, *Machine Learning for Efficient Prediction of Protein Redox Potential: The Flavoproteins Case*, J. Chem. Inf. Model., 62 (2022), pp. 4748–4759.

[82] S. GHISLA AND V. MASSEY, *Mechanisms of flavoprotein-catalyzed reactions*, Eur J Biochem, 181 (1989), pp. 1–17.

[83] S. GHISLA, V. MASSEY, J.-M. LHOSTE, AND S. G. MAYHEW, *Fluorescence and optical characteristics of reduced flavines and flavoproteins*, Biochemistry, 13 (1974), pp. 589–597.

[84] Q. GIBSON, V. MASSEY, AND N. ATHERTON, *The nature of compounds present in mixtures of oxidized and reduced flavin mononucleotides*, Biochemical Journal, 85 (1962), p. 369.

[85] D. GOLDFARB AND S. STOLL, eds., *EPR spectroscopy: fundamentals and methods*, Wiley, Chichester, West Sussex, 2018.

[86] M. González-Viegas, R. K. Kar, A.-F. Miller, and M.-A. Mroginski, *Non-covalent interactions that tune the reactivities of the flavins in bifurcating electron transferring flavoprotein*, Journal of Biological Chemistry, (2023), p. 104762.

[87] F. Grein, A. R. Ramos, S. S. Venceslau, and I. A. Pereira, *Unifying concepts in anaerobic respiration: Insights from dissimilatory sulfur metabolism*, Biochimica et Biophysica Acta (BBA) - Bioenergetics, 1827 (2013), pp. 145–160.

[88] S. Grimaldi, B. Schoepp-Cothenet, P. Ceccaldi, B. Guigliarelli, and A. Magalon, *The prokaryotic Mo/W-bisPGD enzymes family: A catalytic workhorse in bioenergetic*, Biochimica et Biophysica Acta (BBA) - Bioenergetics, 1827 (2013), pp. 1048–1085.

[89] J. Grodkowski, P. Neta, B. W. Carlson, and L. Miller, *One-electron transfer reactions of the couple NAD^+/NADH*, J. Phys. Chem., 87 (1983), pp. 3135–3138.

[90] B. Guigliarelli and P. Bertrand, *Application of EPR Spectroscopy to the Structural and Functional Study of Iron-Sulfur Proteins*, in Advances in Inorganic Chemistry, vol. 47, Elsevier, 1999, pp. 421–497.

[91] M. R. Gunner, J. Madeo, and Z. Zhu, *Modification of quinone electrochemistry by the proteins in the biological electron transfer chains: examples from photosynthetic reaction centers*, J Bioenerg Biomembr, 40 (2008), p. 509.

[92] R. J. Gurbiel, C. J. Batie, M. Sivaraja, A. E. True, J. A. Fee, B. M. Hoffman, and D. P. Ballou, *Electron-nuclear double resonance spectroscopy of nitrogen-15-enriched phthalate dioxygenase from Pseudomonas cepacia proves that two histidines are coordinated to the [2Fe-2S] Rieske-type clusters*, Biochemistry, 28 (1989), pp. 4861–4871.

[93] W. R. Hagen, *EPR spectroscopy of complex biological iron–sulfur systems*, J Biol Inorg Chem, 23 (2018), pp. 623–634.

[94] I. Hazekawa, Y. Nishina, K. Sato, M. Shichiri, R. Miura, and K. Shiga, *A Raman Study on the C(4)=O Stretching Mode of Flavins in Flavoenzymes: Hydrogen Bonding at the C(4)=O Moiety*, Journal of Biochemistry, 121 (1997), pp. 1147–1154.

[95] G. Herrmann, E. Jayamani, G. Mai, and W. Buckel, *Energy Conservation via Electron-Transferring Flavoprotein in Anaerobic Bacteria*, J Bacteriol, 190 (2008), pp. 784–791.

[96] J. P. Hoben, C. E. Lubner, M. W. Ratzloff, G. J. Schut, D. M. Nguyen, K. W. Hempel, M. W. Adams, P. W. King, and A.-F. Miller, *Equilibrium and ultrafast kinetic studies manipulating*

electron transfer: A short-lived flavin semiquinone is not sufficient for electron bifurcation, Journal of Biological Chemistry, 292 (2017), pp. 14039–14049.

[97] R. HUBER, T. A. LANGWORTHY, H. KÖNIG, M. THOMM, C. R. WOESE, U. B. SLEYTR, AND K. O. STETTER, *Thermotoga maritima sp. nov. represents a new genus of unique extremely thermophilic eubacteria growing up to 90°C*, Arch. Microbiol., 144 (1986), pp. 324–333.

[98] J. HUNT, V. MASSEY, W. DUNHAM, AND R. SANDS, *Redox potentials of milk xanthine dehydrogenase. Room temperature measurement of the FAD and 2Fe/2S center potentials.*, Journal of Biological Chemistry, 268 (1993), pp. 18685–18691.

[99] C. HUNTE, J. KOEPKE, C. LANGE, T. ROSSMANITH, AND H. MICHEL, *Structure at 2.3 Å resolution of the cytochrome bc_1 complex from the yeast Saccharomyces cerevisiae co-crystallized with an antibody Fv fragment*, Structure, 8 (2000), pp. 669–684.

[100] H. ISHIKITA, *Influence of the protein environment on the redox potentials of flavodoxins from Clostridium beijerinckii*, Journal of Biological Chemistry, 282 (2007), pp. 25240–25246.

[101] H. ISHIKITA, B. T. EGER, K. OKAMOTO, T. NISHINO, AND E. F. PAI, *Protein conformational gating of enzymatic activity in xanthine oxidoreductase*, Journal of the American Chemical Society, 134 (2012), pp. 999–1009.

[102] H. ISHIKITA AND K. SAITO, *Proton transfer reactions and hydrogen-bond networks in protein environments*, J. R. Soc. Interface., 11 (2014), p. 20130518.

[103] M. IWAKI, G. YAKOVLEV, J. HIRST, A. OSYCZKA, P. L. DUTTON, D. MARSHALL, AND P. R. RICH, *Direct Observation of Redox-Linked Histidine Protonation Changes in the Iron-Sulfur Protein of the Cytochrome bc $_1$ Complex by ATR-FTIR Spectroscopy*, Biochemistry, 44 (2005), pp. 4230–4237.

[104] S. IWATA, J. W. LEE, K. OKADA, J. K. LEE, M. IWATA, B. RASMUSSEN, T. A. LINK, S. RAMASWAMY, AND B. K. JAP, *Complete Structure of the 11-Subunit Bovine Mitochondrial Cytochrome bc $_1$ Complex*, Science, 281 (1998), pp. 64–71.

[105] G. JESCHKE, *EPR techniques for studying radical enzymes*, Biochimica et Biophysica Acta (BBA)-Bioenergetics, 1707 (2005), pp. 91–102.

[106] D. JOLLIE AND J. D. LIPSCOMB, *Formate dehydrogenase from Methylosinus trichosporium OB3b. purification and spectroscopic characterization of the cofactors.*, Journal of Biological Chemistry, 266 (1991), pp. 21853–21863.

[107] A. JUSZCZAK, S. AONO, AND M. ADAMS, *The extremely thermophilic eubacterium, Thermotoga maritima, contains a novel iron-hydrogenase whose cellular activity is dependent upon tungsten*, Journal of Biological Chemistry, 266 (1991), pp. 13834–13841.

[108] M. P. KABIR, Y. OROZCO-GONZALEZ, AND S. GOZEM, *Electronic spectra of flavin in different redox and protonation states: a computational perspective on the effect of the electrostatic environment*, Phys. Chem. Chem. Phys., 21 (2019), pp. 16526–16537.

[109] R. K. KAR, A. MILLER, AND M. MROGINSKI, *Understanding flavin electronic structure and spectra*, WIREs Comput Mol Sci, 12 (2022), p. e1541.

[110] A. KATSYV, S. JAIN, M. BASEN, AND V. MÜLLER, *Electron carriers involved in autotrophic and heterotrophic acetogenesis in the thermophilic bacterium Thermoanaerobacter kivui*, Extremophiles, 25 (2021), pp. 513–526.

[111] A. KATSYV, A. KUMAR, P. SAURA, M. C. PÖVERLEIN, S. A. FREIBERT, S. T. STRIPP, S. JAIN, A. P. GAMIZ-HERNANDEZ, V. R. I. KAILA, V. MÜLLER, AND J. M. SCHULLER, *Molecular Basis of the Electron Bifurcation Mechanism in the [FeFe]-Hydrogenase Complex HydABC*, J. Am. Chem. Soc., 145 (2023), pp. 5696–5709.

[112] K. KAYASTHA, A. KATSYV, C. HIMMRICH, S. WELSCH, J. M. SCHULLER, U. ERMLER, AND V. MÜLLER, *Structure-based electron-confurcation mechanism of the Ldh-EtfAB complex*, eLife, 11 (2022), p. e77095.

[113] K. KAYASTHA, S. VITT, W. BUCKEL, AND U. ERMLER, *Flavins in the electron bifurcation process*, Archives of Biochemistry and Biophysics, 701 (2021), p. 108796.

[114] P. KIERKEGAARD, R. NORRESTAM, P.-E. WERNER, A. EHRENBERG, L. E. G. ERIKSSON, AND F. MÜLLER, *X-Ray structure studies in some flavin derivatives*, Chem. Commun. (London), 0 (1967), pp. 288–289.

[115] A. KPEBE, M. BENVENUTI, C. GUENDON, A. REBAI, V. FERNANDEZ, S. LE LAZ, E. ETIENNE, B. GUIGLIARELLI, G. GARCÍA-MOLINA, A. L. DE LACEY, C. BAFFERT, AND M. BRUGNA, *A new mechanistic model for an o_1-protected electron-bifurcating hydrogenase, Hnd from Desulfovibrio fructosovorans*, Biochimica et Biophysica Acta (BBA) - Bioenergetics, 1859 (2018), pp. 1302–1312.

[116] C. KRAIYA AND D. H. EVANS, *Investigation of potential inversion in the reduction of 9,10-dinitroanthracene and 3,6-dinitrodurene*, Journal of Electroanalytical Chemistry, 565 (2004), pp. 29–35.

[117] F. KRIEGER, A. MÖGLICH, AND T. KIEFHABER, *Effect of proline and glycine residues on dynamics and barriers of loop formation in polypeptide chains*, Journal of the American Chemical Society, 127 (2005), pp. 3346–3352.

[118] A. KUMAR, F. KREMP, J. ROTH, S. A. FREIBERT, V. MÜLLER, AND J. M. SCHULLER, *Molecular architecture and electron transfer pathway of the Stn family transhydrogenase*, Nat Commun, 14 (2023), p. 5484.

[119] R. N. LEDBETTER, A. M. GARCIA COSTAS, C. E. LUBNER, D. W. MULDER, M. TOKMINA-LUKASZEWSKA, J. H. ARTZ, A. PATTERSON, T. S. MAGNUSON, Z. J. JAY, H. D. DUAN, J. MILLER, M. H. PLUNKETT, J. P. HOBEN, B. M. BARNEY, R. P. CARLSON, A.-F. MILLER, B. BOTHNER, P. W. KING, J. W. PETERS, AND L. C. SEEFELDT, *The Electron Bifurcating FixABCX Protein Complex from Azotobacter vinelandii : Generation of Low-Potential Reducing Equivalents for Nitrogenase Catalysis*, Biochemistry, 56 (2017), pp. 4177–4190.

[120] I. S. H. LEE, D. OSTOVIC, AND M. KREEVOY, *Marcus theory of hydride transfer from an anionic reduced deazaflavin to NAD^+ analogs*, J. Am. Chem. Soc., 110 (1988), pp. 3989–3993.

[121] C. LÉGER, K. HEFFRON, H. R. PERSHAD, E. MAKLASHINA, C. LUNA-CHAVEZ, G. CECCHINI, B. A. ACKRELL, AND F. A. ARMSTRONG, *Enzyme electrokinetics: energetics of succinate oxidation by fumarate reductase and succinate dehydrogenase*, Biochemistry, 40 (2001), pp. 11234–11245.

[122] H. LEIF, V. D. SLED, T. OHNISHI, H. WEISS, AND T. FRIEDRICH, *Isolation and characterization of the proton-translocating nadh: ubiquinone oxidoreductase from escherichia coli*, European journal of biochemistry, 230 (1995), pp. 538–548.

[123] B. W. LENNON, C. H. WILLIAMS, AND M. L. LUDWIG, *Crystal structure of reduced thioredoxin reductase from escherichia coli: structural flexibility in the isoalloxazine ring of the flavin adenine dinucleotide cofactor*, Protein Science, 8 (1999), pp. 2366–2379.

[124] V. LESKOVAC, S. TRIVIĆ, G. WOHLFAHRT, J. KANDRAČ, AND D. PERIČIN, *Glucose oxidase from Aspergillus niger: the mechanism of action with molecular oxygen, quinones, and one-electron acceptors*, The international journal of biochemistry & cell biology, 37 (2005), pp. 731–750.

[125] P. LESLIE DUTTON, *[23] Redox potentiometry: Determination of midpoint potentials of oxidation-reduction components of biological electron-transfer systems*, in Methods in Enzymology, vol. 54, Elsevier, 1978, pp. 411–435.

[126] F. LI, J. HINDERBERGER, H. SEEDORF, J. ZHANG, W. BUCKEL, AND R. K. THAUER, *Coupled Ferre-*

doxin and Crotonyl Coenzyme A (CoA) Reduction with NADH Catalyzed by the Butyryl-CoA Dehydrogenase/Etf Complex from Clostridium kluyveri, J Bacteriol, 190 (2008), pp. 843–850.

[127] J. LIANG, H. HUANG, AND S. WANG, *Distribution, Evolution, Catalytic Mechanism, and Physiological Functions of the Flavin-Based Electron-Bifurcating NADH-Dependent Reduced Ferredoxin: $NADP^+$ Oxidoreductase*, Front. Microbiol., 10 (2019), p. 373.

[128] N. A. LOSEY, S. POUDEL, E. S. BOYD, AND M. J. MCINERNEY, *The Beta Subunit of Non-bifurcating NADH-Dependent [FeFe]-Hydrogenases Differs From Those of Multimeric Electron-Bifurcating [FeFe]-Hydrogenases*, Front. Microbiol., 11 (2020), p. 1109.

[129] C. E. LUBNER, D. P. JENNINGS, D. W. MULDER, G. J. SCHUT, O. A. ZADVORNYY, J. P. HOBEN, M. TOKMINA-LUKASZEWSKA, L. BERRY, D. M. NGUYEN, G. L. LIPSCOMB, B. BOTHNER, A. K. JONES, A.-F. MILLER, P. W. KING, M. W. W. ADAMS, AND J. W. PETERS, *Mechanistic insights into energy conservation by flavin-based electron bifurcation*, Nat Chem Biol, 13 (2017), pp. 655–659.

[130] M. L. LUDWIG, K. A. PATTRIDGE, A. L. METZGER, M. M. DIXON, M. EREN, Y. FENG, AND R. P. SWENSON, *Control of Oxidation Reduction Potentials in Flavodoxin from Clostridium beijerinckii : The Role of Conformation Changes*, Biochemistry, 36 (1997), pp. 1259–1280.

[131] S. J. MAIOCCO, A. J. ARCINAS, S. J. BOOKER, AND S. J. ELLIOTT, *Parsing redox potentials of five ferredoxins found within Thermotoga maritima*, Protein Science, 28 (2019), pp. 257–266.

[132] S. O. MANSOORABADI, C. J. THIBODEAUX, AND H.-W. LIU, *The Diverse Roles of Flavin Coenzymes Nature's Most Versatile Thespians*, J. Org. Chem., 72 (2007), pp. 6329–6342.

[133] R. MARCUS AND N. SUTIN, *Electron transfers in chemistry and biology*, Biochimica et Biophysica Acta (BBA) - Reviews on Bioenergetics, 811 (1985), pp. 265–322.

[134] V. MASSEY, *The Chemical and Biological Versatility of Riboflavin*, Biochemical Society Transactions, 28 (2000), pp. 283–296.

[135] V. MASSEY AND H. GANTHER, *On the Interpretation of the Absorption Spectra of Flavoproteins with Special Reference to D-Amino Acid Oxidase* *, Biochemistry, 4 (1965), pp. 1161–1173.

[136] V. MASSEY AND P. HEMMERICH, *Active-site probes of flavoproteins*, Biochemical Society Transactions, 8 (1980), pp. 246–257.

[137] V. MASSEY AND G. PALMER, *On the Existence of Spectrally Distinct Classes of Flavoprotein Semiquinones. A New Method for the Quantitative Production of Flavoprotein Semiquinones*, Biochemistry, 5 (1966), pp. 3181–3189.

[138] R. MATHEWS, S. CHARLTON, R. H. SANDS, AND G. PALMER, *On the Nature of the Spin Coupling between the Iron-Sulfur Clusters in the Eight-Iron Ferredoxins*, Journal of Biological Chemistry, 249 (1974), pp. 4326–4328.

[139] S. G. MAYHEW, *The Redox Potential of Dithionite and SO_2^- from Equilibrium Reactions with Flavodoxins, Methyl Viologen and Hydrogen plus Hydrogenase*, Eur J Biochem, 85 (1978), pp. 535–547.

[140] ——, *The effects of pH and semiquinone formation on the oxidation–reduction potentials of flavin mononucleotide: A reappraisal*, European Journal of Biochemistry, 265 (1999), pp. 698–702.

[141] S. G. MAYHEW AND M. L. LUDWIG, *2 Flavodoxins and Electron-Transferring Flavoproteins*, in The Enzymes, vol. 12, Elsevier, 1975, pp. 57–118.

[142] S. W. MEINHARDT, T. KULA, T. YAGI, T. LILLICH, AND T. OHNISHI, *EPR characterization of the iron-sulfur clusters in the NADH: ubiquinone oxidoreductase segment of the respiratory chain in Paracoccus denitrificans.*, Journal of Biological Chemistry, 262 (1987), pp. 9147–9153.

[143] S. W. MEINHARDT, D. C. WANG, K. HON-NAMI, T. YAGI, T. OSHIMA, AND T. OHNISHI, *Studies on the NADH-menaquinone oxidoreductase segment of the respiratory chain in Thermus thermophilus HB-8.*, Journal of Biological Chemistry, 265 (1990), pp. 1360–1368.

[144] A. L. MENON, H. HENDRIX, A. HUTCHINS, M. F. J. M. VERHAGEN, AND M. W. W. ADAMS, *The δ-Subunit of Pyruvate Ferredoxin Oxidoreductase from Pyrococcus furiosus Is a Redox-Active, Iron-Sulfur Protein: Evidence for an Ancestral Relationship with 8Fe-Type Ferredoxins*, Biochemistry, 37 (1998), pp. 12838–12846.

[145] J. MEYER, *Iron–sulfur protein folds, iron–sulfur chemistry, and evolution*, J Biol Inorg Chem, 13 (2008), pp. 157–170.

[146] J. MEYER, S. L. ANDRADE, AND O. EINSLE, *Thioredoxin-Like [2Fe-2S] Ferredoxin*, in Encyclopedia of Inorganic and Bioinorganic Chemistry, R. A. Scott, ed., Wiley, 2 ed., Dec. 2011.

[147] L. MICHAELIS, *Theory of the reversible two-step oxidation*, Journal of Biological Chemistry, 96 (1932), pp. 703–715.

[148] L. MICHAELIS, M. P. SCHUBERT, AND C. SMYTHE, *Potentiometric study of flavins*, Journal of Biological Chemistry, 116 (1936), pp. 587–607.

[149] L. MICHAELIS AND G. SCHWARZENBACH, *The intermediate forms of oxidation-reduction of the flavins*, Journal of Biological Chemistry, 123 (1938), pp. 527–542.

[150] T. MIKI, M. MIKI, AND Y. ORII, *Membrane potential-linked reversed electron transfer in the beef heart cytochrome bc_1 complex reconstituted into potassium-loaded phospholipid vesicles.*, Journal of Biological Chemistry, 269 (1994), pp. 1827–1833.

[151] A. MILLER, D. DUAN, N. MOHAMED-RASEEK, R. KAR, D. BELL, T. VARNER, S. KHAN, M. GILLIAM, AND S. CHASEN, *Interactions that shape the complementary reactivities of the flavins of bifurcating electron transfer flavoproteins*, FASEB j., 35 (2021), p. fasebj.2021.35.S1.04129.

[152] A.-F. MILLER, H. DUAN, T. VARNER, AND N. MOHAMED RASEEK, *Reduction midpoint potentials of bifurcating electron transfer flavoproteins*, in Methods in Enzymology, vol. 620, Elsevier, 2019, pp. 365–398.

[153] A.-F. MILLER, N. MOHAMED-RASEEK, D. DAS, H. D. DUAN, M. G. VIEGAS, AND M.-A. MROGINSKI, *The Contrasting Roles of Flavins in Electron Bifurcation: How the Protein Environment Makes These Possible*, Biochimica et Biophysica Acta (BBA) - Bioenergetics, 1863 (2022), p. 148603.

[154] P. MITCHELL, *The protonmotive Q cycle: A general formulation*, FEBS Letters, 59 (1975), pp. 137–139.

[155] ——, *Protonmotive redox mechanism of the cytochrome bc_1 complex in the respiratory chain: Protonmotive ubiquinone cycle*, FEBS Letters, 56 (1975), pp. 1–6.

[156] R. MIURA, *Versatility and specificity in flavoenzymes: Control mechanisms of flavin reactivity*, Chem. Record, 1 (2001), pp. 183–194.

[157] N. MOHAMED RASEEK, *Flavin Modification and Redox Tuning in the Bifurcating Electron Transfer Flavoprotein from Rhodopseudomonas palustris: Two Arginines with Different Roles*, PhD thesis, University of Kentucky Libraries, 2021.

[158] N. MOHAMED-RASEEK, C. VAN GALEN, R. STANLEY, AND A.-F. MILLER, *Unusual reactivity of a flavin in a bifurcating electron-transferring flavoprotein leads to flavin modification and a charge-transfer complex*, Journal of Biological Chemistry, 298 (2022), p. 102606.

[159] P. MONDAL, K. SCHWINN, AND M. HUIX-ROTLLANT, *Impact of the redox state of flavin chromophores on the UV–vis spectra, redox and acidity constants and electron affinities*, Journal of Photochemistry and Photobiology A: Chemistry, 387 (2020), p. 112164.

[160] C. C. MOSER, J. M. KESKE, K. WARNCKE, R. S. FARID, AND P. L. DUTTON, *Nature of biological electron transfer*, Nature, 355 (1992), pp. 796–802.

[161] F. MÜLLER, *NMR spectroscopy on flavins and flavoproteins*, Flavins and Flavoproteins: Methods and Protocols, (2014), pp. 229–306.

[162] F. MÜLLER, M. BRÜSTLEIN, P. HEMMERICH, V. MASSEY, AND W. H. WALKER, *Light-Absorption Studies on Neutral Flavin Radicals*, European Journal of Biochemistry, 25 (1972), pp. 573–580.

[163] F. MÜLLER, P. HEMMERICH, A. EHRENBERG, G. PALMER, AND V. MASSEY, *The Chemical and Electronic Structure of the Neutral Flavin Radical as Revealed by Electron Spin Resonance Spectroscopy of Chemically and Isotopically Substituted Derivatives*, Eur J Biochem, 14 (1970), pp. 185–196.

[164] M. B. MURATALIEV, *Application of Electron Spin Resonance (ESR) for Detection and Characterization of Flavoprotein Semiquinones*, in Flavoprotein Protocols, vol. 131, Humana Press, New Jersey, July 1999, pp. 97–110.

[165] S. NAKAI, F. YONEDA, AND T. YAMABE, *Theoretical study on the lowest-frequency mode of the flavin ring*, Theoretical Chemistry Accounts: Theory, Computation, and Modeling (Theoretica Chimica Acta), 103 (1999), pp. 109–116.

[166] D. G. NICHOLLS, *Bioenergetics*, Academic press, 2013.

[167] K. NISHIMOTO, Y. WATANABE, AND K. YAGI, *Hydrogen bonding of flavoprotein. I. Effect of hydrogen bonding on electronic spectra of flavoprotein*, Biochimica et Biophysica Acta (BBA) - Enzymology, 526 (1978), pp. 34–41.

[168] W. NITSCHKE, P. JOLIOT, U. LIEBL, A. W. RUTHERFORD, G. HAUSKA, A. MÜLLER, AND A. RIEDEL, *The pH dependence of the redox midpoint potential of the [2Fe-2S] cluster from cytochrome b_6f complex (the 'Rieske centre')*, Biochimica et Biophysica Acta (BBA) - Bioenergetics, 1102 (1992), pp. 266–268.

[169] W. NITSCHKE AND M. J. RUSSELL, *Redox bifurcations: Mechanisms and importance to life now, and at its origin: A widespread means of energy conversion in biology unfolds...*, BioEssays, 34 (2012), pp. 106–109.

[170] G. NÖLL, *Spectroscopic investigation of flavoproteins: Mechanistic differences between (electro)chemical and photochemical reduction and oxidation*, Journal of Photochemistry and Photobiology A: Chemistry, 200 (2008), pp. 34–38.

[171] J.-I. OH AND B. BOWIEN, *Structural Analysis of the fds Operon Encoding the NAD^+-linked Formate Dehydrogenase of Ralstonia eutropha*, Journal of Biological Chemistry, 273 (1998), pp. 26349–26360.

[172] T. OHNISHI, *Iron–sulfur clusters/semiquinones in Complex I*, Biochimica et Biophysica Acta (BBA) - Bioenergetics, 1364 (1998), pp. 186–206.

[173] T. OHNISHI AND J. C. SALERNO, *Thermodynamic and EPR characteristics of two ferredoxin-type iron-sulfur centers in the succinate-ubiquinone reductase segment of the respiratory chain.*, Journal of Biological Chemistry, 251 (1976), pp. 2094–2104.

[174] A. OSYCZKA, H. ZHANG, C. MATHÉ, P. R. RICH, C. C. MOSER, AND P. L. DUTTON, *Role of the PEWY Glutamate in Hydroquinone-Quinone Oxidation-Reduction Catalysis in the Q_o Site of Cytochrome bc_1*, Biochemistry, 45 (2006), pp. 10492–10503.

[175] C. C. PAGE, C. C. MOSER, X. CHEN, AND P. L. DUTTON, *Natural engineering principles of electron tunnelling in biological oxidation–reduction*, Nature, 402 (1999), pp. 47–52.

[176] J. D. PELLETT, D. F. BECKER, A. K. SAENGER, J. A. FUCHS, AND M. T. STANKOVICH, *Role of Aromatic Stacking Interactions in the Modulation of the Two-Electron Reduction Potentials of Flavin and Substrate/Product in Megasphaera elsdenii Short-Chain Acyl-Coenzyme A Dehydrogenase*, Biochemistry, 40 (2001), pp. 7720–7728.

[177] G. W. PETTIGREW, T. E. MEYER, R. G. BARTSCH, AND M. D. KAMEN, *pH dependence of the oxidation-reduction potential of cytochrome c_2*, Biochimica et Biophysica Acta (BBA) - Bioenergetics, 430 (1976), pp. 197–208.

[178] A. G. PORRAS AND G. PALMER, *The room temperature potentiometry of xanthine oxidase. pH-dependent redox behavior of the flavin, molybdenum, and iron-sulfur centers.*, Journal of Biological Chemistry, 257 (1982), pp. 11617–11626.

[179] J. J. PUEYO, P. G. CURLEY, AND S. G. MAYHEW, *Kinetics and thermodynamics of the binding of riboflavin, riboflavin 5'-phosphate and riboflavin 3',5'-bisphosphate by apoflavodoxins*, Biochemical Journal, 313 (1996), pp. 855–861.

[180] M. QUAN, D. SANCHEZ, M. F. WASYLKIW, AND D. K. SMITH, *Voltammetry of Quinones in Unbuffered Aqueous Solution: Reassessing the Roles of Proton Transfer and Hydrogen Bonding in the Aqueous Electrochemistry of Quinones*, J. Am. Chem. Soc., 129 (2007), pp. 12847–12856.

[181] H. RAANAN, D. H. PIKE, E. K. MOORE, P. G. FALKOWSKI, AND V. NANDA, *Modular origins of biological electron transfer chains*, Proc. Natl. Acad. Sci. U.S.A., 115 (2018), pp. 1280–1285.

[182] T. REDA, C. D. BARKER, AND J. HIRST, *Reduction of the iron- sulfur clusters in mitochondrial nadh: Ubiquinone oxidoreductase (complex i) by euii-dtpa, a very low potential reductant*, Biochemistry, 47 (2008), pp. 8885–8893.

[183] P. R. RICH, *Electron transfer reactions between quinols and quinones in aqueous and aprotic media*, Biochimica et Biophysica Acta (BBA) - Bioenergetics, 637 (1981), pp. 28–33.

[184] R. M. G. ROBERTS, D. OSTOVI, AND M. M. KREEVOY, *Hydride transfer between NAD^+ analogues*, Faraday Discuss. Chem. Soc., 74 (1982), p. 257.

[185] H. RUPP, K. RAO, D. HALL, AND R. CAMMACK, *Electron spin relaxation of iron-sulphur proteins studied by microwave power saturation*, Biochimica et Biophysica Acta (BBA) - Protein Structure, 537 (1978), pp. 255–269.

[186] H. RÜTERJANS, G. FLEISCHMANN, M. KNAUF, F. LÖHR, M. BLÜMEL, F. LEDERER, S. MAYHEW, AND F. MÜLLER, *NMR studies of flavoproteins*, 1996.

[187] M. SAARINEN, F. K. GLEASON, AND H. EKLUND, *Crystal structure of thioredoxin-2 from Anabaena*, Structure, 3 (1995), pp. 1097–1108.

[188] J. C. SALERNO AND T. OHNISHI, *Studies on the stabilized ubisemiquinone species in the succinate-cytochrome c reductase segment of the intact mitochondrial membrane system*, Biochemical Journal, 192 (1980), pp. 769–781.

[189] K. SATO, Y. NISHINA, AND K. SHIGA, *Interaction between NADH and electron-transferring flavoprotein from Megasphaera elsdenii*, Journal of Biochemistry, 153 (2013), pp. 565–572.

[190] B. SCHOEPP-COTHENET, R. VAN LIS, A. ATTEIA, F. BAYMANN, L. CAPOWIEZ, A.-L. DUCLUZEAU, S. DUVAL, F. TEN BRINK, M. J. RUSSELL, AND W. NITSCHKE, *On the universal core of bioenergetics*, Biochimica et Biophysica Acta (BBA) - Bioenergetics, 1827 (2013), pp. 79–93.

[191] L. SCHOPFER, M. LUDWIG, AND V. MASSEY, *A working proposal for the role of the apoprotein in determining the redox potential of the flavin in flavoproteins: correlations between potentials and flavin pk_s*, Flavins and flavoproteins, (1990), pp. 399–404.

[192] K. SCHUCHMANN AND V. MÜLLER, *A Bacterial Electron-bifurcating Hydrogenase*, Journal of Biological Chemistry, 287 (2012), pp. 31165–31171.

[193] M. SCHULTE, K. FRICK, E. GNANDT, S. JURKOVIC, S. BURSCHEL, R. LABATZKE, K. AIERSTOCK, D. FIEGEN, D. WOHLWEND, S. GERHARDT, O. EINSLE, AND T. FRIEDRICH, *A mechanism to prevent*

production of reactive oxygen species by Escherichia coli respiratory complex I, Nat Commun, 10 (2019), p. 2551.

[194] G. J. SCHUT AND M. W. W. ADAMS, *The Iron-Hydrogenase of Thermotoga maritima Utilizes Ferredoxin and NADH Synergistically: a New Perspective on Anaerobic Hydrogen Production*, J Bacteriol, 191 (2009), pp. 4451–4457.

[195] M. SCHÜTZ, M. BRUGNA, E. LEBRUN, F. BAYMANN, R. HUBER, K.-O. STETTER, G. HAUSKA, R. TOCI, D. LEMESLE-MEUNIER, P. TRON, C. SCHMIDT, AND W. NITSCHKE, *Early Evolution of Cytochrome bc Complexes*, Journal of Molecular Biology, 300 (2000), pp. 663–675.

[196] W.-H. SHIN AND D. KIHARA, *55 Years of the Rossmann Fold*, in Protein Supersecondary Structures, A. E. Kister, ed., vol. 1958, Springer New York, New York, NY, 2019, pp. 1–13. Series Title: Methods in Molecular Biology.

[197] Y. SHOMURA, M. TAKETA, H. NAKASHIMA, H. TAI, H. NAKAGAWA, Y. IKEDA, M. ISHII, Y. IGARASHI, H. NISHIHARA, K.-S. YOON, ET AL., *Structural basis of the redox switches in the NAD$^+$-reducing soluble [NiFe]-hydrogenase*, Science, 357 (2017), pp. 928–932.

[198] V. D. SLED', T. FRIEDRICH, H. LEIF, H. WEISS, S. W. MEINHARDT, Y. FUKUMORI, M. W. CALHOUN, R. B. GENNIS, AND T. OHNISHI, *Bacterial NADH-quinone oxidoreductases: Iron-sulfur clusters and related problems*, J Bioenerg Biomembr, 25 (1993), pp. 347–356.

[199] E. T. SMITH, D. W. BENNETT, AND B. A. FEINBERG, *Redox properties of 2[4Fe-4S] ferredoxins*, Analytica Chimica Acta, 251 (1991), pp. 27–33.

[200] W. W. SMITH, R. M. BURNETT, G. D. DARLING, AND M. L. LUDWIG, *Structure of the semiquinone form of flavodoxin from Clostridium MP: Extension of 1.8 Å resolution and some comparisons with the oxidized state*, Journal of Molecular Biology, 117 (1977), pp. 195–225.

[201] P. SOBRADO, *Noncanonical Reactions of Flavoenzymes*, IJMS, 13 (2012), pp. 14219–14242.

[202] Y. SONG AND G. R. BUETTNER, *Thermodynamic and kinetic considerations for the reaction of semiquinone radicals to form superoxide and hydrogen peroxide*, Free Radical Biology and Medicine, 49 (2010), pp. 919–962.

[203] F. L. SOUSA, R. J. ALVES, M. A. RIBEIRO, J. B. PEREIRA-LEAL, M. TEIXEIRA, AND M. M. PEREIRA, *The superfamily of heme–copper oxygen reductases: Types and evolutionary considerations*, Biochimica et Biophysica Acta (BBA) - Bioenergetics, 1817 (2012), pp. 629–637.

[204] M. STANKOVICH, L. SCHOPFER, AND V. MASSEY, *Determination of glucose oxidase oxidation-reduction potentials and the oxygen reactivity of fully reduced and semiquinoid forms.*, Journal of Biological Chemistry, 253 (1978), pp. 4971–4979.

[205] P. J. STEPHENS, D. R. JOLLIE, AND A. WARSHEL, *Protein Control of Redox Potentials of Iron-Sulfur Proteins*, Chem. Rev., 96 (1996), pp. 2491–2514.

[206] J. SUCHARITAKUL, S. BUTTRANON, T. WONGNATE, N. P. CHOWDHURY, M. PRONGJIT, W. BUCKEL, AND P. CHAIYEN, *Modulations of the reduction potentials of flavin-based electron bifurcation complexes and semiquinone stabilities are key to control directional electron flow*, The FEBS Journal, 288 (2021), pp. 1008–1026.

[207] K.-I. TAKAMIYA AND P. DUTTON, *Ubiquinone in Rhodopseudomonas sphaeroides. Some thermodynamic properties*, Biochimica et Biophysica Acta (BBA) - Bioenergetics, 546 (1979), pp. 1–16.

[208] S. L. J. TAN, J. M. KAN, AND R. D. WEBSTER, *Differences in Proton-Coupled Electron-Transfer Reactions of Flavin Mononucleotide (FMN) and Flavin Adenine Dinucleotide (FAD) between Buffered and Unbuffered Aqueous Solutions*, J. Phys. Chem. B, 117 (2013), pp. 13755–13766.

[209] S. L. J. TAN, M. L. NOVIANTI, AND R. D. WEBSTER, *Effects of Low to Intermediate Water Concentrations on Proton-Coupled Electron Transfer (PCET) Reactions of Flavins in Aprotic Solvents and a Comparison with the PCET Reactions of Quinones*, J. Phys. Chem. B, 119 (2015), pp. 14053–14064.

[210] R. THAUER, K. JUNGERMANN, AND K. DECKER, *Energy Conservation in Chemotrophic Anaerobic Bacteria*, Bacteriol Rev, 41 (1977), pp. 809–809.

[211] M. TIETZE, A. BEUCHLE, I. LAMLA, N. ORTH, M. DEHLER, G. GREINER, AND U. BEIFUSS, *Redox Potentials of Methanophenazine and CoB-S-S-CoM, Factors Involved in Electron Transport in Methanogenic Archaea*, ChemBioChem, 4 (2003), pp. 333–335.

[212] H. S. TOOGOOD, A. VAN THIEL, J. BASRAN, M. J. SUTCLIFFE, N. S. SCRUTTON, AND D. LEYS, *Extensive Domain Motion and Electron Transfer in the Human Electron Transferring Flavoprotein·Medium Chain Acyl-CoA Dehydrogenase Complex*, Journal of Biological Chemistry, 279 (2004), pp. 32904–32912.

[213] A. TRAN-BETCKE, U. WARNECKE, C. BÖCKER, C. ZABOROSCH, AND B. FRIEDRICH, *Cloning and nucleotide sequences of the genes for the subunits of NAD^+-reducing hydrogenase of Alcaligenes eutrophus H16*, J Bacteriol, 172 (1990), pp. 2920–2929.

[214] M. A. VANONI, *Iron-sulfur flavoenzymes: the added value of making the most ancient redox cofactors and the versatile flavins work together*, Open Biol., 11 (2021), p. 210010.

[215] M. F. VERHAGEN, T. O'ROURKE, AND M. W. ADAMS, *The hyperthermophilic bacterium, Thermotoga maritima, contains an unusually complex iron-hydrogenase: amino acid sequence analyses versus biochemical characterization*, Biochimica et Biophysica Acta (BBA) - Bioenergetics, 1412 (1999), pp. 212–229.

[216] M. F. VERHAGEN, T. W. O'ROURKE, A. L. MENON, AND M. W. ADAMS, *Heterologous expression and properties of the γ-subunit of the Fe-only hydrogenase from Thermotoga maritima*, Biochimica et Biophysica Acta (BBA) - Bioenergetics, 1505 (2001), pp. 209–219.

[217] M. L. VERKHOVSKAYA, N. BELEVICH, L. EURO, M. WIKSTRÖM, AND M. I. VERKHOVSKY, *Real-time electron transfer in respiratory complex i*, Proceedings of the National Academy of Sciences, 105 (2008), pp. 3763–3767.

[218] D. VICTORIA, R. BURTON, AND A. R. CROFTS, *Role of the PEWY-glutamate in catalysis at the Q_o-site of the cyt bc_1 complex*, Biochimica et Biophysica Acta (BBA) - Bioenergetics, 1827 (2013), pp. 365–386.

[219] W. VIGIL, D. NIKS, S. FRANZ-BADUR, N. CHOWDHURY, W. BUCKEL, AND R. HILLE, *Spectral deconvolution of redox species in the crotonyl-CoA-dependent NADH:ferredoxin oxidoreductase from Megasphaera elsdenii. A flavin-dependent bifurcating enzyme*, Archives of Biochemistry and Biophysics, 701 (2021), p. 108793.

[220] W. VIGIL, J. TRAN, D. NIKS, G. J. SCHUT, X. GE, M. W. ADAMS, AND R. HILLE, *The reductive half-reaction of two bifurcating electron-transferring flavoproteins*, Journal of Biological Chemistry, 298 (2022), p. 101927.

[221] A. J. W. G. VISSER, J. L. DE WIT, F. MÜLLER, AND H. J. C. BERENDSEN, *Water relaxation measurements on semiquinones of various Flavoproteins*, Helvetica Chimica Acta, 65 (1982), pp. 2422–2430.

[222] T. WAGNER, J. KOCH, U. ERMLER, AND S. SHIMA, *Methanogenic heterodisulfide reductase (HdrABC-MvhAGD) uses two noncubane [4Fe-4S] clusters for reduction*, Science, 357 (2017), pp. 699–703.

[223] C. WALSH, *Flavin coenzymes: at the crossroads of biological redox chemistry*, Acc. Chem. Res., 13 (1980), pp. 148–155.

[224] J. D. WALSH AND A.-F. MILLER, *Flavin reduction potential tuning by substitution and bending*, Journal of Molecular Structure: THEOCHEM, 623 (2003), pp. 185–195.

[225] S. WANG, H. HUANG, J. KAHNT, A. P. MUELLER, M. KÖPKE, AND R. K. THAUER, *Nadp-specific electron-bifurcating [fefe]-hydrogenase in a functional complex with formate dehydrogenase in clostridium autoethanogenum grown on co*, Journal of bacteriology, 195 (2013), pp. 4373–4386.

[226] S. WANG, H. HUANG, J. KAHNT, AND R. K. THAUER, *A Reversible Electron-Bifurcating Ferredoxin- and NAD^+-Dependent [FeFe]-Hydrogenase (HydABC) in Moorella thermoacetica*, Journal of Bacteriology, 195 (2013), pp. 1267–1275.

[227] V. WASER AND T. R. WARD, *Aqueous stability and redox chemistry of synthetic [4Fe4S] clusters*, Coordination Chemistry Reviews, 495 (2023), p. 215377.

[228] T. WATANABE, O. PFEIL-GARDINER, J. KAHNT, J. KOCH, S. SHIMA, AND B. J. MURPHY, *Three-megadalton complex of methanogenic electron-bifurcating and CO_2-fixing enzymes*, Science, 373 (2021), pp. 1151–1156.

[229] W. WATT, A. TULINSKY, R. P. SWENSON, AND K. D. WATENPAUGH, *Comparison of the crystal structures of a flavodoxin in its three oxidation states at cryogenic temperatures*, Journal of molecular biology, 218 (1991), pp. 195–208.

[230] M. K. WIKSTRÖM AND J. A. BERDEN, *Oxidoreduction of cytochrome b in the presence of antimycin*, Biochimica et Biophysica Acta (BBA) - Bioenergetics, 283 (1972), pp. 403–420.

[231] C. E. WISE, A. E. LEDININA, D. W. MULDER, K. J. CHOU, J. W. PETERS, P. W. KING, AND C. E. LUBNER, *An uncharacteristically low-potential flavin governs the energy landscape of electron bifurcation*, Proc. Natl. Acad. Sci. U.S.A., 119 (2022), p. e2117882119.

[232] J. J. WRIGHT, E. SALVADORI, H. R. BRIDGES, J. HIRST, AND M. M. ROESSLER, *Small-volume potentiometric titrations: EPR investigations of Fe-S cluster N2 in mitochondrial complex I*, Journal of Inorganic Biochemistry, 162 (2016), pp. 201–206.

[233] F. Y. H. WU, R. E. MACKENZIE, AND D. B. MCCORMICK, *Kinetics and mechanism of oxidation-reduction reactions between pyridine nucleotides and flavins*, Biochemistry, 9 (1970), pp. 2219–2224.

[234] D. XIA, L. ESSER, L. YU, AND C.-A. YU, *Structural basis for the mechanism of electron bifurcation at the quinol oxidation site of the cytochrome bc_1 complex*, Photosynthesis research, 92 (2007), pp. 17–34.

[235] D. Xia, C.-A. Yu, H. Kim, J.-Z. Xia, A. M. Kachurin, L. Zhang, L. Yu, and J. Deisenhofer, *Crystal Structure of the Cytochrome bc $_1$ Complex from Bovine Heart Mitochondria*, Science, 277 (1997), pp. 60–66.

[236] L. Xiao, G. G. Wildgoose, and R. G. Compton, *Investigating the voltammetric reduction of methylviologen at gold and carbon based electrode materials. evidence for a surface bound adsorption mechanism leading to electrode 'protection'using multi-walled carbon nanotubes*, New Journal of Chemistry, 32 (2008), pp. 1628–1633.

[237] Y. Xu, J. Salerno, Y. Wei, and T. E. King, *Stabilized ubisemiquinone in reconstituted succinate ubiquinone reductase*, Biochemical and Biophysical Research Communications, 144 (1987), pp. 315–322.

[238] K. Yagi, N. Ohishi, K. Nishimoto, J. D. Choi, and P.-S. Song, *Effect of hydrogen bonding on electronic spectra and reactivity of flavins*, Biochemistry, 19 (1980), pp. 1553–1557.

[239] G. N. Yalloway, S. G. Mayhew, J. P. G. Malthouse, M. E. Gallagher, and G. P. Curley, *pH-Dependent Spectroscopic Changes Associated with the Hydroquinone of FMN in Flavodoxins*, Biochemistry, 38 (1999), pp. 3753–3762.

[240] Z. Yan, M. Wang, and J. G. Ferry, *A Ferredoxin- and F $_{420}$ H $_2$ -Dependent, Electron-Bifurcating, Heterodisulfide Reductase with Homologs in the Domains Bacteria and Archaea*, mBio, 8 (2017), pp. e02285–16.

[241] K.-Y. Yang and R. P. Swenson, *Modulation of the Redox Properties of the Flavin Cofactor through Hydrogen-Bonding Interactions with the N(5) Atom: Role of α-Ser254 in the Electron-Transfer Flavoprotein from the Methylotrophic Bacterium W3A1*, Biochemistry, 46 (2007), pp. 2289–2297.

[242] T. Yano, S. Magnitsky, and T. Ohnishi, *Characterization of the complex I-associated ubisemiquinone species: toward the understanding of their functional roles in the electron/proton transfer reaction*, Biochimica et Biophysica Acta (BBA) - Bioenergetics, 1459 (2000), pp. 299–304.

[243] T. Yano, V. D. Sled, T. Ohnishi, and T. Yagi, *Expression and characterization of the flavoprotein subcomplex composed of 50-kda (nqo1) and 25-kda (nqo2) subunits of the proton-translocating nadh-quinone oxidoreductase of Paracoccus denitrificans ()*, Journal of Biological Chemistry, 271 (1996), pp. 5907–5913.

[244] A. P. YEH, C. CHATELET, S. SOLTIS, P. KUHN, J. MEYER, AND D. C. REES, *Structure of a thioredoxin-like [2Fe-2S] ferredoxin from Aquifex aeolicus*, Journal of Molecular Biology, 300 (2000), pp. 587–595.

[245] T. YOUNG, D. NIKS, S. HAKOPIAN, T. K. TAM, X. YU, R. HILLE, AND G. M. BLAHA, *Crystallographic and kinetic analyses of the fdsbg subcomplex of the cytosolic formate dehydrogenase fdsabg from Cupriavidus necator*, Journal of Biological Chemistry, 295 (2020), pp. 6570–6585.

[246] J. L. YULY, P. ZHANG, C. E. LUBNER, J. W. PETERS, AND D. N. BERATAN, *Universal free-energy landscape produces efficient and reversible electron bifurcation*, Proc. Natl. Acad. Sci. U.S.A., 117 (2020), pp. 21045–21051.

[247] P. ZANELLO, *The competition between chemistry and biology in assembling iron–sulfur derivatives. Molecular structures and electrochemistry. Part V.[Fe4S4](SCysγ)4 proteins*, Coordination Chemistry Reviews, 335 (2017), pp. 172–227.

[248] H. ZHANG, S. E. CHOBOT, A. OSYCZKA, C. A. WRAIGHT, P. L. DUTTON, AND C. C. MOSER, *Quinone and non-quinone redox couples in Complex III*, J Bioenerg Biomembr, 40 (2008), p. 493.

[249] H. ZHANG, A. OSYCZKA, P. L. DUTTON, AND C. C. MOSER, *Exposing the Complex III Q_o semiquinone radical*, Biochimica et Biophysica Acta (BBA) - Bioenergetics, 1767 (2007), pp. 883–887.

[250] P. ZHANG, J. L. YULY, C. E. LUBNER, D. W. MULDER, P. W. KING, J. W. PETERS, AND D. N. BERATAN, *Electron Bifurcation: Thermodynamics and Kinetics of Two-Electron Brokering in Biological Redox Chemistry*, Acc. Chem. Res., 50 (2017), pp. 2410–2417.

[251] Z. ZHANG, L. HUANG, V. M. SHULMEISTER, Y.-I. CHI, K. K. KIM, L.-W. HUNG, A. R. CROFTS, E. A. BERRY, AND S.-H. KIM, *Electron transfer by domain movement in cytochrome bc_1*, Nature, 392 (1998), pp. 677–684.

[252] Y. ZHENG, J. KAHNT, I. H. KWON, R. I. MACKIE, AND R. K. THAUER, *Hydrogen Formation and Its Regulation in Ruminococcus albus: Involvement of an Electron-Bifurcating [FeFe]-Hydrogenase, of a Non-Electron-Bifurcating [FeFe]-Hydrogenase, and of a Putative Hydrogen-Sensing [FeFe]-Hydrogenase*, J Bacteriol, 196 (2014), pp. 3840–3852.

[253] Y.-J. ZHENG AND R. L. ORNSTEIN, *A Theoretical Study of the Structures of Flavin in Different Oxidation and Protonation States*, J. Am. Chem. Soc., 118 (1996), pp. 9402–9408.

[254] G. ZHU, H. ZENG, S. ZHANG, J. JULI, X. PANG, J. HOFFMANN, Y. ZHANG, N. MORGNER, Y. ZHU, G. PENG, H. MICHEL, AND F. SUN, *A 3.3 Å-Resolution Structure of Hyperthermophilic Respiratory*

Complex III Reveals the Mechanism of Its Thermal Stability, Angew Chem Int Ed, 59 (2020), pp. 343–351.

[255] J. ZHU, T. EGAWA, S.-R. YEH, L. YU, AND C.-A. YU, *Simultaneous reduction of iron–sulfur protein and cytochrome b $_l$ during ubiquinol oxidation in cytochrome bc $_1$ complex*, Proc. Natl. Acad. Sci. U.S.A., 104 (2007), pp. 4864–4869.

[256] Y. ZU, S. DI BERNARDO, T. YAGI, AND J. HIRST, *Redox Properties of the [2Fe-2S] Center in the 24 kDa (NQO2) Subunit of NADH:Ubiquinone Oxidoreductase (Complex I)*, Biochemistry, 41 (2002), pp. 10056–10069.

[257] K. ZUCHAN, *Energetics of the bifurcating electron transfer in Nfn.*, PhD thesis, University of Bayreuth, 2019.

[258] K. ZUCHAN, F. BAYMANN, C. BAFFERT, M. BRUGNA, AND W. NITSCHKE, *The dyad of the Y-junction-and a flavin module unites diverse redox enzymes*, Biochimica et Biophysica Acta (BBA) - Bioenergetics, 1862 (2021), p. 148401.

Abstract The [FeFe]-hydrogenase, HydABC(D), represents a group of flavoenzymes that catalyze the recently discovered reaction of flavin-based electron bifurcation/confurcation (FBEB/FBEC), in a mechanistically not yet understood manner.

This complex shares its modular architecture with other bioenergetic NAD(P)H dehydrogenases such as respiratory complex I, [NiFe]-hydrogenases and formate dehydrogenase. They exhibit two distinctive protein modules, here termed "Y-junction"- and "flavin"-modules, that assure electron transfer between $NAD(P)^+$/NAD(P)H and various bioenergetic substrates. The Y-junction module harbors three [4Fe-4S]- and one [2Fe-2S]-cluster in a Y-shaped arrangement. The flavin module has a single FMN, with two neighboring FeS-clusters, a [2Fe-2S]-cluster of the thioredoxin-type and a [4Fe4S]-cluster, in a branching architecture. Our phylogenetic analysis of this flavin-module led to a clustering of these enzymes into two groups that are distinguished by specific sequence signatures that were congruent with their proposed capacity to use ferredoxin as a second, thermodynamically-coupled substrate besides $NAD(P)^+$/NAD(P)H. The experimentally demonstrated requirement for both substrates, as one defining attribute of FBEB/FBEC, in HydABC alongside other ferredoxin-dependent members of this family was shown to correlate with the expression of additional FeS-cluster-containing domains in the HydBC-subcomplex, which exhibit different degrees of conformational rearrangements and have never been thermodynamically characterized.

Here, for the first time the complete set of equilibrium redox midpoint potentials and spectral signatures of all but one FeS cluster was determined for the heterologously expressed, electron-confurcating apo-HydABC and its constitutive subunits from *Thermotoga maritima*. The redox properties of the single flavin in the isolated HydB subunit feature a redox midpoint potential for the first electron reduction ($E_{OX/SR}$) of -160 mV at pH below 7 with a $pK_{a,OX}$-value of 7 that was attributed to the protonation of the isoalloxazine's nitrogen, N(5), of the FMN. Another redox midpoint potential below -500 mV for the second electron transition ($E_{SR/RED}$) is indicative for a strongly stabilized neutral semi-reduced flavin-state characterized by a $\log(K_s)$ around 6.8. These redox properties of the FMN in the isolated HydB subunit may reflect an observed conformational state of the HydABC complex in which the mobile thioredoxin-like C1 [2Fe-2S]-cluster domain of the HydC subunit is far from the adjacent flavin-binding site in HydB. In the apo-HydABC, the redox properties of the flavin are different with the two individual redox transitions much closer together, occurring at overall higher potentials ($E^\circ \sim$ -120 mV) as compared to the neighboring FeS-clusters ($E\sim$ -400 mV).

In none of the investigated samples, HydB or apo-HydABC, the redox properties of the flavin and the surrounding FeS-clusters fulfill the requirements for a flavin-based electron confurcating reaction, in analogy to the redox scheme determined for the Q_o-site in Rieske/cyt*b*-complexes, with the flavin redox potentials exhibiting strong positive cooperativity and the overall two-electron midpoint potential ($E_{OX/RED}$) of the flavin located in between the redox potentials of two adjacent one-electron donors.

The spectral characteristics of redox cofactors in HydABC mirror those in other NAD(P)H dehydrogenase family members, specifically the clusters proximal to the flavin. This provides the basis for the experimental investigations of additional family members with a focus on thermodynamic properties of the flavin and its adjacent cofactors, to elucidate the catalytic abilities of FMN and its implication in FBEB/FBEC.

Résumé L' hydrogénase à [FeFe], HydABC(D), représente un groupe de flavoenzymes catalysant la réaction de la bifurcation/confurcation des électrons qui a été découverte récemment. Le mécanisme de cette réaction, catalysé par la flavine, n'est pas encore compris.

HydABC(D) partage son architecture modulaire avec d'autres déshydrogénases à NAD(P)H telles que le complexe I de la chaîne respiratoire, les hydrogénases à [NiFe] et la formiate déshydrogénase. Toutes comportent deux modules protéiques distincts, ici appelés modules "jonction Y" et module à "flavine", qui assurent le transfert d'électrons entre le $NAD(P)^+$/NAD(P)H et divers substrats bioénergétiques. Le module jonction Y héberge trois centres [4Fe-4S] et un centre [2Fe-2S] disposés en forme de Y. Le module à flavine comporte un seul FMN, avec deux clusters FeS voisins, un cluster [2Fe-2S] de type thiorédoxine et un cluster [4Fe-4S], disposés en triangle. Notre analyse phylogénétique de ce module à flavine a conduit à un regroupement de ces enzymes en deux groupes distincts qui sont caractérisés par des signatures de séquences spécifiques qui corrèlent avec leur capacité à coupler la réduction/oxydation de la ferrédoxine à celle du $NAD(P)^+$/NAD(P)H. La présence requise des deux substrats, démontrée expérimentalement pour HydABC ainsi que pour les autres membres de la famille de ces déhydrogénases à NADPH dépendant de la présence la ferrédoxine, définit le mécanisme de la bifurcation ou de la confurcation des électrons au niveau de la flavine (FBEB/FBEC). Elle va de pair avec la présence de certains domaines mobiles à centres FeS du sous-complexe HydBC. Les paramètres physico-chimiques de l'ensemble des cofacteurs de ce groupe d'enzymes n'ont pas encore été caractérisés.

Dans ce travail, les caractéristiques spectrales et les potentiels rédox de 10 des 11 cofacteurs de l'apo-HydABC de *Thermotoga maritima*, produite de façon hétérologue chez *Escherichia coli*, ainsi que de ses sous-unités isolées, ont été déterminés. La flavine de HydB montre, à des valeurs de pH inférieures à 7, un potentiel rédox de -160 mV pour la première transition électronique ($E_{OX/SR}$). Un $pK_{a,OX}$ de 7 peut être attribué à la protonation de l'azote N(5) des cycles isoalloxazine de la FMN. La deuxième transition électronique ($E_{SR/RED}$) ayant lieu en dessous de -500 mV, indiquant un état semi-réduit neutre de la flavine est fortement stabilisé avec un $\log(K_s)$ d'environ 6.8. Ces propriétés rédox du FMN dans la sous-unité isolée HydB pourraient correspondre à l'état de ce cofacteur dans le complex entier, dans lequel le domaine adjacent à HydB, c'est-à-dire la partie de HydC mobile portant le cluster [2Fe-2S] de type thiorédoxine est dans une position loin de HydB. Dans l'apo-HydABC, des propriétés rédox différentes ont été déterminées pour la flavine avec les deux transitions rédox individuelles beaucoup plus rapprochées l'une de l'autre et autour de -120 mV (pH 7), ce qui est bien plus élevé que celles des centres FeS voisins autour -400 mV.

Dans aucun des échantillons étudiés, HydB ou apo-HydABC, les propriétés rédox de la flavine et des clusters FeS environnants ne satisfont aux exigences d'une réaction de confurcation des électrons comme celle décrite pour le site Qtextsubscripto des complexes Rieske/cyt*b*, avec les potentiels rédox de la flavine présentant une forte coopérativité positive et le potentiel rédox global à deux électrons ($E_{OX/RED}$) de la flavine situé entre les potentiels rédox des deux donneurs d'électrons.

Cependant, les caractéristiques spectrales des cofacteurs rédox dans HydABC reflètent celles d'autres membres de la famille des NAD(P)H-déshydrogénases, en particulier en ce qui concerne les clusters FeS proches de la flavine. Ceci fournit la base pour les investigations expérimentales d'autres membres de la famille, en mettant l'accent sur les propriétés thermodynamiques de la flavine et des cofacteurs adjacents, pour élucider les capacités catalytiques du FMN et ses implications dans la FBEB/FBEC.